# USE OF ALGAL BIOMARKERS FROM MARINE SEDIMENTS FOR RECONSTRUCTING ANTARCTIC ENVIRONMENTAL CHANGE IN THE HOLOCENE

by

KATE ASHLEY

A thesis submitted to the University of Birmingham for the degree of

DOCTOR OF PHILOSOPHY

Department of Earth Sciences

School of Geography, Earth and Environmental Sciences

College of Life and Environmental Sciences

University of Birmingham

December 2019

UNIVERSITY OF
BIRMINGHAM

## University of Birmingham Research Archive

### e-theses repository

This unpublished thesis/dissertation is copyright of the author and/or third parties. The intellectual property rights of the author or third parties in respect of this work are as defined by The Copyright Designs and Patents Act 1988 or as modified by any successor legislation.

Any use made of information contained in this thesis/dissertation must be in accordance with that legislation and must be properly acknowledged. Further distribution or reproduction in any format is prohibited without the permission of the copyright holder.

**ABSTRACT**

Antarctic coastal zones play a key role in regulating global climate, through sea level change, ocean circulation and the global carbon cycle. Observations over recent decades have documented changes such as thinning of ice sheets, freshening of the surrounding ocean and changes in sea ice extent. However, these records are only short and sparse leaving many questions yet to be answered about the drivers of such changes and environmental implications. Palaeoenvironmental records provide the potential to reconstruct such changes over the past and extend observations back through time. This requires a robust understanding of how different proxies work and thus what signal they are recording. This thesis aims to assess the use of two biomarker proxies for reconstructing past environmental conditions in the Antarctic coastal zone, namely compound-specific carbon isotopes of fatty acids and the $TEX_{86}^{L}$ sea surface temperature proxy, as well as applying these and other proxies to reconstruct past environmental conditions. Two marine sediment cores recovered from off the coast of Adélie Land, East Antarctica, are used for this work: a short core spanning roughly the past four centuries, and another core spanning the Holocene.

Changes in concentrations and carbon isotopes of two fatty acids in sediment samples are analysed in the short core and compared with down-core changes in other proxy data. Different possible drivers of fatty acid $\delta^{13}C$ are explored, of which primary productivity changes appear to be the most likely driver. The $C_{24}$ fatty acid $\delta^{13}C$ is suggested to be predominantly reflecting productivity in open water environments, while $C_{18}$ fatty acid $\delta^{13}C$ is reflecting productivity in the marginal ice zone. Fatty acid $\delta^{13}C$ is applied to the Holocene sediment core to reconstruct primary productivity changes. These data suggest that primary productivity was spatially variable over the Holocene. Open water productivity appears to be highest and most stable during the middle and late Holocene periods, after local ice sheets

have retreated. Despite a rapid and widespread increase in sea ice concentration in the Late Holocene, open water productivity remains high, possibly reflecting conditions within the Mertz Glacier Polynya, up-wind from the core site. In contrast, ice edge productivity reaches the lowest levels, perhaps due to a shorter ice-free season leading to a lack of stratified, nutrient-rich water.

A high-resolution record of $TEX_{86}^{L}$ from off the coast of Adélie Land, East Antarctica is presented spanning the last four centuries. The $TEX_{86}^{L}$ record, however, shows no correlation with air temperature in this region over the period of temporal overlap. This, in addition to a consistent over-prediction of temperatures compared to known sea surface temperatures (SST) in the region, and the deviation of glycerol dialkyl glycerol tetraether (GDGT) distributions from the global core top dataset, suggest that $TEX_{86}^{L}$ is not recording SST. A correlation between $TEX_{86}^{L}$ and Sand% suggests that $TEX_{86}^{L}$ is being driven by changes in the strength of the westward coastal currents. We hypothesise that stronger currents are leading to greater advection of GDGTs from further east, where modified Circumpolar Deep Water (MCDW) upwells. MCDW is known to have a greater diversity of archaeal communities and thus, greater advection may lead to greater inputs of GDGTs produced by different archaea, for which the relationship between GDGT cyclisation and temperature may differ.

A range of proxies are applied to both sediment cores to reconstruct past changes in different environmental conditions. In the Holocene sediment core, fatty acid hydrogen isotopes indicate a peak in meltwater input during the mid-Holocene which coincides with a widespread increase in sea-ice around the coast, persisting towards the modern day. This is hypothesised to reflect the development of a large ice-shelf cavity in the Ross Sea which fundamentally alters ice-ocean interactions and surface water properties. These surface waters

are transported west, enhancing sea ice formation around the coast. This provides a new insight into ice shelf-ocean-sea ice interactions with implications for the incorporation of ice shelves into climate models. Proxy data from the short-core provides a high-resolution insight into the relationship between different environmental factors over the past four centuries. These data highlight the key role of sea ice in driving changes in ice-edge primary productivity, inputs of glacial meltwater and strength of the westward coastal current. Ice-edge primary productivity broadly increases when both fast and pack ice are low. Productivity in more open waters, however, appears to be less sensitive to changes in sea ice. Inputs of glacial meltwater also appear to be controlled by sea ice concentrations, perhaps due to isotopically-depleted meltwater being locked up in sea ice and released when extensive melting of sea ice occurs. The strength of the westward current appears to be affected by the concentration of fast ice attached to the coast, due to its effect on wind stress. Comparison with instrumental data is difficult due to the short-term nature of the overlapping datasets. However, there is some indication that wind direction may play a key role in determining sea ice concentrations in this location which, in turn, affects many other environmental conditions offshore Adélie Land.

**ACKNOWLEDGEMENTS**

I am grateful to so many people who have helped and supported me during this PhD. My first thanks must go to James Bendle who has been a great supervisor over the past 5 years! Thanks for supporting and encouraging me through the ups and downs of the PhD, helping me to become more confident in myself, and enabling me to take many exciting opportunities during the PhD, including the chance to attend conferences and meetings around the world. Sarah Greene and Yvette Eley have been great supervisors over the latter part of the PhD, providing many useful discussions and continually encouraging me. This PhD would not have been possible without Rob McKay, Xavier Crosta and Johan Etourneau who have been incredibly helpful, providing data and samples to use in this PhD as well as many discussions helping me understand the complexities of the Adélie and how all the data fits together, and for the wonderful opportunities to visit Wellington and Bordeaux! Thank you also to Christina Riesselman, Francis Jiménez-Espejo and Alan Condron who also provided useful data and discussions for this thesis.

I am grateful to Hannah Gruszczynska and Alison Kuhl for running samples at Bristol for me, and for letting me visit the facility. Heiko Moossen and Matt O'Callaghan are thanked for their technical support in the labs at Birmingham. In particular, Heiko taught me a huge amount in the lab, without which I would have struggled to complete my analyses. Harry Gilchrist and Uthmaan Ibraheem helped with the lab work for core DTGC2011, extracting samples and doing column chromatography which was essential for this project. I must thank Rob Berstan and Elementar for the CASE partnership to this PhD and for letting me spend two weeks working with them. Many of the analyses would not have been possible without Rob's help.

I have been very fortunate to have a wonderful group of office mates supporting me over the past few years, providing lots of fun, laughter and encouragement, an endless supply of biscuits, games nights, cooked breakfasts, fungi hunts and more – thank you Dan, Nicola, Ally, Davey, Bridget, Luke, Lisa, Struan, Alice, plus Terri, Simiao, Jack, JP and many others in the Earth Sciences department. I also want to thank SPICe for providing the incredible opportunity to take 3 months out during my write up to delve into the world of science policy and salmon!

My husband James has been an incredible support throughout the whole PhD. Thank you for your constant love, patience and encouragement to help me get through it. And also all my family for their prayers and encouragement throughout.

Thank you to NERC/CENTA for funding this PhD and NERC for funding the analyses at Bristol.

## TABLE OF CONTENTS

ABSTRACT ..... i
ACKNOWLEDGEMENTS ..... v
TABLE OF CONTENTS ..... vii
LIST OF FIGURES ..... xi
LIST OF TABLES ..... xiii
ACRONYMNS ..... xiv

**Chapter 1: INTRODUCTION ..... 1**
1.1 Introduction ..... 1
1.2 Aims of this thesis ..... 2
1.3 Thesis outline ..... 3
1.4 Contributions to this thesis ..... 5

**Chapter 2: BACKGROUND CONTEXT ..... 9**
2.1 Environmental setting ..... 9
2.1.1 Location ..... 9
2.1.2 Ice dynamics ..... 10
2.1.3 Polynyas ..... 11
2.1.4 Primary productivity ..... 11
2.1.5 Climatology ..... 12
2.1.6 Currents ..... 12
2.2 Current knowledge on environmental processes in the Antarctic coastal zone. ..... 13
2.2.1 Glacial retreat ..... 13
2.2.2 Sea ice changes ..... 15
2.2.3 The oceanic carbon cycle and primary productivity ..... 20
2.3 Antarctic Holocene climate change ..... 29
2.4 The need for sedimentary archives ..... 30
2.5 Molecular and compound-specific isotope proxies ..... 31
2.5.1 Compound-specific carbon isotopes ..... 32
2.5.2 Compound-specific hydrogen isotopes ..... 34
2.5.3 Glycerol dialkyl glycerol tetraethers ..... 36

**Chapter 3: ORGANIC GEOCHEMISTRY METHODS ..... 43**
3.1 Introduction ..... 43
3.2 Glassware ..... 43
3.3 Solvents and reagents ..... 43

3.4 Biomarker extraction and separation ..... 44
3.4.1 Sediment sample preparation ..... 44
3.4.2 Lipid extractions ..... 44
3.4.3 Acid-neutral split of lipid extracts ..... 45
3.4.4 Clean up of neutral fractions ..... 46
3.4.5 Derivatization and clean-up of acid fractions ..... 46
3.5 Quantification of samples by gas chromatography ..... 47
3.6 Standards ..... 48
3.7 Identification of samples by mass spectrometry ..... 49
3.8 Carbon isotope analysis of fatty acids ..... 49
3.9 Liquid Chromatography analysis of GDGTs ..... 53
3.10 Hydrogen isotope analysis of fatty acids ..... 54

**Chapter 4: MID-HOLOCENE ANTARCTIC SEA-ICE INCREASE DRIVEN BY MARINE ICE SHEET RETREAT ..... 57**

Abstract ..... 57
4.1 Introduction ..... 58
4.2 Early Holocene ..... 61
4.3 Middle Holocene ..... 63
4.4 What drove the Neoglacial transition? ..... 67
4.5 Methods ..... 71
4.5.1 Organic geochemical analyses ..... 71
4.5.2 Inorganic geochemical analysis and electronic microscopy ..... 72
4.5.3 Grain size analyses ..... 73
4.5.4 Highly branched isoprenoids (HBI) ..... 74
4.5.5 Biogenic silica ..... 75
4.5.6 Model simulations ..... 75
SUPPLEMENTARY INFORMATION ..... 77
S1 Environmental setting ..... 77
S2 Age model ..... 80
S3 Justification for interpretation of proxy data ..... 83
S3.1 $\delta^2H_{FA}$ ..... 83
S3.1.1 Source of fatty acids ..... 83
S3.1.2 Interpretation of hydrogen isotopes ..... 86
S3.2 Ba/Ti ratio excess as a meltwater pulse proxy ..... 92
S3.3 Grain size ..... 93

S3.4 Highly-branched isoprenoids (HBI) ..... 99
S4 Ross Sea deglaciation history ..... 100
S5 Data-Model mismatch ..... 103

**Chapter 5: USE OF FATTY ACID CARBON ISOTOPES AS A PALAEOPRODUCTIVITY PROXY IN A HIGHLY PRODUCTIVE ANTARCTIC POLYNYA ENVIRONMENT ..... 105**

Abstract ..... 105
5.1 Introduction ..... 105
5.2 Materials and Methods ..... 106
5.3 Fatty acids within DTGC2011 ..... 107
5.3.1 Fatty acid concentrations ..... 108
5.3.2 Potential sources of the C18 fatty acid ..... 110
5.3.3 Potential sources of the C24 fatty acid ..... 112
5.3.4 Microbial degradation and diagenetic effects on fatty acid concentration ..... 114
5.3.5 Comparison of fatty acid concentrations with highly branched isoprenoid alkenes ..... 116
5.4 Carbon isotopes of fatty acids ..... 120
5.4.1 Controls on carbon isotopes of particulate organic matter ..... 122
5.4.2 Controls on photosynthetic fractionation (εp) ..... 125
5.4.3 Comparison of fatty acid $\delta^{13}C$ with other proxy data ..... 133
5.5 Conclusions ..... 136

**Chapter 6: RECONSTRUCTION OF HOLOCENE PRIMARY PRODUCTIVITY OFFSHORE ADÉLIE LAND, EAST ANTARCTICA, USING COMPOUND-SPECIFIC CARBON ISOTOPES ..... 139**

Abstract ..... 139
6.1 Introduction ..... 139
6.2 Methods ..... 141
6.3 Results and Discussion ..... 142
6.3.1 Early Holocene (11.4 – 8.2 ka BP) ..... 142
6.3.2 Mid-Holocene (8.2 – 4.5 ka BP) ..... 146
6.3.3 Late Holocene (4.5 ka BP – present) ..... 147
6.4 Conclusions ..... 150

**Chapter 7: APPLICATION OF THE $TEX_{86}^{L}$ SEA SURFACE TEMPERATURE PROXY TO HIGHLY RESOLVED SEDIMENTS IN THE ANTARCTIC COASTAL ZONE ..... 153**

Abstract ..... 153
7.1 Introduction ..... 153
7.2 Methods ..... 155
7.3 $TEX_{86}^{L}$ and sea surface temperatures ..... 155

7.4 GDGT distributions ..... 158
7.5 Possible drivers of $TEX_{86}^{L}$ in DTGC2011 ..... 161
7.6 Grain size distributions and $TEX_{86}^{L}$ ..... 166
7.7 Conclusions ..... 173

**Chapter 8: PRODUCTIVITY, ICE AND WATER MASS CHANGE IN THE DUMONT D'URVILLE TROUGH OVER THE PAST FOUR CENTURIES ..... 175**
Abstract ..... 175
8.1 Introduction ..... 175
8.2 Methods ..... 177
8.3 Interpretation of proxy records ..... 177
8.4 Reconstruction of palaeoenvironmental conditions offshore Adélie Land ..... 178
8.4.1 The 1587 to 1725 C.E. period ..... 178
8.4.2 The 1725 to 1890 C.E. period ..... 181
8.4.3 The 1890 to 1999 C.E. period ..... 182
8.5 Conclusions ..... 187

**Chapter 9: CONCLUSIONS AND FUTURE WORK ..... 189**
9.1 Main findings from this thesis ..... 289
9.1 Directions for future work ..... 192

**REFERENCES ..... 195**
**APPENDICES ..... 233**
A1 Chapter 4 data ..... 233
A2 Chapter 5 data ..... 261
A3 Chapter 6 data ..... 269
A4 Chapter 7 data ..... 275
A5 Chapter 8 data ..... 280

## LIST OF FIGURES

Figure 2.1 Location of Site DTGC2011 on bathymetric map of the Adélie Land region .....9
Figure 2.2 NASA MODIS satellite image of the study region .....10
Figure 2.3 Structures of marine GDGTs referred to in the text. .....38
Figure 3.1 δ13C values of each F8 compound at different peak heights. .....52
Figure 4.1 Location of Sites U1357 and MD03-2601 .....58
Fig. 4.2 Holocene Adélie Land proxy records from IODP Site U1357 and other circum-Antarctic sites. .....62
Fig. 4.3 MITgcm simulations of meltwater release from along the edge of the Ross Ice Shelf. .....65
Fig. 4.4 Conceptual model of evolving Holocene glacial and oceanographic conditions in the Ross Sea region. .....69
Figure S1. Simulated salinity anomalies over time at Site U1357 for the five meltwater release experiments. .....79
Figure S2. Age-depth plot of U1357B, using the default outputs from the BACON software.. .....81
Figure S3. Age-depth plot of MD03-2601, using the default outputs from the BACON software....82
Figure S4. Authigenic marine barite (red circle, size > 300nm) observed in Ba/Ti enriched interval. .....93
Figure S5 Holocene Adélie Land proxy records from IODP Site U1357. .....95
Figure S6 3.5 kHz seismic profile of the Adélie drift. .....98
Figure S7 Absolute concentrations of highly branched isoprenoids (HBIs) measured in U1357...100
Figure S8 Comparison of sea ice data from the Adélie region with TraCE-21k simulations. .....103
Figure 5.1 Location of Site DTGC2011 on bathymetric map of the Adélie Land region. .....106
Figure 5.2 Typical chromatogram of the fatty acid fraction of DTGC2011 samples.....107
Figure 5.3 Fatty acid concentrations (µg/g of dry sediment) with depth from core DTGC2011. ....110
Figure 5.4 Concentrations of the C18 fatty acid, the HBI triene, HBI diene, C24 fatty acid from core DTGC2011 .....117
Figure 5.5 δ13C measurements of the C18 and C24 fatty acids in core DTGC2011.....121
Figure 5.6 δ13C values of the C24 fatty acid and relative abundances (%) of the open water diatom Fragilariopsis kerguelensis. Also shown are relative abundances of the four most abundant diatom groups in DTGC2011.. .....132
Figure 5.7 δ13C of the C24 and C18 fatty acid, HBI diene concentrations and relative abundances of Fragilariopsis curta plus Fragilariopsis cylindrus.....134
Figure 6.1 Holocene proxy record from offshore Adélie land. .....144
Figure 7.1 TEX86L derived sea surface temperatures in core DTGC2011 .....156
Figure 7.2 Spatial variation in sea surface temperature around the Antarctic coast from Adélie Land to the Ross Sea.. .....157
Figure 7.3 TEX86L derived sea surface temperatures in core DTGC2011 and air temperatures measured at Dumont d'Urville weather station between 1950 and 2000 C.E.. .....157

Figure 7.4 ΔRI of samples from DTGC2011 over time ..... 159

Figure 7.5 Ring index plotted against TEX86 for core top samples used in Zhang et al. (2016) and DTGC2011 samples ..... 160

Figure 7.6 Methane index plotted against ΔRI for samples from DTGC2011 ..... 161

Figure 7.7 δ13C from C24 and C18 fatty acid compared to TEX86L derived SSTs from core DTGC2011 ..... 164

Figure 7.8 TEX86L derived sea surface temperatures and sand percent from core DTGC2011. .. 167

Figure 7.9 R2 values between sand percent and TEX86L after adjusting the age scale of the TEX86L back by 1 to 10 years. ..... 167

Figure 7.10 Sand percent and TEX86L derived sea surface temperatures from core DTGC2011 after resampling by linear interpolation and shifting the age scale of the TEX86L back by 5 years. ..... 168

Figure 8.1 Proxy data from core DTGC2011 ..... 179

Figure 8.2 Proxy data from core DTGC2011 for the most recent period (1890 to 1999 C.E.) ..... 183

## LIST OF TABLES

Table 3.1 Solvents and reagents used during this thesis and their abbreviations used .....44

Table 3.2 Details of the different fractions collected during column chromatography of the total neutral fraction .....46

Table 3.3. Compounds included in the in-house standard and their abbreviations used .....48

Table 3.4 Fatty acid compounds included in the F8 standard and their abbreviations used. .....50

Table 5.1 $R^2$ values for fatty acid concentrations throughout core DTGC2011 .....108

Table 5.2 $R^2$ values for fatty acid concentrations in core DTGC2011 below 25 cm only .....109

Table 5.3 Summary of several studies where long-chain fatty acids have been shown to be produced by aquatic organisms .....113

**ACRONYMNS**

**AABW** – Antarctic Bottom Water

**AACC** – Antarctic Coastal Current

**AASW** – Antarctic Surface Water

**ALBW** – Adélie Land Bottom Water

**ASC** – Antarctic Slope Current

**ASF** – Antarctic Slope Front

**BF3** – Boron trifluoride

**BIT** – Branched and isoprenoid tetraether index

**BP** – Before present

**C.E**. – Common era

**CDW -** Circumpolar Deep Water

**Chl a** – Chlorophyll a

**Cren** – Crenarchaeol

**Cren' -** Isomer of crenarchaeol

**CRS** – Chaetoceros resting spores

**CuO** – Cupper oxide

**DCM** – Dichloromethane

**DDUP** – Dumont D'Urville Polynya

**DDUT** – Dumont D'Urville Trough

**DIC** – Dissolved Inorganic Carbon

**EAIS** – East Antarctic Ice Sheet

**FA** – Fatty acid

**FAME** – Fatty acid methyl esther

**Fe** – Iron

**FID** – Flame ionisation detector

**GC** – Gas chromatography

**GC-MS** – Gas chromatograph mass spectrometer

**GDGT** – Glycerol dialkyl glycerol tetraether

**HBI** – Highly branched isoprenoid alkenes

**HPLC** – High performance liquid chromatography

**HSSW** – High Salinity Shelf Water

**IODP** – Integrated Ocean Drilling Program

**IRD** – Ice rafted debris

**IRMS** – Isotope ratio mass spectrometer

**ISO** – Isopropyl alcohol

**ISW** – Ice shelf water

**ka** – Thousand years

**LCFA** – Long chained fatty acid

**LPSA** – Laser Diffraction Particle Size Analyser

**MAR** – Mass accumulation rate

**MCDW** – Modified Circumpolar Deep Water

**MeOH** – Methanol

**MG-I** – Marine Group I

**MG-II** – Marine Group II

**MGP** – Mertz Glacier Polynya

**MI** – Methane Index

**MIZ** – Marginal ice zone

**MLD** – Mixed layer depth

**MSLP** – Mean sea level pressure

**nA** – nanoamps

**$Na_2SO_4$** – Sodium sulphate

**NGR** – Natural gamma radiation

**NPP** – Net Primary Productivity

**P – E** – Precipitation minus evaporation

**PO4** – Phosphate

**POOZ -** Permanently open-ocean zone

**RI** – Ring Index

**RIS** – Ross Ice Shelf

**SAM** – Southern Annular Mode

**Sand% -** Sand percentage

**SCFA** – Short chained fatty acid

**SiO2** – Silica

**SIZ** – Sea ice zone

**SST** – Sea surface temperature

**TEX86** –TetraEther indeX of tetraethers consisting of 86 carbon atoms

**THC** – Thermohaline circulation

**TLE -** Total lipid extract

**TNF** – Total neutral fraction

**Uk37'** – Alkenone unsaturation index

**XRF** – X-ray fluorescence

**WAIS** – West Antarctic Ice Sheet

**WOA18** – World Ocean Atlas 2018

# Chapter 1

# INTRODUCTION

## 1.1 Introduction

The Antarctic continent and its surrounding ocean are important players in regulating global climate. Not only does the melting of large volumes of ice have the potential for widespread sea-level rise (Mengel and Levermann, 2014; Pollard and Deconto, 2016; Robel et al., 2019), it can also have direct and indirect effects on global ocean circulation (Rintoul, 2007; Orsi et al., 1999) and the carbon cycle (Sigman and Boyle, 2000; Arrigo et al., 2008), in combination with other processes such as primary productivity, upwelling and sea ice production (Sigman et al., 2010; Bintanja et al., 2015; Shadwick et al., 2014; Arrigo and van Dijken, 2003). These in turn can affect both regional and global climates.

Over recent decades, observations from instrumental and satellite records have documented increased freshening of surface and bottom waters along the Antarctic continental margin (Jacobs et al., 2002; Rintoul, 2007; Jacobs and Giulivi, 2010; Aoki et al., 2013; Khazendar et al., 2016) thinning of ice shelves (Paolo et al., 2015; Shepherd et al., 2004; Rignot et al., 2014; Khazendar et al., 2016) and an increase in sea ice extent (Gagné et al., 2015; Turner et al., 2016). Understanding the drivers and feedbacks involved in such changes is hampered by the limited meteorological records from the Antarctic, currently being too short, sparse and discontinuous to fully constrain these changes (Steig et al., 2009). These uncertainties create difficulties in making predictions of future changes in climate and sea level rise (IPCC, 2013), leaving large inter-model variability in projected 21st century climate change (Sen Gupta et al., 2009).

Palaeoenvironmental reconstructions can provide a longer-term view of these changes. While ice cores have provided much information on changes in atmospheric variability (Jouzel et al., 2007; Masson-Delmotte et al., 2011; Masson et al., 2000; Steig et al., 2000; Petit et al., 1999), fewer oceanic records exist, which are required for understanding changes in conditions such as water masses and sea ice (e.g. Pike et al., 2013; Shevenell et al., 2004; Crosta et al., 2007). Marine sediment cores from the Antarctic coastal zone have the potential for reconstructing interactions between the atmosphere, ocean, ice and biological productivity.

Various proxies have been developed to reconstruct a range of environmental conditions from marine sediments. In particular, lipid biomarkers have the potential to record a wide range of information about the environment they were formed in. These are organic molecules produced by various different organisms, preserved within marine sediments. Changes in the abundance, structure and isotopic composition of biomarkers can record environmental conditions at the time of their formation (Gaines et al., 2009). A good understanding of how these proxies work and the type of environmental information they record is vital if they are to provide a useful insight into past environmental changes.

### 1.2 Aims of this thesis

This thesis uses material from two marine sediment cores recovered from the same location, in the Dumont D'Urville Trough, just off the coast of Adélie Land, East Antarctica. Core DTGC2011 is 4.6 m in length and covers the period 1587 to 1999 C.E. Core U1357B is 171 m in length and covers the period ca. 11,400 to 100 years before present.

Broadly, the main aims of this thesis are twofold:

1) *Assess the utility of biomarker proxies for reconstructing palaeoenvironmental conditions offshore Adélie Land, East Antarctica.*

The East Antarctic coastal zone is a complex environment affected by various water masses, glacial meltwater inputs, sea ice cover and high rates of primary productivity. In particular, the use of both the $TEX_{86}^{L}$ sea surface temperature proxy (based on the distributions of glycerol dialkyl glycerol tetraethers; GDGTs) and the compound-specific carbon isotope composition of fatty acids, are assessed as proxies for reconstructing palaeoenvironmental conditions in this type of environment.

2) *Reconstruct changes in palaeoenvironmental conditions offshore Adélie Land, East Antarctica.*

   A range of biomarkers and other proxies are applied to cores U1357B and DTGC2011 to reconstruct changes over the Holocene and over the past four centuries, respectively.

### 1.3 Thesis outline

*Chapter 2: Background Context*

This chapter provides the relevant background information to the thesis, including details about the environmental setting. By reviewing the literature, current understanding and recent observed trends of physical and biological processes in the Antarctic are summarised, along with current understanding on Holocene climate change in Antarctica, and the background to the main proxies used in this thesis.

*Chapter 3: Methods*

This chapter details the organic geochemical methods which were used to produce data for this thesis.

*Chapter 4: Mid-Holocene Antarctic sea-ice increase driven by marine ice sheet retreat*

This chapter jumps straight into addressing the second aim of this thesis, by using a variety of palaeoclimate proxies from core U1357B to reconstruct environmental conditions over the Holocene. Compound-specific hydrogen isotopes of fatty acids are used to reconstruct changes in glacial meltwater input and compared with other proxies to understand the interactions between glacial retreat and ice shelf development in the Ross Sea, and sea ice conditions around the East Antarctic coast.

*Chapter 5: Use of fatty acid carbon isotopes as a palaeoproductivity proxy in a highly productive Antarctic polynya environment*

This chapter addresses the first aim of the thesis and assesses the use of compound-specific carbon isotopes of two fatty acid compounds for reconstructing past changes in primary productivity. This uses material from core DTGC2011 and compares changes in fatty acid carbon isotopes over time with other proxies, notably highly-branched isoprenoid alkenes (HBIs), and diatom abundances, to determine the most likely driver of the carbon isotopes.

*Chapter 6: Reconstruction of Holocene primary productivity offshore Adélie Land, East Antarctica, using compound-specific carbon isotopes*

This chapter builds directly on the conclusions of Chapter 4 and addresses the second aim of this thesis. Compound-specific carbon isotopes of two fatty acids compounds are measured from core U1357B and are applied as a proxy to reconstruct primary productivity over the Holocene.

*Chapter 7: Application of the $TEX_{86}^{L}$ sea surface temperature proxy to highly resolved sediments in the Antarctic coastal zone*

This chapter addresses the first aim of the thesis and assesses the use of the $TEX_{86}^{L}$ sea surface temperature proxy in recent sediments offshore Adélie Land. Through close

assessment of GDGT distributions and comparisons with other proxy data in core DTGC2011, the most likely driver of changes in $TEX_{86}^{L}$ is determined.

*Chapter 8: Productivity, ice and water mass change in the Dumont D'Urville Trough over the past four centuries*

This chapter addresses the second aim of the thesis and builds directly on the conclusions of Chapters 4 and 6. A range of proxies from core DTGC2011 are used to reconstruct environmental conditions offshore Adélie Land over the past four centuries, with some comparison to instrumental records where overlap occurs. This aims to provide an insight into interactions between climate, sea ice, currents and primary productivity.

*Chapter 9: Conclusions and future work*

This chapter summarises the main findings from the thesis and discusses outstanding questions and potential areas of future work which can build on the results of this thesis.

**1.4 Contributions to this thesis**

Most of the work in this thesis has been part of international collaborations with many different researchers. As such, various people have contributed unpublished datasets to be used alongside data generated by myself, as detailed below:

*Chapter 4:*

The data used in this chapter was generated prior to the PhD project, as part of IODP Expedition 318 which took place in 2010. Dr James Bendle and Dr Osamu Seki provided compound-specific hydrogen isotopes of fatty acids, generated at Hokkaido University. HBIs were measured by Dr Johan Etourneau and Dr Guillaume Massé at Laboratoire d'Océanographie et du Climat: Experimentations et Approches Numériques. Dr Francis J.

Jimenez-Espejo generated the Ba/Ti data at the at the IODP-Core Repository/Texas A&M University laboratories. Dr Christina Riesselmann provided biogenic silica generated at the University of Otago. Dr Alan Condron ran model simulations at the Massachusetts Institute of Technology. Grain size analyses were generated by Dr Rob McKay and Anya Albot at Victoria University Wellington. The age model for core U1357 was generated by Dr Rob Dunbar, Dr Rob McKay, Dr Xavier Crosta and Dr Guillaume Masse.

*Chapter 5:*

HBI concentrations, diatom abundances and the age model for core DTGC2011 were generated as part of Phillipine Campagne's PhD thesis at the Université de Bordeaux. Fatty acids were extracted and separated via column chromatography by myself with assistance from undergraduate students Uthmaan Ibraheem and Harry Gilchrist. Fatty acid concentration for measured by Harry Gilchrist and me. Carbon isotope measurements were generated by me.

*Chapter 6:*

The majority of fatty acid $\delta^{13}C$ data was generated at the University of Birmingham, as an MSci thesis prior to this PhD, presented in Newton (2015). However, the data quality was reassessed by me during this PhD in order to meet the same standards as the data used in Chapters 5 and 8. This involved removing data points where standard deviations between duplicate runs were above the threshold defined in Chapter 3. In addition, fifteen extra samples were analysed and added to the dataset, following the methods described in Chapter 3. Bulk sediment $\delta^{13}C$ was generated by Dr Christina Riesselmann at the University of Otago.

*Chapter 7:*

GDGTs were extracted from the sediments by Uthmaan Ibraheem and myself. Samples were filtered for LC-MS analysis by me. GDGT distributions were analysed at the University of Bristol by Hannah Gruszczyska and myself as part of a NERC grant funded during this PhD project. Grain size analyses were conducted by Dr Rob McKay at Victoria University Wellington.

*Chapter 8:*

In addition to the data mentioned in Chapters 5 and 7, compound-specific fatty acid hydrogen isotope measurements were analysed at the University of Bristol by Alison Kuhl as part of a NERC grant funded during this PhD project.

## Chapter 2

# BACKGROUND CONTEXT

## 2.1 Environmental setting

### 2.1.1 Location

Sediment cores U1357B and DTGC2011 were both retrieved from the Adélie drift, located in the Dumont D'Urville Trough of the Adélie Basin, ca. 35 km offshore from Adélie Land (66.24°S, 140.25°E; Fig 2.1). This is a 1000 m deep, glacially scoured depression on the East Antarctic continental shelf, bounded to the east by the Adélie Bank. Further east lays the Adélie Depression and the Mertz Bank, the latter located north of the Mertz Glacier floating ice tongue (Fig. 2.1). The Adélie Land region is dissected by several glaciers which could potentially contribute glacial meltwater and terrigenous sediment into the coastal zone with

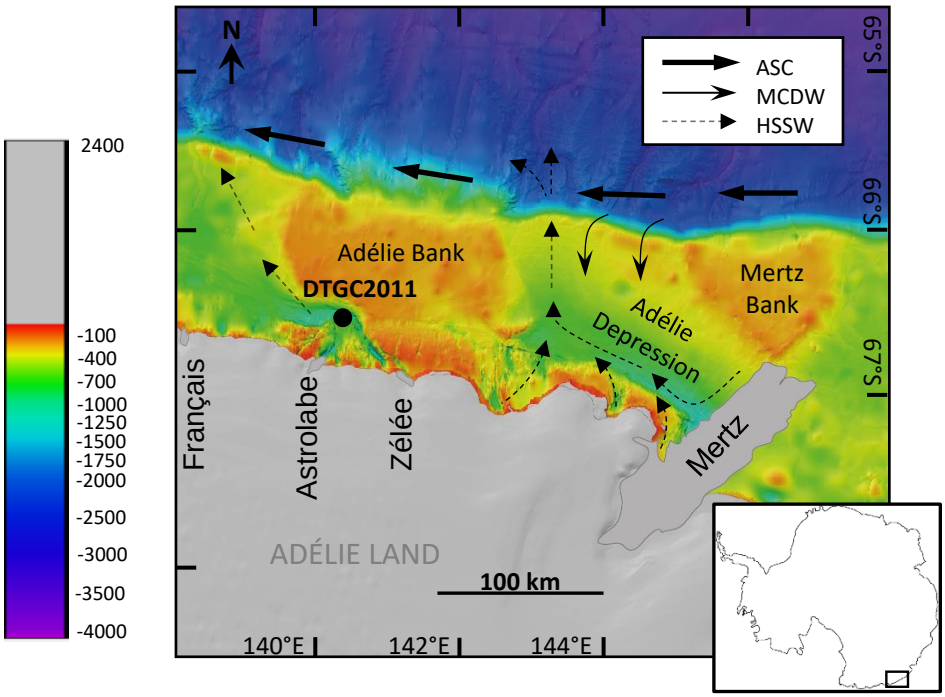



**Figure 2.1** Location of Site DTGC2011 on bathymetric map of the Adélie Land region (modified from Beaman et al., 2011), indicating positions of the main glaciers (prior to Mertz Glacier Tongue collapse in 2010) and pathways of the main water masses affecting the region: Antarctic Slope Current (ASC), Modified Circumpolar Deep Water (MCDW) and High Shelf Salinity Water (HSSW).

the core site located 40 km to the north of the Astrolabe Glacier, and ca. 75 and 300 km northwest of the Zélée and Mertz glaciers, respectively.

### 2.1.2 Ice dynamics

Sea ice plays a key role on the dynamics of the region, with both fast ice and pack ice present off the coast of Adélie Land. Fast ice is sea ice which forms and becomes attached to the coast (Massom et al., 2010). Offshore Adélie Land, a large bank of fast ice forms annually between 135 and 142°E, and extends ca. 100-120 km away from the coast (Fig. 2.2a). Grounded icebergs play a key role in the fast ice distribution, by providing anchor points for ice growth and aiding the trapping of pack ice (Massom et al., 2001, 2009, 2010). On the north edge of this fast ice buttress is an inlet of open water forming a polynya, an area of open water surrounded by sea ice (Bindoff et al., 2000). In contrast, pack ice is a much more dynamic form of sea ice, in constant motion in response to ocean currents and winds (Massom et al., 2009) (Fig. 2.2a). In the summer, most of the sea ice melts, allowing large phytoplankton

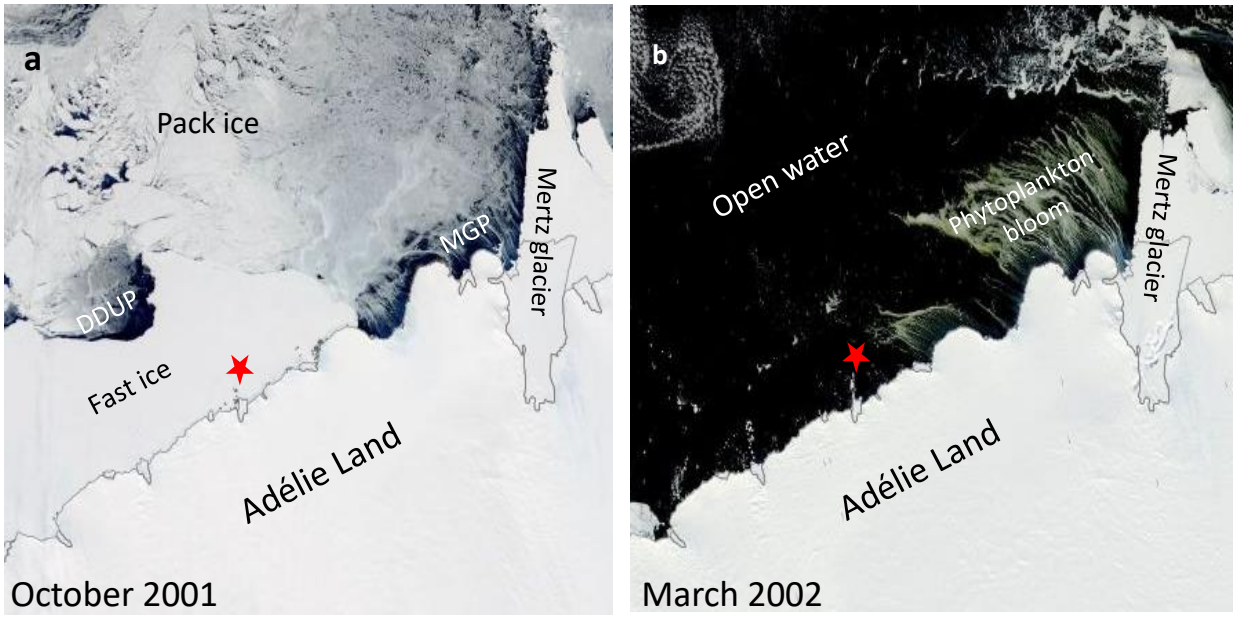



**Figure 2.2** NASA MODIS satellite image of the study region (from https://worldview.earthdata.nasa.gov/). Red star indicates location of the core site. a) October 2001 showing the cover of fast ice and pack ice off the coast and the presence of the two polynyas: Dumont D'Urville Polynya (DDUP) and Mertz Glacier Polynya (MGP) b) March 2002 showing open water over the site and the presence of a large phytoplankton bloom.

blooms to form in the open water offshore Adélie Land (Massom et al., 2009; Arrigo and van Dijken, 2003) (Fig 2.2b).

### 2.1.3 Polynyas

The site itself is located close to the Dumont D'Urville polynya (DDUP), which has a summer (winter) extent of 13,020 $km^2$ (920 $km^2$), but is also directly downwind and downcurrent of the much larger and highly productive Mertz Glacier polynya (MGP) to the east, with a summer (winter) extent of 26,600 $km^2$ (591 $km^2$) (Arrigo and van Dijken, 2003) (Fig. 2.2a). The MGP forms as a result of reduced advection of sea-ice from the east due to the presence of the Mertz Glacier Tongue (Massom et al., 2001) (Fig. 2.2b) and strong katabatic winds which blow off the Antarctic ice sheet with temperatures below -30°C (Bindoff et al., 2000). Katabatic winds freeze the surface waters and blow newly formed ice away from the coast, making the polynya an efficient sea-ice 'factory', with higher rates of sea-ice formation in comparison to non-polynya ocean areas which undergo seasonal sea ice formation (Kusahara et al., 2010). Despite occupying a region of less than 0.1% of the total Antarctic sea ice extent, the MGP produces 1.3% of the total Southern Ocean sea ice volume (Marsland et al., 2004).

### 2.1.4 Primary productivity

As a result of the polynya environments, the area along the Adélie Coast is characterized by extremely high primary productivity, with phytoplankton assemblages dominated by diatoms (Beans et al., 2008). The lack of ice cover means polynyas are the first polar marine systems exposed to spring solar radiation, making them regions of enhanced biological productivity compared to adjacent waters (Arrigo and van Dijken, 2003). The Mertz Glacier zone (ca. 144°E) to the east of the core site, is generally characterized by stratified waters in the

summer, due to seasonal ice melt, with these conditions resulting in diatom communities of low diversity dominated by small diatoms species such as *Fragilariopsis* spp. (Beans et al., 2008). In contrast, the surface waters above the core site (140°E) are more well-mixed with a diverse diatom assemblage characterized by larger diatoms such as *Rhizosolenia* spp. (Beans et al., 2008)

### 2.1.5 Climatology

The nearest weather station is the Dumont D'Urville station (66.40°S, 140.l°E). Here, mean annual air temperature has been measured as -10.8°C, with monthly mean temperatures always below freezing. Surface melting events do occur, in which temperatures can reach above 10°C, between November and March. The dominant wind direction is southeast (120 - 160°) as a result of the strong katabatic winds. The annual mean wind speed is 9.4 m $s^{-1}$, but can be greater than 50 m $s^{-1}$ (König-Langlo et al., 1998).

### 2.1.6 Currents

The region is affected by various water masses. High Salinity Shelf Water (HSSW) is formed on the shelf in coastal polynyas as a result of sea ice production and the associated brine rejection. HSSW flows out of the shelf through the Adélie sill at 143°E (Fig. 2.1). Modified Circumpolar Deep Water (MCDW) is a warm and salty water mass which upwells onto the continental shelf through channels in the shelf break. MCDW has been observed to upwell across the shelf break near the Mertz Glacier at 144°E (Williams et al., 2008) (Fig. 2.1). Around Antarctica, a strong gradient in water mass properties between the shelf waters and Circumpolar Deep Water (CDW) offshore forms the Antarctic Slope Front (ASF) and Antarctic Slope Current (ASC), the latter flowing westward along the continental slope (Fig.

2.1). The ASC acts as a barrier, controlling the transport of heat onto the continental shelf and acting as a link between processes on the coast and the rest of the ocean. Surface wind stress plays an important role in driving the ASC (Thompson et al., 2018). Poleward of the ASC is the Antarctic Coastal Current (AACC), also known as the East Wind Drift, also flowing westward often adjacent to ice shelves (Thompson et al., 2018). The Antarctic Surface Water (AASW) is a widespread water mass which extends across the continental shelf and has a surface mixed layer varying from a shallow (ca. 10 m), warmer and fresher layer in summer to a deeper (ca. 100 m), colder layer in winter. This is also transported westward along with the AACC (Martin et al., 2017).

The majority of material, including biological material produced within the DDUP and MGP, is transported via the westward flowing AASW and AACC. The location of the core site in a deep trough surrounded by the Adélie Bank means that a large volume of material is deposited here. This results in a remarkably high sedimentation rate of ca. 1.5-2 cm $year^{-1}$ at Site U1357 (Escutia et al., 2011).

## 2.2 Current knowledge on environmental processes in the Antarctic coastal zone

### 2.2.1 Glacial retreat

The vast majority of Antarctic ice retreat has occurred in the West Antarctic Ice Sheet (WAIS) (Paolo et al., 2015; Robel et al., 2019) most notably ice streams in the Amundsen Sea Embayment (Khazendar et al., 2016), where significant air (Steig et al., 2009) and ocean (Schmidtko et al., 2014) warming has been observed. Although the East Antarctic Ice Sheet (EAIS) has remained relatively stable in comparison (Gardner et al., 2018), the Totten and Moscow University ice shelves have also shown comparable melt rates to the WAIS in recent years (Li et al., 2016; Silvano et al., 2017). Indeed, various studies suggest that the EAIS has

contributed several metres to sea level rise in the past (Fogwill et al., 2014; Cook et al., 2013) and has the potential to in the future (Mengel and Levermann, 2014). Thus, understanding both the drivers and environmental implications of retreat are important for future projections.

Ocean warming has been proposed a key driver of glacial retreat in the WAIS, with the most significant ice losses observed where warm CDW has access below ice shelves (Shepherd et al., 2004; Pritchard et al., 2012; Cook et al., 2016), driven by large scale changes in Southern Ocean wind forcing (Pritchard et al., 2012). In other areas, atmospheric warming is also shown to be important, particularly in the Antarctic Peninsula where significant increases in air temperature have been recorded at a rate of 3.7±1.6°C century$^{-1}$ (Vaughan et al., 2003). During this time, widespread retreat of glaciers has been observed on the Peninsula and associated islands (Cook et al., 2005). Recent studies have suggested this could also be important in parts of East Antarctica (Miles et al., 2013) and the Ross Ice Shelf (Nicolas et al., 2017).

Sea ice and ice shelves themselves have been shown to have an important influence on glacial retreat in some places, acting as buttresses to glacial ice, reducing the destructive effect of ocean swells (Massom et al., 2018; Miles et al., 2016, 2017). Widespread retreat of glaciers across Wilkes Land, between 2000 and 2012 corresponded with a decrease in sea ice duration by an average of 11.5 sea ice days per year (Miles et al., 2016). Multi-year fast ice (thicker fast ice which persists year round) is also suggested to stabilize and delay calving of the Mertz Glacier Tongue (Massom et al., 2010).

Furthermore, the bathymetry underlying an ice sheet is important, whereby a small retreat on a reverse sloping bed can lead to positive feedback and rapid, irreversible retreat (Robel et al., 2019).

### 2.2.2 Sea ice changes

In addition to stabilising ice streams, Antarctic sea ice can also have a direct influence on climate change, through its links with the global thermohaline circulation (THC) and more locally through albedo changes, as well as modulating air-sea gas exchange and playing a role in driving primary productivity.

The production of sea ice in the Antarctic plays a key role on the THC, through the formation of cool, dense bottom waters. Brine rejection during sea ice formation leads to an increase in salinity, forming dense waters which eventually flow down the continental shelf into the abyssal depths. This forms the Antarctic Bottom Water (AABW), the coldest and densest water found in the deep ocean, making it one of the most important water masses in the globe (Bindoff et al., 2000). Despite comprising just 3.5% the volume of the world's oceans, the AABW's low temperature means it has a disproportionately strong impact on the climate, with both the strength of AABW formation and its equatorward flow being key controls on the THC (Orsi et al., 1999). The THC is the dominant mechanism for ocean heat transport, thus can influence global climate (Rintoul, 2007).

Particularly important in sea ice formation are polynyas, areas of open water surrounded by sea ice, often formed along the coast by strong katabatic winds which flow down the Antarctic ice sheet and blow newly formed sea ice away from the coast (Bindoff et al., 2000). In polynyas, heat from the ocean is insufficient to maintain open water meaning new sea ice is continually formed as soon as the previous ice is mechanically moved offshore. This means that sea ice production, and hence, brine rejection, is significantly greater in polynyas than in the surrounding sea ice zone (Zwally et al., 1985). Furthermore, the open water in polynyas formed by katabatic winds (known as latent heat polynyas) leads to a high heat flux which

cools the warm MCDW flowing towards the shelf which additionally increases the density of the water contributing to bottom water formation (Bindoff et al., 2000).

The AABW has three main sources, found in the Weddell Sea, offshore Adélie Land, and the western Ross Sea, respectively contributing 68%, 24% and 8% of the volume of AABW (Bindoff et al., 2000). Each of these sources is associated with the presence of a large polynya (Arrigo et al., 2015). The MGP, one of the largest polynyas in the East Antarctic (Arrigo and van Dijken, 2003), plays a central role in the production of Adélie Land Bottom Water (ALBW), through brine rejection associated with sea ice formation as well as its high heat flux (Bindoff et al., 2000). Observations of temperature, salinity and chlorofluorocarbon concentrations have confirmed the production and export of ALBW offshore the Adélie Coast, forming a layer up to a few hundred metres thick in some regions (Rintoul and Bullister, 1999).

Thus, changes in sea ice production in these coastal polynyas can have a direct role in controlling the THC and global ocean heat transport, as has already been observed in some places. Using a model simulation, Masuda et al. (2010) linked bottom water warming observed in the North Pacific between 1985 and 1999 to changes in the surface air-sea heat flux offshore Adélie Land. Between 1945 and 1959, sea ice concentrations off the Adélie Coast, as determined from methanesulphonic acid concentrations in the Law Dome ice core, declined, resulting in an increased air-sea heat flux. This in turn led to a warming of the bottom water formed, which the simulations suggest was then transmitted toward the North Pacific via internal topographic Kelvin and Rossby waves.

In addition to their role in the thermohaline circulation, sea ice changes can also directly affect regional temperature through feedbacks associated with albedo changes. This has been

clearly observed in the Arctic where reductions in sea ice cover and thickness have led to temperature amplification in recent decades (Screen and Simmonds, 2010). In the Antarctic, however, the feedback process is slightly more complex due to the presence of snow on the sea ice, and the fact that sea ice melts from the bottom up due to warming oceans (Laine, 2008). Snow has a higher albedo than bare ice, so the highest albedos are often found on snow covered ice. Thus where ice melt is driven by ocean warming it melts from the bottom up, meaning that the snow cover is retained on the ice for longer than it would if it was melting from above. This also means that increased snow, as a result of a warming climate, could lead to an increase in albedo (Laine, 2008).

In contrast to the Arctic, Antarctic sea ice has broadly increased over recent decades (Parkinson and Cavalieri, 2012; Turner et al., 2016) and positive spring-summer albedo trends have been observed in the Antarctic sea ice zone between 1981 and 2000 (Laine, 2008). This has been coupled with strong negative spring-summer temperature trends (cooling) in the Antarctic, and thus a negative correlation between temperature and albedo. In contrast, parts of the Ross Sea have exhibited an opposing trend, with the strongest increase in sea ice temperature of more than 5°C observed over this period, and a negative trend in albedo (Laine, 2008).

Various processes can affect sea ice concentrations, including air and sea surface temperatures, wind, ocean currents, precipitation and tides (Zwally et al., 1985; Turner et al., 2016). In the Arctic, sea ice concentrations have rapidly declined over recent decades as a result of climate change (Serreze and Stroeve, 2015). However, the relationship between sea ice and climate is clearly less straightforward in the Antarctic, where sea ice has predominantly increased, despite a warming ocean and atmosphere (Parkinson and Cavalieri, 2012). Sea ice simulations from the CMIP5 multimodel ensemble simulate a decline in sea ice

over the historical period in direct contrast to observational evidence (Swart and Fyfe, 2013). Various hypotheses have been put forward to try and explain this mismatch, including changes in winds (Holland and Kwok, 2012), snow (Manabe et al., 1992), ocean heat flux (Zhang, 2007) and surface water freshening (Bintanja et al., 2013).

Strong correlations between ice motion and wind trends in the sea ice zone have been observed, suggesting that winds may be the key driver of recent increases in ice extent. Using satellite-tracked ice motion data and 10m winds from the ERA-Interim atmospheric reanalysis, Holland and Kwok (2012) demonstrated that in West Antarctica, this is mainly the result of dynamic processes, i.e. the physical transport of ice from the south. In East Antarctica, however, they showed that the correlation with winds is predominantly due to thermodynamic processes, i.e. atmospheric cooling through advection of cool, polar air masses. In the Ross Sea, an increase in southerly winds and sea ice extent has been shown to be linked to a deepening of the Amundsen Sea Low, but within its natural variability (Turner et al., 2016).

Accelerated basal melting of glacial ice has also been suggested as a potential driver behind recent sea ice increases, as a result of a strong negative feedback. Bintanja et al. (2013) performed sensitivity experiments using a coupled climate model with an enhanced meltwater flux from the Antarctic ice sheet, equivalent to observed changes over the previous decade. They showed that, due to its low density, meltwater accumulates in a cool, fresh surface ocean layer (100m), which reduces vertical mixing with warmer subsurface waters, meaning the surface layer can be cooled more by the atmosphere and freezes more easily, resulting in a simulated sea ice expansion. Further to this, Bintanja et al. (2015) showed that in model simulations of future sea ice trends, while the absence of freshwater forcing projected a strong

decline in sea ice, the addition of freshwater in model simulations reduced this decline in sea ice and even reversed it in the highest freshwater flux scenario.

However, Bintanja et al. (2013, 2015)'s results differed from those from similar model runs by Swart and Fyfe (2013). In a simulation involving a circumpolar distribution of freshwater forcing from glacial ice, the level of sea ice loss compared to the control run (no freshwater) was reduced. However, even the strongest rates of freshwater forcing were unable to reverse the negative trend in sea ice produced in the control. In the latter scenario, sea ice loss was reduced by 64% by 2020, but for the scenario closest to the observed rates of mass loss, sea ice was reduced only by 11% by 2020 compared to the control. While some areas did display a sea ice concentration increase, these were both in the wrong location and significantly smaller than observations (Swart and Fyfe, 2013).

However, Pauling et al. (2016) point out that the freshwater amounts added in model runs from both studies are minor compared to the increase in precipitation minus evaporation (P – E) observed since the pre-industrial, the latter being 5 – 22 times larger than the mass imbalance of ice sheets and ice shelves. In their model simulations, the volume of freshwater they add is 10% on top of the freshwater already added by P – E. This results in a freshening and cooling of the upper layers of the Southern Ocean, but does not result in an expansion over time. In comparison, simulations by Bintanja et al. (2013, 2015) had a significant response in sea ice from a freshwater forcing an order of magnitude lower. Why such different outcomes result from similar model simulations is difficult to understand, but may be due to differences in the models such as the representation of water column stratification (Pauling et al., 2016).

Using a global coupled ocean-atmosphere model, Manabe et al. (1991) show that increased precipitation itself can drive an increase in sea ice concentration under high $CO_2$ conditions. They simulate an increase in $CO_2$ concentrations at a rate of 1% $year^{-1}$ for 100 years, which leads to a marked increase in precipitation rate at high latitudes with only a small increase in evaporation. This excess precipitation results in reduced salinity in the upper ocean layers around Antarctica and reduces mixing of the cold surface water with the warmer subsurface layers. As a result, SSTs are shown to decrease, leading to an increase in sea ice thickness. However, this result may be a slight overestimate due to a known bias in the model towards overestimating precipitation in high latitudes.

It is clear that, while various mechanisms have been put forward to explain the recent increase in sea ice under a warming climate, no one driver can solely explain these trends. This suggests that various different factors may have contributed together, however, a compelling explanation for recent trends remains to be found.

Sea ice and ice edge environments are also hugely important in that they provide a vital habitat for a large proportion of Southern Ocean phytoplankton. The seasonal melting of sea ice produces a fresh, shallow surface layer which enhances vertical stability promoting phytoplankton growth. Consequently, extensive phytoplankton blooms are commonly observed here. Many ice-associated phytoplankton species (e.g. *Fragilariopsis curta*) have been observed both within the sea ice itself and in ice-edge communities, which suggests that these blooms may be seeded by the release of ice algae (Wilson et al., 1986). Thus, the concentration and duration of sea ice cover can have implications for the productivity of the region, which in turn affects both carbon cycling and wider ecosystem dynamics.

### 2.2.3 The oceanic carbon cycle and primary productivity

On millennial timescales, the deep ocean is the largest store of $CO_2$ which is in exchange with the atmosphere (via the surface water), giving it a key role in controlling atmospheric $CO_2$ concentrations. The large glacial-interglacial fluctuations in atmospheric $CO_2$ are hypothesised to have been driven largely by changes in the amount of $CO_2$ released from, or drawn down, into this deep ocean store (Sigman and Boyle, 2000). Antarctica's continental shelves are important ventilation sites due to the production of AABW. As high-salinity waters, formed during sea ice production, sink to form bottom water, waters rich in nutrients and $CO_2$ are upwelled to the surface, increasing surface water $pCO_2$. However, the increased nutrient concentration leads to intense phytoplankton blooms which rapidly reduce $pCO_2$ to low levels through photosynthesis (Arrigo et al., 2008). Unlike the low-latitudes, in the Southern Ocean there is incomplete utilization of upwelled nutrients by photosynthesising algae, meaning some of this $CO_2$ from the deep ocean is 'leaked' into the atmosphere. As a result, any change in the consumption of these nutrients by phytoplankton can play a key role in the air-sea $CO_2$ exchange in this region, through the 'biological pump', since greater nutrient consumption will be associated with enhanced photosynthetic drawdown of $CO_2$ from the surface waters. Where this carbon is eventually exported to the deep sea and buried, it can lead to a lowering of atmospheric $CO_2$ concentrations (Sigman and Boyle, 2000; Köhler and Fischer, 2006).

In the Antarctic, coastal polynyas are hotpots of primary productivity, often drawing down significant amounts of $CO_2$ through photosynthesis during the spring and summer months (Arrigo and van Dijken, 2003). As mentioned above, both sea ice and ice edge environments provide important habitats for phytoplankton (Wilson et al., 1986), thus polynyas are particularly important because of the large area of ice edge habitat. Furthermore, polynyas are

exposed to increasing springtime solar radiation earlier than other polar marine systems under sea ice, further enhancing their biological productivity (Arrigo et al., 2003).

In addition to biological processes, changes in the proportion of deep water being upwelled to the surface and the amount of sea ice covering the surface waters are also important modulators of $CO_2$ exchange (Sigman et al., 2010; Köhler and Fischer, 2006). Supersaturation of the surface waters have been observed in the Ross Sea polynya during the winter months, with pCO2 up to 425 μatm measured in November (almost 60 μatm higher than atmospheric CO2) due to upwelling onto the shelf and convective mixing (Sweeney, 2003). The Southern Annular Mode (SAM), which is the principal mode of atmospheric variability in the Southern Hemisphere, has a strong control on upwelling, through influencing surface pressure, geopotential height, surface temperature and zonal wind. The SAM is defined as the difference in mean sea level pressure between 40° and 65°S (Marshall, 2003) and has been shown to drive large scale variability of the Southern Ocean (Hall and Visbeck, 2002). A trend towards a more 'positive' SAM has been reported in recent decades, driving an intensification and southerly shift of the westerlies around Antarctica (Marshall, 2003). Between 1981 and 2004, Le Quéré et al. (2007) found that variability in the Southern Ocean $CO_2$ flux correlated with the SAM, with an increase in $CO_2$ outgassing during positive SAM phases, suggesting that wind-driven upwelling and ventilation of C-rich subsurface waters dominates the variability in $CO_2$ flux. Over this time, an overall weakening of the $CO_2$ sink was estimated in response to the increase in winds.

Sea ice itself also has a direct effect on air-sea $CO_2$ fluxes, not only through acting as a barrier to gas exchange, but also through production of high salinity waters which transfer C into the deep ocean (Shadwick et al., 2014). HSSW is formed on the shelf through the rejection of brine during sea ice formation in the winter months. At the beginning of the sea ice formation

period, the surface waters have been modified by the intense phytoplankton blooms in the summer, and thus are depleted in dissolved inorganic carbon (DIC) and enhanced in particulate organic matter. These waters are exported from the shelf predominantly between June and December. Shadwick et al. (2014) calculated that 3 – 6 Tg of anthropogenic C is exported per year from the MGP via dense shelf water outflows, and suggest that this is an effective mechanism to transfer anthropogenic C into the deep ocean. Changes in the balance between biological processes (i.e. photosynthetic drawdown of $CO_2$) and physical processes (i.e. upwelling and sea ice production) will determine the magnitude and direction of air-sea $CO_2$ fluxes in the Southern Ocean.

In the last few decades, the global oceans are estimated to have taken up 25% of anthropogenic $CO_2$ emissions (Le Quéré et al., 2007). The Southern Ocean is thought to be one of the largest oceanic sinks, although estimates as to the magnitude of this sink vary greatly (Lenton et al., 2013). Furthermore, there is uncertainty over whether the Antarctic zone (south of 58°) is currently acting as a sink or a source for anthropogenic carbon emissions. For the entire Southern Ocean, different approaches to estimating recent sea-air $CO_2$ fluxes vary between -0.27 and -0.43 Pg C $yr^{-1}$, all indicating that this region as a whole acts as a carbon sink. For the Antarctic zone, however, all approaches suggest a much smaller flux but disagree as to whether it is a small $CO_2$ sink or a small net flux to the atmosphere (Lenton et al., 2013).

However, the role of coastal regions, particularly polynyas, where biological drawdown of $CO_2$ is high, may be severely underrepresented in these studies, and it is possible this area may be a greater sink than currently suggested. Coupled physical/ocean biogeochemical model simulations in the Ross Sea polynya do suggest that this more southerly region is a strong sink for anthropogenic $CO_2$, due to high biological productivity, intense winds, high

ventilation rates, and extensive winter sea ice cover (Arrigo et al., 2008). Various studies in this region have confirmed the intense biological drawdown of $CO_2$, with summer surface water $pCO_2$ as low as 100 ppm during a phytoplankton bloom (Tortell et al., 2011). Similar observations of summer surface water undersaturation have been made in the MGP (Shadwick et al., 2014) and Amundsen Sea polynya (Mu et al., 2014), as a result of strong biological drawdown. These data suggest high productivity coastal regions do have the potential to act as a strong sink for anthropogenic $CO_2$, so understanding how this may change could be of vital importance for future atmospheric $CO_2$ projections.

Although high productivity rates have been measured within coastal polynyas, *annual* primary productivity in open waters offshore has been measured as 100 g C $m^2$ $yr^{-1}$ – greater than all except the seven largest polynyas in the Southern Ocean (Arrigo and van Dijken, 2003). Overall, Arrigo et al. (1998) found the marginal ice zone (associated with the retreating ice edge) and continental shelf to contribute 11.3% of total primary productivity below 50°S, the rest occurring in the pelagic zone (the latter comprising a larger area). The higher annual productivity rate offshore is due to the fact that it remains ice free, meaning primary productivity takes place year round. However, peak production in January averaged across 37 polynyas was found to be 3 times higher than the average offshore (Arrigo and van Dijken, 2003).

Thus, although annual productivity rates may be, on average, lower than offshore, polynyas provide highly concentrated sources of primary productivity at the coast during the spring and summer months. As well as being important sites for carbon sequestration, this also makes them incredibly important ecosystems supporting high densities of higher trophic level organisms (Arrigo et al., 2015). Distributions of krill and their predators, baleen whales and seabirds, are directly related to the distribution of primary productivity (Nicol et al., 2000).

Thus, understanding how primary productivity in these environments might change in future has important implications for both atmospheric $CO_2$ and marine ecosystems. It is therefore important to determine the key drivers of phytoplankton in the Southern Ocean. One such factor which has been suggested to control productivity levels in this region is Fe concentration (Boyd et al., 2000; Blain et al., 2007; Arrigo et al., 2003). While macronutrients such as nitrate and phosphate are generally abundant in Antarctic waters, trace metals such as Fe are often found to be limited, resulting in incomplete utilization of upwelled nutrients (Martin et al., 1990). Fe is integral for phytoplankton, playing a key part in photosynthesis (Alderkamp et al., 2012). An increase in dust deposition (a key source of Fe) during glacial periods, has been observed in marine sediments and ice cores, particularly in high latitudes, when atmospheric $CO_2$ levels were significantly reduced (Mahowald et al., 1999). The resultant increase in Fe supplied to the oceans has been hypothesised to have driven an increase in primary productivity, by allowing a greater use of upwelled nutrients, resulting in enhanced drawdown of atmospheric $CO_2$ (Mahowald et al., 1999; Martin et al., 1990, Martínez-Garcia et al., 2011). Indeed, some Fe fertilization experiments in Southern Ocean have shown a rapid response of phytoplankton, particularly diatoms, with large blooms and significant drawdown of $pCO_2$ observed in the subsequent days after Fe release (Boyd et al., 2000).

In a study of 46 Antarctic coastal polynyas, Arrigo et al. (2015) found that six features were able to explain 78% and 82% of variability in Chl *a* and net primary productivity (NPP). Observed correlations with three of these features, namely open water area, continental shelf width and basal melt rate, can all be linked to their effect on Fe concentrations (Arrigo et al., 2015). Melting of both ice shelves and sea ice can release dissolved Fe into the surface waters (Sedwick and DiTullio, 1997; Death et al., 2014). Basal melt rate was found to be the most

important factor controlling phytoplankton production, likely due to phytoplankton responding directly to the amount of Fe released. Larger polynyas are likely to hold a greater area of sea ice melt, and thus greater open water area will result in more Fe released in this way (Arrigo et al., 2015). Similarly, enhanced primary productivity has been observed within a few kilometres of icebergs in the Southern Ocean due to the release of iron and other nutrients (Duprat et al., 2016). The correlation with continental shelf width is likely to be due to the increase in sediment derived Fe mixed into surface water. Continental shelf waters are generally enriched in dissolved Fe due to their greater proximity to Fe rich sediments (Arrigo et al., 2015), therefore a greater shelf width will result in more Fe and thus, primary productivity. It is clear that the abundance of Fe is an important driver of primary productivity, particularly diatoms, with various features controlling the amount of Fe available for phytoplankton.

Arrigo et al. (2015) also found large variations in both open water duration and photosynthetically usable radiation across polynyas, but these had only weak correlations with primary productivity. In contrast, SST was found to be strongly correlated with NPP and Chl *a*, despite only small SST differences between polynyas. Metabolic activity of microalgae has been shown to be affected by temperature, doubling for every 10°C increase (Arrigo, 2007). Since only small temperature differences were observed, this would not be able to directly explain the level of variation in NPP. However, the effect of mixed layer depths (MLD), which controls light levels in the upper water column and directly affects phytoplankton growth rates, was not able to be assessed. Arrigo et al. (2015) suggest that the strong correlation between SST and both Chl *a* and NPP may instead be explained by the relationship between MLD and SST. Shallow MLDs result in higher SSTs, due to the

concentration of surface heating in a thinner surface layer, but also allow greater light availability which will enhance primary productivity.

Arrigo (2007) also found that cloud cover had a very strong relationship with primary productivity in the Ross Sea Polynya. However, cloud cover is negatively correlated with polynya size, which may be due to the influence open water has on cloud cover. Thus, the relationship between primary productivity and cloud cover cannot be separated from the effects of open water area and, ultimately, sea ice.

It should be noted that while these different drivers may apply broadly to primary productivity in the Southern Ocean, there may be different drivers for individual polynyas and also for different species. In the MGP, for example, light and nutrient availability are suggested to be the most important drivers (Arrigo, 2007).

Diatoms and *Phaeocystis sp.* are the most abundant phytoplankton in Antarctic waters (Arrigo et al., 1999; Wright et al., 2010). Physiological differences mean they may respond differently to certain environmental drivers. In the Ross Sea, for example, *Phaeocystis antarctica* has been observed to dominate the phytoplankton assemblage in spring when mixed layers are deeper and weakly stratified. Later in the season, when sea ice melt results in intense stratification, diatoms dominate the bloom (Tortell et al., 2011; Arrigo et al., 1999). Physiological studies have shown that *P. antarctica* has photosynthetic properties adapted for efficient use of light in deep mixed layers and underneath sea ice where light levels are highly variable (Mills et al., 2010; Moisan and Mitchell, 1999). Furthermore, various studies have suggested *P. antarctica* may have lower Fe requirements than diatoms (Sedwick et al., 2000; Alderkamp et al., 2012). Since sea ice melt is a key source of Fe, Fe concentrations tend to be higher in shallow MLDs where diatoms thrive, but much lower in deeper MLDs where *P.*

*antarctica* dominates (Sedwick et al., 2000), suggesting Fe may not be as important for *Phaeocystis*. Fe is integral to photosynthesis meaning Fe limitation affects the response of algae to different levels of irradiance (Alderkamp et al., 2012). In culture experiments, Alderkamp et al. (2012) compared the growth rates of *P. antarctica* and the diatom *Fragilariopsis cylindrus* under Fe limitation and varying irradiance levels. They found that *P. antarctica* was able to sustain high growth rates under Fe limitation whereas attempts to grow *Fragilariopsis cylindrus* required additional Fe to avoid eventual death of the culture. Furthermore, Fe limitation was shown to increase the photophysiological differences between the two taxa. They suggest that this increases photoprotection in *F. cylindrus* meaning it will outcompete *P. antarctica* in shallow MLDs with high irradiance, while *P. antarctica* was found to efficiently use a wider range of light levels for C fixation under both Fe-replete and Fe-limited conditions.

*P. antarctica* is also found to be better adapted in low $CO_2$ conditions. During bloom conditions, surface water pH increases and $CO_2$ can become low enough to limit growth. However, *Phaeocystis sp*. has the ability to convert $HCO_3^-$ into $CO_2$ which is beneficial when dissolved $CO_2$ concentrations become very low (Schoemann et al., 2005). *Phaeocystis* dominance under low $CO_2$ conditions was observed in the equatorial Pacific, with diatoms decreasing by ~50% under low compared to high $CO_2$ conditions while *Phaeocystis* increased by ~60% (Tortell et al., 2002). Furthermore, the fact that *Phaeocystis* often blooms in colonies, as well as surviving as free-living cells, is also thought to be part of their success. Their colony matrix can act as a nutrient and energy reservoir making them more competitive when resources are limited, and it may also help to deter grazers (Schoemann et al., 2005).

Diatoms and *P. antarctica* have also been found to have different rates of $CO_2$ drawdown. Arrigo et al. (1999) found that ratios of C:$PO_4$ were much higher in *P. antarctica* suggesting that *P. antarctica* take up ~56% more $CO_2$ than diatoms. Thus, understanding how phytoplankton community structure responds to different environmental conditions, as well as overall phytoplankton abundances, is important for predicting how $CO_2$ drawdown could change in future. Arrigo et al. (1999) suggest that enhanced stratification (e.g. from greater ice melt) may result in a shift to more diatoms which could reduce $CO_2$ drawdown by ~36%.

### 2.3 Antarctic Holocene climate change

Changes in continental scale Holocene climate and atmospheric conditions in the Antarctic are relatively well constrained by ice core records (Masson-Delmotte et al., 2011; Steig et al., 2000; Jouzel et al., 2007; Petit et al., 1999). Masson et al. (2000) looked at water isotopes (oxygen and hydrogen) from 11 different sites across Antarctica, to reconstruct air temperature and elevation changes through the Holocene. All ice cores with long-term datasets record an early Holocene temperature optimum (11.5 – 9 ka) across Antarctica, indicating warming of around 0.2 to 2.5°C. This is followed by a cooling trend, with most sites recording a minimum at about 8 ka BP. Mid-Holocene warm periods are then recorded at ~8 – 6 ka in the Ross Sea sector, ~6 – 3 ka in most inland East Antarctic regions, and centred on ~3 ka at other inland sites, including the Byrd ice core in the WAIS, Dome C in the EAIS and Dominion Range in the Transantarctic Mountains. Masson-Delmotte et al. (2011) use principal components analysis to identify the common signals in 5 of these ice cores (Vostok, Dome C, Dronning Maud Land,Dome Fuji and TALDICE). The 1$^{st}$ principal component picks out the broad trends described above, showing an early Holocene optimum 11.5 to 10 ka BP, followed by a minimum around 8 ka and a secondary maximum at 4 ka. The 2$^{nd}$ principal component indicates a temperature optimum around 12 ka followed by a long-term

cooling trend until 2 ka. The ice core water isotope records appear to record larger fluctuations at coastal sites compared to those further in land, possibly due to ice shelf/sea ice feedbacks. However, it is important to note that these records will also be reflecting temperature change associated with elevation fluctuations, rather than climate change alone (Masson et al., 2000).

Coeval ocean and cryosphere changes during the Holocene, and their relationship with climate, are less well understood. Reconstruction of the timing and pattern of glacial retreat since the Holocene have been based on geomorphological and geological data, including cosmogenic dating (Mackintosh et al., 2011; Anderson et al., 2014; Hein et al., 2016). However, these data are sparse and limited in resolution. For example, the timing of WAIS deglaciation since the Last Glacial Maximum, including break-up of the Ross Ice Shelf (RIS) (McKay et al., 2008; Anderson et al., 2014), the largest ice shelf in the world, has been difficult to constrain, and, consequently, there are differing views as to whether Antarctic ice contributed significantly to late Holocene sea-level changes or not (Lambeck and Purcell, 2005; Bradley et al., 2016).

### 2.4 The need for sedimentary archives

Palaeo-records from marine sediment cores recovered from Antarctic coastal zones provide an opportunity to put recent changes into a longer-term perspective. These can complement ice-core records by providing additional information on environmental conditions, such as changes in meltwater input, sea ice, water masses and primary productivity, not captured by the ice-cores.

Terrestrial archives such as tree rings, speleothems and ice cores often continue up to the present day and thus environmental proxies can be ‘ground-truthed’ against instrumental data.

However, this is rarely the case in marine sediments due to the slow accumulation rate (often less than 1 cm 1000 $yr^{-1}$ (BOSCORF, 2019) meaning there is often very little overlap with the instrumental era. Furthermore, deep sea drilling techniques (e.g. the Advanced Piston Corer, or Extended Core Barrel systems deployed by the Integrated Ocean Drilling Programme (IODP, n.d.) are not always able to recover the sediment-water interface, further preventing analysis of modern sediment. Thus, environmental proxies from marine sediments can be difficult to ground-truth leaving uncertainties as to their reliability and accuracy in reconstructing past conditions.

### 2.5 Molecular and compound-specific isotope proxies

A multitude of proxies have been developed over the years to reconstruct changes in past environmental conditions from marine sediments. These include microfossils, trace elements, stable and radiogenic isotopes, sedimentary properties and lipid biomarkers (Bradley, 2015).

Lipid biomarkers are the main focus of this thesis. These are organic molecules produced by a wide range of organisms, preserved within marine sediments or other geological archives. Changes in the abundance, structure and isotopic composition of biomarkers can record environmental conditions at the time of their formation. Furthermore, they can be preserved for long periods of time even when the rest of a fossil (e.g. a shell or other hard parts) may have degraded (Gaines et al., 2009). Biomarker proxies have been developed for over > 50 years and can be used to reconstruct changes in a wide variety of environmental conditions, such as sea surface temperatures (Brassell et al., 1986, Conte et al., 2006; Schouten et al., 2002), sea ice (Smik et al., 2016; Belt, 2018), salinity (Sachse et al., 2012), $pCO_2$ (Freeman and Hayes, 1992), vegetation changes (Huang et al., 2007) and more.

The main biomarkers employed in this research are fatty acids and glycerol diakyl glycerol tetraethers (GDGTs), with a particular focus on compound-specific isotope analysis of fatty acids. The use of these biomarker proxies is discussed below. Other proxy data used in this thesis, but generated elsewhere, include highly branched isoprenoid alkene (HBI) biomarkers, diatom relative abundances and grain size distributions.

### 2.5.1 Compound-specific carbon isotopes

Carbon isotope measurements on marine biomarkers have traditionally focussed on attempts to reconstruct palaeo-$CO_2$ in ancient greenhouse worlds. Marine photosynthetic carbon fractionation, known as $\varepsilon_p$, has been shown to correlate with $CO_{2(aq)}$ concentration in seawater, and was therefore recognised for its potential to provide an indication of atmospheric $CO_2$ in the past (Freeman and Hayes, 1992). A palaeo-$CO_2$ proxy was developed using compound-specific $\delta^{13}C$ of the di-unsaturated $C_{37}$ alkenone, a biomarker produced by haptophyte algae, and the $\delta^{13}C$ of planktic forams (Pagani, 2014). This proxy is based on the premise that the surface waters of the ocean (where the phytoplankton reside) are broadly in equilibrium with the atmosphere, at least on the relatively long timescales (millions of years) on which this proxy is generally applied. Over long time scales, other effects on surface water $CO_2$, such as upwelling or productivity changes, are assumed to be relatively minor, meaning shifts in atmospheric $CO_2$ will be the dominant driver of surface water $CO_2$ (Pagani, 2014).

However, on shorter timescales (i.e. sub-millennial) when atmospheric $CO_2$ changes are relatively subtle, this surface water signal may be overridden by other factors. In particular, hotspots of primary productivity in the ocean can result in significant levels of $CO_2$ drawdown, leaving the surface waters significantly undersaturated with respect to $CO_2$

(Tortell et al., 2011). In this instance, changes in primary productivity over time may become the dominant driver of algal biomarker $\delta^{13}C$.

One such hotspot is the Ross Sea, where some of the highest rates of productivity in the Antarctic coastal region have been observed (Arrigo and van Dijken, 2003). As a result, large seasonal variations exist in surface water $CO_2$, with one study measuring a range of 425 μatm to 150 μatm between winter and summer (Sweeney, 2003), indicating significant undersaturation of $CO_2$ with respect to the atmosphere during summer. Very low $pCO_2$ values correspond with the growing season for phytoplankton (Tortell et al., 2011). Similarly, large spatial variations of $pCO_2$ exist in the surface water corresponding broadly to phytoplankton abundances (Tortell et al., 2011). Villinski et al. (2008) found that the spatial variation in $pCO_2$ in the Ross Sea was associated with a variation in the $\delta^{13}C$ of sedimentary organic carbon and sterol biomarkers, and that this could not be explained by the effects of different species, heterotrophy or growth rates. They concluded that the isotopic zonation is most likely due to a change in isotopic fractionation associated with the photosynthetic drawdown of $CO_2$. Their results demonstrate that the spatial variation in surface water $CO_2$ is recorded in sedimentary organic matter and sterol biomarkers, which paves the way for using algal biomarkers from older sediments to reconstruct such changes in primary productivity and $CO_2$ drawdown over time.

This provides the basis for the application of compound-specific carbon isotopes of fatty acids in sediments offshore Adélie Land in this thesis. This is an area of high primary productivity proximal to two coastal polynyas (Arrigo and van Dijken, 2003) (Chapter 2.1) and, although less well studied than the Ross Sea polynya, has also been observed to have a seasonal variation in surface water $CO_2$ associated with primary productivity (Shadwick et al., 2014). Thus, the same processes of $CO_2$ drawdown are assumed to be occurring here.

As well as being used for reconstructing changes in the carbon cycle, the $\delta^{13}C$ of biomarkers – in the case of this thesis, fatty acids – can also help determine their source. For example, (Budge et al., 2008) looked at $\delta^{13}C$ values of fatty acids from fifteen different organisms in the Arctic, ranging from ice algae and phytoplankton at the bottom of the food web, up to bowhead whales and ringed seals at the top. Phytoplankton were found to have the most negative $\delta^{13}C$ values of all species measured (mean of -30.7‰ for the C16:4n-1 fatty acid), while ice algae had some of the highest values (mean of -24.0‰). Brine channels within sea ice are known to have much lower $CO_2$ concentrations than the surface waters, meaning fractionation of algae living within these channels is reduced compared to open water species, explaining the elevated $\delta^{13}C$ values in ice algae (Gibson et al., 1999).

Although few studies have looked specifically at the $\delta^{13}C$ of fatty acids from different organisms in Antarctic food webs, one study of suspended particulate organic matter $\delta^{13}C$ near Prydz Bay found that higher $\delta^{13}C$ values were associated with diatoms and large heterotrophic dinoflagellates, whereas lower $\delta^{13}C$ values were characterized by *Phaeocystis sp.* and autotrophic dinoflagellates (Kopczynska et al., 1995).

This knowledge of the $\delta^{13}C$ of different organisms in polar food webs will help determine the most likely source of fatty acids from samples used in this thesis, which is essential for understanding the signals they may record.

### 2.5.2 Compound-specific hydrogen isotopes

Hydrogen isotopes of organic matter in sediments have commonly been used as palaeohydrological proxies. This is based on the knowledge that primary producers can often record the isotopic composition of water used during photosynthesis (Sachse et al., 2012). In particular, focus has been made on hydrogen isotope measurements of individual compounds,

since bulk organic material contains complex mixtures of compounds from different sources, which may have highly varying isotope values due to different biosynthetic pathways. The $\delta^2H$ of lipid biomarkers from both marine and terrestrial organisms are generally highly correlated with the water source used, but with an offset due to biosynthetic processes (Sachse et al., 2012). As a result, $\delta^2H$ measurements of preserved sedimentary lipids have the potential to yield a record of changes in the isotopic composition of the water source over time, with implications for understanding the associated hydrological changes which drove them.

The $\delta^2H$ of precipitation is known to vary over space and time, controlled by 'Rayleigh' fractionation processes which occur during evaporation and condensation. During evaporation, the lighter isotope $^1H$ evaporates faster than $^2H$, meaning that the $\delta^2H$ value of the water vapour becomes lower (depleted in $^2H$) while the residual water mass $\delta^2H$ is higher (enriched in $^2H$). When the water vapour condenses, $^2H$ is more easily removed in the form of precipitation, meaning that precipitation is enriched in $^2H$ relative to the water vapour, thus having a higher $\delta^2H$ value (Dansgaard, 1964).

As a result, the $\delta^2H$ value of precipitation in space and time can be seen as a function of these processes, with predictable patterns in response to various environmental factors, such as the amount of precipitation falling ("amount effect") and the distance over a continent an air mass has travelled ("continental effect"). Of particular importance in this thesis is the "temperature effect", whereby the rainout process and isotopic fractionation are strongly correlated with temperature. At colder temperatures, the fractionation between the condensed water and water vapour is greater, meaning precipitation can become highly depleted in $^2H$ over the Antarctic continent, with very negative $\delta^2H$ values (Sachse et al., 2012).

The water isotopes locked up within Antarctica's ice sheet have some of the most negative $\delta^2H$ values known. The EPICA Dome C ice core in the East Antarctic, for example, records $\delta^2H$ values varying between -412 and -377‰ (Jouzel et al., 2007). Although $\delta^2H$ measurements of ocean water are less abundant than for $\delta^{18}O$, available $\delta^2H$ data ranges from ca. -60‰ in the Baltic Sea (Frohlich et al., 1988), up to ca. 10.4‰ in the eastern Mediterranean Sea (Gat et al., 1996). Even with the most negative measurements of ocean water $\delta^2H$, this provides two end members (glacial ice and ocean water) with highly contrasting $\delta^2H$ values. Thus, inputs of glacial meltwater from Antarctic ice into the coastal waters has the potential to drive large changes in surface water $\delta^2H$. Since the $\delta^2H$ of lipid biomarkers of marine phytoplankton are known to correlate with the hydrogen isotope value of the water source used, such changes in glacial meltwater input are hypothesised to be recorded within sedimentary lipids of marine phytoplankton residing within the surface waters. In this case, greater glacial meltwater inputs will lead to more negative $\delta^2H$ of algal biomarkers such as fatty acids.

It must be noted that lipid $\delta^2H$ can also be affected by changes in the fractionation occurring between source water and the lipid ($\varepsilon_{l/w}$) (i.e. vital effects), in which various environmental factors play a part (Sachse et al., 2012). This will be affected by salinity and temperature, whereby $\delta^2H$ increases by 1-4‰ per increase in practical salinity unit (Schouten et al., 2006) and decreases by 2-4‰ per degree C increase (Zhang et al., 2009). These must be taken into account when interpreting lipid $\delta^2H$ values, however, these effects are likely to be minor compared to any substantial changes in glacial meltwater input.

### 2.5.3 Glycerol dialkyl glycerol tetraethers

GDGTs are membrane lipids biosynthesised by thermophilic archaea, which contain up to eight cyclopentane rings (Schouten et al., 2002). Culture and observational studies have demonstrated a relationship between the temperature of the water and the distribution of GDGT rings (Gliozzi et al., 1983; Schouten et al., 2002), suggesting that the biosynthesis of cyclopentane rings in these archaeal lipids are a mechanism for temperature adaptation of the membrane (Schouten et al., 2002).

Schouten et al. (2002) analysed GDGTs derived from marine crenarchaeota in core top sediments from 14 locations distributed across the globe. They found a significant positive relationship ($R^2 = 0.92$, n = 43) between SST and the $TEX_{86}$ index (TetraEther indeX of tetraethers consisting of 86 carbon atoms) which they introduced as a new SST proxy. This is defined as:

$$TEX_{86} = \frac{[GDGT-2] + [GDGT-3] + Cren'}{[GDGT-1] + [GDGT-2] + [GDGT-3] + Cren'}$$

whereby GDGT-1, GDGT-2 and GDGT-3 are GDGTs with one, two and three cyclopentane rings, respectively, and Cren' is the isomer of crenarchaeol (Fig. 2.3).

The measured relationship with SST has a linear equation of:

$$TEX_{86} = 0.015T + 0.92$$

whereby T is the annual mean SST in °C. This provides a means of using sedimentary GDGTs for reconstructing SST.

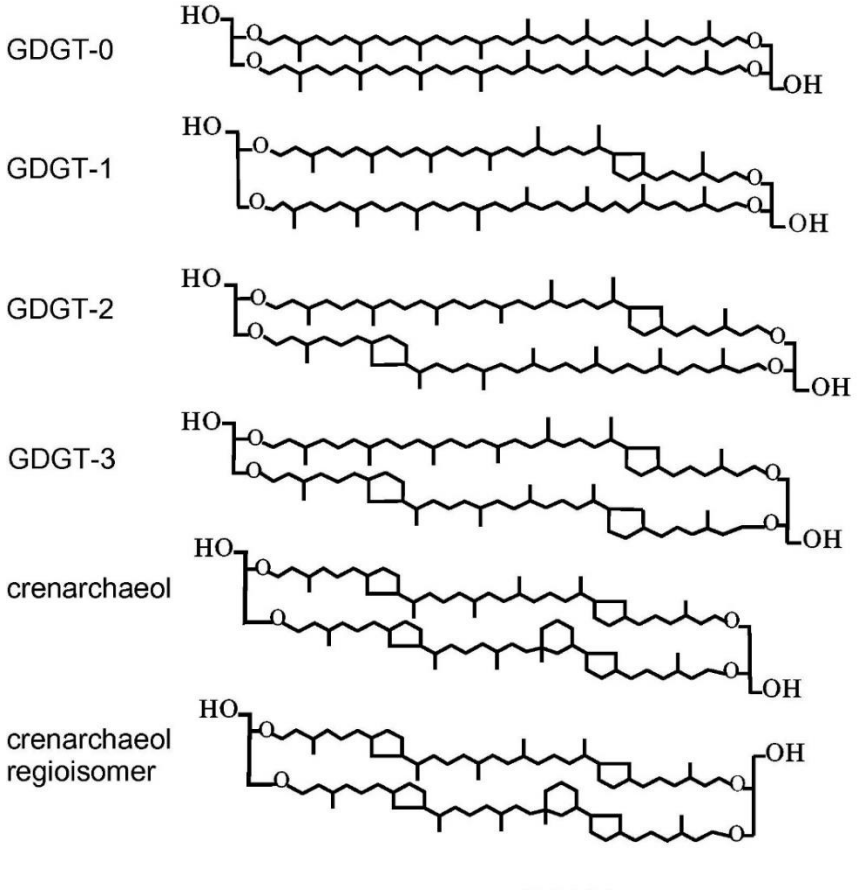



**Figure 2.3** Structures of marine GDGTs referred to in the text. From Yang et al. (2018)

The $TEX_{86}$ proxy has been widely used for reconstructing past SSTs from sediments throughout the Cenozoic and even as far back as the Jurassic (Jenkyns et al., 2012). One key advantage GDGTs have for reconstructing SSTs is their ubiquitous nature throughout the oceans (Schouten et al., 2013), whereas the alkenone based SST proxy, $U^{K}_{37}$', cannot be applied at high southern latitudes due to a lack of alkenones south of 62°S (Sikes et al., 1997).

Following on from Schouten et al. (2002), Kim et al. (2008) undertook a more extensive core-top calibration of $TEX_{86}$ using 287 globally distributed samples. However, they found a large amount of scatter in the calibration below 5°C which they suggest is due to a non-linear response of $TEX_{86}$ at lower temperatures. Many samples from the polar regions were found to

give $TEX_{86}$ values higher than expected and there was no significant relationship between $TEX_{86}$ and temperature below 5°C. As a result, they argue that $TEX_{86}$ is not suitable for reconstructing SSTs at low temperatures.

In response, Kim et al. (2010) analysed GDGT distributions from additional core-top samples from polar and sub-polar regions. Their results continued to show large scatter at temperature below 5°C. Using their new core-top dataset (excluding data from the Red Sea), they define a new core-top calibration (called $TEX_{86}^{L}$) which correlates more strongly with SST ($R^2$=0.86, n = 396). Unlike $TEX_{86}$, this does not include the isomer of crenarchaeol and is defined as follows:

$$TEX_{86}^{L} = log \frac{[GDGT-2]}{[GDGT-1]+[GDGT-2]+[GDGT-3]}$$

The standard error in SST reconstruction using this calibration is 4°C. Kim et al. (2010) suggest this index is more appropriate for low temperature regions than $TEX_{86}$.

However, as use of these proxies has increased, deviations between GDGT-derived temperatures and other SST proxies in many palaeo reconstructions have become apparent (Huguet et al., 2006; Zhang et al., 2016). Various studies have suggested that factors other than temperature may influence GDGT distributions, including ammonia oxidation rate (Hurley et al., 2016), pH (Boyd et al., 2011), salinity (Dawson et al., 2012), terrestrial input (Hopmans et al., 2004), and contributions from other archaeal communities (Lincoln et al., 2014).

In attempt to identify when non-thermal influences maybe be affecting GDGTs, Zhang et al. (2016) introduced the Ring Index (RI), the weighted average of cyclopentane rings. This is defined as:

$$RI = 0 * [GDGT - 0] + 1 * [GDGT - 1] + 2 * [GDGT - 2] + 3 * [GDGT - 3] + 4 * [Cren] + 4 * [Cren']$$

For the global core-top dataset, the ring index correlates strongly with $TEX_{86}$. Any deviation from this relationship is suggested to indicate the influence of factors other than temperature. This deviation is calculated using ΔRI – the difference between the RI (as defined above) and the calculated RI from the global core top RI-$TEX_{86}$ relationship. Zhang et al. (2016) suggest that ΔRI values > 0.3 indicate non-thermal factors are likely to be impacting GDGT abundances and should be removed from SST calculations.

Similarly, the Methane Index (MI) and the branched and isoprenoid tetraether (BIT) index were also develop in attempt to identify influences of methanotrophic Euryarchaeota and terrestrial inputs, respectively (Zhang et al., 2011; Hopmans et al., 2004).

The MI is used to identify influences of methanotrophic Euryarchaeota, which is assumed to be represented by GDGT-1, -2 and -3, in contrast to thaumarchaeota, which is represented by crenarchaeota (Cren) and its regioisomer (Cren') (Zhang et al., 2011). It is defined as:

$$MI = \frac{[GDGT - 1] + [GDGT - 2] + [GDGT - 3]}{[GDGT - 1] + [GDGT - 2] + [GDGT - 3] + Cren + Cren'}$$

MI values > 0.3 are suggested to indicate an influence of methanotrophic Euryarchaeota (Zhang et al., 2011).

The BIT index is used to identify inputs of terrestrially derived GDGTs, through comparison of crenarchaeol abundances, produced in the water column, with abundances of branched GDGTs which are produced within soils (Hopmans et al., 2004).

The BIT index is defined as:

$$BIT = \frac{brGDGT3a + brGDGT2a + brGDGT1a}{brGDGT3a + brGDGT2a + brGDGT1a + Cren}$$

Where the BIT index is >0.4, the input of GDGTs from soils is regarded to be substantial, leading to $TEX_{86}$-derived SST deviations of >2°C (Weijers et al., 2006).

The $TEX_{86}$ proxy has been applied to Holocene sediments in the Antarctic in a handful of studies. Shevenell et al. (2011) generated a Holocene record from west of the Antarctic Peninsula, using a modified $TEX_{86}$ calibration that integrates regional core-top data with a global data set. Their reconstructed SST record gives a very high SST range of -2.9 to 10.5°C. Whilst the authors recognise that absolute temperature values may not be accurate (especially at the lower end where reconstructed temperatures are below freezing), they argue that the overall trends are robust and follow local spring insolation. Etourneau et al. (2013) similarly generated a Holocene SST record from a nearby site west of the Antarctic Peninsula, using $TEX_{86}^{L}$. Their reconstructions showed a much smaller temperature range than that of Shevenell et al. (2011) which they suggest is down to the different indices used ($TEX_{86}$ vs $TEX_{86}^{L}$) and the fact that they calibrated their $TEX_{86}^{L}$ index to 0 – 200m depth rather than sea surface temperatures.

From the East Antarctic, Kim et al. (2012) also generated a Holocene $TEX_{86}^{L}$ record from core MD03-2601 offshore Adélie Land, calibrated to 0 – 200 m depth. Their Holocene record showed a pronounced peak in temperatures ca. 6 ka BP, however, the low resolution nature of this record means that this warming is limited to just two data points.

Due to the focus on Antarctic sediments, where SSTs are low, the $TEX_{86}^{L}$ calibration is applied to GDGT distributions presented in this thesis. However, as a result of the complexities of GDGT based proxies discussed above, close examination of GDGT

distributions relative to global core-top data will be made, with careful consideration as to the most likely driver(s) of $TEX_{86}^{L}$ changes.

**Summary**

This chapter has summarised the environmental setting for this thesis, a very dynamic environment, with complex interactions between the atmosphere, ocean, ice and the carbon cycle. Based on a review of the literature, the current understanding of these relationships, including observations of recent trends and our knowledge of Holocene climate and environmental changes have been summarised. It is clear from this review that many uncertainties exist, which has implications for our understanding of future changes.

Palaeoenvironmental proxies from coastal marine sediment cores, have the potential to provide an insight into air-ocean-ice interactions where instrumental records are unavailable. In particular, the use of lipid biomarkers and compound-specific isotopes (carbon and hydrogen) in this type of environment have been reviewed and will be the focus of analysis for this thesis. It is clear that a good understanding of how different proxies work and the type of environmental information they record is vital if they are to provide a useful insight into past environmental changes.

## Chapter 3

# ORGANIC GEOCHEMISTRY METHODS

## 3.1 Introduction

The methods described in this chapter are specific to the data presented in Chapters 5, 7 and 8 from sediment core DTGC2011. The methods for data used in the other chapters are described elsewhere.

## 3.2 Glassware

All disposable glassware including pipettes and Gas Chromatography (GC) vials were wrapped in aluminium foil and furnaced at 450°C for 8 hours prior to use. Reusable glassware was cleaned in between use by soaking in a bucket of tap water with Lipsol™ detergent for 12-24 hours. Glassware was scrubbed with a brush before being transferred to a clean bucket of 5% Lipsol™ detergent in tap water where they were left for 24 hours. Water and Lipsol™ in the bucket was changed periodically (once every few months or when the water appeared discoloured) to maintain cleanliness of the water. Glassware was then removed from the bucket and thoroughly rinsed in tap water before being left to dry naturally. Once dry, glassware was wrapped in aluminium foil and furnaced at 450°C for 8 hours.

## 3.3 Solvents and reagents

All solvents used were high-performance liquid chromatography (HPLC) grade to reduce potential contamination, supplied by Fisher Scientific, Loughborough, U.K. The solvents and reagents used are listed in the table below.

**Table 3.1** Solvents and reagents used during this thesis and their abbreviations used.

| Solvent/reagent | Abbreviation used |
|---|---|
| *n*-Hexane* | Hexane |
| Methanol* | MeOH |
| Dichloromethane* | DCM |
| Isopropyl alcohol* | ISO |
| Diethyl ether* | - |
| Acetic acid* | - |
| Boron trifluoride-methanol solution (14% in methanol)† | $BF_3$ |
| Silica 60A, 30-75 µm, Davisil® chromatography grade* | $SiO_2$ gel |
| 3-aminopropyl-functionalized silica gel† | Aminopropyl- $SiO_2$ gel |
| Sodium sulphate* | $Na_2SO_4$ |

* Fisher Scientific, Loughborough, U.K. ** Thermo Scientific †Sigma Aldrich, Germany

### 3.4 Biomarker extraction and separation

Lipid extraction of samples from core DTGC2011 and compound separation was performed at the University of Birmingham in the School of Geography, Earth and Environmental Sciences, unless specified otherwise.

#### 3.4.1 Sediment sample preparation

All sediment samples were freeze dried prior to extraction to remove any moisture. These were then ground into a powder using a glass pestle and mortar, transferred to a clean, pre-weighted 30ml glass test tube and weighed. The pestle and mortar was solvent-rinsed with hexane and DCM prior to and in between samples.

#### 3.4.2 Lipid extractions

Samples were extracted in batches of twelve, including one blank sample (using purified sea sand) every other batch. 20ml of DCM/MeOH (3:1 v/v) was added to each sample and mixed

vigorously using a Fisherbrand™ WhirliMixer™. Samples were then ultrasonicated for 20 minutes and then placed on a heating block at 50°C for 1 hour. Samples were then centrifuged in the test tubes at 1000 rpm for 3 minutes or until the sediment and solvent were cleanly separated. The supernatant was transferred into a BÜCHI™ Polyvap vial using a pipette and another 10 ml of DCM/MeOH (3:1 v/v) was added to each sample. The whole process was repeated using 10ml of solvent three times or until no more colour was visible within the solvent extract.

Once all solvent extract had been collected in the BÜCHI vials, these were transferred into a BÜCHI™ Syncore® Polyvap, where they were heated to 40°C and rotated at 200 rpm. This was attached to a BÜCHI™ V-700 vacuum pump which was set to a pressure of 850 mbar to evaporate DMC and gradually reduced to 200 mbar to evaporate MeOH, until little to no solvent remained in the vial.

Where dried total lipid extracts (TLE) appeared to contain water or sediment, these were filtered through a column using 4 cm of $NaSO_4$ in a Pasteur pipette. The sample was re-dissolved in 0.5 ml of DCM/MeOH (9:1 v/v) and eluted through the column adding 0.5 ml of DCM/MeOH at a time and collected in a glass vial until the solvent coming through became clear.

The TLE was then transferred into a 1.5 ml GC vial using ~0.5 ml of DCM and MeOH and a Pasteur pipette until the GC vial was full. These were then left either to dry naturally over ~24 hours in the fume hood covered in a clean piece of paper towel, or dried under a gentle stream of filtered $N_2$. The sample was then re-dissolved in 100 µl of hexane and 50 µl was transferred into a glass GC vial insert, and again, left to dry.

### 3.4.3 Acid-neutral split of lipid extracts

Column chromatography was used to separate the TLE into acid and neutral fractions. 4 cm of dry aminopropyl-$SiO_2$ gel was packed into a Pasteur pipette plugged with glass wool at the bottom, and conditioned with 3 ml of DCM/ISO (1:1 v/v). The TLE was re-dissolved in 0.5 ml DCM/ISO (1:1 v/v) and loaded onto the column and the total neutral fraction (TNF) eluted into a glass vial using an addition 3.5 ml of DCM/ISO (1:1 v/v) in total. The total acid fraction (TAF) was then eluted into another glass vial using 4 ml of diethyl ether with 4% acetic acid. These were then either left to dry naturally over ~24 hours in the fume hood covered in a clean piece of paper towel, or dried under a gentle stream of filtered $N_2$.

### 3.4.4 Clean up of neutral fractions

Column chromatography was used to separate the TNF into three different fractions. 4 cm of furnaced silica gel was packed into Pasteur pipette plugged with glass wool and conditioned using 3 ml of hexane. The sample was re-dissolved in 0.5 ml hexane and the three fractions (N1-N3) were eluted using solvents, as described in Table 3.2, and collected in clean, labelled glass vials.

**Table 3.2** Details of the different fractions collected during column chromatography of the total neutral fraction.

| Fraction | Solvent | Compounds of interest |
|---|---|---|
| N1 | 4 ml n-hexane | Aliphatic hydrocarbons |
| N2 | 4 ml DCM | Aromatic hydrocarbons, alcohols, aldehydes, ketones and esters |
| N3 | 4 ml DCM/MeOH (95:5 v/v) | Sterols and glycerol dialkyl glycerol tetraethers (GDGTs) |

### 3.4.5 Derivatization and clean-up of acid fractions

The TAF was derivatized by adding 200 µl of $BF_3$ (14 % in MeOH (v/v)) to the sample vial, sealed and placed in a heating cupboard at 70°C for one hour. The sample was then dried

under a gentle stream of $N_2$ and then re-dissolved in 0.5 ml hexane for further clean up by column chromatography. 3 cm of $SiO_2$ gel was packed into a Pasteur pipette and conditioned using 3 ml of hexane. The dissolved TAF was loaded onto the column and eluted with 4 ml of hexane in total and collected in a clean, labelled glass vial. Fatty acid methyl esters (FAMEs) were then eluted using 4 ml of DCM and collected in a clean, labelled glass vial. These samples were then either left to dry naturally over ~24 hours in the fume hood covered in a clean piece of paper towel, or dried under a gentle stream of filtered $N_2$. The hexane fraction was not required for analysis but was maintained until FAMEs had been checked by GC.

Once dry, FAME samples were transferred into GC vials using 0.5 ml of DCM at a time until the GC vial was nearly full. These were again either left to dry naturally over ~24 hours in the fume hood covered in a clean piece of paper towel, or dried under a gentle stream of filtered $N_2$. The sample was then re-dissolved in 100 µl of hexane and 50 µl was transferred into a glass GC vial insert, and again, left to dry.

### 3.5 Quantification of samples by gas chromatography

Concentrations of fatty acids (FA) within samples were determined using an Agilent 7890B GC-flame ionization detector (FID) at the University of Birmingham. Samples were injected in splitless mode using an Agilent 7693 autosampler. The front inlet and back detector were held at 330°C. Hydrogen was the carrier gas with a constant flow rate of 2 ml $min^{-1}$. An Rtx™-200 column (105 m, 250µm internal diameter, 0.25µm film thickness) which has a poly(trifluoropropylmethylsiloxane) stationary phase was used for FA analyses to enable the best separation possible. The oven programme was: 70°C, held for 1 min, increased to 150°C at a rate of 30°C/min, increased to 320°C at a rate of 3°C/min, then held for 10 minutes. Agilent OpenLab software was used to integrate sample peaks.

FA concentrations were quantified by addition of a $C_{19}$ alkane as an internal standard, prepared in-house to the concentration of 10 ng/μl. The peak areas of FAs and the internal standard were used to calculate the concentration of each compound.

### 3.6 Standards

An in-house standard was prepared in the lab and was run in between every 5-10 samples to check performance of the GC-FID and GC-MS instruments. This contained 16 organic compounds listed below, each with the concentration of 10 ng/μl.

**Table 3.3** Compounds included in the in-house standard and their abbreviations used.

| Compound | Abbreviation |
|---|---|
| Hexadecane | $C_{16}$ |
| Octadecane | $C_{18}$ |
| Nonadecane | $C_{19}$ |
| Eicosane | $C_{20}$ |
| Tricosane | $C_{23}$ |
| Pentacosane | $C_{25}$ |
| Hexacosane | $C_{26}$ |
| Octacosane | $C_{28}$ |
| 5α-cholestane | Chol |
| Octadecanone | $C_{18}$-O |
| Triacontane | $C_{30}$ |
| Dotriacontane | $C_{32}$ |
| Heptatriacontane | $C_{37}$ |
| Behenic acid methyl ester | BAME |
| Pristane | Pr |
| Squalane | Sq |

10 mg of each compound was weighed out individually and dissolved in 10 ml hexane to create a stock solution, 10μl of which was added to 1ml of hexane for each compound, to create a standard containing all 16 compounds each at a concentration of 10 ng/μl.

Where standard peaks on the GC-FID or GC-MS were showing contamination or peak heights becoming inconsistent (in particular, the height of the last peak falling relative to the rest), the front of the column was trimmed using a ceramic blade and the inlet liner and septum was changed.

### 3.7 Identification of samples by mass spectrometry

A selection of FA samples were analysed by an Agilent 7890B GC coupled to an Agilent 5977A MSD to identify compounds present within the sample. For the FA samples, a BP5-MS (SGE) column (60m, 320µm internal diameter, 0.25µm film thickness) was used. Helium was used as the carrier gas set at a constant flow rate of 2 ml/min. The MSD was run in scan mode with a scan width of 50 to 800 mass units.

Samples were identified by looking at the m/z of fragments within each compound and compared to a reference library.

### 3.8 Carbon isotope analysis of fatty acids

The $\delta^{13}C$ composition of fatty acids are described in delta notation:

$$\delta^{13}C\ (‰) = (({}^{12}C/{}^{13}C)_{sample} / ({}^{12}C/{}^{13}C)_{standard} - 1) \times 1000$$

whereby the standard is Vienna Pee Dee Belemnite.

FA samples were analysed using an Agilent 7890A GC coupled to an Isoprime GC5 furnace and an Isoprime 100 isotope ratio mass spectrometer (IRMS). The Isoprime GC5 furnace contained a CuO furnace tube kept at 850°C. Helium was used as the carrier gas set at a constant flow of 1.7 ml/min and $CO_2$ was used as the reference gas. The GC had a VF-200ms column (60 m, 250µm internal diameter, 0.25µm film thickness) which also has a poly(trifluoropropylmethylsiloxane) stationary phase. The oven programme was: 70°C, held

for 1 min, increased to 150°C at a rate of 30°C/min, increased to 320°C at a rate of 3°C/min, then held for 5 minutes. Most samples were run using an Agilent 7693 autosampler from dilutions of 10 – 100 μl. Where concentrations were very low, samples were dissolved in <10 μl and were manually injected. Most samples were ran in duplicate except for a few cases where the sample concentration was so low that the entire sample had to be injected in one run.

Machine performance was routinely checked using a FA ester mix (F8; Arndt Schimmelmann, Indiana University) containing eight FA compounds. This was run before the start of analysis and after every five duplicate samples. These compounds and abbreviations are listed in Table 3.4.

**Table 3.4** Fatty acid compounds included in the F8 standard and their abbreviations used.

| Compound name | Abbreviation used |
|---|---|
| Tetradecanoic acid methyl ester | C14-Me |
| Tetradecanoic acid ethyl ester | C14-Et |
| Hexadecanoic acid methyl ester | C16-Me |
| Hexadecanoic acid ethyl ester | C16-Et |
| Octadecanoic acid methyl ester | C18-Me |
| Octadecanoic acid ethyl ester | C18-Et |
| Icosanoic acid methyl ester | C20-Me |
| Icosanoic acid ethyl ester | C20-Et |

Samples were only run where the r-squared value between measured and actual $\delta^{13}C$ values of the eight F8 compounds was greater than 0.99, and when the standard deviation of consecutive standard runs was <0.3. The F8 standard was also used to calibrate samples onto the VDPB scale, using the linear relationship between measured and actual $\delta^{13}C$ values.

A dilution series was run on the GC-IRMS to determine the sensitivity of $\delta^{13}C$ measurements at different peak heights, in which an F8 standard was analysed nine times at different concentrations. Peak heights for the eight compounds across the different runs ranged from an average of 0.49 nA (range 0.43 to 0.52 nA) up to an average of 6.4 nA (range 5.52 to 7.55 nA). The average standard deviation of $\delta^{13}C$ for all eight compounds across the nine runs is 0.21‰, but ranges from 0.11‰ for the C14-Et up to 0.59‰ for the C20-Et. However, it should be noted that the $\delta^{13}C$ value of the C20-Et for the highest concentration dilution deviates significantly from the $\delta^{13}C$ value measured during the other analyses, while other compounds at this peak height remain relatively stable (Fig. 3.1).

Fig 3.1 shows a plot of peak height against $\delta^{13}C$ for each of the eight compounds. With the exception of the C20-Et outlier (with a peak height of 5.64 nA), the highest level of variability is evident below 0.9 nA. The most notable offset is the second lowest concentration which has an average peak height of 0.65 nA. $\delta^{13}C$ values of compounds at this dilution level increase by an average of 0.38‰ compared to the previous dilution (average peak height 0.88 nA), with a maximum increase of 0.74‰ for the C20-Et. The average standard deviation for all compounds excluding the lowest two dilutions is 0.17‰ (and 0.11‰ if the outlying C20-Et datapoint is also excluded). This suggests that the $\delta^{13}C$ analysis is most accurate when peaks heights are ca. 0.9 nA and above. For FA samples from DTGC2011, analyses where peak heights were less than 1 nA were removed from the final dataset to account for this source of error.

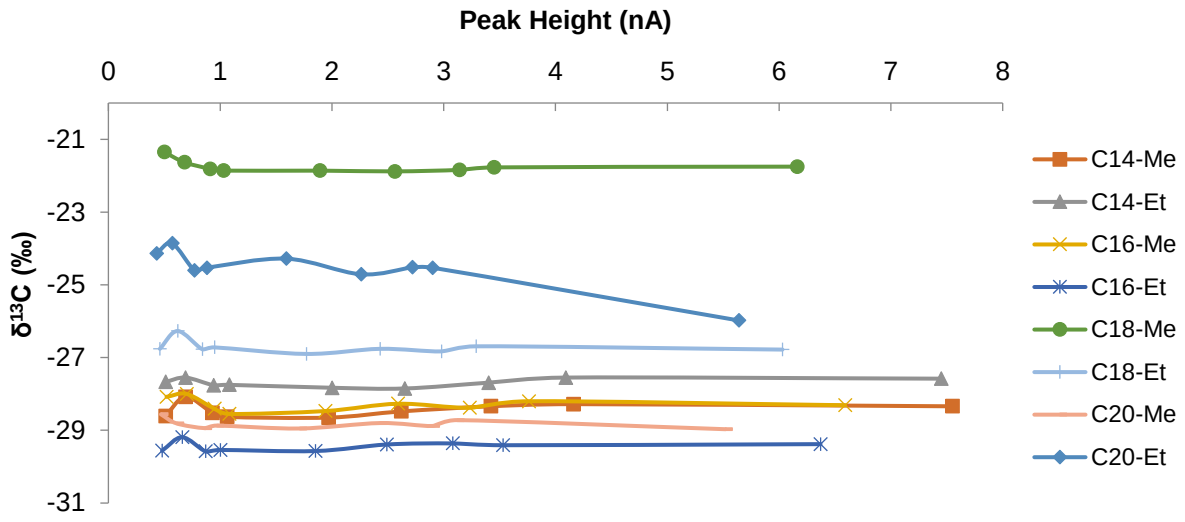



**Figure 3.1** $\delta^{13}C$ values of each F8 compound at different peak heights.

The final $\delta^{13}C$ data set excluded any samples in which the standard deviation of duplicate samples runs was greater than 0.4‰ and where peak height was below 1 nA. Peak separation was also assessed for each analysis and where high levels of co-elution occurred, samples were excluded from the final dataset. Errors were calculated based on the difference between duplicate analyses where available, which were only accepted where less than 0.5‰. Where no duplicates were available, the error was taken as the average difference of the duplicate analyses.

To correct for the additional carbon added during MeOH derivatization, three FA standards were analysed for their bulk carbon isotope value using an Elementar Pyrocube at the University of Birmingham. Samples were combusted at 920°C before being passed through a reduction column and the isotopic composition of sample gases was then determined on an Isoprime continuous flow mass-spectrometer. These samples were then derivatized, using the methods described in Section 3.4.5, and then analysed on the GC-IRMS for the $\delta^{13}C$ value of the FAME. The $\delta^{13}C$ of the FA ($\delta^{13}C_{FA}$) and FAME ($\delta^{13}C_{FAME}$) were used to calculate the $\delta^{13}C$ of the MeOH ($\delta^{13}C_{MeOH}$) as follows:

$$\delta^{13}C_{MeOH} = (n_{FAME} * \delta^{13}C_{FAME}) - (n_{FA} * \delta^{13}C_{FA})$$

whereby $n_{FAME}$ is the number of carbons in the FAME and $n_{FA}$ is the number of carbons in the FA. $\delta^{13}C_{MeOH}$ was calculated to be ca. -40.8‰ and the $\delta^{13}C_{FAME}$ values were corrected using:

$$\delta^{13}C_{FA} = ((n_{FAME} * \delta^{13}C_{FAME}) + 40.8) / n_{FA}$$

### 3.9 Liquid Chromatography analysis of GDGTs

Relative GDGT abundances in 145 marine samples were analysed at the NERC Life Sciences Mass Spectrometry Facility, at the University of Bristol's Organic Geochemistry Unit, using HPLC-atmospheric pressure chemical ionisation-mass spectrometry. The N3 fraction (containing the GDGT compounds; Table 3.3) was filtered using a 0.45 μm PTFE filter prior to sending to Bristol and subsequently re-dissolved in 100 or 200 μL HPLC grade hexane: ISO mixture (99:1 *v/v*, Rathburn) with sonication prior to instrumental analysis.

Analyses of all samples were conducted on a Thermo Fisher Scientific TSQ Quantum Access triple quadrupole mass spectrometer equipped with an Acela autosampler and Acela pump. The data were acquired and analysed using Xcalibur software (Version 2.06; Thermo Fisher Scientific). Normal phase separation was achieved using two identical ultra-high-performance silica columns (Aquity columns, length 150 mm × ID 2.1 mm; particle size: 1.7 μm; pore size: 130 Å; Waters) fitted with a 2.1 mm × 5 mm guard cartridge and maintained at 2ºC, after Hopmans et al. (2016). The HPLC pump was operated at a flow rate of 200 μL $min^{-1}$, resulting in a maximum back pressure of 300 bar for this system.

GDGT determinations were based on single injections. In-house marine and peat standards were measured daily to assess system performance and monitor instrumental drift following the same analytical sequence as the samples and measured over the same period. These were

measured repeatedly at the start, end and typically every 7 samples throughout the sequence and integrated in the same way as the unknowns. Analytical precision (standard deviation, σ) is based on repeat analyses of these standards, giving an error of 0.01 for $TEX_{86}^{L}$ values.

A 15 μL aliquot was injected *via* an autosampler, with analyte separation performed under a gradient elution, where A was hexane and B was hexane: ISO (90:10 *v/v*, Rathburn). Samples were initially eluted isocratically with 82% A and 18% B for 25 minutes. Then the concentration of B was increased to 35% on a linear gradient over the next 25 minutes. Finally, the concentration of B was increased up to 100% using a linear gradient over 30 minutes. At the end of each run, the column was re-equilibrated to the initial conditions (82% A and 18% B) for 10 minutes prior to the next injection. A 45-minute washout period was applied between injections, whereby the column was flushed by injecting 25 μL hexane: ISO (99:1 *v/v*, Rathburn). GDGT peaks were integrated manually using Xcalibur software (Version 3.0.63, Thermo Fisher Scientific).

### 3.10 Hydrogen isotope analysis of fatty acids

FA hydrogen isotope analysis was undertaken at the NERC Life Sciences Mass Spectrometry Facility at the University of Bristol's Organic Geochemistry Unit. Each sample was dissolved in a solution of hexane which contained sacrificial compounds ethyl decanoate and pentadecane at ~0.3 mg per $cm^3$. The $\delta^2H$ values were determined using a ThermoScientific Delta V with GC Isolink and Conflow IV in electron ionisation mode. 1 μl of each sample was injected onto an Rtx-1 column (30m x 0.25mm internal diameter x 0.25um film thickness) with a flow rate of 0.8ml/min with He as the carrier gas. The oven programme was as follows: initial temperature 50°C, held for 1 minute, ramped 8°C per minute up to 120°C

then 3°C per minute up to 300°C then held for 10 minutes. FAs were analysed in duplicate except where concentrations were high enough for only one injection.

Data were initially calibrated to two $H_2$ reference peaks injected directly into the ion source, before being normalized using the equation of a line from a plot of measured against known $\delta^2H$ values for a standard suite of 15 n-alkanes (C16-C30; Mixture B3, Arndt Schimmelmann, Indiana University) which was injected prior to every two sample runs. Instrument error was typically less than 5‰, calculated using the same n-alkane standard.

Errors were calculated based on the difference between duplicate analyses. Where no duplicates were available, the error was taken as the average difference of the duplicate analyses.

***Note:*** *This chapter has been written for publication in a short-format journal. Hence, the style may differ from other chapters and some information may have been repeated.*

**Chapter 4**

# MID-HOLOCENE ANTARCTIC SEA-ICE INCREASE DRIVEN BY MARINE ICE SHEET RETREAT

Kate E. Ashley, James Bendle, Robert McKay, Johan Etourneau, Francisco J. Jimenez-Espejo, Alan Condron, Anya Albot, Xavier Crosta, Christina Riesselman, Osamu Seki, Guillaume Masse, Nicholas R. Golledge, Edward Gasson, Daniel P. Lowry, Nicholas E. Barrand, Nancy Bertler, Carlota Escutia and Robert Dunbar

## Abstract

Over recent decades Antarctic sea-ice extent has broadly increased, alongside widespread ice shelf thinning and freshening of waters along the Antarctic margin. In contrast, Earth system models generally simulate a decrease in sea ice. Circulation of water masses beneath large cavity ice shelves is not included in current models and may be a driver of this phenomena. We examine a Holocene sediment core off East Antarctica that records the Neoglacial transition, the last major baseline shift of Antarctic sea-ice, and part of a late-Holocene global cooling trend. Our record, supported by high-resolution ocean modelling, shows that a rapid Antarctic sea-ice increase occurred against a backdrop of increasing glacial meltwater input and gradual climate warming. We suggest that mid-Holocene ice shelf cavity expansion led to supercooling of surface waters and sea-ice growth which slowed basal ice shelf melting.

Incorporating this feedback mechanism into global climate models will be important for future projections of Antarctic changes.

### 4.1 Introduction

Ice shelves and sea ice are intrinsically linked and represent fundamental components of the global climate system, impacting ice-sheet dynamics, large-scale ocean circulation, and the Southern Ocean biosphere. Antarctic ice-shelves with large sub-shelf cavities (e.g. Ross, Filchner-Ronne) play a key role in regional sea-ice variations, by cooling and freshening surface ocean waters for hundreds of kilometres beyond the ice shelf edge (Hughes et al., 2014; Hellmer, 2004). Antarctic sea ice has broadly expanded over the past few decades, particularly in the western Ross Sea region (Turner et al., 2016), alongside widespread thinning of ice shelves (Paolo et al., 2015) and freshening along the Antarctic margin (Jacobs et al., 2002; Aoki et al., 2013). The drivers and feedbacks involved in these decadal trends are still poorly understood, hampered by the sparse and short-term nature of meteorological,

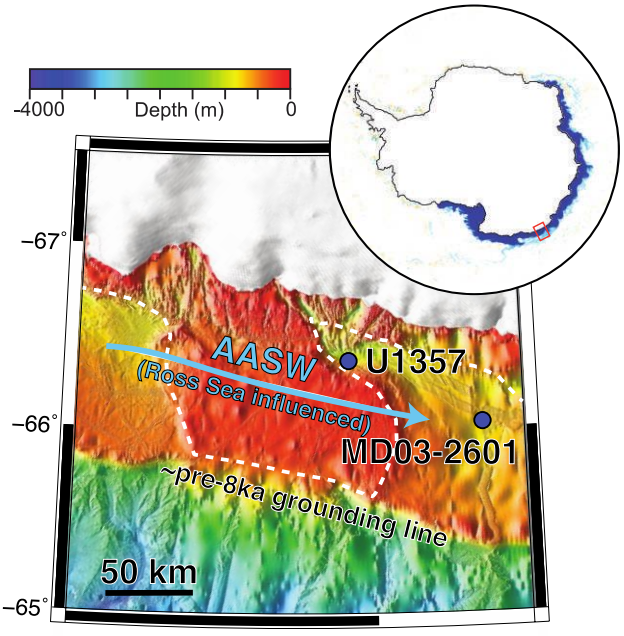



**Figure 4.1 Location of Sites U1357 and MD03-2601 (blue dots).** The ice sheet grounding line formed a calving-bay environment (dashed white line) prior to 11.4 ka, but since at least 8.2 ka Antarctic Surface Water flow is largely advected from the Ross Sea (blue line). Inset map: pathway of freshwater (dark blue) after 1 year of 1 Sv meltwater released from along the edge of the Ross Ice Shelf in a model simulation (Supplementary Information).

oceanographic and glaciological observations (Jones et al., 2016), and thus establishing the long-term trajectory for Antarctic sea ice on the background of accelerated ice sheet loss remains a challenge. Marine sediment cores provide a longer-term perspective and highlight a major baseline shift in coastal sea ice ~4.5 ka BP (Crosta et al., 2008; Steig et al., 1998; Denis et al., 2010) which characterizes the mid-Holocene 'Neoglacial' transition in the Antarctic. A mechanistic driver for this climate shift currently remains unresolved, but we propose that two interrelated aspects of the last deglaciation are significantly underrepresented in current models of this transition: (i) the retreat of grounded ice sheets from the continental shelves of Antarctica, and (ii) the subsequent development of large ice shelf cavities during the Holocene. Both factors would significantly alter water mass formation on Antarctica's continental shelves, which today are major source regions of Antarctic Bottom Water (AABW) and Antarctic Surface Water (AASW). These interrelated processes are not included in many coupled ocean-atmosphere models (e.g. Collins et al., 2006) which currently do not simulate the timing, magnitude and rapid onset of the Neoglacial (Supplementary Information).

Integrated Ocean Drilling Program (IODP) Expedition 318 cored a 171 m thick deposit of laminated diatomaceous ooze at Site U1357 offshore Adélie Land (Fig. 4.1), deposited over the past 11,400 years. Here, we present a new Holocene record of glacial meltwater, sedimentary input and local sea ice concentrations from Site U1357 using compound-specific hydrogen isotopes of fatty acid (FA) biomarkers ($\delta^2H_{FA}$), terrigenous grain size, biogenic silica accumulation, highly-branched isoprenoid alkenes (HBIs) and Ba/Ti ratios (Fig. 4.2 and S5).

We interpret $\delta^2H_{FA}$ (Fig. 4.2) fluctuations in Adélie Drift sediments as a record of meltwater input from isotopically-depleted glacial ice (Supplementary Information). Antarctic glacial ice is highly depleted in $^2H$ compared to ocean water, thus creating highly contrasting end-member values for the two major H source pools. Grain size (sand and mud percentage and sorting), natural gamma radiation (NGR) and terrigenous and biosiliceous mass accumulation rates (MARs) reflect changing sediment delivery either driven via local glacial meltwater discharge or advection of suspended sediment by oceanic currents. The diene/triene HBI ratio is used as a proxy for coastal sea ice presence (Massé et al., 2011). Ba/Ti enrichment is considered to reflect enhanced primary productivity. These records allow a unique opportunity to reconstruct the magnitude of the coupled response of the ocean and ice sheet during the Neoglacial transition. Details on all proxies and associated uncertainties can be found in the Supplementary Information.

The Adélie drift deposit is built up predominantly through advection of siliceous diatom frustules derived from local hyperproductive polynyas (Arrigo and van Dijken, 2003), and erosion of terrigenous material from local bathymetric highs. Most of these components are transported from regions to the east and concentrated within the drift via the westward-flowing Antarctic Coastal Current (Fig. 4.1; Supplementary Information), resulting in the predominantly east-west elongation of the drift deposit. While several small glaciers within Adélie Land may contribute meltwater to the site, the region is also likely to be influenced significantly by changes in Ross Sea waters. To demonstrate this, we employed a series of sensitivity tests from a high-resolution numerical ocean model by releasing a range of meltwater volumes (0.01 to 1 Sv) from along the front of the Ross Ice Shelf (RIS) to determine its pathway. This demonstrates that, even under the lowest flux scenarios, freshwater is transported anticlockwise, entrained within the coastal current (Fig. 4.3 and

Supplementary Fig. S1), and reaches Site U1357 within a year. Moreover, the simulations show a strong linear relationship between meltwater flux and salinity change at the core site (Fig 4.3), suggesting the magnitude of the signal recorded at Site U1357 is directly related to the magnitude of meltwater released. Thus, we argue that any changes in Ross Sea water mass properties (salinity and temperature) would have a direct influence on surface water mass properties at Site U1357 during the Holocene.

The stratigraphy of U1357B is divided into three units: the lowermost 10 cm recovered Last Glacial Maximum (LGM) till (Unit III), overlain by 15 m of laminated mud-rich diatom oozes with ice rafted debris (IRD) (Unit II), and the upper most 171 m (Unit I) consists of laminated diatom ooze with a general lack of IRD and a significant reduction in terrigenous sediment (Escutia et al., 2011). The sedimentology and geometry of the drift prior to ~11.4 ka (Unit II) is consistent with the calving bay reentrant model (Leventer et al., 2006; Domack et al., 2006) (Fig. 4.1 and Fig. S6; Supplementary Information), whereby LGM ice retreated in the deeper troughs while remaining grounded on shallower banks and ridges. Sediment laden meltwater and IRD content in Unit II (>11.4 ka) is thus likely derived from local outlet glaciers. However, anomalously old radiocarbon ages due to glacial reworking precludes development of a reliable age model prior to the Holocene (Supplementary Information).

**4.2 Early Holocene (11.4 – 8.2 ka BP)**

The base of the drift deposit shows downlapping of material suggesting a supply from the south, indicating that local focusing of meltwater and terrigenous material was the dominating influence until 11.4 ka (Supplementary Information). This is overlain by onlapping strata (Unit I) with the drift forming an east-west elongation on the northern flank of the Dumont d'Urville Trough, which is more consistent with advection of material from the east than with

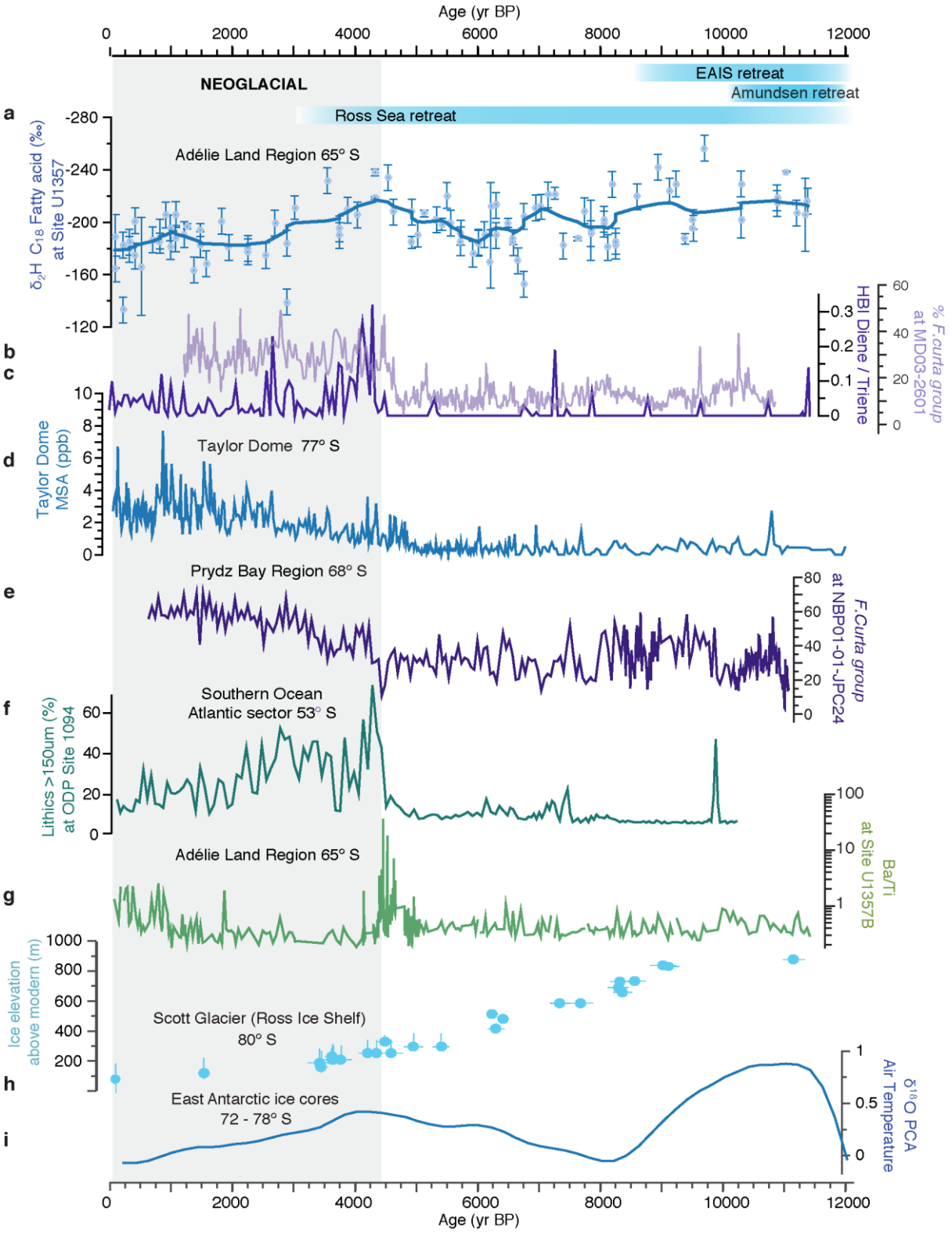



**Fig. 4.2 Holocene Adélie Land proxy records from IODP Site U1357 and other circum-Antarctic sites.** Glacial retreat chronologies are shown as bars at the top as discussed in the text. a) $\delta^2H$ $C_{18}$ fatty acid at Site U1357 (errors bars based on replicates), with robust locally weighted smoothing (rlowss). b) *Fragilariopsis curta* group (*F. curta* and *F. cylindrus*) relative abundance at MD03-2601, as a proxy of sea-ice conditions (Crosta et al., 2008) (c) di-unsaturated HBI ($C_{25:2}$; Diene)/tri-unsaturated HBI isomer ($C_{25:3}$; Triene) ratio at Site U1357 d) Methanesulfonate (MSA) concentrations (ppb) from Taylor Dome ice core e) *F. curta* group relative abundances in core NBP-01-JPC24 f) Coarse lithic (ice-rafted) content at ODP 1094 (Nielsen et al., 2007) g) Ba/Ti (logarithmic scale) at Site U1357 h) $^{10}Be$ cosmogenic nuclide ages from Scott Glacier in the SW Ross Ice Shelf region (Spector et al., 2017) i) Temperature signal from principal component analyses of five $\delta^{18}O$ records in five East Antarctic ice cores (Vostok, EPICA Dome C, EPICA Dronning Maud Land, Dome Fuji and Talos Dome) (Masson-Delmotte et al., 2011).

delivery from local outlet glaciers to the south. Thus, an increased meltwater influence from the Ross Sea is likely since this time (Supplementary Information).

Due to the potential for competing sources of glacial meltwater in the earliest Holocene, we focus our study on Unit I, where there is less influence of calving bay processes (Escutia et al., 2011). However, the earliest part of Unit I (11.4 to 8 ka BP), which includes the most negative $\delta^2H_{FA}$ values, is characterized by a very gradual upcore increase of sorting in the terrigenous sediment supply, decreasing natural gamma ray (NGR) values (Supplementary Fig. S5) and a general lack of IRD. We conservatively interpret this as potentially maintaining some local glacial meltwater input from local outlet glaciers in the lowermost interval of Unit I. Nevertheless, this process was probably greatly reduced relative to Unit II deposition and it is likely much of this signal between 11.4 and 8 ka could still be derived from water masses advecting to the site from the east (e.g. the Ross Sea).

An overall trend to more positive $\delta^2H_{FA}$ values, from the most negative value of the record at ~9.6 ka, to ~8 ka indicates decreasing meltwater (Fig. 4.2a), thus suggesting a gradually diminished input from either local outlet glaciers or the Ross Sea (Supplementary Fig. S5). This is associated with an increase in mass accumulation rates (MARs), between 10 and 8 ka, and is tentatively interpreted to represent the final retreat of residual ice from local bathymetric highs allowing more material to advect into the drift (Supplementary Fig. S6). Although there is millennial scale variability, MARs remain relatively high until 4.5 ka. However, $\delta^2H_{FA}$ and MARs show greater coherence at the millennial-scale after 7 ka BP, suggesting that increased fluxes of glacial meltwater broadly corresponded to stronger easterly currents, which advected biogenic and terrigenous material into the drift.

### 4.3 Middle Holocene (8.2 – 4.5 ka BP)

A negative excursion in $\delta^2H_{FA}$ starting from 6 ka and culminating at 4.5 ka is interpreted to record a period of enhanced glacial meltwater flux to the site relating to a final retreat phase of the major ice sheet grounding line in the Ross Sea embayment (Fig. 4.4). A marked enrichment of Ba/Ti ratios also occurs at 4.5 ka, reaching values of 36.1, on a background of baseline fluctuations between 0.1 and 2.7 (Fig. 4.2g), which suggests enhanced primary productivity, potentially driven by meltwater-induced stratification. Ongoing Holocene retreat in the Ross Sea is interpreted to be primarily the consequence of marine ice sheet instability processes resulting from the overdeepened continental shelf in that sector (McKay et al., 2016).

The $\delta^2H_{FA}$ peak at 4.5 ka in U1357B coincides directly with a rapid shift in HBI biomarker ratios at the site, as well as sea ice proxies recorded in nearby site MD03-2601, in the Ross embayment (Taylor Dome ice core (Steig et al., 1998) following a revised age model by Baggenstos et al., 2018) and Prydz Bay (JPC24) (Denis et al., 2010) (Fig. 4.2), reflecting a widespread increase in coastal sea-ice concentration and duration. We interpret decreasing MAR and finer-grained terrigenous content (e.g. increased mud percent) at Site U1357 after 4.5 ka (Fig. S5) to also be a consequence of increased coastal sea ice, reducing wind stress on the ocean surface and limiting the easterly advection of detritus to the drift deposit.

Coastal sea-ice concentration and duration remain high throughout the rest of the Holocene (this study and Crosta et al. (2008), Steig et al. (1998), Denis et al. (2010)), compared to the period before 4.5 ka, despite a decrease in glacial meltwater flux to the U1357 site. In addition, meltwater input prior to 4.5 ka does not have a major influence on sea ice extent. Thus, an increase in meltwater flux cannot explain the Neoglacial intensification of sea ice at ~4.5 ka. Here, we propose that greater coastal sea ice cover since 4.5 ka is related to the

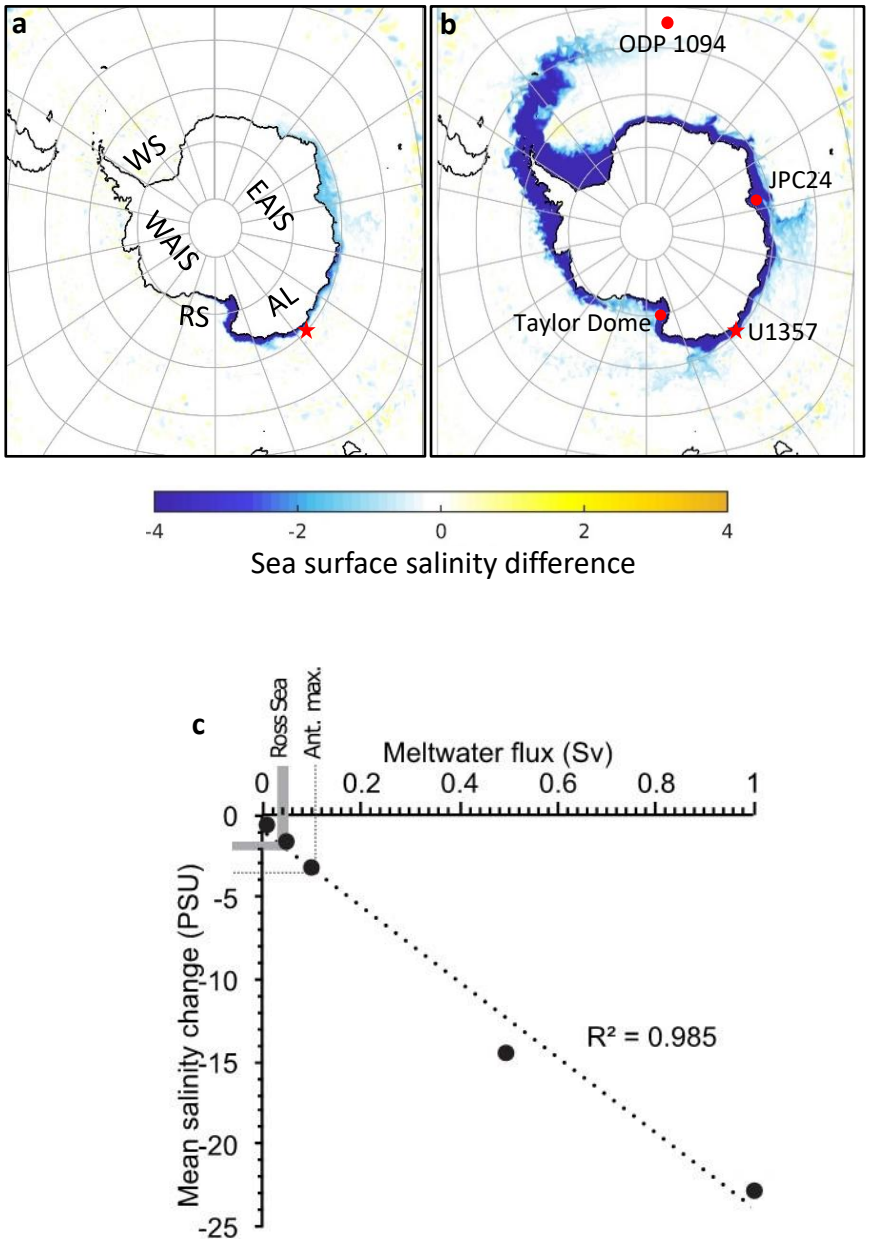



**Fig. 4.3 MITgcm simulations of meltwater release from along the edge of the Ross Ice Shelf**. First two images show sea-surface salinity difference (in practical salinity units) after 3.5 model years resulting from meltwater release volumes of a) 0.1 Sv and b) 1 Sv. Red star indicates position of Site U1357 (this study) and red dots show positions of other core sites mentioned in this study where a Mid Holocene increase in sea ice and/or cooling is recorded: Taylor Dome (Steig et al., 1998; Baggenstos et al., 2018), JPC24 (Denis et al., 2010) and ODP 1094 (Nielsen et al., 2007). AL = Adélie Land, RS = Ross Sea, WS = Weddell Sea, EAIS = East Antarctic Ice Sheet, WAIS = West Antarctic Ice Sheet. c) Scatter plot of simulated meltwater flux (Sv) against mean salinity difference at U1357 core site. Grey band indicates range of plausible Holocene to deglacial Ross Sea meltwater inputs. Dotted line indicates maximum Antarctic meltwater during the Holocene.

development of a large ice-shelf cavity in the Ross Sea as the ice sheet retreats (Fig. 4.4),

which pervasively modified ice shelf-ocean interactions and increased sea ice production.

Models suggest a large cavity on the continental shelf increases contact between basal-ice and circulating ocean water, driving the formation of a cool, fresh water mass feeding into the AASW, stabilizing the water column and enhancing the production of sea ice (Hellmer, 2004) (Fig. 4.4). However, under small cavities such as in the modern Amundsen Sea influenced by warm-water incursions, ice-shelf melting results in an "ice pump" enhancement of sub-ice shelf circulation. This increases flow of warm Circumpolar Deep Water (CDW) under the ice shelf that is 100-500 times the rate of melt, and this volume of water does not allow for supercooling. Small cavity ice shelf outflows are therefore warm and act to restrict sea ice at the ice shelf front (Jourdain et al., 2017). Thus, during the Holocene, the size of the cavity must have reached a threshold after which this positive warming feedback switched to a negative feedback. We argue that such a tipping point takes place at 4.5 ka BP, when our proxy data suggest meltwater peaks, and would explain why the increase in sea-ice concentration appears rapid and only occurs at the peak of the meltwater input, and not during its prior increase, or previous meltwater inputs (Fig. 4.2a-g).

Although the glacial meltwater volume is greatly reduced after 4.5 ka BP, the volume of Ice Shelf Water (ISW) produced beneath the modern RIS is estimated at 0.86 Sv-1.6 Sv (Smethie and Jacobs, 2005; Holland et al., 2003). We note that ISW is not glacial meltwater, but it is defined as a supercooled water mass formed through interaction with the base of the RIS, but once formed, acts to modify other water masses in the Ross Sea. A significant proportion of ISW is high salinity and is thus advected northwards at intermediate waters depth to ultimately form AABW. However, a significant volume of ISW is lower salinity and buoyant, due to development of frazil ice, and acts to mix with surface waters (Robinson et al., 2014). Currently, a 0.4 Sv plume of ISW in the western margin of the Ross Ice Shelf (Robinson et al., 2014) is directly delivered to the surface resulting in enhanced sea ice production, while

seasonal melt of this enhanced sea ice further acts to cool and freshen surface waters. Although unrealistic in the context of a post-LGM meltwater flux from the Ross Sea alone, the larger meltwater release scenarios in our simulations (0.5 to 1 Sv) show the potential pathways that a cool, fresher surface water mass collecting and forming on the broad Ross Sea continental shelf would follow (Fig. 4.3). These waters are transported in easterly coastal currents to the Weddell Sea and the Antarctic Peninsula. This eventually retroflects to join the Antarctic Circumpolar Current (Fig. 4.3b), and thus has potential for cooling and freshening in the South Atlantic far offshore, as the ice shelf cavity increased in the Ross Sea. Indeed, offshore site ODP 1094 records increased lithics in the South Atlantic after 4.5 ka (Fig. 4.2f), relative to the period before, suggested to have been predominantly transported by sea ice indicating a cooling in sea surface temperatures and increase in sea-ice extent in the South Atlantic at this time (Nielsen et al., 2007). However, it also is feasible that this circum-Antarctic cooling signal indicates similar melt processes may have been occurring in the Weddell Sea at ~4.5 ka, as suggested by cosmogenic nuclide data (Hein et al., 2016).

### 4.4 What drove the Neoglacial transition?

Our observed coastal sea-ice increase is part of a widespread transition to Neoglacial conditions both globally and at high southern latitudes (Masson-Delmotte et al., 2011; Marcott et al., 2013; Kim et al., 2002; Solomina et al., 2015). However, most current climate models do not simulate this cooling trend, resulting in a significant data-model mismatch (Liu et al., 2014) (Supplementary Fig. S8). Marine ice sheet retreat along the entire Pacific margin of West Antarctica has previously been proposed to be triggered by enhanced wind-driven incursions of warm CDW onto the continental shelves in the early Holocene (Hillenbrand et al., 2017), with continued retreat in the Ross Sea being the consequence of the overdeepened continental shelf and marine ice sheet instability processes (McKay et al., 2016). However,

we propose that a series of negative feedbacks associated with this retreat and RIS cavity expansion occurred in the mid-Holocene, with similar processes possibly occurring in the Weddell Sea, leading to the onset and continuation of Neoglacial conditions. Widespread albedo changes associated with increased coastal sea ice would have amplified regional cooling trends (Masson-Delmotte et al., 2011), whilst increased stratification resulting from seasonal sea-ice melt and increased ISW production drove the deepening of the fresher water surface isopycnal at the continental shelf break. Grounding line retreat creates new space for continental shelf water masses to form, while ice shelf cavity expansion promotes supercooling and freshening of AASW. Thus, as seasonal sea ice melt and ice shelf supercooling processes played a greater role in enhancing AASW production on the continental shelf, they would have acted to restrict warmer subsurface water transport onto the continental shelf (Smith Jr. et al., 2012) (Fig. 4.4). Furthermore, the Neoglacial sea-ice increase itself may have been associated with a stabilising feedback mechanism (which also is not resolved in ice-ocean models) through its role in dampening ocean-induced wave flexural stresses at ice shelf margins, reducing their vulnerability to catastrophic collapse (Massom et al., 2018). We suggest that some combination of the above processes slowed the rate of Ross Sea grounding line retreat (Supplementary Information) and reduced basal ice shelf melt as indicated by a trend towards more positive $\delta^2H_{FA}$ values in U1357B between 4.5 and 3 ka (Fig. 4.2a). Furthermore, large Antarctic ice shelves currently have large zones of marine accreted ice resulting from supercooling (Rignot et al., 2013), thus the signature of $\delta^2H_{FA}$ is anticipated to become more positive as the ice shelf approaches a steady state of mass balance, relative to the thinning phases when basal melt rates exceed that of accretion. The stabilization of $\delta^2H_{FA}$ values observed at 3 ka in U1357B suggests the RIS has maintained a relatively steady state of mass balance since this time.

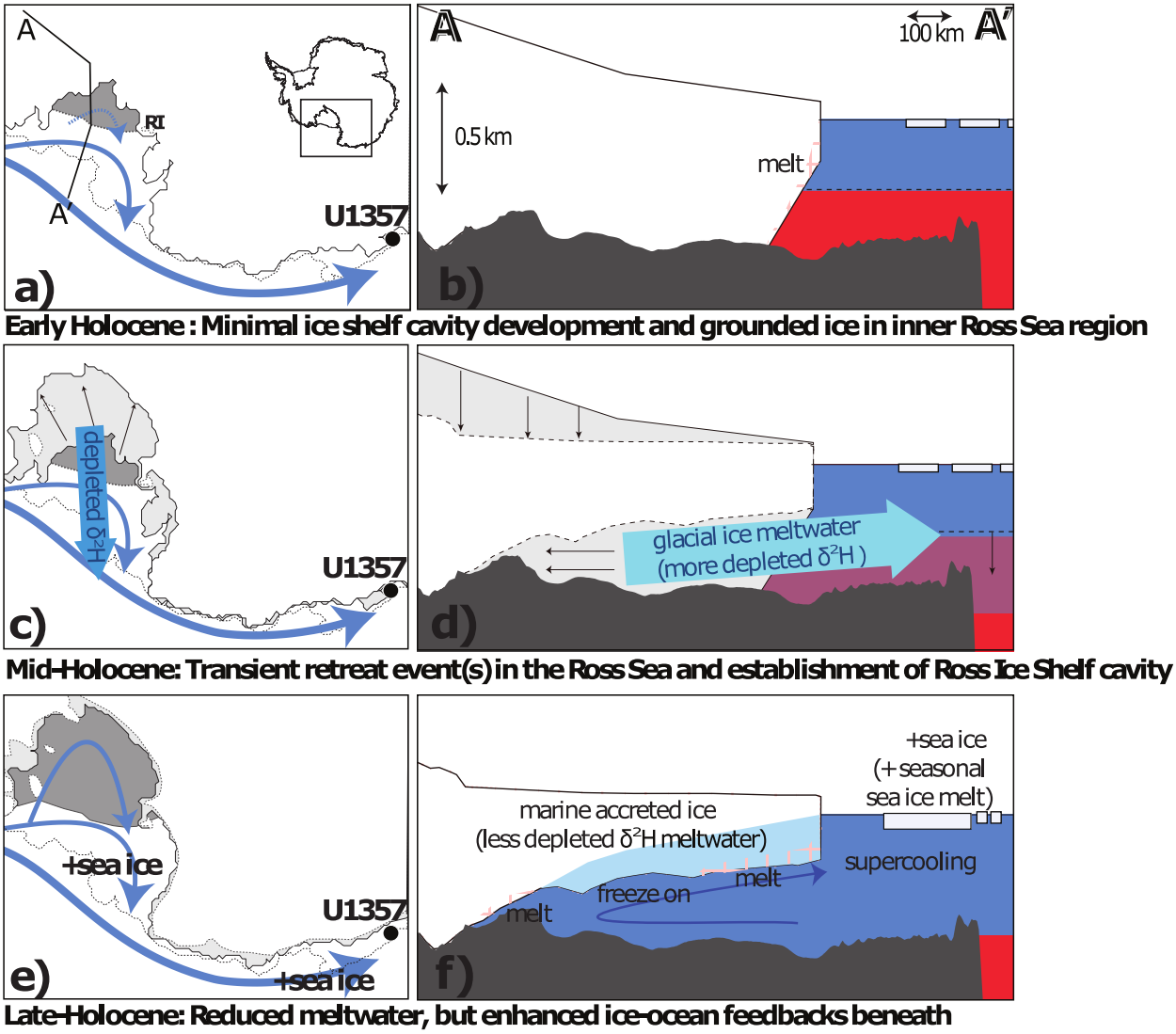



**Fig. 4.4 Conceptual model of evolving Holocene glacial and oceanographic conditions in the Ross Sea region.** Panels on the left show modelled grounding line positions (McKay et al., 2016), and proposed circulation of surface and sub-ice shelf circulating waters (light blue arrows). Panels on the right show cross sections of the Ross Ice Shelf (RIS) and ice-ocean interactions. Dark blue = cool surface waters, Red = warm subsurface waters. a) The grounding line in Adélie Land is near its modern location, but near Ross Island (RI) in the Ross Sea, and ice shelf cavity (dark grey shading) is reduced in size relative to today (McKay et al., 2016). b) Continental shelf profile A-A' (panel a) shows a Ross Sea grounding line in a mid-continental shelf location in close proximity to the RIS calving line (McKay et al., 2016), with subsurface warming on the continental shelf triggering WAIS deglaciation (Hillenbrand et al., 2017). c) Most grounding line retreat south of RI occurred between 9 and 4.5 ka (light grey shading with black arrows represents area of retreat over this period), proposed to be the consequence of marine ice sheet instability, but the ice shelf calving line remained near its present position (McKay et al., 2016; Spector et al., 2017). d) Grounding line retreat and ice shelf thinning released meltwater with negative $\delta^2H$ into the surface waters. Increasing ice shelf-oceanic interactions with the development of the ice shelf cavity (dark grey) led to enhanced Antarctic Surface Water formation; f) Minimal grounding line retreat has occurred since 4.5 ka, and the RIS supercools AASW leading to enhanced sea-ice formation despite reduced glacial meltwater flux. Seasonal sea ice meltwater further freshens and cools AASW. Increased production of AASW on the continental shelf leads to isopycnal deepening (dotted line) and limits flow onto the continental shelf slowing further grounding line retreat. However, as the ice shelf is near steady state mass balance and there is a component of marine accreted ice at the base of the ice shelf (Rignot et al., 2013), the strength of the $\delta^2H$ signal is reduced relative to periods of mass balance loss.

A recent study implies an increase in katabatic winds since at least 3.6 ka in the Ross Sea (Mezgec et al., 2017) (Supplementary Information), leading to enhanced polynya activity.

During colder Antarctic climates, increased latitudinal temperature gradients enhanced katabatic winds in the Ross Sea (Rhodes et al., 2012). We interpret this katabatic wind and polynya activity signal to be a response to the preceding Neoglacial cooling at 4.5 ka and evolution of the modern ocean-ice shelf connectivity, which our data suggest was primarily driven by ice shelf cavity expansion.

Furthermore, this transition takes place on the background of declining winter insolation (Berger and Loutre, 1991) which would have acted to further enhance and maintain these changes. This insolation decline has previously been hypothesised as a driver of the Neoglacial increase in coastal sea ice (Denis et al., 2010), however this monotonic decrease contrasts with the markedly rapid increase in sea ice observed in many records (Fig 4.2). Our mechanism of ice shelf cavity expansion, reaching a threshold that promoted significant supercooling of continental shelf water masses, reconciles both the rapidity and timing of Neoglacial onset in the mid-Holocene.

The lack of these coupled ice-ocean processes is apparent in recent Earth system model experiments, in particular the incorporation of evolving ice shelf cavities, with Trace-21k for example, instead simulating a decrease in Antarctic sea-ice extent and thickness after 5 ka (Supplementary Fig. S8). These model outputs are in direct contrast to multiple lines of proxy data in this study and previous work (Crosta et al., 2008; Steig et al., 1998; Denis et al., 2010). Consequently, our results provide insights into the magnitude of this data-model mismatch, as well as a mechanism for rapid sea-ice change and grounding line stabilisation on the background of a warming climate (Liu et al., 2014), both on modern and Holocene time

scales. Better representation of the role of evolving ice shelf cavities on oceanic water mass evolution and sea-ice dynamics, which our data indicate acted as a strong negative feedback, will be fundamental to understanding the oceanographic and glaciological implications of future ice shelf loss in the Antarctic.

## 4.5 Methods

### 4.5.1 Organic geochemical analyses

Lipid extraction of sediment samples was performed at the Royal Netherlands Institute for Sea Research (NIOZ). Freeze-dried and homogenized samples were extracted by Dionex™ accelerated solvent extraction (DIONEX ASE 200) using a mixture of dichloromethane (DCM)/methanol (MeOH) (9:1, v/v) at a temperature of 100°C and a pressure of $7.6 \times 10^6$ Pa (Kim et al., 2010).

Two-thirds of the total lipid extract were sent to the University of Glasgow, UK and separated over an aminopropyl silica gel column where the total neutral fraction was eluted with 4ml of DCM/ isopropanol (1:1 v/v), and the total acid fractions were eluted into an 8ml vial with 4% acetic acid in ethyl-ether solution (Huang et al., 1999). Derivatisation to Fatty Acid Methyl Ester (FAME) was achieved by adding 200 µl of MeOH containing 14% v/v Boron triflouride to the 8ml vial containing the TAF. The vial was sealed and placed in the drying cabinet at 70°C for one hour. The MeOH was dried under $N_2$ and the FAMEs were recovered and cleaned up by eluting through a pre-cleaned 3cm silica gel column (60 A; 35-70) with 4ml of hexane and 4ml of DCM (containing the FAMEs). The recovered FAMEs fraction was split 50:50 and one half used for hydrogen isotope analysis. $\delta^2H$ values indicate depletion against the international standard Vienna Standard Mean Ocean Water (V-SMOW).

Compound specific hydrogen isotope analyses of FAMES was performed at the Institute of Low Temperature Science, Hokkaido University. $\delta^2H$ values were obtained using an isotope-ratio mass spectrometer system with a HP 6890 gas chromatograph and a ThermoQuest Finnigan MAT Delta Plus XL mass spectrometer. Separation of the FAMES was achieved with a HP-5 MS fused silica capillary column (30 m, 0.32 mm internal diameter, 0.25 μm film thickness) with a cooled on-column injector. An *n*-alkane and a reference gas whose isotopic values were known was co-injected with the samples as an internal isotopic standard for $\delta^2H$. A laboratory standard (Mix F8 of FAs from Indiana University) containing $C_{10}$–$C_{30}$ FAs was analyzed daily to check the accuracy and the drift of the instrument and to normalize the data to the SMOW isotopic scale. The $H^{3+}$ factor was measured every three days.

The FA $\delta^2H$ was plotted with a robust locally weighted smoothing (rlowss) to highlight the longer term centennial to millennial scale trends. This is preferable to a running mean (or similar) because the FA $\delta^2H$ data are patchy in resolution (due to some parts of the core having weaker FA concentrations than others) and have some high amplitude changes in signal. This means that an rlowss gives a smoothing curve which visually picks out the longer terms changes well, whereas a running mean results in some strange artefacts due to the changes in resolution, e.g. step wise changes which do not reflect longer term changes well.

### 4.5.2 Inorganic geochemical analysis and electronic microscopy

Major element concentrations were obtained using X-Ray Fluorescence Scanner on 412 analyses measured directly over undisturbed sediment sections. The bulk major element composition included in this study was measured between sections U1357B-1H-2 to U1357-19H-5 continuously each 50 cm. We used an Avaatech XRF core scanner at the IODP-Core Repository/Texas A&M University laboratories (USA) during December 2010. Non-

destructive XRF core-scanning measurements were performed over 1 $cm^2$ area with slit size of 10 mm, a current of 0.8 mA and sampling time of 45 seconds at 10 kV in order to measure the relative content of titanium (Ti) and barium (Ba).

Field emission scanning electron microscopy (FESEM) images and corresponding spectrum were obtained with an AURIGA FIB-FESEM Carl Zeiss SMT at Centro de Instrumentación Científica, Granada University, Spain

### 4.5.3 Grain size analyses

A total of 341 samples were prepared for grain size analysis. Samples were treated for removal of biogenic opal with a 1M sodium hydroxide NaOH solution and incubated in a water bath at 80°C for 24 hours. This procedure was repeated twice due to an incomplete dissolution of diatoms observed in smear slides. The samples were then treated with $H_2O_2$ to remove organic material at 80°C for 24 hours. Samples were measured using a Beckman Coulter LS 13 320 Laser Diffraction Particle Size Analyser (LPSA). The LPSA has a relatively narrow range of optimum obscuration which is determined by the sample surface area, in turn determined by sample concentration and sample distribution. Prior to grain size analysis, ~30 mL of 0.5 g/L Calgon (sodium hexametaphosphate) was added to the samples, and sonicated and stirred in order to disperse the grains and prevent clumping. The range in sample mass for most of the post-treatment samples varied from ~0.035-0.8 grams. Random biases propagating through this process cannot be ruled out, especially when taking account of susceptibility of grains <10 μm to clump (McCave et al., 1995) and random cohesion of grains due to any remaining organic content. The aqueous liquid module in the LPSA also does not accurately record the <2 μm clay that may compromise a significant part of the size spectrum in glacial environments (McCave et al., 1995; McCave and Hall, 2006). Given these

considerations, subsamples were taken from a total of 84 samples to test reproducibility of the data relating to sub-sampling biases, with a least squares regression showing a high reproducibility with an $r^2$ value of 0.744. An additional 12 samples were sub-sampled before the chemical treatment in order to test the reproducibility of the treatment methodology, with a least squares regression showing a high reproducibility with an $r^2$ value of 0.752.

### 4.5.4 Highly branched isoprenoids (HBI)

HBIs were extracted at Laboratoire d'Océanographie et du Climat: Experimentations et Approches Numériques using a mixture of 9mL $CH_2Cl_2$/MeOH (2:1, v:v), to which internal standards were added and applying several sonication and centrifugation steps in order to extract the selected compounds (Etourneau et al., 2013). After drying with $N_2$ at 35°C, the total lipid extract was fractionated over a silica column into an apolar and a polar fraction using 3 mL hexane and 6 mL $CH_2Cl_2$/MeOH (1:1, v:v), respectively. HBIs were obtained from the apolar fraction by fractionation over a silica column using hexane as eluent following the procedures reported by (Belt et al., 2007; Massé et al., 2011). After removing the solvent with $N_2$ at 35°C, elemental sulfur was removed using the TBA (Tetrabutylammonium) sulfite method (Jensen et al., 1977; Riis and Babel, 1999). The obtained hydrocarbon fraction was analyzed within an Agilent 7890A gas chomatograph (GC) fitted with a 30 m fused silica Agilent J&C GC column (0.25 mm internal diameter, 0.25 µm film thickness), coupled to an Agilent 5975C Series mass selective detector (MSD). Spectra were collected using the Agilent MS-Chemstation software. Individual HBIs were identified on the basis of comparison between their GC retention times and mass spectra with those of previously authenticated HBIs e.g. Johns et al. (1999) using the Mass Hunter software. Values are expressed as concentration relative to the internal standard.

### 4.5.5 Biogenic silica

Biogenic silica concentrations (wt% BSi) were measured on 349 discrete samples using a molybdate blue spectrophotometric method modified from Strickland and Parsons (1970) and DeMaster (1981). Analytical runs included replicates from the previous sample group and from within the run, and each run was controlled by 10 standards and a blank with dissolved silica concentrations ranging from 0 µM to 1200 µM. For each analysis, ~7 mg of dry, homogenized sediment was leached in 0.1M NaOH at 85°C, and sequential aliquots were collected after 2, 3, and 4 hours. Following addition of reagents, absorbance of the 812 nm wavelength was measured using a Shimadzu UV-1800 spectrophotometer. Dissolved silica concentration of each unknown was calculated using the standard curve, and data from the three sampling hours were regressed following the method of DeMaster (1981) to calculate wt% BSi. In our U1357B samples, wt% BSi ranges from maximum of ~60% in early and mid-Holocene light laminae to a minimum of 31% in late Holocene dark laminae. The average standard deviation of replicate measurements is 0.5%.

### 4.5.6 Model simulations

All numerical calculations were performed using the Massachusetts Institute of Technology general circulation model (MITgcm; Marshall et al.,1997); a three-dimensional, ocean sea-ice, hydrostatic, primitive equation model. The experiments presented here were integrated on a global domain projected onto a cube-sphere grid to permit a relatively even grid spacing and to avoid polar singularities (Adcroft et al., 2004; Condron and Winsor, 2012). The ocean grid had a mean, eddy-permitting, horizontal grid spacing of 1/6° (18-km) with 50 vertical levels ranging in thickness from 10m near the surface to approximately 450m at the maximum model depth. The ocean model is coupled to a sea-ice model in which ice motion is driven by

forces generated by the wind, ocean, Coriolis force, and surface elevation of the ocean, while internal ice stresses are calculated using a viscous-plastic (VP) rheology, as described in Zhang and Hibler (1997). In all experiments, the numerical model is configured to simulate present-day (modern) conditions: Atmospheric forcings (wind, radiation, rain, humidity etc.) are prescribed using 6-hourly climatological (1979-2000) data from the ERA-40 reanalysis product produced by the European Centre for Medium-range Weather Forecasts and background rates of runoff from the ice sheet to the ocean are based on the numerical ice sheet model of Pollard and Deconto (2016) integrated over the same period (1979-2000). To study the pathway of meltwater in the ocean, additional fresh (i.e. 0 psu) water was released into the surface layer of the ocean model at the grid points closest to the front of the Ross Ice Shelf. Five different discharge experiments were performed by releasing meltwater into this region at rates of 0.01 Sv (Sv = $10^6$ m3/s), 0.05 Sv, 0.1 Sv, 0.5 Sv, and 1 Sv for the entire duration of each experiment (~3.5 years).

# SUPPLEMENTARY INFORMATION

## S1. Environmental setting

Site U1357 is located in the Dumont D'Urville Trough of the Adélie Basin, ca. 35 km offshore from Adélie Land (66°24.7990'S, 140°25.5705'E; Fig 4.1). This is a >1000 m deep, glacially scoured depression on the East Antarctic continental shelf, bounded to the east by the Adélie Bank. Further east lays the Adélie Depression and the Mertz Bank, the latter located north of the Mertz Glacier floating ice tongue. The Adélie Land region is dissected by several glaciers which could potentially contribute terrigenous sediment into the coastal zone with the core site located 40 km to the north of the Astrolabe Glacier, and ca. 75 and 300 km northwest of the Zélée and Mertz glaciers, respectively.

The site itself is located within the Dumont d'Urville polynya (DDUP), which has a summer (winter) extent of 13,020 $km^2$ (920 $km^2$), but is also directly downwind and downcurrent of the much larger and highly productive Mertz Glacier polynya (MGP) to the east, with a summer (winter) extent of 26,600 $km^2$ (591 $km^2$) (Arrigo and van Dijken, 2003). The MGP forms as a result of reduced sea-ice westward advection due to the presence of the Mertz Glacier Tongue (Massom et al., 2001) and strong katabatic winds which blow off the Antarctic ice sheet with temperatures below -30°C (Bindoff et al., 2000). Katabatic winds freeze the surface waters and blow newly formed ice away from the coast, making the polynya an efficient sea-ice 'factory', with higher rates of sea-ice formation in comparison to non-polynya ocean areas which undergo seasonal sea ice formation (Kusahara et al., 2010). The MGP produces 1.3% of the total Southern Ocean sea ice volume despite occupying less than 0.1% of total Antarctic sea ice extent (Marsland et al., 2004).

As a result of the upwelling polynya environments, the area along the Adélie Coast is characterized by extremely high primary productivity, with the water column known to host significant amounts of phytoplankton, dominated by diatoms (Beans et al., 2008). The Mertz Glacier zone is generally characterized by stratified waters in the summer, due to seasonal ice melt, with these conditions corresponding to the highest phytoplankton biomass. The lack of ice cover means polynyas are the first polar marine systems exposed to spring solar radiation, making them regions of enhanced biological productivity compared to adjacent waters. A considerable amount of resultant sedimentation is focused via the westward flowing currents from both of these polynyas within the deep, protected Adélie Basin, resulting in a remarkably high sedimentation rate of ca. 1.5-2 cm $year^{-1}$ at Site U1357 (Escutia et al., 2011).

Although biogenic and terrigenous sediment is interpreted to be sourced locally in the Adélie Land region, the mass accumulation rate of these sediments in this drift is associated with the intensity of westward flowing currents (Section 3c). Critically, these westward currents also act to transport water masses from further afield, and Site U1357 is directly oceanographically downstream of the Ross Sea, meaning the continental shelf in this region receives significant Antarctic Surface Water (ASSW) transported by the Polar Easterlies and the Antarctic Slope Current (ASC) from the Ross Sea embayment (Fig 4.3). Thus, changes in the surface waters of the Ross Sea influence Site U1357. Whitworth et al. (1998) confirm the continuity of the westward flowing ASC between the Ross Sea and the Wilkes Land margin. This flow is largely associated with the Antarctic Slope Front, which reflects the strong density contrast between AASW and Circumpolar Deep Water (CDW). McCartney and Donohue (2007) estimate that the transport in the westward ASC, which links the Ross Sea to the Wilkes Land margin, reaches 76 Sv ($10^6/m^3/s$). This contributes to a cyclonic gyre, which together with the ASC dominate the circulation at Site U1357. The gyre transports around 35 Sv, and comes

mainly from the Ross Sea region, with a lesser contribution from a westward flow associated with the Antarctic Circumpolar Current.

Freshwater release simulations from the Ross Ice Shelf (RIS) confirm this oceanographic continuity between the Ross Sea and the Wilkes region (Fig 4.3). Five simulations with fluxes from 0.01 to 1 Sv released from the edge of the RIS all indicate that meltwater is almost completely entrained within the westward coastal surface current and reaches Site U1357 within 4 months to 1 year (Fig S1). These fluxes cover a wide range of meltwater inputs, and show a strong linear relationship with salinity at the core site (Fig. 4.3). This suggests that the

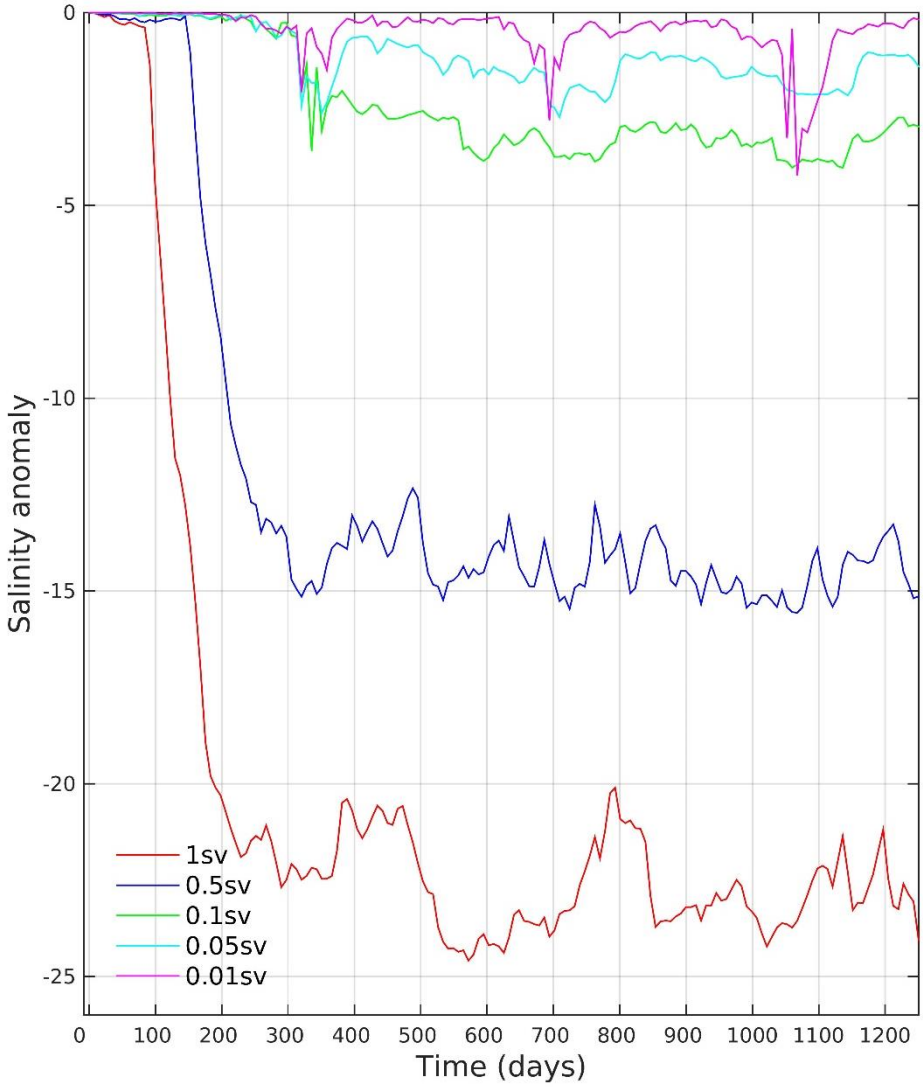



**Figure S1**. Simulated salinity anomalies over time at Site U1357 for the five meltwater release experiments.

magnitude of the signal recorded at Site U1357 is directly related to the magnitude of meltwater.

Local processes do also play a critical role in this region. For example, episodic calving events of the Mertz Glacier tongue release fast ice over the drill site and create strong surface water stratification, cutting off local AABW production (Campagne et al., 2015). Although appearing to be only a local process, there is still a regional (Ross Sea) influence, as this fast ice that builds up behind the Mertz Glacier is formed by the freezing of fresher AASW transported from the Ross Sea (Fig 4.3). Thus, conditions in the Ross Sea, such as the melting of isotopically depleted glacial ice, would influence both the isotopic composition and amount of this sea ice.

**S2. Age model**

We developed an age model for core U1357B based on 87 $^{14}C$ analyses on bulk organic carbon (Fig. S2). In the standard IODP CSF-A depth scale, recovery often exceeds 100% and to correct for this, the standard IODP procedure is to apply a linear compression algorithm which is based on the assumption that expansion is uniform in the core. However, in U1357B, expansion due to biogenic gas was particularly high and resulted in discrete sections of core being pushed apart creating voids in the depth scale that did not represent real gaps in the stratigraphy. To account for this, the voids are numerically removed and depth scale adjusted prior to linear compression being applied (if recovery still exceeds 100%).

The model was calibrated with a reservoir age correction of 1200±100 years and depth to age conversions achieved by using BACON. This is a Bayesian iteration scheme that invokes memory from dates above any given horizon, and produces a weighted mean and median age-depth curve (Blaauw and Christeny, 2011). The top depth of 3 m is consistent with the

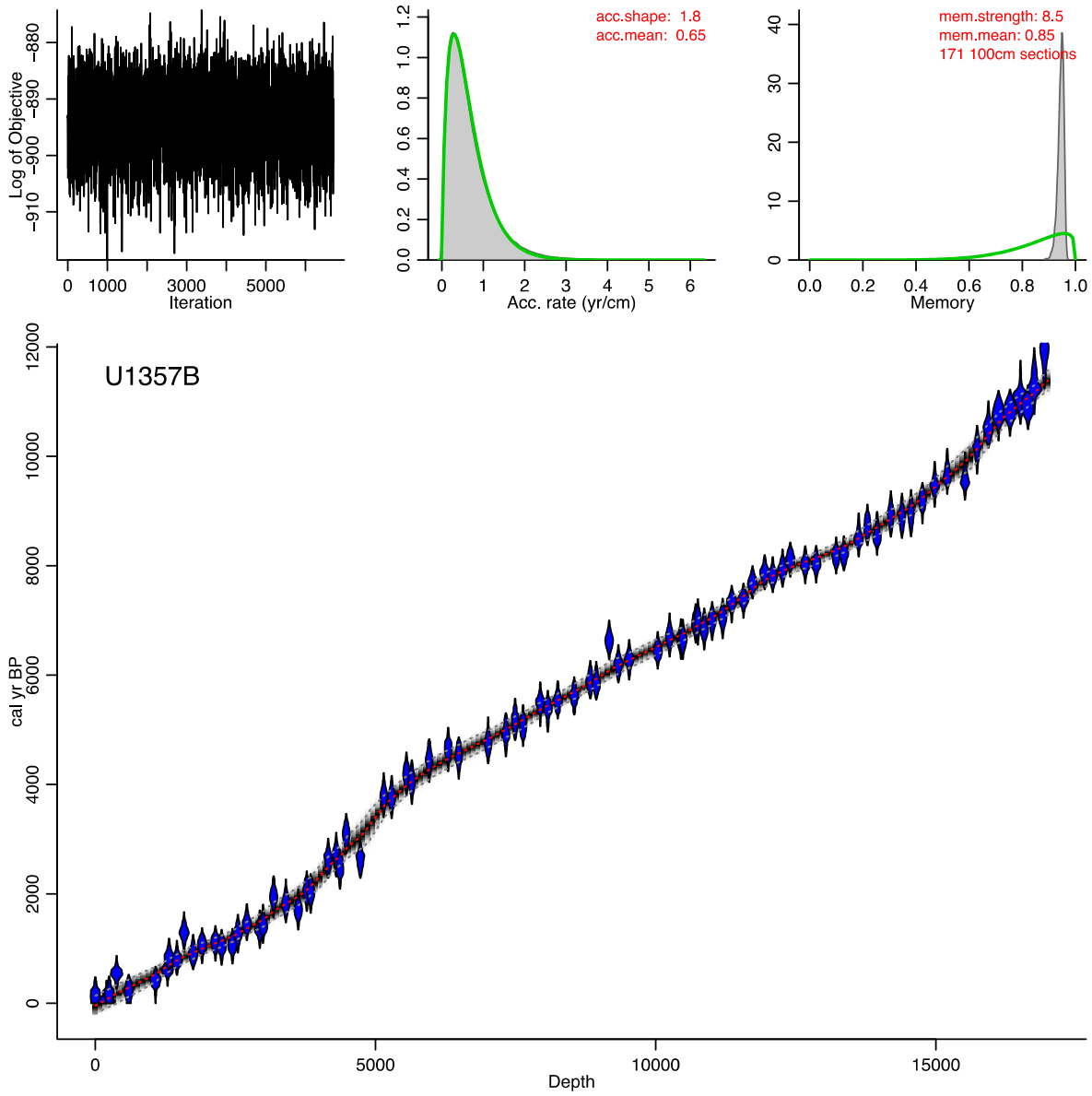



**Figure S2**. Age-depth plot of U1357B, using the default outputs from the BACON software. Upper panels show (from left to right): a stationary distribution of the Markov Chain Monte Carlo iterations; prior (green curve) and posterior (grey curve) distribution for the accumulation rate; prior (green curve) and posterior (grey curve) distribution for memory. Bottom panel shows the calibrated $^{14}$C dates (blue) and age depth model with 95% confidence intervals.

reservoir age in the Southern Ocean (Hall et al., 2010). Bulk organic carbon ages in the Antarctic are commonly compromised by reworking of older carbon in the sediment column (Andrews et al., 1999), which is compounded by extreme sediment starvation of post-LGM sequences in the Antarctic. However, due to extremely high input of autochthonous carbon associated with the Adélie Drift deposit, which is a predominately seasonally deposited

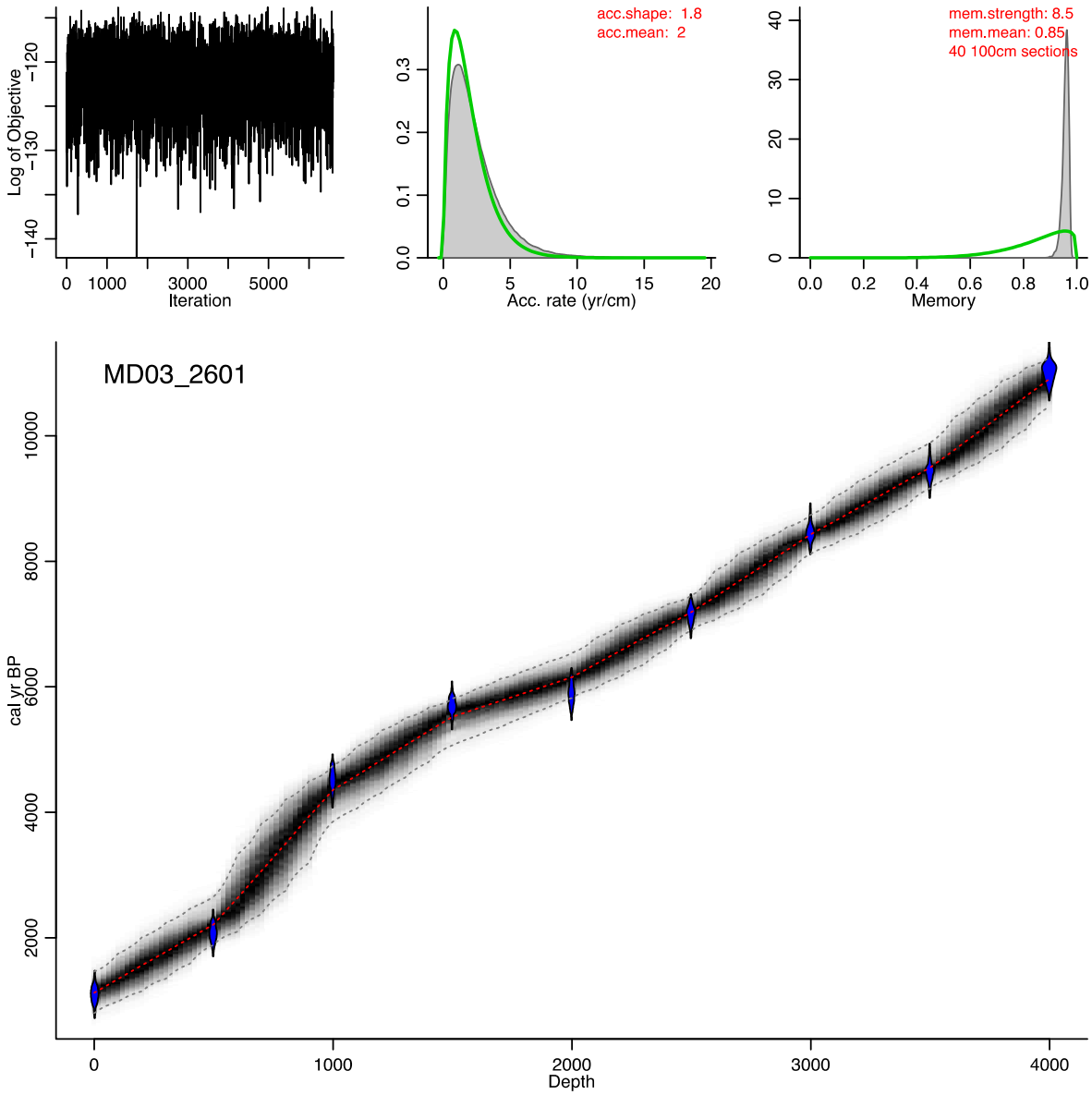



**Figure S3**. Age-depth plot of MD03-2601, using the default outputs from the BACON software. Upper panels show (from left to right): a stationary distribution of the Markov Chain Monte Carlo iterations; prior (green curve) and posterior (grey curve) distribution for the accumulation rate; prior (green curve) and posterior (grey curve) distribution for memory. Bottom panel shows the calibrated $^{14}$C dates (blue) and age depth model with 95% confidence intervals.

diatom bloom, this reworking is expected to be minimal at the U1357 site, and is only a potential issue at the base of the core (Unit II), due to increased proximity to glacial influences from the Adélie Land coast during the deglaciation (e.g. > 11.4 ka). This is supported by the radiocarbon ages, maintaining a strong stratigraphic order (within error),

relatively consistent sedimentation rates throughout the deposited interval, and core top ages that are consistent with the expected reservoir age.

We also recalibrated the age-model for MD03-2601 applying the BACON methodology using the $^{14}C$ dates presented in Crosta et al. (2008) (Fig. S3). This age model differs from that of Denis et al. (2009a), who discarded two $^{14}C$ ages bracketing the mid-Holocene (4.4 and 5.6 cal ka BP), on the basis of an inferred meteorite impact at ca. 15 m and correlated this to an event at 4 ka BP. We note that this impact correlation does not provide a unique absolute age constraint, with our revised age model instead indicating an age of 5.4 cal ka BP for this impact event. Critically, comparison between the age model for U1357B and the revised age model for MD03-2601 now indicates a strong similarity regarding changes in the sedimentation rates at ca. 4.5 ka and ca. 2 ka BP, indicating that both sites are influenced by similar depositional processes.

## S3. Justification for interpretation of proxy data

### S3.1 $\delta^2H_{FA}$

#### *S3.1.1. Source of fatty acids*

To best interpret the hydrogen isotope signal recorded by the $C_{18}$ FA, it is important to determine the most likely source these compounds are derived from, and thus the habitat in which they are produced. The $C_{18}$ FA, however, is known to be produced by a wide range of organisms and so we cannot preclude the possibility of multiple sources, especially in a highly diverse and productive region such as the surface waters of offshore Adélie Land. However, we can attempt to determine the most dominant producer(s), which will help us understand the main signal being recorded by the isotopes.

An analysis of the FAs within eight classes of microalgae by Dalsgaard et al. (2003) (compiling results from multiple studies) showed *Cryptophyceae, Chlorophyceae, Prasinophyceae* and *Prymnesiophyceae* to be the most dominant producers of total $C_{18}$ FAs. The *Bacillariophyceae* class, on the other hand, which includes the diatoms, were found to produce only minor amounts of $C_{18}$ FA, instead synthesizing abundant $C_{16:1}$ FAs. Thus, despite the water column offshore Adélie Land being dominated by diatoms, these are unlikely to be a major source of the $C_{18}$ FA within U1357B (Beans et al., 2008; Riaux-Gobin et al., 2011).

Of the four microalgae classes dominating $C_{18}$ production (Dalsgaard et al., 2003), species from the Chlorophyceae and Prymnesiophyceae classes have been observed within surface waters offshore Adélie Land after spring sea-ice break-up (Riaux-Gobin et al., 2011). Here, *Phaeocystis antarctica* of the Prymnesiophytes was found to dominate the surface water phytoplankton community (representing 16% of the phytoplankton assemblage), whereas Cryptophyceae spp. were found in only minor abundances (Riaux-Gobin et al., 2011). In the Antarctic, *Phaeocystis* is thought to be the most dominant producer of $C_{18}$ FAs (Dalsgaard et al., 2003), and thus is likely to be a key producer of the $C_{18}$ FA in U1357B samples.

To investigate this further, we measured compound-specific carbon isotopes of the $C_{18}$ FAs in U1357B samples, which gives an average $\delta^{13}C$ value of -29.8 ± 1.0 ‰ (n=85). Budge et al. (2008) measured a similar $\delta^{13}C$ value of -30.7 ± 0.8‰ from $C_{16}$ FAs derived from Arctic pelagic phytoplankton, while sea ice algae and higher trophic level organisms all had much higher $\delta^{13}C$ values (sea ice algae having values of -24.0 ± 2.4‰). Assuming similar values apply for the $C_{18}$ FA and for organisms within the water column at our site, this suggests that our $C_{18}$ FA is predominantly derived from pelagic phytoplankton.

Furthermore, $\delta^{13}C$ measurements of suspended particulate organic matter (SPOM) near Prydz Bay, East Antarctica by Kopczynska et al. (1995) showed that sites with high $\delta^{13}C$ SPOM values (-20.1 to -22.4‰) were characterized by diatoms and large heterotrophic dinoflagellates, whereas the lowest $\delta^{13}C$ SPOM values (-29.7 to -31.85‰) were associated with *Phaeocystis*, naked flagellates and autotrophic dinoflagellates. Wong and Sackett (1978) measured the carbon isotope fractionation of seventeen species of marine phytoplankton and showed that Haptophyceae (of which *Phaeocystis* belongs) had the largest fractionation of -35.5‰.

Therefore, based on the known producers of $C_{18}$ FAs, observed phytoplankton assemblages within modern surface waters offshore Adélie Land, and the $\delta^{13}C$ value of $C_{18}$ FAs in U1357B samples, as discussed above, we argue that the $C_{18}$ FA here is predominantly produced by *Phaeocystis* (most likely *P. antarctica*), but with potential minor inputs from other algal species such as Cryptophytes or diatoms.

*Phaeocystis antarctica* is a major phytoplankton species within the Antarctic, dominating spring phytoplankton blooms, particularly in the Ross Sea (Schoemann et al., 2005; DiTullio et al., 2000). It is known to exist both within sea ice and in open water (Tang et al., 2008) and has been observed in surface waters in great abundance following spring sea-ice break-up, at both coastal and offshore sites in Adélie Land (Riaux-Gobin et al., 2011).

Although a large proportion of organic matter produced in the surface water is recycled in the upper water column, the small fraction which is deposited in the sediment reaches the sea floor through large particles sinking from above as “marine snow”. This export production includes large algal cells, fecal pellets, zooplankton carcasses and molts, and amorphous aggregates (Mayer, 1993). In the Ross Sea, aggregates of *P. antarctica*, have been observed to

sink at speeds of more than 200 m $day^{-1}$, meaning they could reach deep water very quickly (Asper and Smith, 1999). In this way, a proportion of the lipid content of *P. antarctica* and other algae is transported and sequestered in the sediments.

Initial diagenesis is characterized by the preferential degradation of more labile organic compounds e.g. sugars, proteins, amino acids. Proportionally, lipids are relatively recalcitrant compared to other biological components and thus are more likely to be preserved as molecular biomarkers on geological timescales, even where the rest of the organism may be completely degraded. The final proportion of lipids that are preserved within sediments are affected by factors including the export production, $O_2$ content, residence time in the water column and at the sediment/water interface before deposition, molecular reactivity, formation of macromolecular complexes, adsorption to mineral surfaces and bioturbation (Killops and Killops, 2004; Meyers and Ishiwatari, 1993). Within lacustrine sediments, a significant shift in FA distribution has been shown to occur younger than 100 years due to early diagenesis, after which the FA distribution remains relatively unaffected by diagenesis (Matsuda, 1978), thus major changes are assumed to reflect primary environmental signals on longer timescales such as in our Holocene record. Due to the hyperproductivity of the surface waters offshore Adélie land, we assume the dominant inputs of the $C_{18}$ FA are from algal sources in overlying waters and upcurrent regions. Allochthonous inputs e.g. long-range aeolian transport of plant material are assumed to be minimal.

### *S3.1.2. Interpretation of hydrogen isotopes*

Compound-specific H isotopes of algal biomarkers are a well-used climate proxy in sediments throughout the Cenozoic (e.g. Pagani et al. (2006), Feakins et al. (2012)). Although diagenetic alteration, including H-exchange, is possible within sedimentary archives, this has shown to

be minimal in sediments younger than 20 Ma (Sessions et al., 2004). Furthermore, if H-exchange had occurred, we would expect $\delta^2H$ values between different FA chain lengths and closely-spaced samples to be driven towards homogeneity, yet large variability remains, suggesting this is not the case. Thus, we are confident that our measured H isotopes are indicating a primary signal throughout the Holocene.

The $\delta^2H$ value preserved in biomarkers is known to be correlated, but offset, with the $\delta^2H$ of the water from which the hydrogen was derived. Measured $\delta^2H$ can therefore be described as a function of either the $\delta^2H$ of the water source, or the fractionation occurring between source water and the lipid ($\varepsilon_{l/w}$) (i.e. vital effects), in which various environmental factors play a part (Sachse et al., 2012).

The main environmental factors controlling $\varepsilon_{l/w}$ are salinity and temperature, with which $\delta^2H$ increases by 1-4‰ per increase in practical salinity unit (psu; Sachse et al., 2012; Schouten et al., 2006) and decreases by 2-4‰ per degree C increase (Zhang et al., 2009), respectively. The $\delta^2H_{FA}$ record from Site U1357 displays an absolute range of ca. 123‰, and millennial to centennial scale variability with an amplitude of ca. 50‰, throughout the core. This would imply extremely large and pervasive variations in temperature (up to ca. 60°C) and salinity (up to 123 psu) if fractionation driven by either of these factors were the main control. One study has shown the salinity of present day Adélie shelf waters to vary between 34 and 34.8 psu (Bindoff et al., 2000), while tetraether-lipid based subsurface (50-200 m) temperature estimates from nearby Site MD03-2601 (about 50 km west of Site U1357) range from -0.17 to 5.35°C over the Holocene (Kim et al., 2010). Therefore, fractionation changes driven by temperature or salinity cannot be invoked as a major control on $\delta^2H_{FA}$ in the Holocene.

Thus, the most parsimonious explanation relates to changes in $\delta^2H$ of the water source (Sachse et al., 2012). In the Adélie Basin, the most apparent controls on this are advection, upwelling or inputs of isotopically depleted glacial meltwater. The $\delta^2H$ value within Antarctic glaciers is highly depleted relative to sea water due to the Rayleigh distillation process, leading to highly negative isotope values for precipitation over the continent.

The glacial meltwater originating from the Ross Ice Shelf is likely to combine ice precipitated throughout the Holocene and glacial period, and from both the East and West Antarctic Ice Sheets. However, as noted by Shackleton and Kennett (1975) in their first oxygen isotope record of the Cenozoic (see their Fig. 6), most of the ice that melts around the margin has been coastally precipitated (due to higher accumulation rates). Since ice precipitated further inland has a greater residence time (Shackleton and Kennett, 1975) and significantly lower accumulation rates it will contribute significantly less to this signal. Thus, the ice that contributed to a marine-based ice sheet collapse along this margin is best represented by average values of coastal ice dome records at a similar latitude to that which melted since the LGM (such as TALDICE and Siple Dome) than more southerly locations. Glacial to Holocene $\delta^2H$ values from TALDICE, located on the western edge of the Ross Sea in the East Antarctic, for example, vary between -276.2 and -330.3‰ (Steig et al., 1998) (converted from $\delta^{18}O$ values following the global meteoric water line (GMWL): $\delta^2H = 8.13\ (\delta^{18}O) + 10.8$), while values from Siple Dome on the eastern edge of the Ross Sea in the West Antarctic, vary from ca. -200 to -293‰ (Brook et al., 2005). Taking the average of these values as a rough estimate for the meltwater gives a $\delta^2H$ value of ca. -275‰. We note our calculations are based on averages of set time periods, which we expect would integrate ice of various ages - rather than extreme values which could relate to specific melt events of ice or biases to certain ages/regions. This seems reasonable - the isotopic signal of coastal surface waters masses

advected from the RIS to the Adélie land (as illustrated in Fig. 3) must integrate a range of source areas across the RIS and from the coast around to Adélie Land.

In comparison to the highly negative glacial ice isotope composition, sea surface water $\delta^{18}O$ measurements taken near the Mertz Glacier offshore Adélie Land (140-150°E) in summer 2000-2001 ranged between -0.47 and 0.05‰ (Jacobs et al., 2004), equivalent to $\delta^{2}H$ values of 6.9 to 11.2‰ (average = 9‰) following the GMWL. Thus, the two major hydrogen source pools (RIS glacial ice and ocean water) have highly contrasting isotope values, meaning inputs of upstream glacial ice could have a large effect on surface water $\delta^{2}H$ values in the Adélie Land region.

Taking the average glacial meltwater $\delta^{2}H$ value as -275‰ and the average modern Adélie surface water $\delta^{2}H$ value of 9‰ as end-members, and assuming a biosynthetic offset between the FA and sea water of 173‰ (see below), we can use a simple mixing model to estimate the percentage of glacial meltwater required in the surface waters to change the $\delta^{2}H_{FA}$ value to those recorded in U1357B samples. The most negative values occur during the early Holocene, 11.4 – 8.2 ka, averaging -214.2‰ (n=18) which, converted to a surface water value of -41‰, requires 17.6% of the surface water to be comprised of glacial meltwater. During this time, we argue that large volumes of meltwater were reaching the core site as local glaciers retreated, leading to intense surface-water stratification. Thus, a relatively high percentage of meltwater in the Adélie Land surface waters seems reasonable. During the mid-Holocene (5-4 ka), the average $\delta^{2}H_{FA}$ is very similar (-213.9‰, n=7), requiring 17.2% of the surface water to be derived from glacial meltwater. During this time, we argue for the dominant meltwater source as coming from the Ross Sea, and interpret this as a major period of glacial retreat (see section 4), during which large volumes of meltwater are injected into the

surface water and transported to the Adélie coast. In contrast, the most recent samples (last 0.5 ka, n=7), which includes the most positive value of the record, has an average $\delta^2H_{FA}$ value of -174.5‰. This brings the surface water value up to -1.5‰, which approaches modern measured values, and requires just 3.7% (e.g. well within uncertainties) of the surface waters in the Adélie Land to be glacial meltwater. However, it is also possible that the meltwater was dominated by more LGM-aged ice. In either case, perturbation of the exact isotopic values still indicate only significant changes in the flux of glacial meltwater can account for this signal. For example, the use of -330‰ (LGM values) for the ice input gives an estimate of 3% of the surface water being comprised of glacial meltwater for latest Holocene values, and 14.7% for pre 8 ka values. Taking -240‰ (Holocene values) for the ice input gives an estimate of 4% for latest Holocene values, and 20% for pre 8 ka values). Thus even with changing isotopic values though the deglacial, this signal of changing meltwater flux would still dominate. We note these are semi-quantitative estimates, as the salinity and temperature fractionation could reduce these estimates further (but cannot account for the whole signal).

Surface water $\delta^{18}O$ values around Antarctica (below 60°S), measured between 1964 and 2006, ranged from -8.52‰ to 0.42‰ (Schmidt et al., 1999), the most negative value having been measured proximal to the George VI Ice Shelf edge, where high melt rates have been observed (Potter and Paren, 1985). If converted to $\delta^2H$ using the global meteoric water line, these values give a $\delta^2H$ range of 83.4‰. Thus, our absolute $\delta^2H_{FA}$ range of 123‰ over the Holocene suggests a range of isotopically depleted meltwater inputs to our core site over this time that are 1.5 times greater than that occurring in different locations around the Antarctic in recent decades. This seems plausible given that geological evidence indicates large glacial retreat and ice mass loss occurred from the Ross Sea sector during the Holocene (McKay et al., 2016), meaning resultant changes in surface water are likely to be greater in magnitude

than observed around the Antarctic in recent decades. This assumes a relatively constant value for the isotopic composition of glacial meltwater, however, there is likely to be some variability due to the possibility of melting ice of different $\delta^2H$ values. But, as discussed above, the meltwater is best represented by the average values of the ice sheet, rather than extreme values, since it must (over the broad expanse of the RIS) include an integrated signal, and thus the actual variation in meltwater $\delta^2H$ will be significantly within the range of the end-members.

Although the biosynthetic fractionation of the $C_{18}$ FAs in U1357B is unknown, we assume that the offset with surface water remains relatively constant throughout the record. Sessions et al. (1999) showed the biosynthetic fractionation of hydrogen isotopes in the $C_{18}$ FA from four different marine algae to range from -189 to -157‰. If we take the average of these values of 173‰ and apply this as a biosynthetic offset to the youngest samples in U1357B (last 0.5 ka, n=7), which includes the most positive value of the record, gives an average $\delta^2H_{FA}$ value of -174.5‰. This brings the surface water value up to -1.5‰, which approaches modern measured values (Jacobs et al., 2004).

Furthermore, it is interesting to note that the biosynthetic offsets measured by Sessions et al. (1999) for the $C_{18}$ FA from different algal species have a total $\delta^2H$ range of 32‰. Although we cannot dismiss changes in the relative contribution of $C_{18}$ from different species in U1357B samples (and thus different biosynthetic fractionations), we argue this would only be a minor control on $\delta^2H$ compared to other influences. As a thought experiment, taking the above end-members for biosynthetic fractionation from Sessions et al. (1999), even with a 100% change in $C_{18}$ producer to a different algal source, this could only explain a quarter of the observed $\delta^2H$ change (i.e. 32‰ of 123‰).

Therefore, we interpret the first order control on $\delta^2H_{FA}$ at Site U1357 as inputs of isotopically depleted glacial meltwater. Such inputs are, in turn, influenced by the mass balance of the proximal or up-current glaciers and ice-shelves.

### *S3.2 Ba/Ti ratio excess as a meltwater pulse proxy*

Ba-based proxies (e.g., Ba/Ti or equivalent Ba/Al) in the Wilkes Land margin sediments have been commonly related to marine productivity (Presti et al., 2011), although studies in other pelagic environments indicate that they can also be sensitive to bottom current intensity (Bahr et al., 2014), meltwater (Plewa et al., 2006), and other processes (Griffith and Paytan, 2012). FESEM analysis and images at Site U1357 indicate the presence of biogenic barite (Fig. S4a), recognized by the elliptical morphologies and sizes between 1 to 3 μm (Paytan et al., 2002). Titanium is found associated with small heavy minerals (ilmenite) with angular and low sphericity shapes.

Along the entire record, Ba/Ti ratios show persistent periodic fluctuations with values between 0.1 and 2.7. Nevertheless, a marked enrichment can be observed at 4.5 ka reaching Ba/Ti ratio values over 36.1 (Fig. 4.2). Pore water analysis indicates that the carbon dioxide (methanic) reduction zone (CRZ) is reached just few cm near sea floor and the upper 20 m already contain sulfate-free interstitial waters (Expedition 318 Scientists, 2011). Observed geochemical conditions indicate that some Barite dissolution could be expected, but there is no diagenetic barite that could justify the obtained enrichment. In addition, at the enriched interval we did not observe any lithological change or enrichment in other elements (e.g., Si). The influence of aeolian dust or fluvial input on Ba input can also be discarded in the glaciated Wilkes Land margin. In the same way, Ba concentration in sea-ice is considered null

because on an annual cycle, sea ice does not constitute a net source or sink of these species to the underlying seawater (Thomas, 2011).

Furthermore, FESEM imaging detected biogenic barite during intervals were the Ba/Ti excess occurs (Fig. S4) pointing to an increase in productivity. This may be driven by water column stratification or greater nutrient availability. This interpretation is coherent with other paleoproductivity reconstructions in this area, in particularly peaks in $^{230}$Th-normalized fluxes of biogenic silica (BSi) and organic carbon content recorded in nearby core MD03-2601 (Denis et al., 2009b) (when using the recalibrated age-model – see S2).

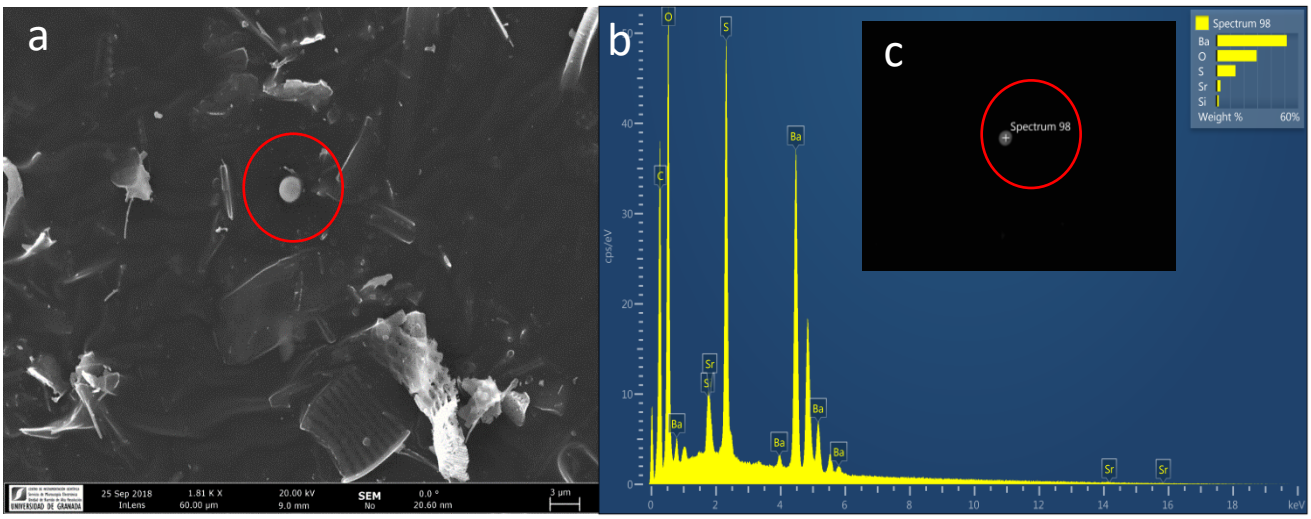



**Figure S4.** Authigenic marine barite (red circle, size > 300nm) observed in Ba/Ti enriched interval (sample U1357B-8H-2A 141-143; age: 4,430 cal yr) a) SEM image obtained with secondary electrons with Inlens detector at 20 kV b) SEM-EDX spectrum (analyzed spot marked with a white cross in image c)) showing barite composition ($BaSO_4$) c) Same barite shown in a backscattered electron (BSE) mode by AsB detector at 20 kV.

### *S3.3 Grain size*

Grainsize analysis was conducted on samples paired with lipid biomarker samples in Unit I. Unit I represents the onset of modern deposition, representing the same lithology found at the site today, and the underlying stratigraphy is discussed in the main text. Between ca. 11.4 and 8 ka, U1357B has a relatively high terrigenous component (i.e. high Natural Gamma

Radiation (NGR) content and low BSi%; Fig S5). The grain size distribution contains coarse tails of fine (125-250 μm) to medium sands (250-500 μm), but only one sample contains coarse sands (>500 μm) that may represent ice-berg rafted debris (IBRD). However, terrigenous content and IBRD is more common in the underlying Unit II, which is interpreted to represent a true "calving bay environment" (Escutia et al., 2011). Shipboard description of the core facies found the presence of small isolated facetted and striated pebbles (lonestones) in Unit II (Escutia et al., 2011), which is supportive of an iceberg component to sediment supply, but these are largely absent in Unit I. The fine grained sands and muds have a distribution with similar modes to overlying intervals, albeit with an increase in the size of the coarse silt and very fine sand modes. The subtle increased sorting up core between ca. 11.4 and ca.8 ka (from very poorly to poorly sorted, Fig. S5) is consistent with an increasingly more distal setting, with less potential for a glacial grounding line sediment supply (Powell and Domack, 1995; McKay et al., 2009). This interval is interpreted to reflect the final post-LGM retreat of local EAIS outlet glacier grounding lines from a proximal (less sorted, more IBRD) to more distal setting (better sorted, less IBRD) from the site, although we note a much larger shift occurs at the Unit I/II boundary at 170.25 mbsf (ca.11.4 ka) (Escutia et al., 2011) and dominant sediment supply from local outlet glaciers probably ceased at this earlier time. It is likely this distal setting was close to the modern day grounding line, as the Dumont d'Urville Trough is overdeepened between Site U1357 and the modern day grounding line, and this bathymetry configuration is inherently unstable for marine-based ice sheets (Thomas and Bentley, 1978; Mackintosh et al., 2014).

Today, Adélie Land glaciers are inferred to have relatively clean basal layers due to the solid bedrock (Kleinschmidt and Talarico, 2000), and distal polar glacimarine settings are usually sediment starved and provide very low inputs of terrigenous sediments (Powell and Domack,

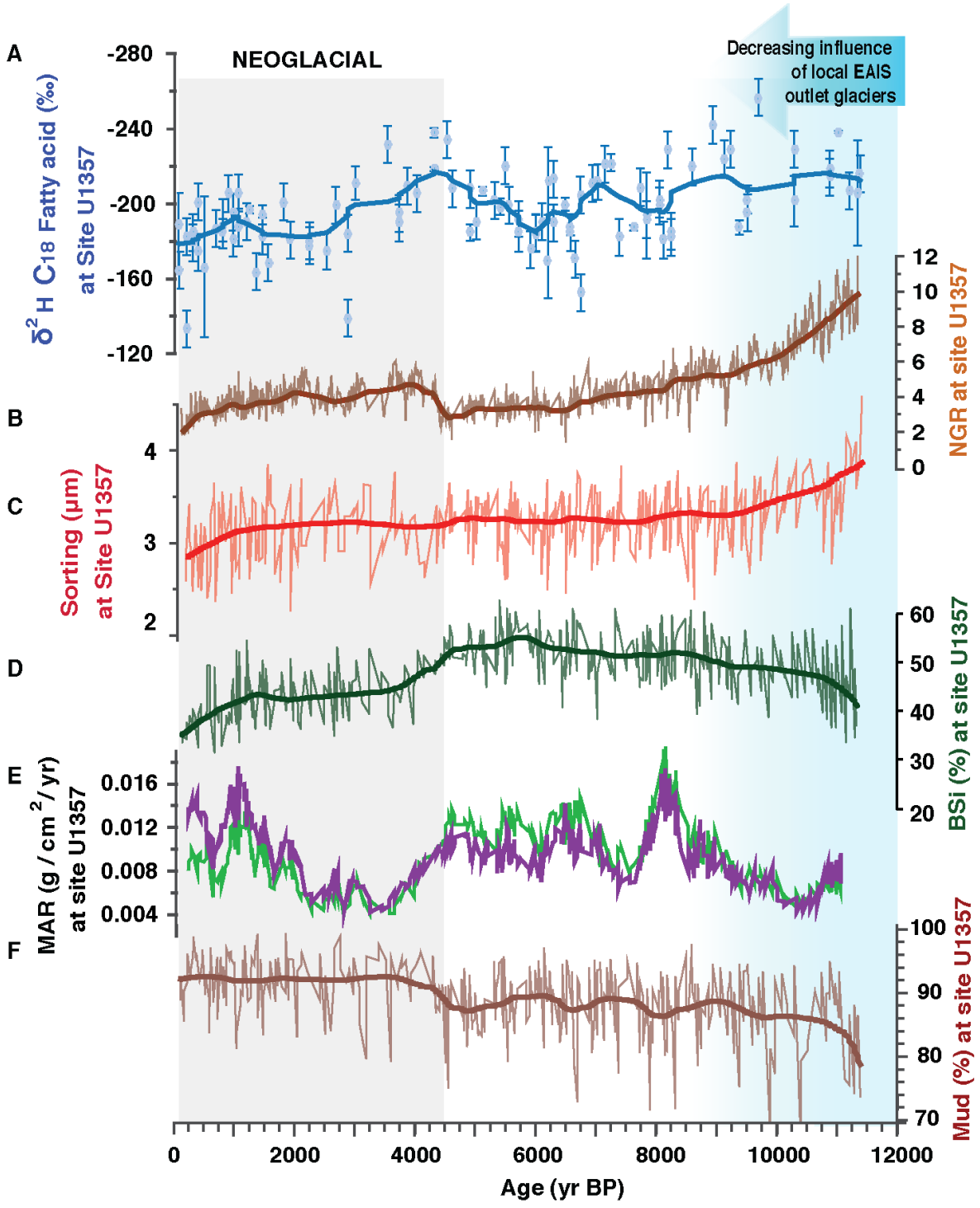



**Figure S5** Holocene Adélie Land proxy records from IODP Site U1357 a) $C_{18}$ fatty acid $\delta^2H$ (errors bars based on replicate analyses), heavy line is a robust locally weighted scatterplot smoothing (rlowss) b) Natural Gamma Radiation, heavy line is a rlowss c) grain sorting (μm) calculated following Folk and Ward (1957), heavy line is a rlowss d) Percentage of biogenic silica (BSi), heavy line is a rlowss; e) Mass accumulation rates of biogenic (green line) and terrigenous (purple line) material f) Percentage of mud, heavy line is a rlowss.

1995; McKay et al., 2009). There are also no large proglacial fans evident at the mouths of these glaciers (Beaman et al., 2011) and consequently, direct sediment discharge from the Mertz and Ninnis Glaciers is unlikely to be of significant quantity to sustain dense overflows delivering sediment over the Adélie Bank and into the Dumont d'Urville Trough. Therefore, the release of terrigenous material through glacial melting is low (to absent) when glacier activity is steady and distal from the site, but is anticipated to increase with increased proximity to the glacier front or with enhanced dynamic ice discharge (which may occur either during a retreat or advance), which would be associated with an increase in IBRD from local outlet glaciers. We note evidence for proglacial fan deposition and IBRD is lacking throughout Unit I (post 11.4 ka).

Between 9 and 4.5 ka, mass accumulation rates (MARs) (both biogenic and terrigenous; Fig. S5) are relatively high, albeit with millennial scale variability. However, the mean grain size and sorting of the terrigenous material is relatively stable throughout the entire interval, and as with the rest of Unit I there is an almost complete lack of IBRD. This suggests that sediment input from grounding line processes were also minimal through this time. Based on the drift morphology (Fig S6), and the prevailing easterly flow of the Antarctic Coastal Current, this interval is interpreted to be the result of sediment advection to the site from the east as residual ice retreated from the bathymetric highs in the region. Diatom frustules and sponge spicules are mainly in the 16 to 63 μm range, much of which is maintained in suspension by weak currents (a few $cms^{-1}$; Dunbar et al., 1985). The greater area of open water for primary production during the summer, combined with an open pathway for advection of biogenic matter from the MGP (Fig. 4.1) can thus explain the significant rise in linear sedimentation and mass accumulation rates for both biogenic and terrigenous material. Most of the terrigenous material after ~8 ka is proposed to have been primarily eroded off the Adélie

Bank by westward flowing currents into the Adélie drift where sediment would have settled out from suspension. Terrigenous sediment younger than 8 ka in this drift is almost entirely finer than 125 μm, while Dunbar et al. (1985) revealed that surface sediments on shallow banks have a grain size distribution that generally exceeds 125 μm. This supports our interpretation that the majority of the terrigenous material in U1357B is winnowed from these banks by bottom currents. The size of the material winnowed implies that maximum current velocities in the region are greater than 18-20 $cms^{-2}$, the minimum velocity required to transport fine sand by intermittent suspension and suspension in poorly sorted glacimarine settings (Singer and Anderson, 1984; McCave and Hall, 2006).

The complete lack of medium to coarse sand in the grainsize distributions of Unit I (<11.4 ka), and from visual observation of the core, that may represent IBRD may be the consequence that icebergs calved from large ice shelves and ice tongues, such as the RIS and Mertz Glacier Tongue, are advected into the region via the Antarctic Coastal Current but usually lack basal debris. While the lack of IBRD could in part be explained as the consequence of the widespread development of the RIS in the Holocene (McKay et al., 2016), it could also be due to the Adélie and Mertz Banks (and Mertz Glacier Tongue) acting to shield Site U1357 from large icebergs passing over the site, as icebergs would have become grounded on the bathymetric highs and deflected north (Massom et al., 2001; Beaman et al., 2011). Notably, this lack of IBRD further supports a lack of shifting glacial dynamics and calving of sediment-laden icebergs from the smaller local Astrolabe and Zéléé outlet glaciers through this time.

There is a rapid increase in mud content at 4.5 ka coincident with a reduction in both the biogenic and terrigenous MARs, although the terrigenous MAR curve shows higher

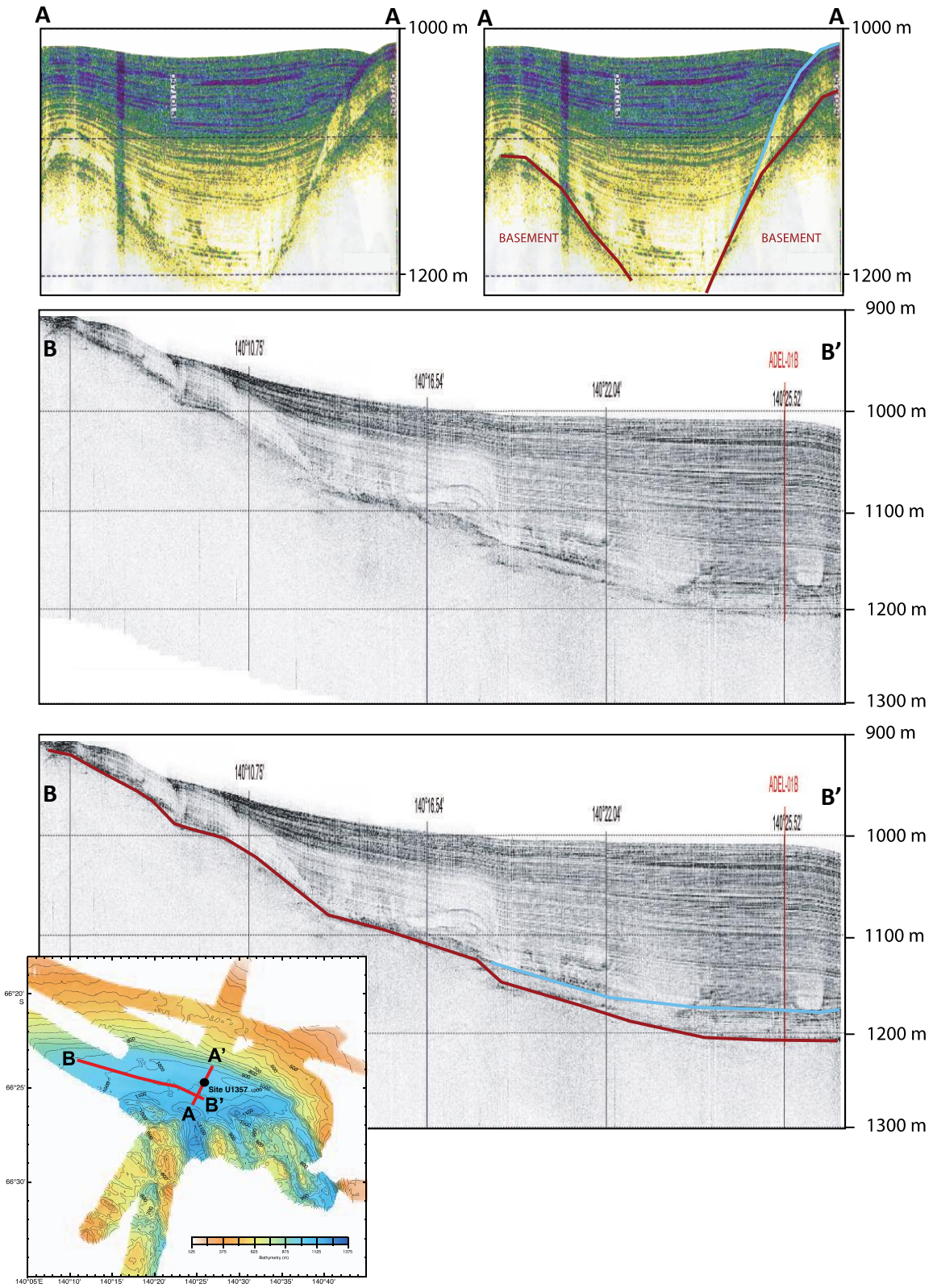



**Figure S6** 3.5 kHz seismic profile of the Adélie drift. Top: South (A) to north (A') profile, showing early Holocene (inferred to be ~11-8.2 ka) strata downlapping on top the basement highs (blue reflector and below). This is overlain by onlapping strata (blue reflector and above). Middle and Bottom: West (B) to East (B') profile, showing that in the depocentre of the basin, the pre-8.2 strata has a different geometry to overlying strata (onlapping onto the northern bank of the Dumont D'Urville Trough), suggesting a supply from the south, while overlying strata form a drift deposit that is thickest on the northern flank of the trough, and infers a drift deposit morphology that is aligned with the flow of easterly Antarctic Coastal Current.

accumulation rates than the biogenic MAR curve (Fig. S5). Hence, less material is being advected to the site, and the maximum current strength acting to winnow and advect material from the Adélie Bank into the Dumont d'Urville Trough is reduced. A reduction in maximum current strength could potentially be explained by more extensive sea ice over the site, which would act to reduce wind stress on the ocean surface and thus the maximum strength of the easterly flow, despite enhanced zonal easterly winds that are predicted with a cooler Antarctic climate (Shin et al., 2003; DeConto et al., 2007).

A final consideration is that aeolian contribution of terrigenous material is known to be of importance in Antarctic coastal areas affected by katabatic winds (Atkins and Dunbar, 2009; Chewings et al., 2014). However, windblown sediment is usually well-sorted, and combined with the lack of exposed sediment in Wilkes Land, and the distance of the core site from the coast, input of aeolian sediment into the ocean from melting sea ice is likely to be a relatively minor component of the sediment population relative to the suspended sediment load derived from the local banks and pelagic processes.

**S3.4. Highly-branched isoprenoids (HBI)**

Several recent studies have highlighted the strong potential of the HBI biomarkers along the Antarctic coast as a robust proxy of sea ice extent. Indeed, it has been shown that the di-unsaturated HBI lipid (i.e. diene II or $C_{25:2}$ alkene) is only synthesized in the modern Antarctic waters by sea ice-associated diatoms (Belt et al., 2016; Massé et al., 2011; Smik et al., 2016). The tri-unsaturated HBI lipid (i.e. triene III or $C_{25:3}$) is in contrast strictly produced by open water diatom species, which have been found to be in highest abundance in the marginal ice zone (Smik et al., 2016). Thus, the calculated diene/triene ratio is a reliable tracer to qualitatively estimate the sea ice extent (sea ice vs open water conditions). As previously

applied in various Antarctic coastal sediments during different period of time (Etourneau et al., 2013; Collins et al., 2012; Barbara et al., 2010), the diene/triene ratio was successfully used to reconstruct the past sea ice history around Antarctica. In particular, it has been shown that the HBIs were not significantly affected by (i) changes in sources (glacial ice vs sea ice), as the diatoms producing the HBIs strictly grow in relation with sea ice (under or at the edge) (ii) bacterial degradation (Robson and Rowland, 1988) or (iii) rapid sulfurization under anoxic conditions (Sinninghe Damsté et al., 2007). Absolute concentrations of the HBI diene and triene compounds are shown in Fig. S7.

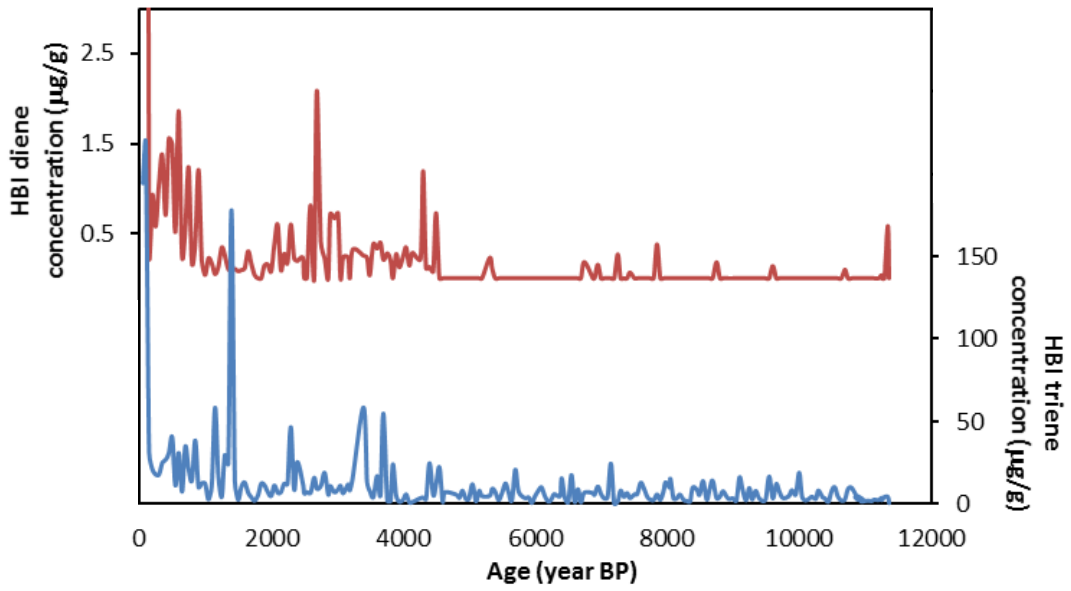



**Figure S7** Absolute concentrations of highly branched isoprenoids (HBIs) measured in U1357B.

## S4. Ross Sea deglaciation history

Our hypothesis is that large (cold) ice shelf cavity development south of Ross Island after ca. 6.5 and 4.5 ka was the driver of major changes in the surface water properties of the Ross Sea and offshore Adélie Land. The history of grounding line retreat to the north of Ross Island is

relatively well-constrained, particularly in the Western Ross Sea, and the loss of residual ice caps appears to be largely complete by ca. 7 ka to the immediate north of Ross Island (Anderson et al., 2014; McKay et al., 2016; Hall et al., 2004; Jones et al., 2015). Indeed, a phase of isotopically depleted glacial melt-water is apparent at Site U1357 between 8 and 7 ka and could be sourced from the Ross Sea, reconciling our model with these chronologies. Prior to 8 ka, any meltwater signal in U1357B is potentially influenced by local glacier retreat, based on the caveats noted earlier in the grainsize and geophysical datasets (Section 3c), although we note a dominant Ross Sea contribution to this signal is possible.

To the south of Ross Island, we use the ice sheet retreat model of McKay et al. (2016) to help constrain the pattern and rate of retreat of the grounding line to the south of Ross Island. This was a higher resolution simulation of the Golledge et al. (2014) model that applies a lower mantle viscosity that is more consistent with the West Antarctic sector of the continent, where the majority of ice loss occurred following the LGM. This allowed for more rapid glacio-isostatic adjustment, slowing down the marine ice sheet instability process, and helped significantly improve data model mismatches to the north of Ross Island. This model suggests that due to the bathymetric configuration of the Ross Sea, Holocene ice sheet retreat to the south of Ross Island is likely to be rapid and would have been completed by the mid-Holocene (ca. 5 ka).

Recent studies are converging on a rapid phase of retreat of the WAIS to its modern-day position (and potentially further south, followed by a short duration readvance of the grounding line) during the mid-Holocene (Hein et al., 2016; Spector et al., 2017; Kingslake et al., 2018). $^{10}$Be exposure ages of erratics in coastal nunataks at the confluence of the Mercer Ice Stream and Reedy Glacier indicate 105 m of ice sheet deflation since 6.8 ka, with only 40

m of this after 4.9 ka (Todd et al., 2010), indicating a rapid phase of retreat between 6.8 ka and 4.9 ka. More recent deflation profiles for the Beardmore Glacier (84°S) and Scott Glacier (86°S) regions show sustained thinning between ca. 9 and 8 ka, but the Scott Glacier experience a second phase of rapid thinning of ca. 200 m between 6.8 and 5.3 ka (Fig. 4.2), followed by a slower rate of thinning of between 5.3 and 3.5 ka of ca. 100 m. Ages younger than this, near the modern surface are thought to be related to surface ablation rather than dynamic thinning. This suggests that the grounding line was at its modern location by ca. 3.5 ka (Spector et al., 2017). Glaciological evidence from radar profiles suggests the development of divide flow on Roosevelt Island occurred sometime between 3 and 4 ka BP, suggesting that the ice sheet thickness was at least 500 m thicker until this time (Conway et al., 1999).

Combined, these lines of evidence suggest the majority of grounding line retreat south of Ross Island occurred after 8 ka, with a sustained retreat occurring after 6.8 ka, consistent with the timing of the glacial meltwater feeding the U1357 site. Most evidence suggest thinning of the outlet glaciers was rapid, and the grounding line was near its modern day position sometime between 4.5 and 3.4 ka. A slighter younger age (e.g. 3 – 3.5 ka) for final establishment of the modern grounding line position is consistent with our interpretation, as we suggest a threshold for ice shelf cavity development was reached at 4.5 ka, whereby ice shelf-ocean interactions lead to the initiation of the negative sea ice feedbacks. However as discussed in the main text, this negative feedback may have acted to slow and stabilise retreat by ca. 3 – 3.5 ka, and values of $\delta^2H$ do not stabilize in U1357B until ca. 3 ka. Thus we infer this was the consequence of the final cessation of significant glacial meltwater source from Ross Sea retreat, noting the timing difference and the range of numerous uncertainties associated with these records, including radiocarbon reservoir ages and production rates for the cosmogenic data.

## S5. Data-Model mismatch

Comparison of sea ice data from the Adélie region (presented in this study), with model output for sea ice thickness and extent from TraCE-21k simulations, indicates a clear mismatch between the observational data and model output over the Holocene (Fig. S8). The rapid mid-Holocene increase in sea ice, recorded at Site U1357 and other sites in the Antarctic coastal zone (Fig. S8c, d), is not seen in the model simulations, which instead indicate a sharp decline in sea ice extent and thickness around the Antarctic and in the Adélie region after ca.

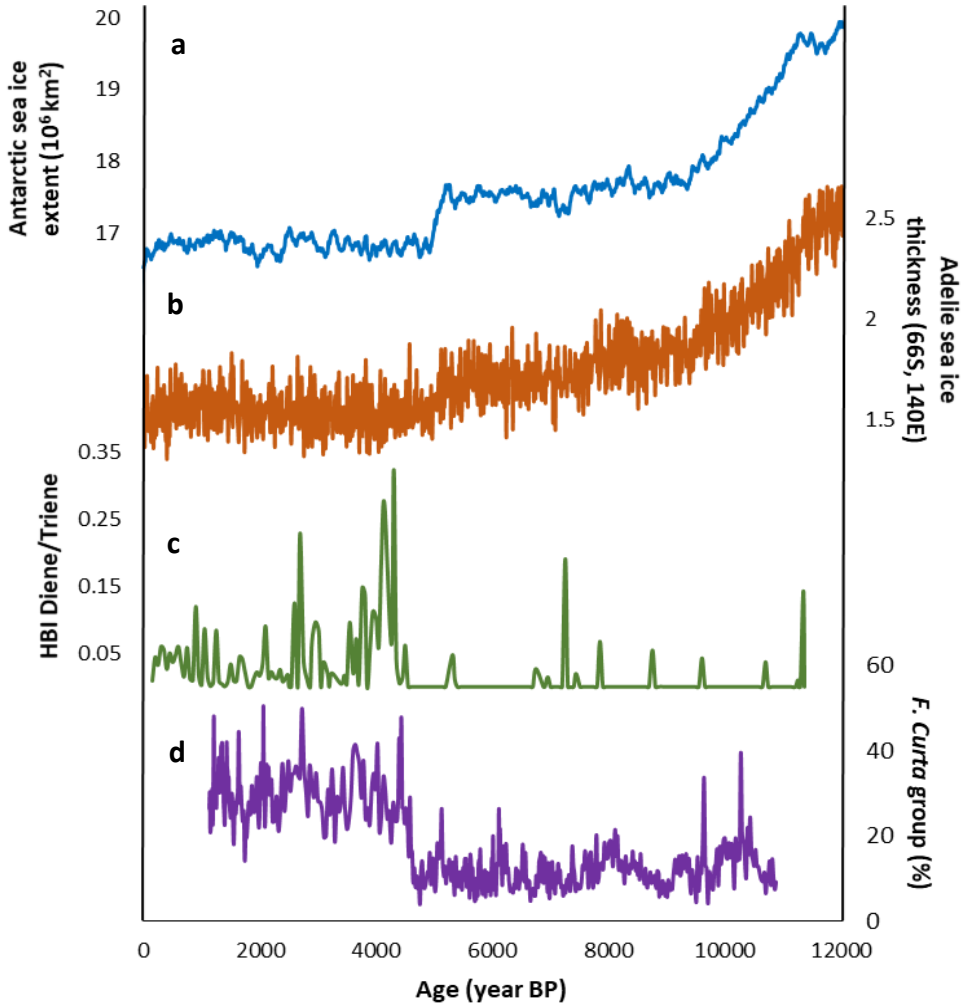



**Figure S8** Comparison of sea ice data from the Adélie region with TraCE-21k simulations a) Antarctic sea ice extent ($10^6$ km$^2$) from TraCE-21k b) Adélie sea ice thickness (66°S, 140°E) from TraCE-21k c) Ratio of the di-unsaturated HBI (C25:2; Diene) and the tri-unsaturated HBI isomer (C25:3; Triene) at Site U1357 d) *Fragilariopsis curta* group relative abundances from MD03-2601.

5 ka (Fig. S8a, b). The Community Climate System Model (CCSM3) used in the simulations lacks a dynamic ice sheet or, instead using a constant prescribed meltwater flux of 1.12 m $ka^{-1}$ from the Antarctic which finishes at 5 ka, which can likely explain the simulated sea-ice decline at ca. 5 ka. Furthermore, it does not incorporate ice-ocean coupling or ice shelf cavities (Collins et al., 2006). We have shown that these processes have an important role on sea ice production and thus are required within models to capture the coupled response between ice sheets and the ocean. We note that some models, such as LOVECLIM (Renssen et al., 2010), do simulate a gradual sea-ice increase and cooling trend in the late Holocene, however the timing (gradual) and magnitude (subtle) of sea-ice trends do not match the abrupt and large changes seen in the proxy data.

## Chapter 5

# USE OF FATTY ACID CARBON ISOTOPES AS A PALAEOPRODUCTIVITY PROXY IN A HIGHLY PRODUCTIVE ANTARCTIC POLYNYA ENVIRONMENT


## Abstract

The Antarctic coastal zone is an area of high primary productivity, particularly within coastal polynyas where large phytoplankton blooms have been observed along with the drawdown of $CO_2$. Reconstruction of primary productivity changes over time can help understand the role of these areas as sinks for atmospheric $CO_2$ and what drives them. Here we investigate the potential for using carbon isotopes of fatty acids in marine sediments as a proxy for primary productivity. We do this using a highly resolved sediment core from off the coast of Adélie Land spanning from ca. 1587 to 2000 C.E and look at the concentrations and carbon isotopes of fatty acids along with other proxy data from the core. We discuss the different possible drivers of fatty acid $\delta^{13}C$ and argue that $C_{24}$ fatty acid $\delta^{13}C$ is predominantly reflecting productivity in open water environments, while $C_{18}$ fatty acid $\delta^{13}C$ is reflecting productivity in the marginal ice zone.


## 5.1 Introduction

Coastal polynyas within the Antarctic margin are areas of very high primary productivity during the spring and summer months. Significant amounts of $CO_2$ can be drawn down from the surface waters through photosynthesis (Arrigo and van Dijken, 2003) and, where this organic matter sinks to the sea floor, export carbon to the deep ocean (Sigman and Boyle, 2000). Reconstructions of changes in $CO_2$ drawdown over time are required to get a better understanding of the strong $CO_2$ coupling between the atmosphere and ocean, what drives it, and their potential importance as sinks for anthropogenic $CO_2$. Here we investigate the use of

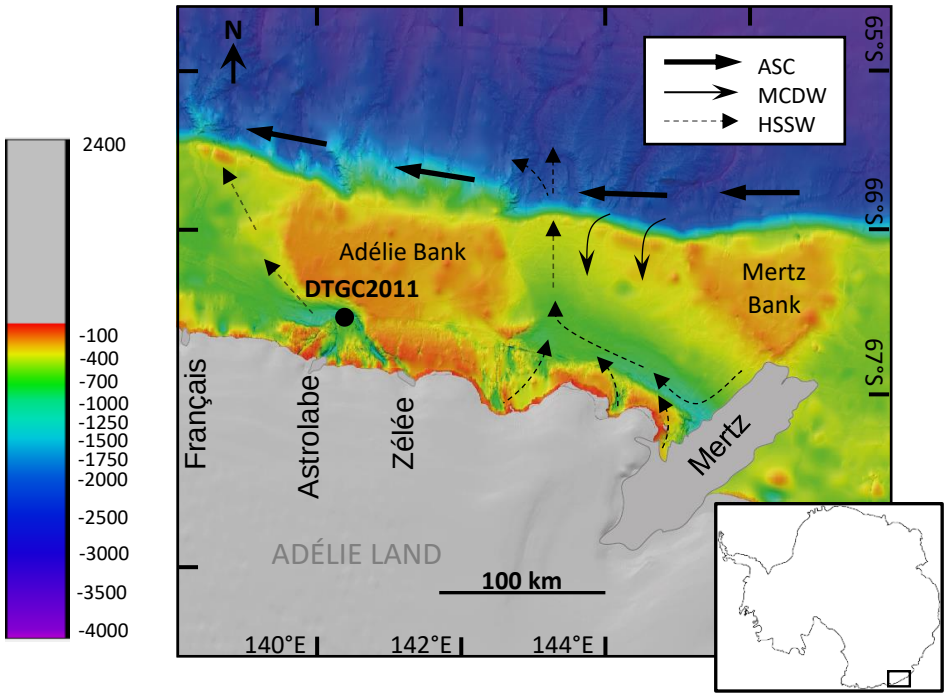



**Figure 5.1** Location of Site DTGC2011 on bathymetric map of the Adélie Land region (modified from Beaman et al., 2011), indicating positions of the main glaciers (prior to Mertz Glacier Tongue collapse in 2010) and pathways of the main water masses affecting the region: Antarctic Slope Current (ASC), Modified Circumpolar Deep Water (MCDW) and High Shelf Salinity Water (HSSW).

compound specific carbon isotope analysis ($\delta^{13}C$) of algal fatty acids (FAs) in marine sediments as a proxy for reconstructing primary productivity in a polynya environment. We do this using sediments from core DTGC2011 recovered from offshore Adélie Land, East Antarctica spanning the last ca. 460 years. In order to understand the signal recorded by the FAs, we estimate the most likely biological source of these compounds and the habitat and season of production. Moreover, we compare downcore changes in FA concentrations and $\delta^{13}C$ with other proxy data from the same core.

## 5.2 Materials and Methods

Sediment core DTGC2011 was recovered from the Dumont D'Urville Trough off the Adélie Land Coast, East Antarctica (Fig. 5.1). The core extends 460 cm and has been dated using radiocarbon and $^{210}Pb$ and spans roughly 1548 to 2000 C.E. The age model has been described in Campagne (2015) and indicates that the sedimentation rate was approximately

1cm per year and relatively stable throughout. One hundred and thirty-five sediment samples were taken for organic geochemical analyses, sampled at 1 cm intervals in the top 50 cm, 2 cm intervals between 50 and 100 cm, and 5 cm intervals until 458 cm.

FAs were extracted at the University of Birmingham, then identified using an Agilent gas chromatograph (GC) coupled to an Agilent mass selective detector (GC-MS) before quantifying their concentrations by GC – flame ionization detector analysis with the inclusion of an internal standard ($C_{19}$ alkane) of known concentration for quantification. Carbon isotopes were measured with an Isoprime 100 isotope ratio-mass spectrometer coupled to an Agilent gas chromatograph-flame ionization detector and a GC5 furnace (see Chapter 2 for more details). Errors are based on the standard deviation of duplicate measures and are all within 0.26‰.

### 5.3 Fatty acids within DTGC2011

Analysis by GC-MS identified seven dominant FAs within the DTGC2011 samples (Fig. 5.2). These have carbon chain lengths of $C_{16}$ to $C_{26}$ and only the saturated forms (i.e. no double

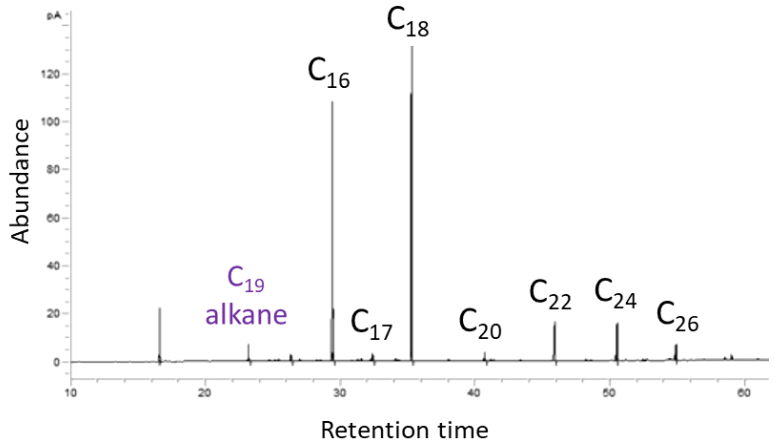



**Figure 5.2** Typical chromatogram of the fatty acid fraction of DTGC2011 samples. Fatty acids are labelled according to their carbon number. An internal standard ($C_{19}$ alkane), which was used for quantification of fatty acids, is labelled in purple.

bonds) were identified. These are predominantly even chain length FAs, with only minor amounts of the $C_{17}$ compound measured (Gilchrist, 2018).

### 5.3.1 Fatty acid concentrations

Down core analysis of FA concentrations reveals clear groupings in concentration changes. In the upper part of the core (ca. 3 – 90 cm depth), equivalent to ~78 years, all FA compounds show a similar pattern, with elevated concentrations, broadly decreasing down-core (Fig. 5.3). Below this, however, two groups clearly diverge. These can be broadly divided into short-chained fatty acids ($C_{16}$ to $C_{20}$; SCFAs) and long-chained fatty acids ($C_{22}$ to $C_{26}$; LCFAs). Within these groups, the concentrations of different compounds show similar trends, but the two groups (SCFAs vs LCFAs) show different trends to each other (Gilchrist, 2018). This is confirmed by $R^2$ values calculated for the linear regression of concentrations of each FA against each other throughout the core (Table 1; n = 135, p <0.001). Correlations between the SCFAs have $R^2$ values between 0.97 and 0.99, while $R^2$ values of LCFAs range between 0.88 and 0.95. Between the two groups, however, $R^2$ values are all lower, ranging between 0.50 and 0.77.

**Table 5.1** $R^2$ values for fatty acid concentrations throughout core DTGC2011. Values are colour coded according to the key on the left. Black border denotes correlations within each group.

| | | $C_{16}$ | $C_{17}$ | $C_{18}$ | $C_{20}$ | $C_{22}$ | $C_{24}$ | $C_{26}$ |
|---|---|---|---|---|---|---|---|---|
| 0.9-0.99 | $C_{16}$ | | 0.97 | 0.98 | 0.97 | 0.72 | 0.53 | 0.58 |
| 0.8-0.89 | $C_{17}$ | 0.97 | | 0.96 | 0.96 | 0.70 | 0.52 | 0.56 |
| 0.7-0.79 | $C_{18}$ | 0.98 | 0.96 | | 0.99 | 0.69 | 0.50 | 0.55 |
| 0.6-0.69 | $C_{20}$ | 0.97 | 0.96 | 0.99 | | 0.77 | 0.59 | 0.64 |
| 0.5-0.59 | $C_{22}$ | 0.72 | 0.70 | 0.69 | 0.77 | | 0.88 | 0.95 |
| | $C_{24}$ | 0.53 | 0.52 | 0.50 | 0.59 | 0.88 | | 0.90 |
| | $C_{26}$ | 0.58 | 0.56 | 0.55 | 0.64 | 0.95 | 0.90 | |

These distinct groupings suggest that compounds within each group (SCFAs and LCFAs) likely have a common precursor organism or group of organisms, but the two groups themselves have different producers from each other. These producers may in turn thrive during different seasons or within different habitats and thus, the isotopic composition of compounds from these different groups may record different environmental signals.

$R^2$ values were also calculated for samples below 25 cm only, to remove correlations associated with preservation changes in the top part of the core (discussed below). Although the $R^2$ values are not quite as high, they broadly confirm these groupings, with the $R^2$ values generally being greater within the two groups (n = 73). $R^2$ values range from 0.93 for the $C_{18}$ with $C_{20}$, down to 0.07 for the $C_{18}$ and $C_{24}$ (Table 2).

**Table 5.2** $R^2$ values for fatty acid concentrations in core DTGC2011 below 25 cm only. Values are colour coded according to the key on the left. Black border denotes correlations within each group.

| |
|---|
| 0.8-0.99 |
| 0.6-0.79 |
| 0.4-0.59 |
| 0.2-0.39 |
| 0.0-0.19 |

| | $C_{16}$ | $C_{17}$ | $C_{18}$ | $C_{20}$ | $C_{22}$ | $C_{24}$ | $C_{26}$ |
|---|---|---|---|---|---|---|---|
| **$C_{16}$** | | 0.74 | 0.87 | 0.80 | 0.24 | 0.09 | 0.21 |
| **$C_{17}$** | 0.74 | | 0.73 | 0.72 | 0.28 | 0.08 | 0.19 |
| **$C_{18}$** | 0.87 | 0.73 | | 0.93 | 0.21 | 0.07 | 0.20 |
| **$C_{20}$** | 0.80 | 0.72 | 0.93 | | 0.39 | 0.15 | 0.31 |
| **$C_{22}$** | 0.24 | 0.28 | 0.21 | 0.39 | | 0.46 | 0.68 |
| **$C_{24}$** | 0.09 | 0.08 | 0.07 | 0.15 | 0.46 | | 0.42 |
| **$C_{26}$** | 0.21 | 0.19 | 0.20 | 0.31 | 0.68 | 0.42 | |

The $C_{18}$ and $C_{24}$ FAs are the most abundant compounds within the SCFA and LCFA groups, respectively, and also the least correlated with each other both in the whole core ($R^2 = 0.5$) and below 25 cm ($R^2 = 0.07$), which suggests they are the most likely to be produced by different organisms. Furthermore, these two compounds yielded the highest quality isotope measurements, due to their greater concentrations, clean baseline and minimal coeluting peaks

(Fig. 5.2). Thus, these two compounds ($C_{18}$ and $C_{24}$) will be the focus of analysis and discussion.

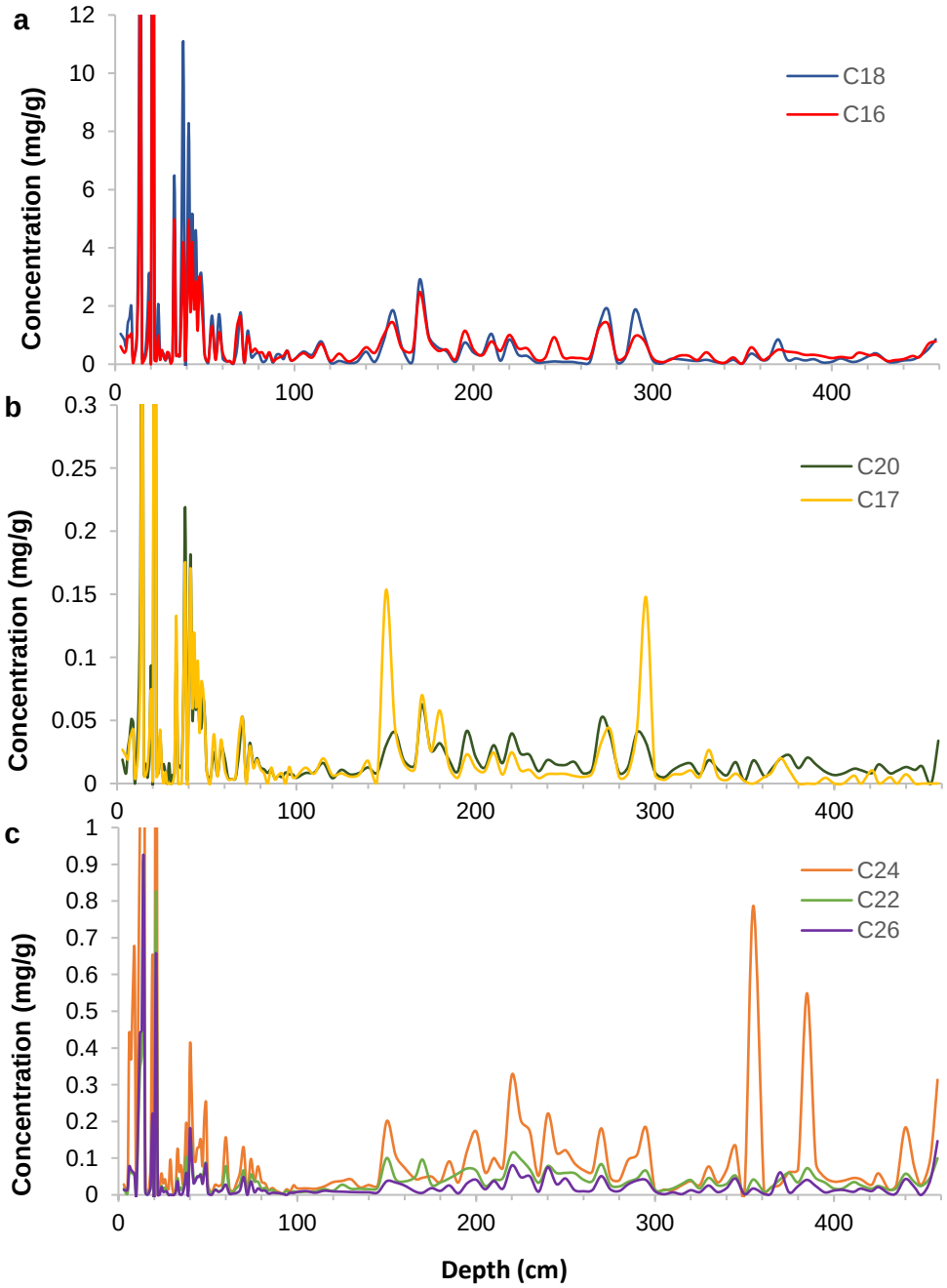



**Figure 5.3** Fatty acid concentrations (µg/g of dry sediment) with depth from core DTGC2011 a) $C_{16}$ and $C_{18}$ fatty acids b) $C_{17}$ and $C_{20}$ fatty acids c) $C_{22}$, $C_{24}$ and $C_{26}$ fatty acids.

### 5.3.2 Potential sources of the $C_{18}$ fatty acid

Potential sources for the $C_{18}$ FA in core U1357 (recovered from the same site as DTGC2011) have been discussed in Chapter 4 (S3.1.1), in which we suggest the prymnesiophyte *Phaeocystis antarctica* is the most likely producer. This is due to it being one of the main known producers of $C_{18}$ in the Antarctic (Dalsgaard et al., 2003); the high observed abundance of *P. antarctica* within modern Adélie surface waters (Riaux-Gobin et al., 2011); and comparison between the measured $\delta^{13}C$ values and those reported in the literature for *P. antarctica* (Kopczynska et al., 1995; Wong and Sackett, 1978). Unfortunately, the poor preservation of *P. antarctica* in sediments (producing no microfossils) precludes the direct comparison of down core trends of this species with FAs. *Phaeocystis antarctica* has been found to live within and underneath sea ice before its break up, as well as in open ocean waters (Riaux-Gobin et al., 2013; Poulton et al., 2007), due to its ability to use a wide range of light intensities for energy production (Moisan and Mitchell, 1999).

Dalsgaard et al. (2003) looked at the FAs of eight major microalgal classes and showed that Prymnesiophyceae and Dinophyceae produce the highest proportions of the saturated $C_{18}$ FA (3.3 and 3.4% of all FAs produced respectively), the former to which *P. antarctica* belongs. Although it seems to represent only a small amount of the total FA fraction, the highest proportions produced were the unsaturated form which are preferentially broken down in the water column and sediments, so less likely to be preserved as discussed in more detail below. Riaux-Gobin et al. (2011) found *P. antarctica* (the only prymnesiophyte species recorded) to dominate the surface waters offshore Adélie Land after spring sea-ice break-up, representing

16% of the phytoplankton assemblage. Although several species of the class Dinophyceae were also recorded, *P. antarctica* was more than 20 times more abundant than the 3 most

abundant Dinophyceae taxa combined. Sambrotto et al. (2003) also observed large blooms of *Phaeocystis* sp. in stable, shallow mixed layer water along the edge of fast ice near the Mertz Glacier.

Furthermore, Skerratt et al. (1998) identified the FAs produced by *P. antarctica* and two Antarctic diatoms, *Chaetoceros simplex* and *Odontella weissflogii,* from culture samples. Of the FAs produced by *P. antarctica,* 52% were saturated FAs ($C_{14}$-$C_{20}$) compared to just 14 and 11% for the two diatoms, respectively, the latter instead producing much more of the mono- and polyunsaturated FAs. The percentage of $C_{18}$ FA produced by *P. antarctica* was also 4.1 and 12.5 times greater than the percentage of $C_{18}$ produced by *C. simplex* and *O. weissflogii,* respectively. This supports the hypothesis of *P. antarctica* being a dominant source of the saturated $C_{18}$ FA in the Adélie basin over other phytoplankton species such as the diatoms and dinoflagellates, but minor contributions of $C_{18}$ from other sources cannot be excluded.

### 5.3.3 Potential sources of the $C_{24}$ fatty acid

Long-chain n-alkyl compounds, including FAs, are major components of vascular plant waxes and their presence within sediments has commonly been used as a biomarker of terrestrial plants (Pancost and Boot, 2004). Although plants such as bryophytes (e.g. mosses) which are present in the Antarctic do also produce LCFAs (Salminen et al., 2018) it is unlikely that FAs from plants make a significant contribution to the water column, due to the limited extent of plants on the continent, and the significant distance from other sources of plants.

However, there is much evidence in the literature for various aquatic sources of LCFAs, a few of which are summarized in Table 3. Although not all of these species are likely to be present within the coastal waters offshore Adélie Land, it highlights the wide range of organisms

**Table 5.3** Summary of several studies where long-chain fatty acids have been shown to be produced by aquatic organisms.

| Study | Fatty Acids | Aquatic Contribution (%) | Location | Source |
|---|---|---|---|---|
| Naraoka and Ishiwatari (2000) | $C_{20}$ - $C_{30}$ | ~ 38 (C30) - 88 (C20) | Northwest Pacific | Unknown |
| Holland et al. (2013) | $C_{24}$ – $C_{28}$ | n/a | Lake El'gygytgyn, Russia | Unknown |
| Volkman et al. (1980) | $C_{24}$ – $C_{28}$ | 30 - 80 | Victoria, Australia, intertidal | Diatoms |
| Schouten et al. (1998) | $C_{28}$ | n/a | Culture | *Scenedesmus communis* (freshwater algae) |
| Yunker et al. (2005) | $C_{20}$ – $C_{28}$ | 46 - 66 | Arctic Ocean | Algae |
| Rogerson and Johns (1996) | $C_{20}$ – $C_{28}$ | 100 | Organic Lake, Antarctica (hypersaline, meromictic) | Bacteria |
| Lawson et al. (1986) | $C_{24}$ – $C_{30}$ | 100 | Westmere Reef, Auckland, New Zealand | *Halichondria moorei* (marine sponge) |
| Koopmans et al. (2014) | $C_{24}$ – $C_{30}$ | 100 | The Oosterschelde Estuary, Netherlands | *Haliclona oculta* and Haliclona *xena* (marine sponges) |
| | | | Lake Veere, Netherlands | *Halichondria panacea* and *Haliclona xena* (marine sponges) |
| | | | Northwest Mediterranean, Spain | *Dysidea avara* and *Aplysina aerophoba* (marine sponges) |
| Viso et al. (1993) | $C_{22}$ – $C_{34}$ | 100 | Mediterranean coasts of France and Greece | *Posidonia oceanica* (seagrass) |
| Leblond and Chapman (2000) | $C_{20}$ – $C_{22}$, trace $C_{24}$ | 100 | Culture | Various dinoflagellate species |

which can produce these compounds, and thus suggests that an autochthonous marine source is entirely possible, especially considering the highly productive nature of this region. However, considering the fact that it is not commonly produced by marine organisms, it is

unlikely that there are many different producers for the $C_{24}$ in DTGC2011. Thus, despite the exact producer(s) remaining unknown we interpret it as having a marine source and look at the carbon isotopes along with other proxy data to determine the most likely signal being recorded.

### 5.3.4 Microbial degradation and diagenetic effects on fatty acid concentration

Both the $C_{18}$ and $C_{24}$ FAs show an overall decrease in concentrations down-core, with significantly higher concentrations in the top 80 cm (representing ~70 years) compared to the rest of the core. Below this point, FAs concentrations remain comparatively stable (Fig. 5.3).

Many studies have shown that significant degradation of FAs occurs both within the water column and surface sediments as a result of microbial activity, and that there is preferential break down of both short-chained and unsaturated FA, compared to longer-chained and saturated FA (Haddad et al., 1992; Matsuda, 1978; Colombo et al., 1997). Haddad et al. (1992) studied the fate of FA within rapidly accumulating (10.3 cm $yr^{-1}$) coastal marine sediments (off the coast of North Carolina, USA) and showed that the vast majority (ca. 90%) of saturated FAs were lost due to degradation within the top 100 cm, in this case representing ~10 years. Below this (100-260 cm), there was minimal change in FA concentrations suggesting that degradation due to diagenesis was largely complete. Similarly, Matsuda and Koyama (1977) show that in slowly accumulating (4 mm $yr^{-1}$) lacustrine sediments from Lake Suwa, Japan, SCFA concentrations decrease rapidly within the top 20 cm of the sediment, representing roughly 50 years, after which they remain relatively stable. Assuming similar processes apply to the DTGC2011 sediments, this suggests that the declining concentrations within the upper part of the core are largely the result of diagenetic effects such as microbial activity occurring within the surface sediments, and thus do not entirely reflect a real change in production of these compounds in the surface waters.

The complete lack of both unsaturated and short chained (fewer than 16 carbon atoms) FA compounds identified within DTGC2011 samples, even within the top layers, suggests that selective breakdown of compounds has already occurred within the water column and on the sea floor (before burial). Wakeham et al. (1984) assessed the loss of FAs with distance during their transport through the water column at a site in the equatorial Atlantic Ocean and estimated that only 0.4 to 2% of total FAs produced in the euphotic zone reached a water depth of 389 m, and even less reaching more than 1,000 m, the vast majority of material being recycled in the upper water column. Their results also show a significant preference for degradation of both unsaturated and short chained compounds over saturated and longer chain length compounds. Although no studies into the fate of lipids within the water column exist for the Adélie region, the >1,000 m water depth at the core site would provide significant opportunity for these compounds to be broken down during transportation through the water column. It is likely, therefore, that the distribution of compounds preserved within the sediments will not be a direct reflection of what is being produced in the surface waters, and explains the preference for saturated FAs with carbon chain lengths of 16 and more.

Although FA concentrations in the top 80 cm of core DTGC2011 are much higher overall than the sediments below and show a broad decline over this section, on closer inspection there is a high level of variability. Concentrations do not decrease uniformly within the top part of the core, as may be expected if concentration change is a first order response to declining microbial activity. The peak in total FAs instead occurs at a depth of 21-22 cm with a concentration more than an order of magnitude higher than in the top layer. This variability creates difficulty in directly determining the effects of diagenesis. However, by 25 cm the concentrations drop to below 1,000 ng $g^{-1}$ and remain so until 32 cm before increasing again. This may suggest that diagenetic effects of FA concentrations are largely complete by 25 cm

(representing ca. 25 years), consistent with results from Haddad et al. (1992) and Matsuda and Koyama (1977), and that subsequent down-core concentration variations predominantly represent real changes in input at the surface, resulting from environmental factors. However, the fluctuating nature of concentrations particularly in the youngest sediments means it is difficult to clearly unpick the effects of diagenesis from actual changes in production of these compounds, and a clear cut-off point for diagenetic effects cannot be determined.

### 5.3.5 Comparison of fatty acid concentrations with highly branched isoprenoid alkenes

It is useful to compare the fatty acid concentrations with concentrations of other organic compounds (whose source is better constrained) in the core to help understand the fatty acid sources. Direct comparison between different organic compounds can be made since both are susceptible to similar processes of diagenesis, in contrast to other proxies such as diatoms. In core DTGC2011, we have concentrations of di- and tri-unsaturated highly branched isoprenoid (HBI) alkenes (referred to as HBI diene and HBI triene, respectively hereafter).

In Antarctic marine sediments HBIs have been used as a tool for reconstructing sea ice, based on the environments in which these compounds are found (Belt et al., 2016, 2017). Smik et al. (2016) compared the concentrations of these compounds in sediment samples offshore East Antarctica from the permanently open-ocean zone (POOZ), the marginal ice zone (MIZ) and the summer sea-ice zone (SIZ). They found the HBI diene reached the highest concentrations in the SIZ and was absent from the POOZ. In contrast, the HBI triene was most abundant in the MIZ, i.e. at the retreating sea ice edge, with much lower concentrations in the SIZ and POOZ. This suggests that the two compounds are produced in contrasting environments but remain sensitive to changes in sea ice.

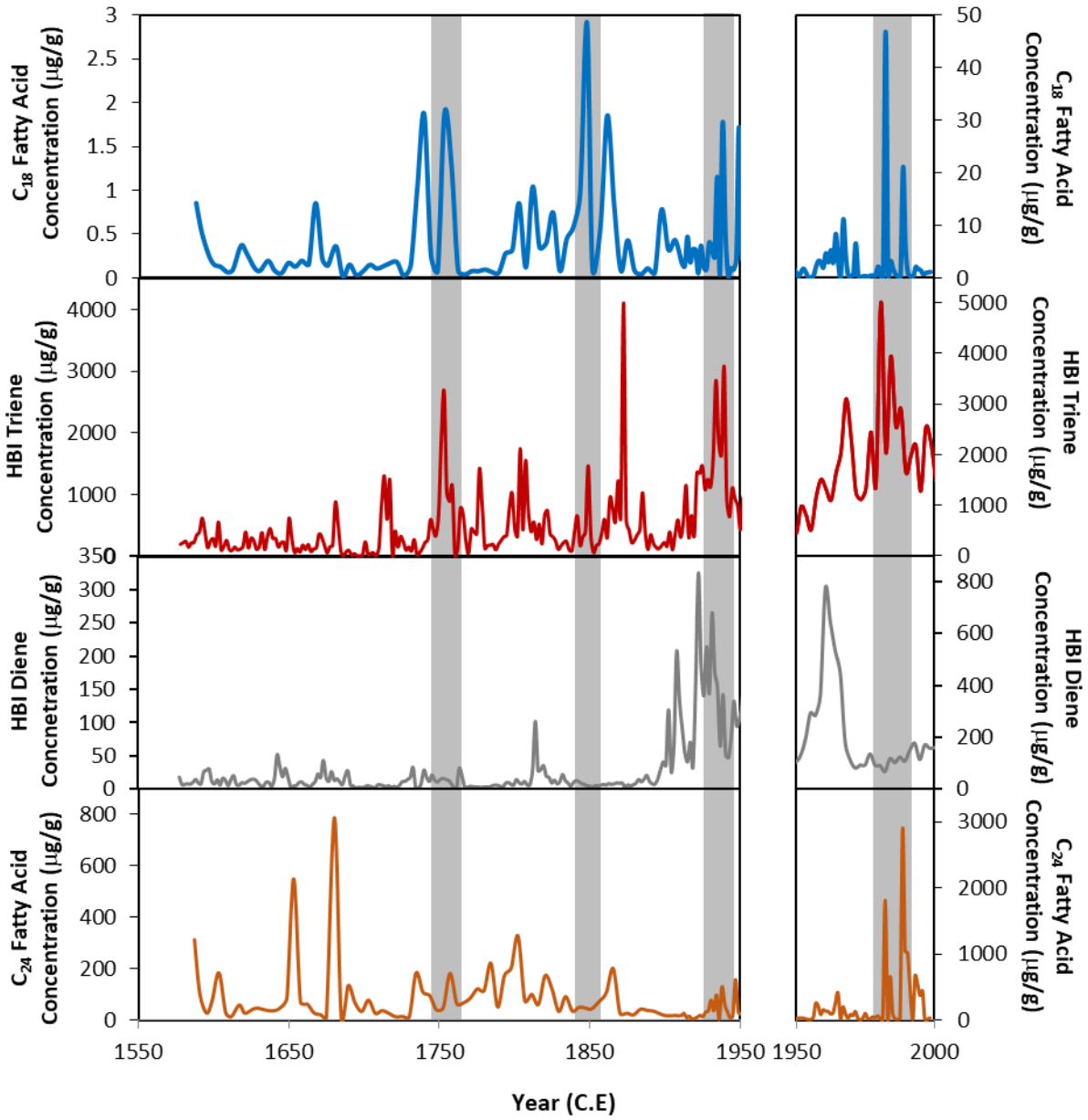



**Figure 5.4** Concentrations of the $C_{18}$ fatty acid (blue), the HBI triene (red), HBI diene (grey) (Campagne, 2015), $C_{24}$ fatty acid (orange) from core DTGC2011. The left hand panels shown 1550 to 1950 C.E. and the right hand panels shown 1950 to 2000 C.E., plotted on different y-axes due to the elevated concentrations in the top part of the core. Grey vertical bands highlights coincident peaks in $C_{18}$ fatty acid and HBI triene records.

The HBI diene biomarker was found by Belt et al. (2016) to be mainly biosynthesised by *Berkeleya adeliensis*, a diatom which resides and blooms within the sea ice matrix, and thus can be used as a proxy for ice attached to the coast (fast ice). In contrast, the presence of the HBI triene mostly in the MIZ is suggestive of a predominantly pelagic phytoplankton source (e.g. *Rhizosolenia* spp, Massé et al., 2011; Smik et al., 2016; Belt et al., 2017), rather than

sea-ice diatoms (Smik et al., 2016). The fact that HBI triene reached its greatest abundance within the MIZ suggests its precursor organism may thrive in the stratified, nutrient-rich surface waters of the sea ice edge.

One key similarity between both the HBI diene and triene, and the FA concentrations is that the highest concentrations are found near the top of the core. Both compounds show broad increases in concentration from 110 cm depth (ca. 1900 C.E) until the top of the core (Fig. 5.3 and 5.4). Concentrations of HBIs are also susceptible to degradation through the water column through visible light induced photo-degradation (Belt and Müller, 2013) and diagenetic effects, as well as reacting with sediments resulting in sulphurisation (Sinninghe Damsté et al., 2007), isomerisation and cyclisation (Belt et al., 2000). Thus, it is certainly possible that the elevated concentrations, and thus the similarity between FA and HBI concentrations, is due to better preservation at the top of the core, with diagenetic effects having an increasing and progressive impact down to ca. 25cm depth.

However, it is clear that, despite an overall increase in HBI and FA concentrations above 110 cm depth, there are clear deviations from this trend. Concentrations of the HBI triene show some broad similarities with FA concentrations. In particular, both the HBI triene and the $C_{18}$ FA have coeval concentration peaks around 1980-88, 1967, 1938, 1961-72, 1848 and 1752 C.E. (Fig. 5.4) These peaks are offset from the HBI diene concentrations, suggesting that these are a result of increased production of these compounds in the surface waters rather than simply changes in preservation. The HBI triene is more susceptible to degradation than the diene (Cabedo Sanz et al., 2016), so while this could explain some of the differences between the diene and triene records, where the triene increases independently of the diene (as in the peaks highlighted above) this is likely to be a genuine reflection of increased production of these compounds at the surface, rather than an artefact of preservation processes.

This close similarity between the $C_{18}$ FA and HBI triene concentrations (Fig. 5.4), suggests that the $C_{18}$ may also be produced by an organism associated with the retreating ice edge. As discussed above, *P. antarctica* has been proposed as a potential producer of the $C_{18}$ in core U1357B (Chapter 4 supplementary). In the Ross Sea, *P. antarctica* has been observed to dominate the phytoplankton bloom during the spring, blooming in deep mixed layers as the sea ice begins to melt, after which the diatoms tend to dominate during the summer (Arrigo et al., 1999; Tortell et al., 2011; DiTullio et al., 2000). However, a few studies in the Adélie region suggest this is not the case there. Offshore Adélie Land, *P. antarctica* has been found to only appear late in the spring/early summer, later than many diatom species. During this time, it was found preferentially within the platelet ice and under-ice water (Riaux-Gobin et al., 2013). Furthermore, Sambrotto et al. (2003) observed a surface bloom of *P. antarctica* near the Mertz Glacier (Fig. 5.1) during the summer months, in very stable waters along the margin of fast ice and Riaux-Gobin et al. (2011) found *P. antarctica* to be abundant in the coastal surface waters eight days after ice break up. This indicates a relationship with cold waters and ice melting conditions. This might explain the close similarity between the $C_{18}$ and HBI triene concentrations, both occupying a similar habitat at the ice edge.

The $C_{24}$ FA does also have some similarity with concentrations of the HBI triene, put this appears to be mostly in the top part of the core where the highest concentrations are found. The reason for this similarity is unclear, especially considering the lack of correlation between the $C_{24}$ and $C_{18}$ FA concentrations, but it may relate to the better preservation in younger samples as discussed above. The weaker correlation between the $C_{24}$ and the HBI triene, and also HBI diene, suggests that the $C_{24}$ FA is predominantly produced by an organism which is not associated with sea ice, and thus perhaps associated instead with more open waters.

Seventy-three diatom species were encountered in Core DTGC2011 (Campagne, 2015), with *Fragilariopsis curta* and *Chaetoceros* resting spores being the most abundant. However, trends in diatom abundances do not show any clear correlations with the $C_{18}$ or $C_{24}$ FA concentrations. While this would lend support to the hypothesis that diatoms are not the main producers of these compounds, the differing effects of diagenesis on the preservation of diatoms and lipids could also explain some of the differences in observed concentrations, particularly in the upper part of the core. The known producer of the HBI diene, *Berkeleya adeliensis*, for example, was not recorded within the core, likely due to their lightly silicified frustules which are more susceptible to dissolution (Belt et al., 2016). Therefore, despite the lack of a correlation between diatom abundances and FA concentrations, we cannot entirely rule out the possibility of a minor contribution of FA by diatoms.

### 5.4 Carbon isotopes of fatty acids

Down-core changes in $\delta^{13}C$ for the $C_{18}$ and $C_{24}$ FAs ($\delta^{13}C_{18FA}$ and $\delta^{13}C_{24FA}$, respectively) (Fig. 5.5) clearly show different trends, with very little similarity between them. This further supports the idea that these compounds are being produced by different species, and also suggests that they are recording different information.

As discussed in Chapter 4, the mean carbon isotope value of $\delta^{13}C_{18FA}$ in Core U1357 of -29.8‰ is suggestive of a pelagic phytoplankton source (Budge et al., 2008). In core DTGC2011 the mean value of $\delta^{13}C_{18FA}$ is -26.2‰ and $\delta^{13}C_{24FA}$ is -27.6‰. This is slightly more positive, but still within the region of a phytoplankton source. There is a slight offset between the mean $\delta^{13}C$ value of the $C_{18}$ and $C_{24}$, with the $C_{18}$ being 1.4‰ more positive. The more positive $\delta^{13}C$ value of the $C_{18}$ could be due to some of the algae producers living within sea ice, since carbon fixation occurring within the closed or semi-closed system of the sea ice

would lead to a higher degree of $CO_2$ utilisation than expected in open waters and thus more positive $\delta^{13}C$ values (Henley et al., 2012). Although no studies on FA $\delta^{13}C$ of different organisms are available for the Southern Ocean, Budge et al. (2008) measured the mean $\delta^{13}C$ value of $C_{16}$ FA from sea ice algae (-24.0‰) at a site in the Arctic to be 6.7‰ higher than pelagic phytoplankton (-30.7‰) from the same region.

The higher $\delta^{13}C$ of the $C_{18}$ FA could therefore be indicative of *P. antarctica* living partly within the sea ice, e.g. during early spring before ice break up. The more negative $\delta^{13}C_{24FA}$ suggests it is more likely to be produced by phytoplankton predominantly within open water, which was also suggested by the limited similarity between the HBI diene and triene which are associated with sea ice.

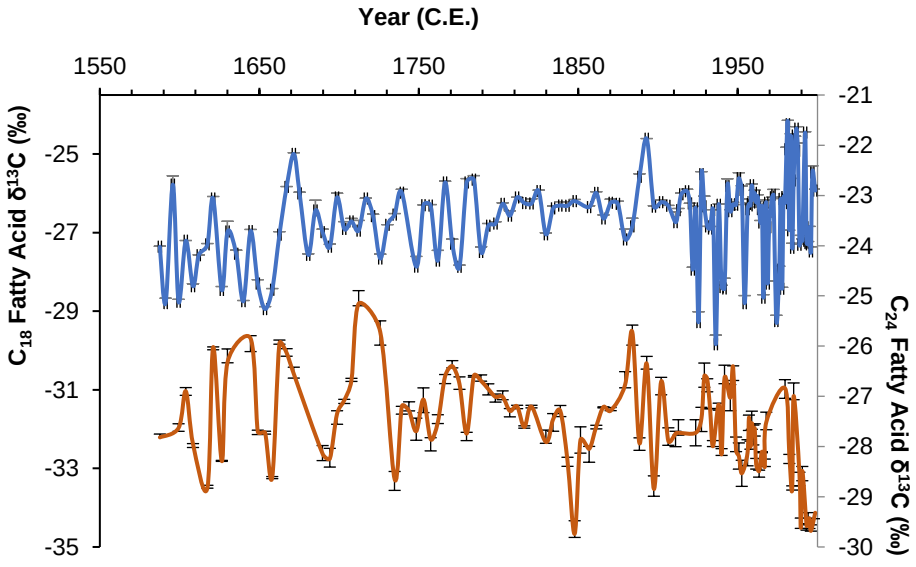



**Figure 5.5** $\delta^{13}C$ measurements of the $C_{18}$ (blue) and $C_{24}$ (orange) fatty acids in core DTGC2011.

### 5.4.1 Controls on carbon isotopes of particulate organic matter

The $\delta^{13}C_{18FA}$ record shows a broadly increasing trend towards more positive values from 1587 until ca. 1920 C.E., with short term fluctuations of up to ~4‰ superimposed on this long term trend (Fig. 5.5). This is followed by a period of higher variability with a full range of 5.6‰ until the most recent material (ca. 1999 C.E.), with more negative $\delta^{13}C$ values between 1921 and 1977 C.E. and a rapid shift toward more positive values after. In contrast, the $\delta^{13}C_{24FA}$ record overall shows a weak, negative trend, with large decadal fluctuations of up to 4.6‰, with a more pronounced negative trend after ca. 1880 C.E. (Fig. 5.5).

There are various factors which may control the carbon isotope value of algal biomarkers produced in the surface waters. Down-core changes in FA $\delta^{13}C$ are likely to be a function of either the $\delta^{13}C$ of the dissolved inorganic carbon (DIC) source, changes in the species producing the biomarkers, diagenesis or changing photosynthetic fractionation ($\varepsilon_p$). The next section outlines the potential influence each of these factors may have and ultimately determine the mostly likely dominant driver of FA $\delta^{13}C$.

#### *5.4.1.1 Isotopic composition of DIC*

The $\delta^{13}C$ of the DIC source can be affected by upwelling or advection of different water masses, or the $\delta^{13}C$ of atmospheric $CO_2$. Around the Antarctic, various water masses have been shown to have unique carbon and oxygen isotope signatures and thus can be used as a water mass tracer. In the Weddell Sea for example, Mackensen (2001) determined the $\delta^{13}C$ value of eight water masses, which ranged from 0.41‰ for Weddell Deep Water (which forms from CDW) and 1.63‰ for AASW. This gives a total range of 1.22‰. A similar range of ~1.5‰ was identified in water masses between the surface and ~5,500m depth along a transect from South Africa to the Antarctic coast (Archambeau et al., 1998). Assuming similar

values apply to these water masses offshore Adélie Land, this range in values would be insufficient to explain the full variation of $\delta^{13}C$ recorded by both $C_{18}$ and $C_{24}$ FA (which have a full range of 5.9 and 4.8‰, respectively), even in the situation of a complete change in water mass over the core site. Furthermore, the location of site DTGC2011 within a 1,000 m deep depression, bounded by the Adélie Bank to the north, means the site is relatively well sheltered from direct upwelling of deep water onto the continental shelf (Fig. 5.1). However, inflow of Modified Circumpolar Deep Water (MCDW) has been shown to occur within the Adélie Depression to the east of the bank (Williams and Bindoff, 2003) and possibly within the Dumont d'Urville Trough. Variations in MCDW inflow may alter surface water DIC and subsequently the $\delta^{13}C$ of FAs produced in that area. However, only very small amplitude changes in $\delta^{13}C$ of benthic foraminifera, tracking upper CDW, have been observed over the Holocene in Palmer Deep, West Antarctica (Shevenell and Kennett, 2002). Although from a different location, this argues against large changes in the isotopic composition of the source of MCDW.

Changes in the $\delta^{13}C$ of atmospheric $CO_2$, which is in exchange with the surface waters could also have the potential to drive changes in the $\delta^{13}C$ of algal biomarkers. Over the last ca. 200 years, the anthropogenic burning of fossil fuels has released of a large amount of $CO_2$ depleted in $^{13}C$, meaning that the $\delta^{13}C$ of $CO_2$ has decreased by ca. 1.5‰, as recorded in the Law Dome ice core. Prior to this, however, the $\delta^{13}C$ of $CO_2$ in the atmosphere remained relatively stable, at least for the last thousand years (Francey et al., 1999). Therefore, this could potentially drive the $\delta^{13}C$ of algal biomarkers towards lighter values within the last 200 years, but this would not be able to explain the full variation of ~5-6‰ in FA $\delta^{13}C$ measured throughout the core. No clear trend towards lighter values is evident in the last 200 years of the FA $\delta^{13}C$ records, which may suggest that this change is insignificant compared to local

and regional interannual variations as a result of other environmental drivers (discussed below).

*5.4.1.2 Changing species*

A shift in the organisms producing the FA could also affect $\delta^{13}C$ where species have different fractionation factors. Changing diatom species have been shown to have an effect on bulk organic matter $\delta^{13}C$ in core MD03-2601, offshore Adélie Land, over the last 5 ka (Crosta et al., 2005). This organic matter would have contained multiple species with different $\delta^{13}C$ values and fractionations, meaning changes in the proportion of species will have an effect on the $\delta^{13}C$ of the bulk organic matter. However, here we are measuring $\delta^{13}C$ of individual biomarkers which are produced by a more restricted group of species (possibly restricted to a few dominant species) compared to bulk $\delta^{13}C$. As discussed above, the $C_{18}$ appears to be produced predominantly by *P. antarctica,* whereas diatoms do not tend to produce this compound (Dalsgaard et al., 2003). However, potential contributions from others species cannot be entirely ruled out.

*5.4.1.3 Effect of diagenesis on lipid $\delta^{13}C$*

As discussed above, diagenesis appears to affect FA concentration. Thus we must acknowledge the possibility of diagenetic effects on the $\delta^{13}C$ record. Sun et al. (2004) looked at the carbon isotope composition of alkenones and FAs during 100 days of incubation in both oxic and anoxic seawater. They observed a shift towards more positive values in FA $\delta^{13}C$, ranging between 2.6‰ for the $C_{14:0}$ and as much as 6.9‰ in the $C_{18:1}$, under anoxic conditions. This suggests that diagenesis could affect FA $\delta^{13}C$ in core DTGC2011. However, these observed changes are rapid (days to months), occurring on timescales which are unresolvable in the FA $\delta^{13}C$ record (annual to decadal), and thus may have no effect on the trends observed in our record. Based on concentration data discussed above, it appears the

main period of potential diagenetic overprint is largely complete by ~25 cm (Fig. 5.3), thus below this point it is unlikely to have a strong control on FA $\delta^{13}C$. In the top 25 cm of the core, $\delta^{13}C_{24FA}$ does show an overall trend towards more positive values downcore ($R^2 = 0.63$, n = 11), increasing by ~2.5‰, while $\delta^{13}C_{18FA}$ instead displays a large variation with no overall trend ($R^2 = 0.12$, n = 20). If diagenesis was driving the changes in $\delta^{13}C$, it is likely that this trend would be observed in all FA compounds. However, the fact that no trend is observed in the $C_{18}$ suggests that it is unlikely to be important.

Taken together, it appears that neither changes in the $\delta^{13}C$ of the DIC, changing diatom species nor diagenesis can explain the full variation of FA $\delta^{13}C$ recorded within DTGC2011. Therefore, we hypothesise that changes in $\varepsilon_p$ are the main driver of $\delta^{13}C_{18FA}$.

### 5.4.2 Controls on photosynthetic fractionation ($\varepsilon_p$)

$\varepsilon_p$ in marine algae has been shown to vary as a result of dissolved surface water $CO_{2(aq)}$ concentration (Rau et al., 1989). Since all plants including phytoplankton preferentially take up the lighter carbon isotope during photosynthesis, when $CO_{2(aq)}$ is high there will be greater fractionation and enhanced uptake of the $^{12}C$. Conversely, when $CO_2$ is low, $^{12}C$ will be depleted quickly meaning there will be greater uptake of the $^{13}C$ and also $HCO_3^-$ (Farquhar et al., 1982; Hollander and McKenzie, 1991). Thus, higher $\delta^{13}C$ values are hypothesised to reflect lower surface water $CO_{2(aq)}$ and vice versa.

Changes in surface water $CO_{2(aq)}$ concentration in turn may be driven by various factors, including changing atmospheric $CO_2$ (Fischer et al., 1997), wind-driven upwelling of deep, carbon-rich water masses (Sigman and Boyle, 2000; Takahashi et al., 2009), sea ice cover (Henley et al., 2012) and/or primary productivity (Villinski et al., 2008). Thus, determining

the main driver(s) of surface water $CO_2$ changes offshore Adélie Land should enable interpretation of the DTGC2011 FA $\delta^{13}C$ records.

*5.4.2.1 Sea ice*

Brine channels within sea ice have very low $CO_2$ concentrations compared to the surface waters, and a limited inflow of seawater. Thus, fractionation of algae living within these channels will be greatly reduced compared to open water species (Gibson et al., 1999), leading to elevated $\delta^{13}C$ values. Thus, it is possible that under conditions of high sea-ice cover, greater FA contribution from sea ice algae could lead to elevated $\delta^{13}C$ values. *Phaeocystis antarctica*, for example, the likely producer of the $C_{18}$ fatty acid, is known to be able to live within and under sea ice before ice break-up (Riaux-gobin et al., 2013; Poulton et al., 2007; Moisan and Mitchell, 1999). HBI diene concentrations within DTGC2011 show a much greater presence of fast ice at the core site ca. 1960 C.E (Fig. 5.4). However, during this time there is no clear elevation in $\delta^{13}C$ concentrations in either $\delta^{13}C_{18FA}$ or $\delta^{13}C_{24FA}$, both instead showing generally lower $\delta^{13}C$ values. In fact, $\delta^{13}C_{18FA}$ shows the lowest values of the whole record between 1925 and 1974 C.E., during which time sea ice, as recorded by the HBI diene, is at its highest. This suggests that inputs in sea ice algae at this time are not driving changes in FA $\delta^{13}C$.

The DTGC2011 core site sits proximal to the Dumont D'Urville polynya, which has a summer area of $13.02 \times 10^3$ km$^2$ and a winter area of $0.96 \times 10^3$ km$^2$ (Arrigo and van Dijken, 2003). Changes in the size of the polynya both on seasonal and inter-annual time scales will effect air-sea $CO_2$ exchange and thus also surface water $pCO_2$ concentration. A reduced polynya may lead to greater supersaturation of $CO_2$ in the surface waters due to a reduced outgassing, allowing $CO_2$ to build up below the ice, leading to lower $\delta^{13}C$ values of algal

biomarkers produced in that habitat (Massé et al., 2011). Thus changes in the extent of sea ice may also affect FA $\delta^{13}C$.

*5.4.2.2 Observed trends in surface water $CO_{2(aq)}$*

If the trend in surface water $CO_{2(aq)}$ paralleled atmospheric $CO_2$, with an increase of over 100 ppm over the last 200 years (MacFarling Meure et al., 2006), we might expect phytoplankton to exert a greater fractionation during photosynthesis in response to elevated surface water $CO_{2(aq)}$ concentration, resulting in more negative $\delta^{13}C$ values. As discussed above, if we also take into account the decline in atmospheric $\delta^{13}CO_2$ over the same period, this would enhance the reduction in phytoplankton $\delta^{13}C$. Fischer et al. (1997) looked at the $\delta^{13}C$ of both sinking matter and surface sediments, and the difference between them, in the South Atlantic and suggested that, since the preindustrial, surface water $CO_2$ in the Southern Ocean has increased much more than in the tropics. They estimate that with a 70 ppm increase in $CO_{2(aq)}$ in South Atlantic waters of 1°C, phytoplankton $\delta^{13}C_{org}$ would decrease by ca. 2.7‰ as a result, or 3.3‰ including the $\delta^{13}CO_2$ change, between preindustrial and 1977-1990 (when the measurements were taken). Since DTGC2011 samples continue until 1999 C.E. – by which time atmospheric $CO_2$ was even higher – based on their calculation, phytoplankton $\delta^{13}C_{org}$ may have decreased even more. However, Fischer et al. (1997)'s data were based on offshore sites, where sea-ice cover and summer primary productivity are likely to be much lower than the Adélie, both of which will affect air-sea gas exchange.

Shadwick et al. (2014) suggest that surface water $pCO_2$ should track the atmosphere in the Mertz Polynya region, despite the seasonal ice cover limiting the time for establishing equilibrium with the atmosphere. They calculated wintertime $pCO_2$ in the shelf waters of the Mertz Polynya region, offshore Adélie Land (Fig. 5.1), measuring ca. 360 μatm in 1996, ca. 396 μatm in 1999, and ca. 385 μatm in 2007, while atmospheric $CO_2$ at the South Pole was

360, 366 and 380ppm, respectively (Keeling et al., 2005). Based on the 1996 and 2007 data only, an increase in $pCO_2$ of ca. 25 μatm is observed over these 11 years, coincident with the 20 ppm atmospheric $CO_2$ increase over this time period. However, high interannual variability (± ca. 30 μatm) is evident (e.g. 396 μatm in 1999) suggesting that other factors, particularly upwelling, may override this trend. The latter was also suggested by Roden et al. (2013) based on winter surface water measurements in Prydz Bay, indicating that decadal-scale carbon cycle variability is nearly twice as large as the anthropogenic $CO_2$ trend alone.

During the austral winter, upwelling of deep water masses causes $CO_2$ to build up in the surface waters, and sea-ice cover limits gas exchange with the atmosphere (Arrigo et al., 2008; Shadwick et al., 2014). Although only limited data, the measurements by Shadwick et al. (2014) suggest slight supersaturation, of up to 30 μatm, occurs in the winter due to mixing with carbon-rich subsurface water, but with high interannual variability. This is compared to undersaturation of 15 to 40 μatm during the summer as a result of biological drawdown of $CO_2$. Roden et al. (2013) also observe varying levels of winter supersaturation in Prydz Bay, East Antarctica, with late winter $pCO_2$ values of 433 μatm in 2011 (45 μatm higher than atmospheric $CO_2$), and suggest that intrusions of C-rich MCDW onto the shelf may play a part in this. Similarly, winter surface water $pCO_2$ of 425 ppm has been measured by Sweeney (2003) in the Ross Sea, before being drawn down to below 150 ppm in the summer as phytoplankton blooms develop.

Enhanced upwelling of deep carbon-rich waters in the Southern Ocean are thought to have played a key role in the deglacial rise of atmospheric $CO_2$, increasing $CO_2$ concentrations by ~80 ppm (Anderson et al., 2009; Burke and Robinson, 2012). Changes in upwelling offshore Adélie Land could therefore drive some interannual variability in surface water $pCO_2$ and

hence FA $\delta^{13}C$ in DTGC2011. However, upwelling tends to occur predominantly during the winter months, when sea-ice formation and subsequent brine rejection is greater and drives mixing with deeper C-rich waters. At this time, there is limited air-sea gas exchange due to sea-ice cover, enhancing the supersaturation of the surface waters (Shadwick et al., 2014). In contrast, the phytoplankton producing FA thrive during the spring and summer months during which time $CO_2$ is rapidly drawn down and the surface waters become undersaturated. However, upwelling cannot be discarded as a possible contributor to surface water $CO_2$ change. As discussed above, the location of the core site is in a relatively sheltered area which suggests it is unlikely to be affected by significant upwelling, though phytoplankton from a wider area may still be represented in the core.

Based on these studies, changes in atmospheric $CO_2$ concentration and $\delta^{13}C$ appear to be unlikely to be a dominant driver of the FA $\delta^{13}C$ record, with interannual variations driven by other factors overriding any longer term trend. As discussed previously, there is no clear decline in the FA $\delta^{13}C$ record over the last 200 years, which supports this hypothesis. Upwelling may play a role, however, since it mostly occurs during winter it is less likely to be a major player during the growing season.

*5.4.2.3 Productivity*

Given that changes in atmospheric $CO_2$, source signal, sea ice algae or diagenesis seem unable to explain the full range of variability seen in the FA $\delta^{13}C$ record, the most plausible driver of these carbon isotopes appears to be changes in surface water primary productivity. Coastal polynya environments in the Antarctic are areas of very high primary productivity (Arrigo and van Dijken, 2003). The DTGC2011 core site sits near to the Dumont D'Urville polynya, and is just downstream of the larger and more productive MGP (Arrigo and van Dijken, 2003). In large polynyas such as the Ross Sea, primary productivity leads to intense

drawdown of $CO_2$ in the surface waters, resulting in reduced fractionation by the phytoplankton during photosynthesis (Villinski et al., 2008). In the Ross Sea, surface water $CO_2$ has been observed to drop to below 100 ppm during times of large phytoplankton blooms (Tortell et al., 2011) demonstrating that primary productivity can play a key role in controlling surface water $CO_2$ concentrations in a productive polynya environment. Arrigo et al. (2015) found the MGP to be the 8$^{th}$ most productive polynya in the Antarctic (out of 46) based on total net primary productivity during their sampling period, and Shadwick et al. (2014) observed $CO_2$ drawdown in the MGP during the summer months.

Therefore, we hypothesise that FA $\delta^{13}C$ recorded in DTGC2011 is predominantly reflecting changes surface water $pCO_2$ driven by primary productivity at the time they are produced. However, they may also be affected to some extent by changes in air-sea $CO_2$ exchange driven by changes in sea ice cover, and upwelling.

Indeed, the potential for the $\delta^{13}C$ of sedimentary lipids to track surface water primary productivity has been recognised in the highly productive Ross Sea polynya. High variability in surface water $pCO_2$ values have been measured across the polynya during the summer months (December – January), ranging from less than 150 ppm in the western Ross Sea near the coast, to >400 ppm on the northern edge of the polynya. This pattern was closely correlated with diatom abundances, indicating intense drawdown of $CO_2$ in the western region where diatom abundances were highest (Tortell et al., 2011). This spatial variation in productivity is recorded in particulate organic carbon (POC) $\delta^{13}C$, and is also tracked in the surface sediments by total organic carbon (TOC) $\delta^{13}C$ and algal sterol $\delta^{13}C$, all of which show significantly higher values in the western Ross Sea. This spatial pattern in sterol $\delta^{13}C$ was concluded to be directly related to $CO_2$ drawdown at the surface, resulting in average sterol

$\delta^{13}C$ values varying from -27.9‰ in the west, where productivity is greatest, down to -33.5‰ further offshore (Villinski et al., 2008).

A similar relationship is evident in Prydz Bay, where POC $\delta^{13}C$ was found to be positively correlated with POC concentration and negatively correlated with nutrient concentration, indicating greater drawdown of $CO_2$ and nutrients under high productivity levels (Zhang et al., 2014).

This suggests it may be possible to apply FA $\delta^{13}C$ as a palaeoproductivity indicator in this highly productive polynya environment. However, it is important to constrain the most likely season and habitat being represented, since phytoplankton assemblages vary both spatially (e.g. ice edge or open water) and temporally (e.g. spring or summer). Surface water $pCO_2$ in the Ross Sea is observed to vary spatially across the polynya, with the lowest $pCO_2$ occurring where primary productivity is high (Tortell et al., 2011; Villinski et al., 2008). The incredibly high sedimentation rate (1-2 cm $yr^{-1}$) within the Adélie Basin where core DTGC2011 was recovered is thought to be the result of syndepositional focusing processes that bring biogenic debris from the higher Adélie and Mertz banks and collect in the ca. 1,000 m deep basin (Escutia et al., 2011). Thus, it is likely that core DTGC2011 contains material from a wide area, including both the Mertz and Dumont d'Urville polynyas, and areas both near the coast and further offshore, meaning it is quite possible that the $C_{18}$ and $C_{24}$ FAs are recording palaeoproductivity changes in different environments, which would explain their different trends. Furthermore, surface water $pCO_2$ can vary spatially, such as in the Ross Sea polynya where Tortell et al. (2011) measured surface water $pCO_2$ values ranging between 100 and 400 ppm. Thus, it is likely that these two areas offshore Adélie Land where the $C_{18}$ and $C_{24}$ FAs are being produced will also have differing surface water $CO_2$ concentrations and trends.

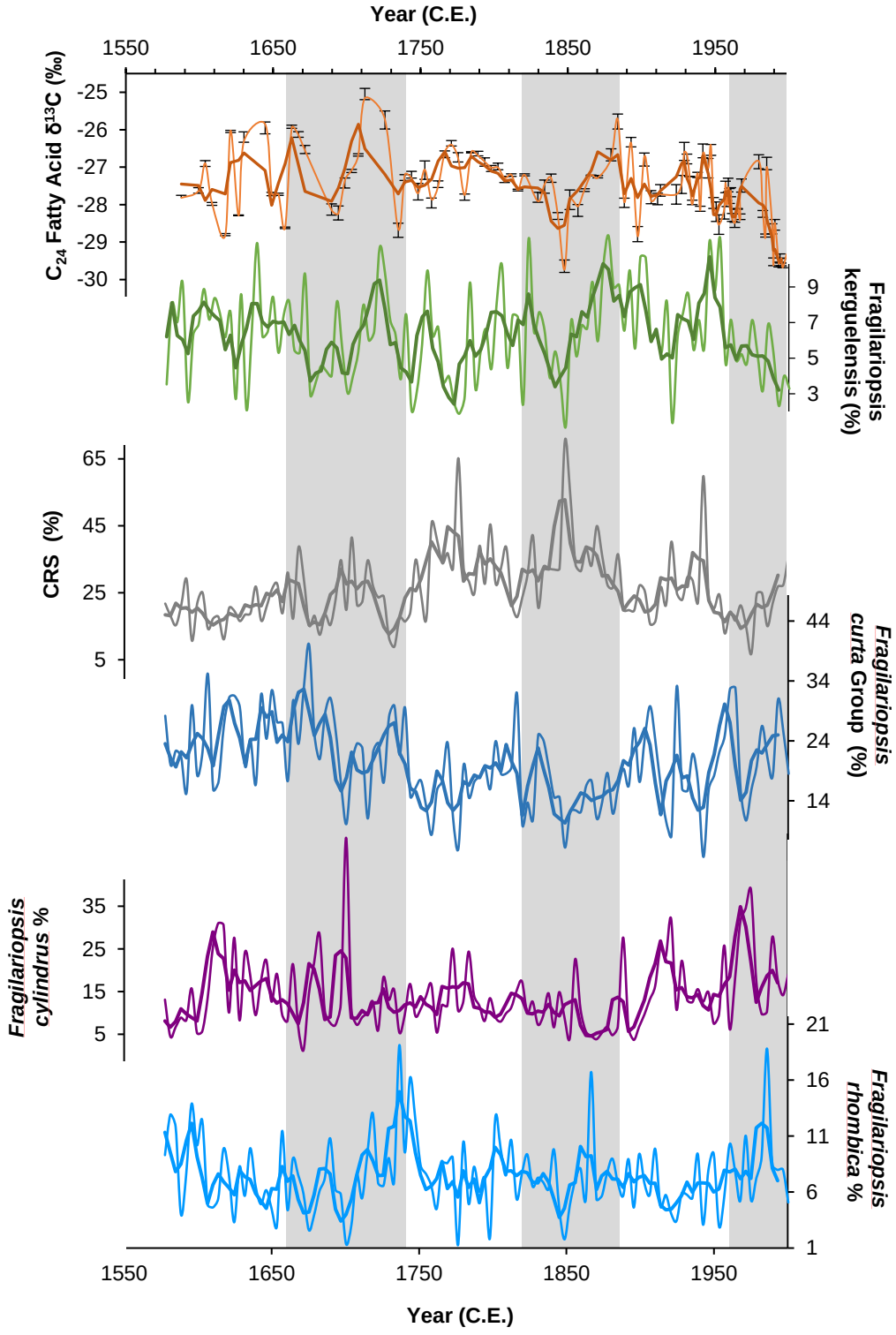



**Figure 5.6** $\delta^{13}C$ values of the $C_{24}$ fatty acid (orange) and relative abundances (%) of the open water diatom *Fragilariopsis kerguelensis* (green). Also shown are relative abundances of the four most abundant diatom groups in DTGC2011. *Chaetoceros* resting spores (CRS; grey line), *Fragilariopsis curta* group (dark blue line), *Fragilariopsis cylindrus* (purple line) and *Fragilariopsis rhombica* (light blue line). Thick line represents 3-point moving average for each. Grey vertical bands highlight periods where $C_{24}$ fatty acid $\delta^{13}C$ is in phase with *F. kerguelensis*.

### 5.4.3 Comparison of fatty acid $\delta^{13}C$ with other proxy data

Comparison of down-core variations in FA $\delta^{13}C$ with other proxy data can also be used to help decipher the main signal being recorded. Comparison between $\delta^{13}C_{24FA}$ and the major diatom species abundances within the core shows a reasonably close coherence with *Fragilariopsis kerguelensis,* particularly since ~1800 C.E. (Fig. 5.6). *Fragilariopsis kerguelensis* is an open water diatom species and one of the most dominant phytoplankton species offshore Adélie Land (Chiba et al., 2000), reaching its peak abundance in the summer (Crosta et al., 2007). This suggests that the $C_{24}$ FA is being produced during the summer months and may indicate that it is reflecting productivity in more open waters, where *F. kerguelensis* thrives. $\delta^{13}C_{24FA}$ also appears to show no response to changes in sea ice, as recorded by both HBI diene concentrations and abundances of *Fragilariopsis curta* (Fig. 5.6 and 5.7). This supports the suggestion that these compounds are being produced in open water during the summer months after sea ice has retreated, thus being relatively unaffected by sea-ice changes.

As discussed above, *P. antarctica* is a likely producer for the $C_{18}$ FA, a prymnesiophyte algae which has been observed in the Adélie region in summer months residing predominantly along the margin of fast ice, but also further offshore (Riaux-Gobin et al., 2013, 2011; Vaillancourt et al., 2003). The aversion of *F. kerguelensis* to sea ice (and thus also the $C_{24}$ FA producer) in contrast to *P. antarctica*, may explain the clear lack of coherence in the down-core trends in $\delta^{13}C_{18FA}$ and $\delta^{13}C_{24FA}$ (Fig. 5.5). Thus, we hypothesise that $\delta^{13}C_{18FA}$ is recording surface water $CO_2$ driven by productivity in the MIZ, whilst $\delta^{13}C_{24FA}$ is recording surface water $CO_2$ in more open water, further from the ice edge.

HBI diene concentrations indicate elevated fast ice cover between ~1919 and 1970 C.E., with a particular peak between 1942 and 1970 C.E., after which concentrations rapidly decline and

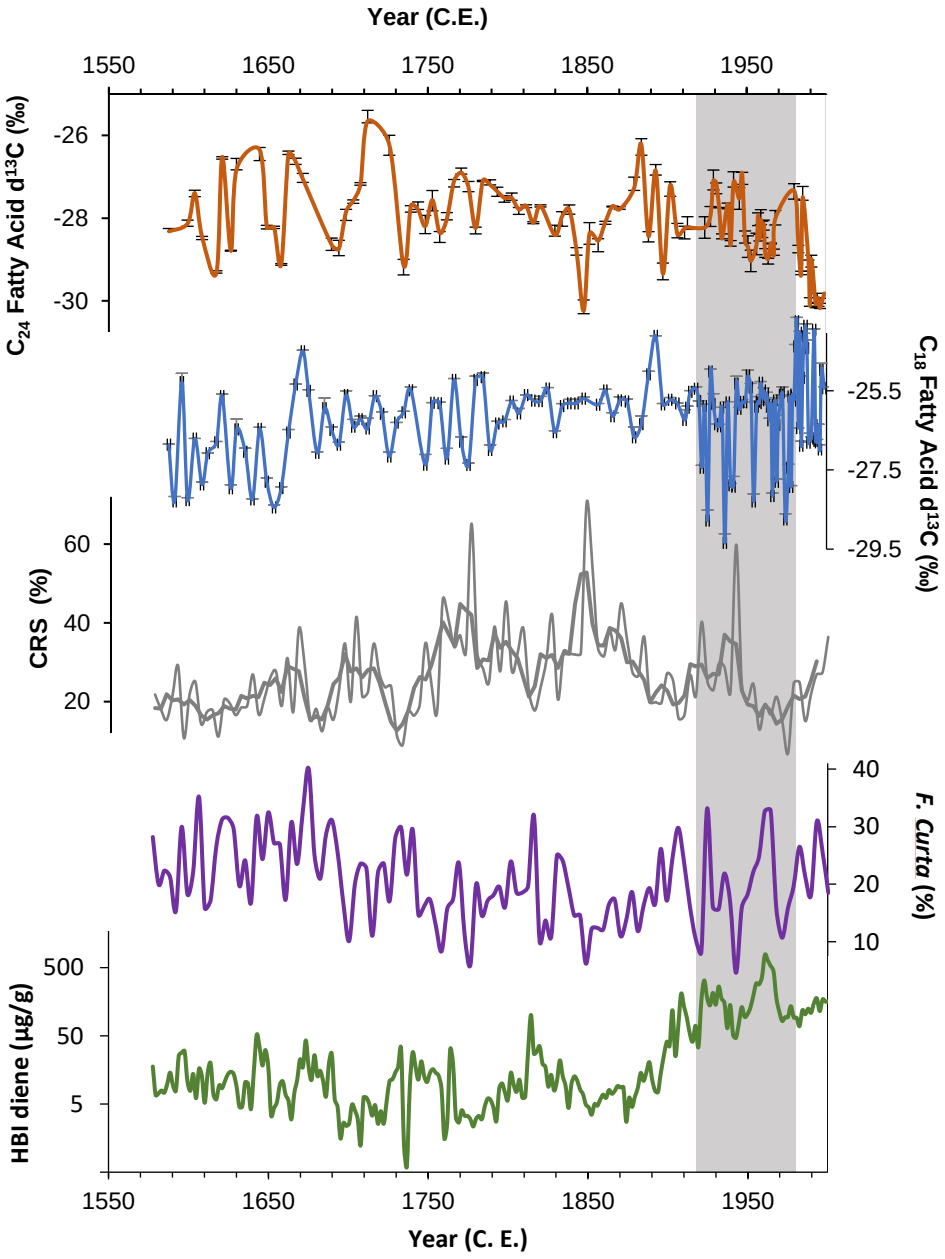



**Figure 5.7** $\delta^{13}C$ of the $C_{24}$ (orange) and $C_{18}$ (blue) fatty acid, HBI diene concentrations (green; plotted on a log scale) and relative abundances of *Fragilariopsis curta* plus *Fragilariopsis cylindrus* (purple). Latter two records reflect sea ice concentrations. Grey vertical band highlights period where low $C_{18}$ $\delta^{13}C$ overlaps with elevated HBI diene concentrations.

remain low until the top of the core. Abundances of *F. curta*, used as a sea ice proxy, similarly show peaks at this time indicate increased sea ice concentration (Campagne, 2015) (Fig. 5.7). $\delta^{13}C_{18FA}$ indicates a period of low productivity between ~1922 and 1977 C.E., broadly overlapping with this period of elevated fast ice concentration (Fig. 5.7), with a mean value of -27.12‰. This is compared to the mean value of -26.23‰ in the subsequent period (~1978 to 1998 C.E.) during which HBI diene concentration remain low (Fig. 5.7). This suggests that productivity in the coastal region was reduced while sea ice was high. This might be expected during a period of enhanced ice cover – perhaps representing a reduction in the amount of open water, or a shorter open water season – since the majority of productivity takes place within open water, such as the ice edge, rather than within or under the ice (Wilson et al., 1986).

Furthermore, $\delta^{13}C_{18FA}$ shows a broad similarity with *Chaetoceros* resting spores (CRS) on a centennial scale, with lower productivity at the start of the record, ca. 1587 to 1662 C.E., followed by an increase in both proxies in the middle part of the record, where $\delta^{13}C_{18FA}$ becomes relatively stable and CRS reaches its highest abundances of the record. This is then followed in the latter part of the record, after ca. 1900 C.E., by both proxies displaying lower values overall. CRS are associated with high nutrient levels and surface water stratification along the edge of receding sea ice, often following high productivity events (Crosta et al., 2008). The broad similarity to CRS, with lower values recorded during periods of high sea-ice concentrations, suggests that $\delta^{13}C_{18FA}$ is similarly responding to productivity in stratified water at the ice edge. This supports the hypothesis that $\delta^{13}C_{18FA}$ is recording primary productivity in the MIZ.

## 5.5 Conclusions

FAs identified within core DTGC2011, recovered from offshore Adélie Land, have been analysed for their concentrations and carbon isotope compositions to assess their utility as a palaeoproductivity proxy in an Antarctic polynya environment. The $C_{18}$ and $C_{24}$ compounds yielded the best isotope measurements and show very different $\delta^{13}C$ trends, suggesting they are being produced by different species in different habitats and/or seasons.

Comparison with other proxy data and information from previous studies suggests that the $C_{18}$ compound may be predominantly produced by *Phaeocystis antarctica*, with $\delta^{13}C_{18FA}$ reflecting productivity changes in the marginal ice zone, where it is sensitive to changes in ice cover. In contrast, $\delta^{13}C_{24FA}$, which compares well with abundances of the open water diatom *Fragilariopsis kerguelensis,* may be reflecting summer productivity further offshore, in open waters where it is less sensitive to fast ice changes. We argue than FA $\delta^{13}C$ can be used as a productivity proxy, but should be used in parallel with other proxies such as diatoms abundances or HBIs. The use of $\delta^{13}C$ analysis of multiple FA compounds, as opposed to individual compounds or bulk isotope analysis, allows a more detailed insight into the palaeoproductivity dynamics of the region, with the potential to separate productivity trends within different habitats.

However, there are clearly uncertainties in interpreting the FA $\delta^{13}C$ and many assumptions have been made here. The producers of the $C_{18}$ and especially the $C_{24}$ FAs is a key source of uncertainty and will require further work to further elucidate. The possibility of inputs of FAs from multiple sources, in particular from organisms further up the food chain, has consequences for their interpretation since this could mean the $\delta^{13}C$ FA is not fully reflecting just surface water conditions. Other key uncertainties are the magnitude of upwelling of $CO_2$

at the site in comparison to drawdown by phytoplankton, and the potential role of changes in air-sea $CO_2$ exchange.

## Chapter 6

# RECONSTRUCTION OF HOLOCENE PRIMARY PRODUCTIVITY OFFSHORE ADÉLIE LAND, EAST ANTARCTICA, USING COMPOUND-SPECIFIC CARBON ISOTOPES


## Abstract

Primary productivity in Antarctic coastal zones plays a key role in drawing down $CO_2$ from the atmosphere. Understanding how primary productivity has changed in the past in relation to different environmental factors can provide important information about the carbon cycle and how it may change in the future. This chapter uses carbon isotopes of two different fatty acids as a proxy for primary productivity in different habitats (ice-edge and open water) over the Holocene from a marine sediment core off the coast of Adélie Land, East Antarctica. The data presented suggest that primary productivity was spatially variable over the Holocene. Open water productivity appears to be highest and most stable during the middle and late Holocene periods, after local ice sheets have retreated. Despite a rapid and widespread increase in sea-ice concentration in the Late Holocene, open water productivity remains high, possibly reflecting conditions within the Mertz Glacier Polynya or within a restricted growing season. In contrast, ice edge productivity reaches the lowest levels in the late Holocene, perhaps due to a shorter ice-free season leading to a lack of stratified, nutrient-rich water.


## 6.1 Introduction

Antarctic coastal zones are important players in the global carbon cycle. A large amount of $CO_2$ from the deep ocean is ventilated here during the production of high-salinity waters, allowing waters rich in nutrients and $CO_2$ to be upwelled to the surface. This leads to intense

phytoplankton blooms which rapidly reduce $pCO_2$ to low levels through photosynthesis (Arrigo et al., 2008). The biological drawdown can result in surface water pCO2 greatly undersaturation with respect to atmospheric $CO_2$ (Tortell et al., 2011). Some of the upwelled $CO_2$ from the deep ocean is 'leaked' into the atmosphere, meaning any change in the consumption of these nutrients by phytoplankton, or a change in phytoplankton community structure, can affect the air-sea $CO_2$ exchange in this region, since greater nutrient consumption is associated with enhanced photosynthetic drawdown of $CO_2$ from the surface waters. Where this carbon is eventually exported to the deep sea and buried, it can lead to a lowering of atmospheric $CO_2$ concentrations (Sigman and Boyle, 2000). Thus understanding how primary productivity has responded to different environmental factors in the past, and how it may change in the future, is important for understanding the carbon cycle in climatically sensitive Antarctic coastal regions.

Sea ice and ice edge environments provide a vital habitat for a large proportion of Southern Ocean phytoplankton and extensive phytoplankton blooms are commonly observed here (Wilson et al., 1986). Coastal polynyas - areas of open water surrounded by sea ice (Bindoff et al., 2000) - are particularly important because of the large area of ice edge habitat. They are often hotspots of primary productivity, drawing down significant amounts of $CO_2$ through photosynthesis during the spring and summer months (Arrigo and van Dijken, 2003).

Understanding how primary productivity and gas exchange in these environments might change in future has important implications for understanding future atmospheric $CO_2$ and climate change. However, many uncertainties remain in terms of what factors drive primary productivity on different time scales, and the role of primary production in Antarctica's coastal zone on atmospheric $pCO_2$. Long-term records of primary productivity are rare, but information reconstructed from marine sediments can provide an insight into how

productivity has changed over time and how it has responded to different environmental drivers.

A 171 m Holocene sediment core U1357B was recovered from a polynya environment offshore Adélie Land, East Antarctica. This is a region of rapid sediment accumulation rate, of ca. 1-2 cm $yr^{-1}$, due in part to the high primary productivity dominated by mostly by diatoms and *Phaeocystis antarctica.* Analysis of algal biomarkers and isotope composition in this sediment core and comparison with nearby records provides the opportunity to reconstruct a range of environmental conditions. In particular, data from U1357B are compared to diatom assemblage data from nearby Holocene sediment core MD03-2601, recovered from a site ca. 100 km west of U1357B.

Analysis of fatty acid carbon isotopes in core DTGC2011, recovered from the same location as U1357B, indicated the potential utility of $C_{18}$ and $C_{24}$ fatty acid $\delta^{13}C$ ($\delta^{13}C_{18FA}$ and $\delta^{13}C_{24FA}$, respectively) as proxies for surface water primary productivity, as discussed in Chapter 5. This chapter concluded that the $C_{18}$ fatty acid is most likely to be produced by *P. antarctica* with $\delta^{13}C_{18FA}$ recording productivity changes predominantly within the marginal ice zone i.e. the stratified waters at the retreating ice edge. In contrast, although the $C_{24}$ fatty acid producer remains unknown, it is more likely to be produced further from the ice edge, with $\delta^{13}C_{24FA}$ recording productivity changes in the open water environment. The aim of this chapter is to apply these fatty acid $\delta^{13}C$ proxies to samples from U1357B to reconstruct palaeoproductivity changes through the Holocene and, through comparisons with other datasets from the region, look at the potential driving factors behind such productivity changes.

## 6.2 Methods

Fatty acids were extracted from 160 sediment samples from core U1357B at the University of Glasgow following the methods described in Chapter 4. Compound specific carbon-isotope analysis was undertaken at the University of Birmingham following the methods described in Chapter 3. One hundred and fifty-five samples successfully yielded isotopes measurements on the $C_{24}$ fatty acid, while the $C_{18}$ fatty acids was only successfully measured on 74 samples due to the lower concentrations. Bulk sediment carbon isotopes were generated at the University of Otago following methods described in Anderson et al. (2018).

## 6.3 Results and Discussion

The $\delta^{13}C_{18FA}$ and $\delta^{13}C_{24FA}$ records show very different trends over the course of the Holocene (Fig. 6.1a and 6.1b), supporting the hypothesis of different biological sources and suggesting that there is significant spatial variation in primary productivity offshore Adélie land. The data has been divided into three time periods based on major patterns in proxy data following Chapter 4.

### 6.3.1 Early Holocene (11.4 – 8.2 ka BP)

The $\delta^{13}C_{24FA}$ has a mean value of -31.1‰ (n = 39) over this period, the lowest value of the three periods, and also the highest standard deviation of 1.1 (Fig. 6.1b). This indicates that the early Holocene was a time of overall low but highly variable productivity. At this time, the geology and geomorphology at the base of the Adélie drift, from which the sediment core was recovered, is suggestive of a 'calving bay re-entrant' situation, as discussed in Chapter 4. This model suggests that parts of the retreating glacial ice from the last glacial maximum remained grounded on the bathymetric highs whilst other parts retreated faster over the deeper troughs, thus creating an ice-walled fjord-like environment at the core site. Fatty acid $\delta^{2}H$ indicate this was a time of high glacial meltwater input, including the most negative $\delta^{2}H$ values of the

record at 9.6 ka, as discussed in Chapter 4. Diatom assemblages from nearby core MD03-2601 also indicate the highest abundances of *Chaetoceros* resting spores (CRS) during the

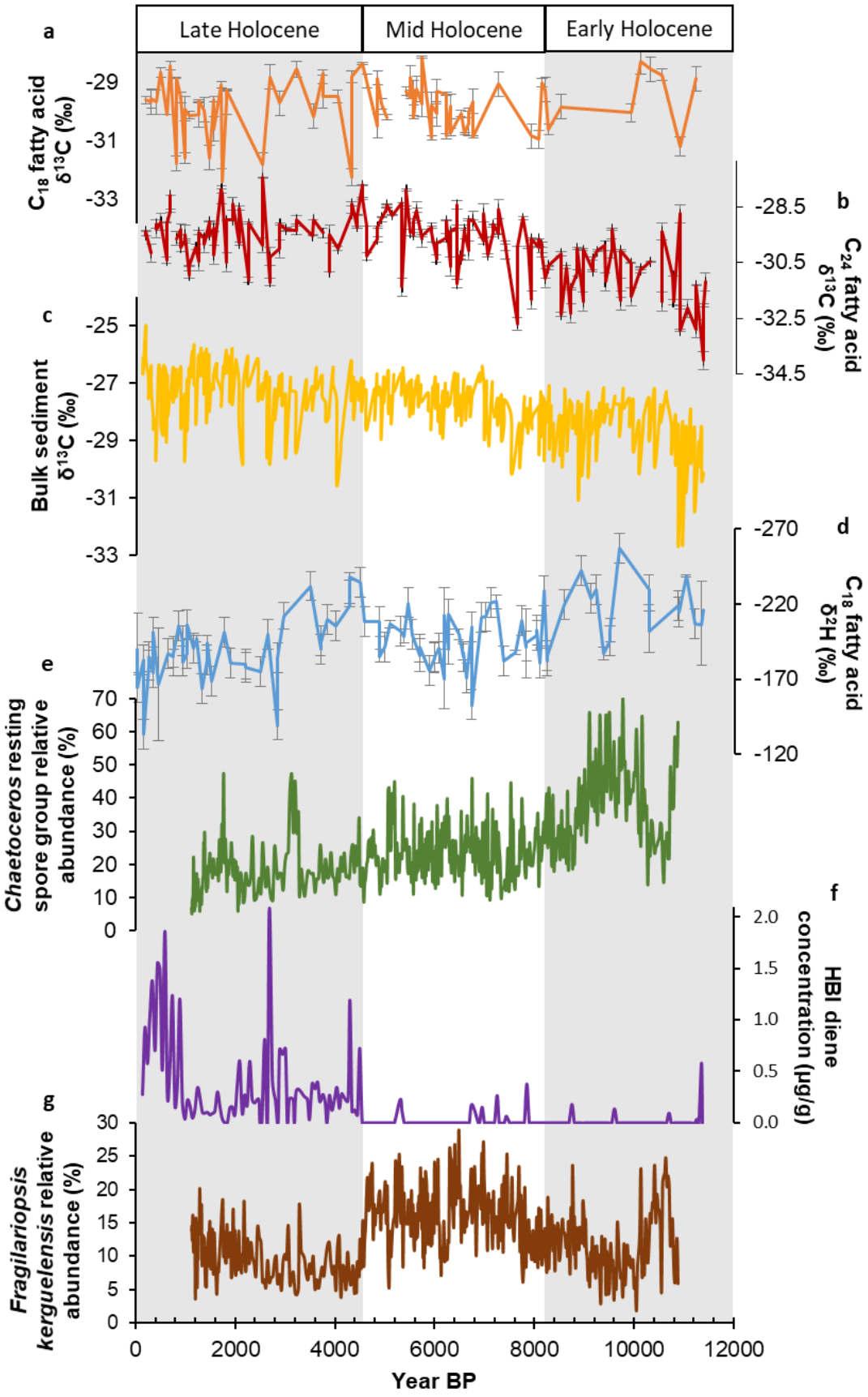



**Figure 6.1** Holocene proxy record from offshore Adélie land a) $C_{18}$ fatty acid $\delta^{13}C$ from U1357B, b) $C_{24}$ fatty acid $\delta^{13}C$ from U1357B, c) Bulk sediment $\delta^{13}C$ from U1357B, d) $C_{18}$ fatty acid $\delta_2H$ from U1357B, e) *Chaetoceros* resting spore group relative abundance (%) from MD03-2601 (Crosta et al., 2007), f) *Fragilariopsis curta* relative abundance (%) from MD03-2601 (Crosta et al., 2007) , g) *Fragilariopsis kerguelensis* relative abundance (%) from MD03-2601 (Crosta et al., 2007). Vertical grey bands indicate boundaries between the periods referred to in the text: Early Holocene (11,400 to 8,200 years BP), Mid-Holocene (8,200 to 4,500 years BP) and Late Holocene (4,500 years BP to present). Error bars for a) b) and d) based on replicate analyses.

early Holocene (Fig. 6.1e). *Chaetoceros* diatom blooms are associated with high nutrient levels and surface water stratification along the edge of sea ice, thus CRS are commonly used to track high productivity events at the receding ice edge (Crosta et al., 2008). Such widespread stratification within the walls of the retreating ice would be likely to limit productivity from phytoplankton associated with open water and deeper mixed layers, explaining the lower productivity recorded by the $\delta^{13}C_{24FA}$. However, the release of important nutrients such as Fe, which is thought to be a key control on Southern Ocean productivity (Boyd et al., 2000), is often associated with glacial ice melt (Death et al., 2014). This may have also benefitted phytoplankton, and so may explain the highly variable nature of the $\delta^{13}C_{24FA.}$

Despite the highly variable nature, $\delta^{13}C_{24FA}$ broadly increases over this period, suggesting that productivity gradually increased as meltwater input declined. Bulk sediment $\delta^{13}C$, which is likely to incorporate a range of phytoplankton species and thus be a broad representation of primary productivity as a whole, similarly shows the most negative values of the record during this period, gradually increasing from the earliest Holocene (Fig. 6.1c). Short term trends in $\delta^{13}C_{24FA}$ and bulk $\delta^{13}C$ are also well correlated, with the lowest values of both records between 11.3 and 10.9 ka BP. This is followed by a rapid but short-lived increase ca. 10.8 ka BP with a subsequent decline in both records. The close similarity between $\delta^{13}C_{24FA}$ and bulk $\delta^{13}C$ may indicate that open water phytoplankton are dominating overall productivity at this time, since bulk $\delta^{13}C$ is likely to record productivity from the wide range of species. However, the bulk $\delta^{13}C$ signal is also going to be affected by changing inputs of different phytoplankton species with varying $\delta^{13}C$ values, as was found to be the case by Crosta et al. (2005) for bulk organic matter $\delta^{13}C$ offshore Adélie Land.

In contrast, the $\delta^{13}C_{18FA}$ has an average value of -29.5‰ (n = 8), the highest of the three periods, suggesting that ice edge productivity was high (Fig. 6.1a). High ice edge productivity is also suggested by the elevated CRS abundances in core MD03-2601, as noted above. This suggests the presence of stratified, nutrient-rich water, benefitting ice-edge phytoplankton species, perhaps enhanced by greater glacial meltwater inputs and associated inputs of Fe, as indicated by highly negative $\delta^{2}H$ values (Fig. 6.1d), and low sea ice cover (Fig. 6.1f).

The $\delta^{13}C_{18FA}$ also has a relatively high standard deviation of 1.1 during this period, as is the case for the $C_{24}$, suggesting ice edge productivity is highly variable. This might be expected at this time of high meltwater input, as indicated by the negative $\delta^{2}H$ values (Fig. 6.1d), and variable surface water conditions, as indicated by fluctuating CRS abundances in MD03-2601 (Fig. 6.1e). However, it should be noted that $\delta^{13}C$ analysis was only completed for the $C_{18}$ on eight samples for the early Holocene, making it difficult to identify any clear trends.

### 6.3.2 Mid-Holocene (8.2 – 4.5 ka BP)

Primary productivity in both open water and ice edge habitats, as recorded by $\delta^{13}C_{18FA}$ and $\delta^{13}C_{24FA}$, appear relatively stable during this period (standard deviation = 0.8 and 0.9, respectively), compared to the early Holocene. $\delta^{13}C_{18FA}$ reaches the highest value of the record at 5.7 ka. Glacial meltwater inputs ($\delta^{2}H$) and CRS abundances both remain relatively low, with greater abundances of open water diatom species *Fragilariopsis kergulenesis* in nearby core MD03-2601 (Fig. 6.1g) (Crosta et al., 2007). This suggests the end of local glacial retreat with the establishment of a more stable, open water environment. Sea ice, as recorded by the highly branched isoprenoid alkene (HBI) diene biomarker (Fig 6.1f), and *F. curta* in core MD03-2601 (Chapter 4, Fig. 6.2), also remain low during this period. The mid-Holocene is associated with increasing air temperatures in East Antarctica, as recorded by the

EPICA Dome C ice core (the most proximal to Adélie Land), and generally warmer temperatures across Antarctica as a whole (Masson-Delmotte et al., 2011). The overall higher productivity for this period may indicate that these warmer, open water conditions were favourable to phytoplankton as a whole, perhaps through sea ice melt and a longer growing season. $\delta^{13}C_{24FA}$ continues to increase throughout the period which may suggest that open water productivity is responding positively to the warming air temperatures.

### 6.3.3 Late Holocene (4.5 ka BP – present)

This period begins with a peak in both the $\delta^{13}C_{18FA}$ and $\delta^{13}C_{24FA}$, with the $\delta^{13}C_{24FA}$ reaching the highest value of the record so far at 4.5 ka, suggesting a peak in productivity in both ice edge and open water habitats. This is followed by a rapid decline in $\delta^{13}C_{18FA}$ which reaches the lowest value of the record so far at 4.3 ka. The $\delta^{13}C_{24FA}$ similarly declines, although more gradually and to a lesser extent than the $C_{18}$, until 3.9 ka. Bulk $\delta^{13}C$ also shows a substantial but short-lived decline, reaching the lowest value since the Early Holocene at 4 ka. A period of enhanced glacial meltwater input is evident from the $\delta^{2}H$ record (Fig. 6.1d), peaking at ca. 4.5 ka, coinciding with a rapid increase in sea-ice concentration at the coast. This is hypothesised to represent the last major grounding line retreat of the Ross Ice Shelf and the development of a large ice-shelf cavity in the Ross Sea, the latter altering ice sheet-ocean interactions leading to enhanced sea ice production around the coast (Chapter 4).

The coincidence of the peak in meltwater, 4.3 – 4.5 ka, with peaks in productivity from both the $\delta^{13}C_{18FA}$ and $\delta^{13}C_{24FA}$ at 4.5 ka, suggests that this freshening of the surface waters created a favourable environment for phytoplankton, at least prior to the onset of enhanced sea ice conditions. Glacial meltwater is an important contributor of Fe in the surface waters (Death et al., 2014; Arrigo et al., 2015), thus the enhanced meltwater input may have increased the

amount of Fe available for phytoplankton, leading to an increase in productivity. There is also a substantial peak in Ba/Ti in core U1357B at this time, centred on ca. 4.5 ka, interpreted in Chapter 4 as representing enhanced primary productivity (Fig. 4.2). However, this productivity peak is short-lived, declining soon after in all proxies. Abundances of open water species such as *F. kerguelensis* from core MD03-2601, also drops substantially, and remain low for the rest of the period (Fig. 6.1g). In contrast, sea ice associated species such as *F. curta* increase rapidly after this point. The rapid increase in sea-ice concentration, which closely followed the meltwater peak at 4.4 ka, clearly had substantial impacts on coastal phytoplankton communities. The $\delta^{13}C$ data suggests that the shift to a sea-ice dominated environment initially had a negative impact on productivity, with a reduction in open water habitat near the coast perhaps due to a reduced polynya size. However, based on the $\delta^{13}C$, this reduction in productivity appears to be short lived for both the $C_{18}$ and $C_{24}$ FA.

It is interesting to note that $\delta^{13}C_{24FA}$ is the highest overall during the late Holocene (-29.47‰, n = 57) and also the most stable (standard deviation = 0.8). Bulk sediment $\delta^{13}C$ similarly reaches the highest values during this period. The high values recorded by the $\delta^{13}C_{24FA}$ and bulk $\delta^{13}C$ is surprising, especially if the former is recording open water productivity, given that an increase in sea ice is likely to reduce the amount of open water habitat available. Indeed, ice-associated species such a *F. curta* increase, while open water species such as *F. kerguelensis* decline, in core MD03-2601.

There are various potential explanations for this apparent divergence between $\delta^{13}C_{24FA}$ and diatom abundances from MD03-2601. One possibility is that there is a shift in the producers of the $C_{24}$ fatty acids, meaning that $\delta^{13}C_{24FA}$ is no longer representing open water productivity. For example, an increased contribution of the $C_{24}$ fatty acid from algae which thrive in icy

conditions could explain the higher $\delta^{13}C$ values during this period – either reflecting greater productivity in the sea ice zone or reflecting the higher $\delta^{13}C$ of sea ice algae (Gibson et al., 1999). This hypothesis is difficult to test due to the uncertainties in identifying a clear precursor organism.

Another explanation could relate to a reduction in growth season duration, due to the increased concentration of sea ice. Crosta et al. (2007) argued that greater *F. curta* abundances indicate a reduced growing season due to the elevated ice cover and a later waning of the ice. In such a case, productivity may be reduced on an annual scale, which would explain why *F. kerguelensis* declines, but the intensity of productivity during the growing season – during which time the $C_{24}$ fatty acid is most likely to be produced – may remain high. As the fatty acids are only recording productivity during the lifetime of the precursor organism, $\delta^{13}C_{24FA}$ could remain high as it will not record the reduced productivity outside of the growing season.

A further explanation may be due to the spatial heterogeneity of the environment, as the *F. kerguelensis* data is from core MD03-2601, which is located ~100 km away from core U1357B. It is possible that these two sites experience different conditions during this period, with productivity being higher close to U1357B than MD03-2601. For example, although U1357B is situated near the Dumont d'Urville Polynya (DDUP), it is also downstream from the much larger and more productive Mertz Glacier Polynya (MGP). Core MD03-2601 is less likely to receive inputs from the MGP as it is ~100 km further downstream. The MGP is formed in the lee of the Mertz Glacier ice tongue, which acts as a physical barrier to sea ice transported around the coast, which is instead deflected northwards. This means water to the west of the ice tongue remains largely ice free. Thus, despite the increase in sea ice in the Late Holocene, the Mertz polynya is more likely to remain open throughout the year than the

DDUP, as long as the Mertz Glacier ice tongue is protruding from the coast. Thus, the difference between the two records may reflect a reduction in productivity in the DDUP, but continued or even enhanced productivity levels in the MGP.

After reaching the lowest values of the record at 4.3 ka, the $\delta^{13}C_{18FA}$ rebounds quickly but remains highly variable throughout this period. In contrast to $\delta^{13}C_{24FA}$, the $\delta^{13}C_{18FA}$ has on average the lowest value (-29.9‰, n = 33) and highest variation (standard deviation = 1.1) during this period. The low values suggest that, at times, ice-edge productivity is reduced during this period. Overall abundances of CRS in MD03-2601 are also low during this period, suggesting a lack of stratified, nutrient-rich waters. The increased sea-ice cover during this period may mean that polynyas were reduced in size leaving little ice edge habitat available, or that sea-ice melt is occurring later in the phytoplankton growing season. The highly variable nature of the $\delta^{13}C_{18FA}$ during this period may indicate variation between periods of highly compacted sea ice cover, leading to low productivity, and periods of enhanced sea ice melt with stratification and Fe release, leading to high productivity events at the ice edge. The HBI diene record also indicates high variability in the concentration of fast ice during this period, supporting this hypothesis.

### 6.4 Conclusions

In this chapter, $C_{18}$ and $C_{24}$ fatty acid $\delta^{13}C$ from core U1357B have been applied as proxies for palaeoproductivity over the course of the Holocene. These are hypothesised to represent ice edge and open water productivity, respectively. The two records show very different long term trends, suggesting that there is a spatial variation in productivity trends offshore Adélie Land. Open water productivity appears to be highest and most stable during the middle and late Holocene periods, after local ice sheets have retreated to near their present day position.

Despite a rapid and widespread increase in sea-ice concentration in the Late Holocene, open water productivity appears to remain relatively high overall, including reaching its highest level during this period whilst ice edge productivity reaches the lowest. This is in contrast to what might be expected, especially as ice-associated species such as *F. curta* increase while open water species such as *F. kerguelensis* decline, as recorded in nearby core MD03-601. Various hypotheses are proposed to explain this disparity, including high productivity conditions within the MGP (but remaining low within the DDUP), a reduction in growth season duration (with productivity retained at high levels during the shorter season), or a shift in fatty acid producer(s). Reduced $\delta^{13}C_{18FA}$ during this period indicates reduced ice edge productivity, suggesting a lack of stratified, nutrient-rich water, possibly due to later melting of sea ice. Based on the data presented here, it is not possible to fully determine the reason for this discrepancy, especially due to a lack of diatom abundance data from core U1357B. However, these data have provided a new insight into the Holocene carbon cycling dynamics offshore Adélie Land.

## Chapter 7

# APPLICATION OF THE $TEX_{86}^{L}$ SEA SURFACE TEMPERATURE PROXY TO HIGHLY RESOLVED SEDIMENTS IN THE ANTARCTIC COASTAL ZONE


## Abstract

$TEX_{86}^{L}$ has been developed as a sea surface temperature (SST) proxy in low temperature regions, based on the distribution of glycerol dialkyl glycerol tetraethers (GDGTs). However, large calibration error bars and scatter in the temperature relationship below 5°C suggests there are uncertainties in our understanding of the role of temperature versus other factors driving GDGT distributions. This chapter presents a high-resolution record of $TEX_{86}^{L}$ from off the coast of Adélie Land, East Antarctica along with other proxy data from the last four centuries, including a period of overlap with a nearby instrumental record of air temperature. This provides the chance to assess the most likely drivers of GDGTs in this environment. The $TEX_{86}^{L}$ record, however, shows no correlation with air temperature in this region. This, in addition to a consistent over-prediction of temperatures compared to known SSTs in the region, and the deviation of GDGT distributions from the global core top dataset, suggest that $TEX_{86}^{L}$ is not recording SST. A correlation between $TEX_{86}^{L}$ and Sand% suggests that $TEX_{86}^{L}$ is being driven by changes in the strength of the westward coastal currents. We hypothesise that stronger currents are leading to greater advection of GDGTs from further east, where MCDW upwells. MCDW is known to have a greater diversity of archaeal communities and thus, greater advection may lead to greater inputs of GDGTs produced by different archaea, for which the relationship between GDGT cyclisation and temperature may differ.


## 7.1 Introduction

The $TEX_{86}^{L}$ palaeotemperature proxy is based on the distribution of glycerol dialkyl glycerol tetraethers (GDGTs), derived from archaea (Schouten et al., 2002). The development, application and interpretation of this proxy is discussed in Chapter 2.5.3. GDGT-based proxies have been applied to sediments recovered from around the globe and as far back in time as the Jurassic (Jenkyns et al., 2012). Various calibration studies involving core-top, seawater and culture samples have furthered the development and interpretation of these proxies in the marine realm (e.g. Schouten et al., 2002; Kim et al., 2010; Elling et al., 2015; Hurley et al., 2016; Lee et al., 2008), while various GDGT based reconstructions have been compared with other sea surface temperatures (SST) proxies (e.g. Huguet et al., 2006; Castañeda et al., 2010).

However, very few GDGT-based SST records exist from recent sediments with high enough temporal resolution to provide an overlap, and thus comparison, with instrumental temperature records. This means there has been no direct testing of this proxy against known temperature trends over time. Furthermore, the $TEX_{86}$ proxy shows a large amount of scatter at temperatures below 5°C, suggesting there may be a different relationship between GDGTs and SST in polar regions, compared to the rest of the globe (Schouten et al., 2002). The $TEX_{86}^{L}$ calibration was subsequently developed, incorporating more core-top samples from the Southern Ocean, yet a considerable amount of scatter in the calibration remains for low temperatures, leading to a large calibration error of 4°C (Kim et al., 2010). As a result, uncertainties remain as to the role of temperature versus other effects on GDGT distributions in the polar regions, particularly in the Antarctic coastal zone where average temperature are often below 0°C. Although some specific calibrations have been developed in the Antarctic (e.g. Shevenell et al., 2011) for the West Antarctic Peninsula, this is unlikely to be widely

applicable since it based on regional core-top data. $TEX_{86}$ variations from this calibration still give an extremely large and unrealistic range of temperature estimates (-2.9 to 10.9°C).

Sediment core DTGC2011 provides an opportunity to look at GDGT distributions off the coast of East Antarctica in high resolution (annual to sub-decadal) over the last few centuries (ca. 1587 to 1999 C.E.). This allows comparison to instrumental records of temperature for the most recent period, as well as proxy records of other environmental conditions, to help determine the most likely drivers of $TEX_{86}^{L}$ in this region.

### 7.2 Methods

Sediment samples were extracted at the University of Birmingham following methods described in Chapter 2. GDGTs were quantified at the University of Bristol on one hundred and forty-three samples (Chapter 2). Grain size analyses were conducted at Victoria University of Wellington following the methods described in Chapter 4.5.3.

### 7.3 $TEX_{86}^{L}$ and sea surface temperatures

To understand the record from DTGC2011 it is important to first decipher whether $TEX_{86}^{L}$ in this location is likely to be recording a signal of temperature or not, through comparison of $TEX_{86}^{L}$ derived SSTs with known temperatures in the region, as well as close analysis of GDGT distributions compared to global core-top samples.

The youngest measured sample in DTGC2011, dated to 1999 C.E. has a $TEX_{86}^{L}$ derived SST of 2.6°C. According to the World Ocean Atlas 2018 (WOA18) the average SST for the decade 1995-2004 in grid square 66.5°S, 142.5°E (the closest to the core site) is -1.1°C (Locarnini et al., 2018). This gives an offset of 3.7°C from the $TEX_{86}^{L}$ derived SST, which is still within the calibration error for $TEX_{86}^{L}$ of 4°C (Kim et al., 2010). However, comparing mean decadal temperatures from DTGC2011 and WOA18 (where SST data is available for

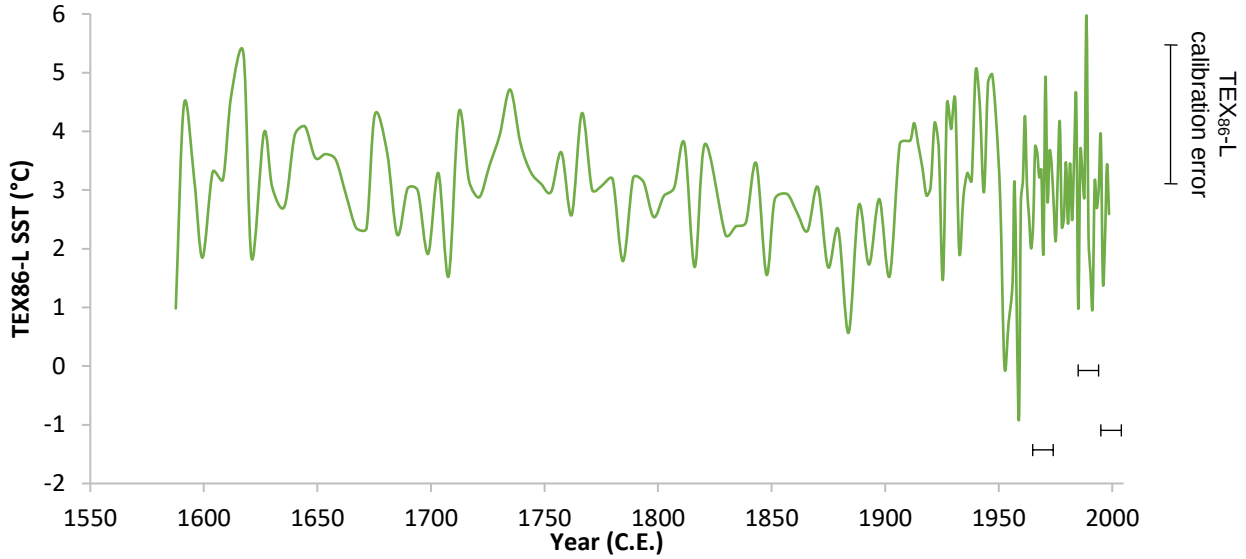



**Figure 7.1** $TEX_{86}^{L}$ derived sea surface temperatures in core DTGC2011. Horizontal bars show mean sea surface temperatures according to the World Ocean Atlas 2018 for three decades (1965-74, 1985-94, 1995-04) from 66.5°S, 142.5°E.

grid square 66.5°S, 142.5°E), there is an offset of 2.8°C for 1985-1994 and 4.7°C for 1965-1974, with the $TEX_{86}^{L}$ derived SST consistently predicting warmer temperatures (Fig. 7.1). The latter offset is greater than the 4°C calibration error which may suggest that something other than temperature is influencing GDGT distributions in this location.

The grid square these WOA18 temperatures are taken from is more than 50 km to the west of the core site (located at 66.2°S, 140.3°E), meaning it is possible that some of the offset may be due to local differences in surface temperatures. However, it is unlikely to be able to explain such large differences, since direct measurements of water temperature from offshore Adélie Land in recent years also record temperatures predominantly around -1°C (Shadwick et al., 2014; Lacarra et al., 2011). WOA18 data from this region indicates similar temperatures around the East Antarctic coast (Fig. 7.2), suggesting that large spatial heterogeneity is highly unlikely. Only the lowest $TEX_{86}^{L}$ derived SST of the record, -0.93°C in ca. 1958 C.E., comes close to the measured surface temperature in this region.

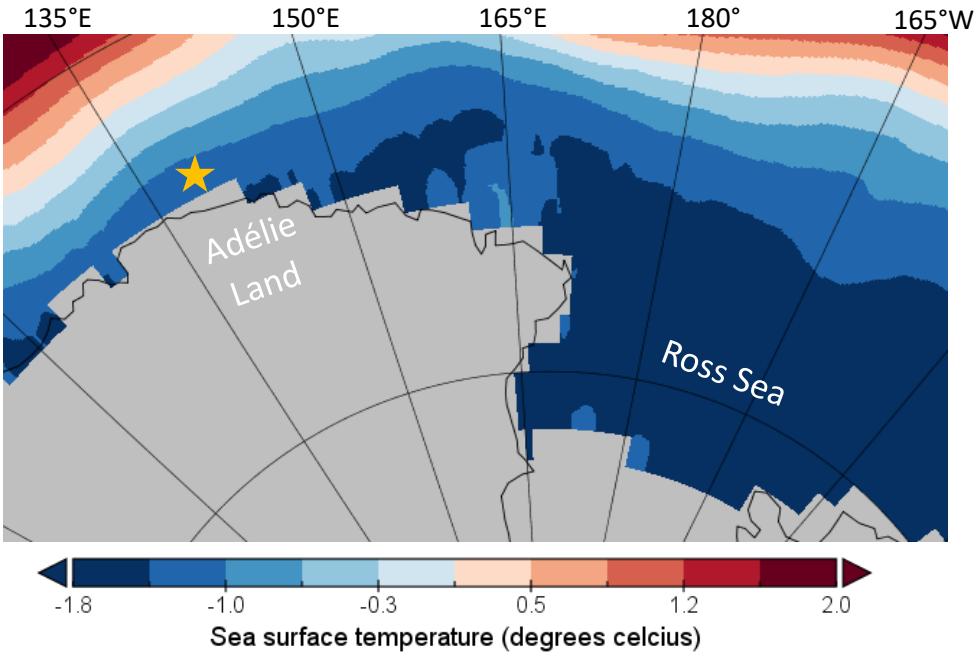



**Figure 7.2** Spatial variation in sea surface temperature around the Antarctic coast from Adélie Land to the Ross Sea. Data taken from the World Ocean Atlas 2018 averaged over the decade 1995 – 2004 and plotted using Panoply Data Viewer.

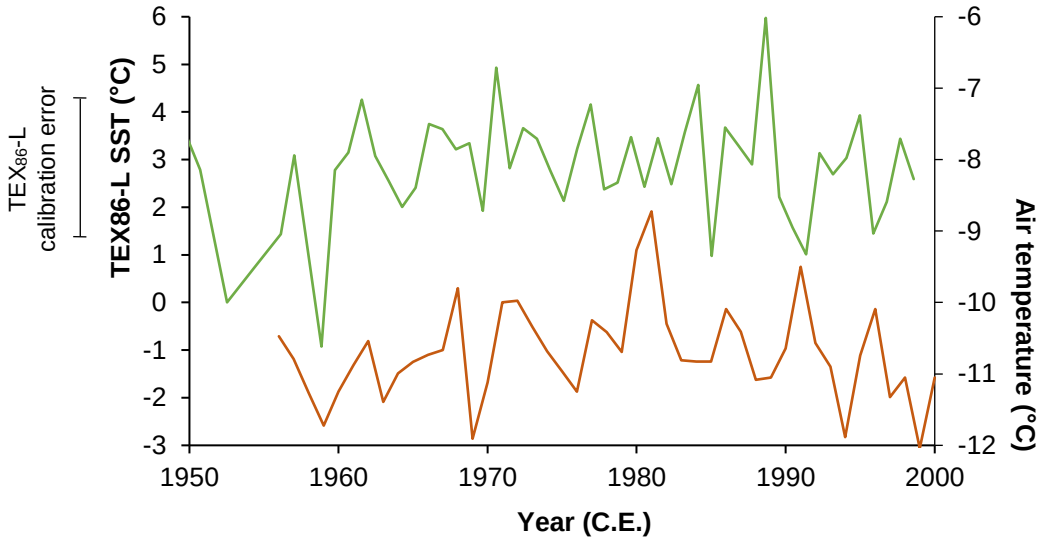



**Figure 7.3** $TEX_{86}^{L}$ derived sea surface temperatures in core DTGC2011 (green line) and air temperatures measured at Dumont D'Urville weather station (orange line) between 1950 and 2000 C.E.

Air temperatures have been measured at the Dumont d'Urville Station (66.6°S, 140.0°E) since 1956. Between 1956 and 2000 C.E., mean annual air temperatures have varied from -12.0°C to -8.7°C, a range of 3.3°C (BAS, 2019). If $TEX_{86}^{L}$ values were predominantly reflecting SSTs, they would be expected to follow a similar pattern to local air temperatures. However,

comparison between the two records (Fig. 7.3) shows no clear similarity. This is supported by regression analysis which gives an $R^2$ value of 0.02 (n = 43) suggesting there is no relationship between the two. Furthermore, $TEX_{86}^L$ SST values vary by 6.9°C over this period – more than twice the range of the mean annual air temperature. This is perhaps surprising given that ocean temperatures are known to vary more slowly than air temperature as a result of the thermal inertia of the ocean (Brown et al., 1989), further suggesting that the $TEX_{86}^L$ record may not be reflecting temperature.

### 7.4 GDGT distributions

Various indices have been introduced as a means of evaluating the likely role of influences other than temperatures on GDGT distributions and $TEX_{86}$ values. These have been discussed briefly in Chapter 1.6.3. and include the methane index (MI) (Zhang et al., 2011), branched and isoprenoid tetraether (BIT) index (Hopmans et al., 2004) and the ring index (RI) (Zhang et al., 2016).

Abundances of branched GDGTs (terrestrially derived) in DTGC2011 were observed to be very weak in all samples compared to isoprenoid GDGTs (marine derived) suggesting minimal input from soils, as would be expected from the ice-covered East Antarctic region with limited exposure of soils. The BIT index of samples are typically two orders of magnitude below the limit of 0.4 defined by Weijers et al. (2006) (e.g. 0.04), indicating negligible terrestrial input. Thus, GDGT input from soils can be disregarded as a likely influence on the $TEX_{86}^L$ record.

In DTGC2011, MI values vary between 0.05 and 0.11, well below the proposed threshold of 0.3 (Zhang et al., 2011), suggesting that GDGT inputs from methanotrophic Euryarchaeota are also likely to be minimal.

The RI and ΔRI were proposed by Zhang et al. (2016) to identify when non-thermal influences may be affecting GDGTs, the latter indicating the deviation from the global core-top relationship between RI and $TEX_{86}$. This is based on the premise that $TEX_{86}$ and RI are linked through a common temperature control on GDGT distributions. ΔRI values > 0.3 are suggested to indicate the influence of factors other than temperature (Zhang et al., 2016).

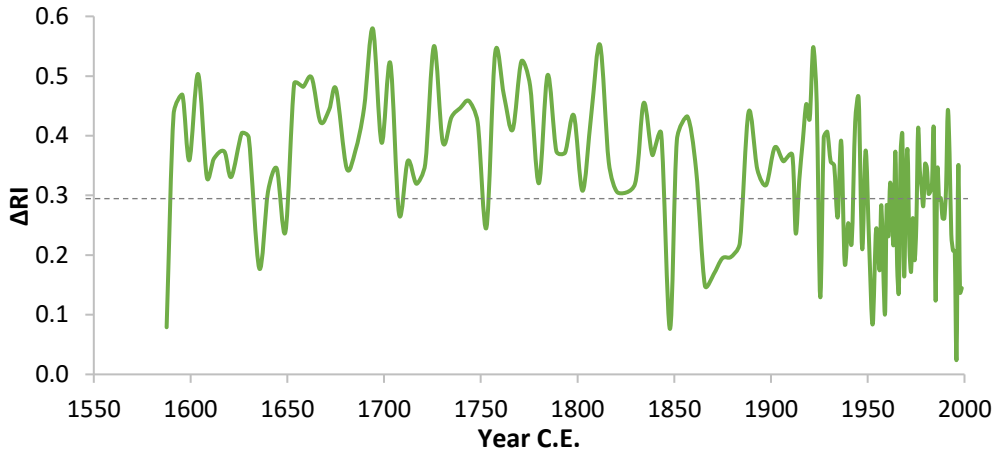



**Figure 7.4** ΔRI of samples from DTGC2011 over time. Horizontal dashed line indicates the 0.3 threshold defined by Zhang et al. (2016) used to indicate potential influence of non-thermal effects.

In DTGC2011, ΔRI values range between 0.03 and 0.58, with 93 samples lying above the 0.3 threshold, and only 50 samples below it (Fig. 7.4). This suggests that there may be non-thermal influences acting on GDGT distributions, affecting the reconstructed temperatures. In addition, DTGC2011 samples show no correlation between RI and $TEX_{86}$ ($R^2 = 0.00$), in contrast to the global core top data used by (Zhang et al., 2016) which shows a strong polynomial regression between the two ($R^2 = 0.87$, n = 531) (Fig. 7.5).

Interestingly, ΔRI has a weak but significant, positive correlation with both $TEX_{86}$ ($R^2 = 0.15$, $p < 0.001$, n = 143) and $TEX_{86}^L$ ($R^2=0.12$, $p < 0.001$, n = 143) in DTGC2011. Broadly speaking, samples with a high ΔRI have a higher $TEX_{86}^L$ value and vice versa, which may suggest that samples with higher $TEX_{86}^L$ values are more likely to be influenced by non-thermal factors. The two lowest $TEX_{86}^L$ SSTs of -0.93°C and 0.00°C (closest to measured

SSTs from the region), for example, have ΔRI values of 0.10 and 0.08, well below the threshold of 0.3. In contrast, global core-top GDGT data (Tierney and Tingley, 2015; Seki et al., 2014) show no relationship between ΔRI and $TEX_{86}$ ($R^2$=0.01, n = 854).

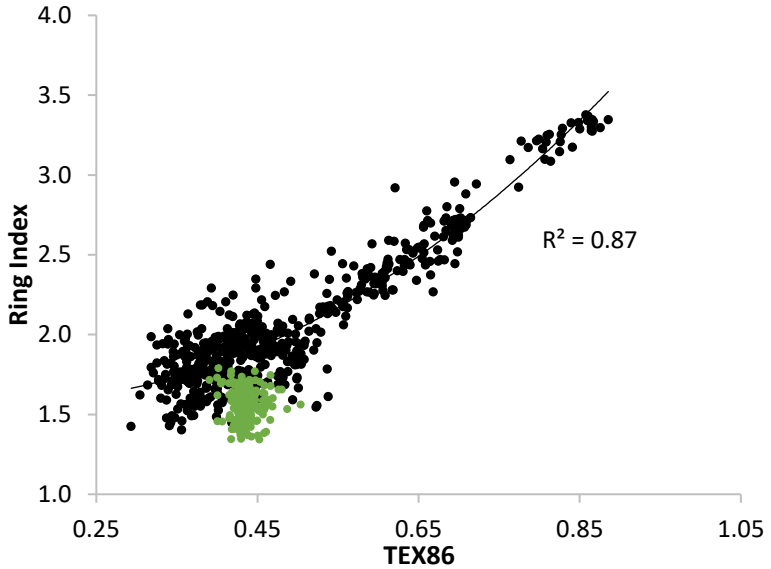



**Figure 7.5** Ring index plotted against TEX86 for core top samples used in Zhang et al. (2016) (black dots) and DTGC2011 samples (green dots). Black line is second order polynomial plotted through data points used in Zhang et al. (2016).

Furthermore, ΔRI values in DTGC2011 have a strong and significant, positive correlation with MI ($R^2$ = 0.69, p < 0.001; Fig. 7.6), suggesting that ΔRI may be sensitive to methane impacts, despite the fact that MI values are all < 0.3. In comparison, this relationship is much weaker ($R^2$ = 0.14, p < 0.001) in global core-top samples (Tierney and Tingley, 2015; Seki et al., 2014). However, Zhang et al. (2016) showed that in samples affected by methanotrophy, the MI had a strong positive correlation with ΔRI ($R^2$ = 0.85).

The analysis of GDGT distributions in relation to global core-top samples, and comparison to known sea surface and air temperatures from the region, suggests that non-thermal influences may be impacting the $TEX_{86}^L$ record in DTGC2011. Higher $TEX_{86}^L$ values generally deviate more from global core top distributions than lower $TEX_{86}^L$ values, based on the positive (albeit, weak) relationship between ΔRI and $TEX_{86}^L$. This could potentially indicate that

higher $TEX_{86}^{L}$ values are being driven more by other factors, compared to lower values which may be predominantly temperature driven. Thus, it is worth considering potential alternative influences on $TEX_{86}^{L}$, in addition to temperature, in core DTGC2011.

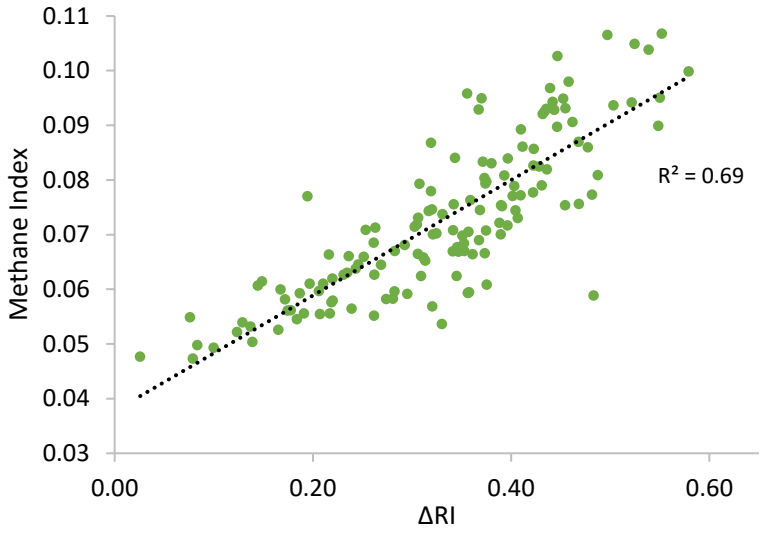



**Figure 7.6** Methane index plotted against ΔRI for samples from DTGC2011

## 7.5 Possible drivers of $TEX_{86}^{L}$ in DTGC2011

Various factors other than temperature have been suggested to influence GDGT distributions, including ammonia oxidation rate (Hurley et al., 2016), pH (Boyd et al., 2011), salinity (Dawson et al., 2012), and contributions from other archaeal communities (Lincoln et al., 2014a).

Various studies have shown an effect of pH on GDGT distributions. However, many of these have focussed on archaea grown in very low pH environments (ca. pH 1 – 5), such as hot springs (Boyd et al., 2011; Macalady et al., 2004; Shimada et al., 2008). In comparison, pH variations within marine environments are relatively minor and thought to have less effect on $TEX_{86}$ values (Schouten et al., 2013). In summer 2007/8, (Shadwick et al., 2014) measured

pH of surface water in the Adélie-Mertz region (65-67°S, 139-147°E) ranging from pH 8 – 8.15. Although this may not take into account the full range of pH in the region (e.g. seasonal or inter-annual change), it does suggest pH change is likely to be minimal. However, in a culture study involving water of pH 7.3 – 7.9 at 28°C, Elling et al. (2015) did find $TEX_{86}$-derived temperature changes with pH of up to 2°C within this smaller pH range. Thus it is possible that pH could have some effect on samples from Adélie Land. However, with a $TEX_{86}^{L}$-derived SST range of 6.9°C in core DTGC2011, current evidence suggests it is very unlikely that pH changes would be able to drive this level of variation. We therefore argue that pH is not a key driver of GDGT distribution in DTGC2011.

Similarly, while Dawson et al. (2012) showed that salinity can also affect GDGT cyclisation, this was over a much larger salinity range (10 – 30% NaCl, w/v), than in the marine environment. In contrast, Elling et al. (2015) looked at changes in GDGT cyclisation at salt concentrations of 27 – 51% but found no significant effects. Modern surface water salinity in the Adélie region has been shown to range between ca. 3.40 and 3.48% (w/v) (Bindoff et al., 2000) which is very minor compared to these other studies, suggesting that salinity changes are also unlikely to effect $TEX_{86}^{L}$ values.

Ammonia oxidation rate has also been suggested as a driver of GDGT cyclization (Hurley et al., 2016). Thaumarchaeota are predominantly ammonia-oxidisers (Könneke et al., 2005) and are suggested to use ammonia generated by the decay of phytoplankton (Herfort et al., 2007). Hurley et al. (2016) showed that higher $TEX_{86}$ values occurred at low ammonia oxidation rates, which are often associated with low oxygen concentrations (Qin et al., 2015). In an equatorial upwelling zone where nutrients and productivity are high, $TEX_{86}$-derived SSTs were found to be colder than *in-situ* temperature measurements, with the minimum $TEX_{86}$ values associated with maximum $NO_2^-$ concentrations. In contrast, $TEX_{86}$ values were greater

deeper in the water column, increasing with decreasing nitrification rates, despite actual temperatures decreasing (Hurley et al., 2016). Thus, changes in ammonia oxidation rates, associated with changes in primary productivity, could have a control on $TEX_{86}$ (and hence $TEX_{86}^{L}$) values in core DTGC2011.

If ammonia oxidation rate was a key driver of $TEX_{86}$ values, responding to conditions over the core site, we might expect $TEX_{86}^{L}$ values to show some coherence with primary productivity proxies such as carbon isotopes and diatom abundances within the core. However, both the $C_{18}$ and $C_{24}$ fatty acid $\delta^{13}C$ records, hypothesised to predominantly reflect ice edge and open water productivity offshore Adélie Land, respectively (Chapter 5), show little to no resemblance to the $TEX_{86}^{L}$ record (Fig. 7.7). In particular, the highest level of variability in the $TEX_{86}^{L}$ record occurs between ca. 1947 and 1966 in which it fluctuates from recording high temperatures (5.0°C) at ca. 1947 to low (-0.9°C) at ca. 1959 and back to high (3.7°C) at ca. 1966. In contrast, the $C_{18}$ $\delta^{13}C$ record shows relatively low $\delta^{13}C$ throughout this period and the $C_{24}$ $\delta^{13}C$ is relatively stable, with neither recording large shifts similar to the $TEX_{86}^{L}$ record. Similarly, diatom abundances show little similarity to $TEX_{86}^{L}$ over this period. Overall diatom abundances show a peak at ca. 1942 at which point $TEX_{86}^{L}$ is relatively high. If ammonia oxidation rate were the main control, the peak abundance should be associated with lower $TEX_{86}^{L}$, but instead the opposite is true. Both diatom and carbon isotope records suggest that the $TEX_{86}^{L}$ record is varying independently of primary productivity and, thus, this suggests that ammonia oxidation rate is unlikely to be a key driver of $TEX_{86}^{L}$ in DTGC2011.

Another possibility to explore is input of different GDGTs resulting from changes in archaeal community composition. One of the underlying assumptions of the $TEX_{86}$ proxy is that the GDGTs are produced by archaea of the phylum Thaumarchaeota (also known as Marine

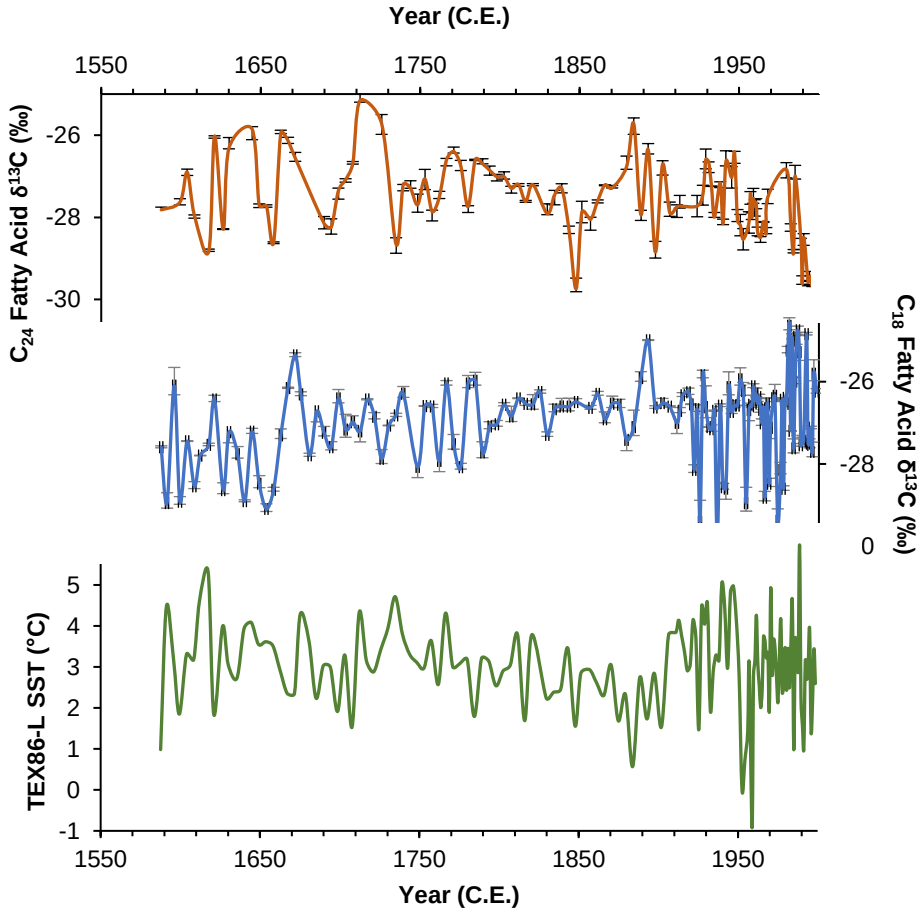



**Figure 7.7** $\delta^{13}C$ from $C_{24}$ (orange line) and $C_{18}$ (blue line) fatty acid compared to TEX86-L derived SSTs from core DTGC2011

Group I; MG I) which are known to be abundant in the global oceans (Schouten et al., 2002). However, the composition of archaea which produced the GDGTs preserved within sediments is generally unknown. Planktonic thaumarchaeota are highly diverse in the ocean with multiple types coexisting in the environment (Tully et al., 2012). Many culture studies have focussed on the species *Nitrosopumilus maritimus*, which is abundant throughout the oceans (Walker et al., 2010; Elling et al., 2015; Hurley et al., 2016). However, much less is known about GDGTs produced by other MG I species, as well as archaea from the three other groups of planktic archaea known to exist within the marine environment which belong to the phylum Euryarchaeota (MG II, III and IV) (Lincoln et al., 2014a).

A study by Lincoln et al. (2014a) suggested that MG-II Euryarchaeota are a major producer of cyclic GDGTs in the surface waters of the North Pacific Subtropical Gyre, based on DNA and lipid analyses of water samples at different depths. This could have serious implications for interpretation of $TEX_{86}$-derived SST reconstructions, since GDGT cyclization in heterotrophic Euryarchaeota is likely to be influenced by different ecological factors than chemolithoautotrophic Thaumarchaeota (Lincoln et al., 2014a). However, these results were contentious (Schouten et al., 2014; Lincoln et al., 2014b). A later study instead suggested that Euryarchaeota are unlikely to be a source of cyclic GDGTs in the North Pacific Subtropical Gyre, based on analysis of the proteins essential for GDGT ring formation and comparison with North Pacific Subtropical Gyre metagenomes from a genome database (Zeng et al., 2019).

While contributions from Euryarchaeota may not be important, there could still be important contributions from different archaea from the Thaumarchaeota phylum. A culture study of three thaumarchaeal strains, including *N. maritimus*, Elling et al. (2015), showed that variations in community composition can result in deviations in the $TEX_{86}$-temperature relationship by up ca. 20°C. Of the three thaumarchaeal strains, $TEX_{86}$ values were found to increase with growth temperature in two strains, but showed no significant change with temperature in the third. The $TEX_{86}$-temperature relationship also diverged from the global $TEX_{86}$ calibration. They suggest that the role of GDGT cyclization in Thaumarchaeota might be species dependant and argue that changes in community composition may play an important role on $TEX_{86}$ in the water column.

The above studies highlight how little is actually known about the archaeal producers of GDGTs in different regions and the effect it may have on $TEX_{86}^{L}$. This in contrast to other SST proxies such as the $U^{k}_{37}$' index, in which the modern alkenone producers have been

constrained almost to a single species. Few studies have looked at the potential producers of GDGTs from the Southern Ocean.

A study of archaeal communities in the Ross and Amundsen Seas, Antarctica, found that Circumpolar Deep Water (CDW) and Modified Circumpolar Deep Water (MCDW) had significantly higher archaeal species richness than any other water mass, including shelf waters and Antarctic surface waters (AASW). Many of the archaeal communities observed within CDW were distinct from communities within the other water masses. This included abundant levels of MG-II Euryarchaeota as well as various different types of MG-I Thaumarchaeota (Alonso-Sáez et al., 2011). Therefore, if GDGTs are being produced by multiple archaea species – a scenario which cannot be ruled out – there is potential for GDGT distributions in Antarctic waters to be prone to changes in community composition, particularly where CDW or MCDW upwells to the surface.

The effect of changes in archaeal community composition should therefore be considered as a potential control on $TEX_{86}^{L}$ alongside temperature. Comparison of downcore changes in $TEX_{86}^{L}$ with other proxy data in the core can help us understand the role of other environmental factors.

### 7.6 Grain size distributions and $TEX_{86}^{L}$

The $TEX_{86}^{L}$ record shows a notable coherency with grain size distributions in core DTGC2011 over time. In particular, higher $TEX_{86}^{L}$ values co-occur with a higher percentage of sand (Fig. 7.8) as well as the level of grain sorting (the standard deviation of grain size distributions) within the core. This coherency appears to persist throughout the record, but with an apparent offset of ca. 5 – 8 years, in which the $TEX_{86}^{L}$ record lags behind sand

percent (Fig. 7.8). This close association suggests that there may be a connection between GDGT distributions and the physical processes which drive the distribution of grain size.

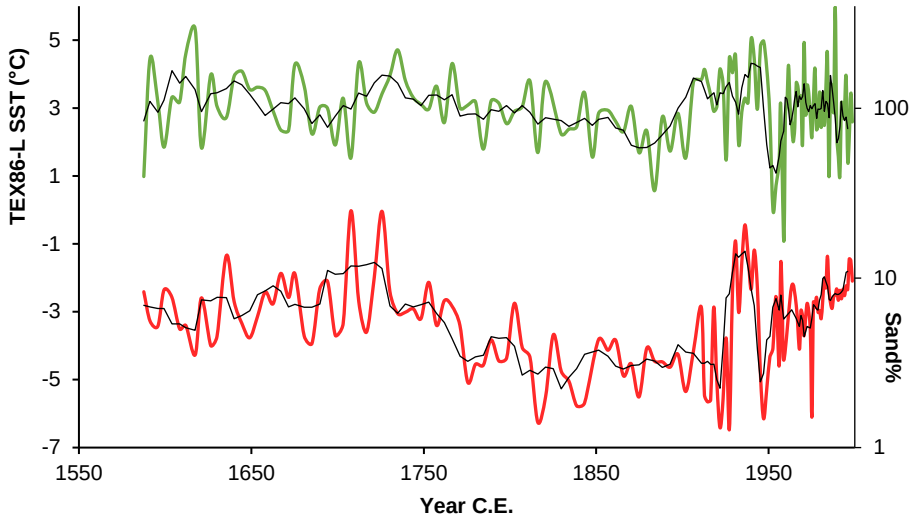



**Figure 7.8** $TEX_{86}^{L}$ derived sea surface temperatures (green line) and sand percent (red line, plotted on log scale) from core DTGC2011. Both fitted with a 4-point moving average (black lines).

Regression analysis between the two records indicates a lack of a linear relationship ($R^2$ = 0.002, n = 126). However, this does not take into account the apparent lag between the two records. As a rough test to determine the length of this lag, the $TEX_{86}^{L}$ and sand percent records were resampled (using the Paleontological Statistics software package (Hammer et al., 2001) by linearly interpolating to a constant spacing of one year. Although this may introduce

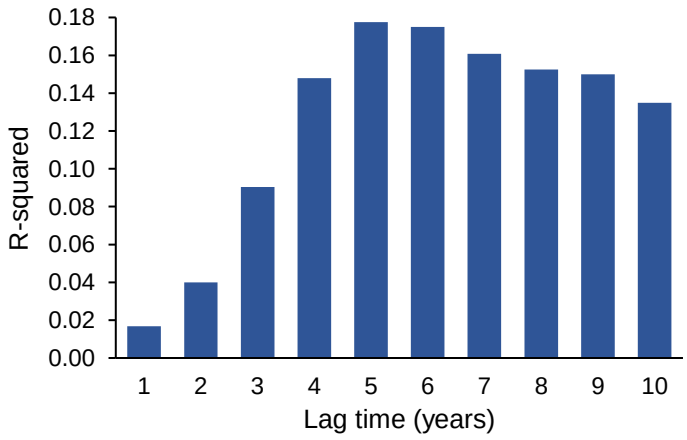



**Figure 7.9** $R^2$ values between sand percent and $TEX_{86}^{L}$ after adjusting the age scale of the $TEX_{86}^{L}$ back by 1 to 10 years.

a small amount of error, the overall pattern of both records remains the same. This interpolation onto an annual scale meant the age of the $TEX_{86}^{L}$ record could be manually adjusted back by 1 year at a time and the coefficient of determination ($R^2$ value) against sand percent calculated to determine the most likely lag time and the strength of any correlation.

Shifting the age of the $TEX_{86}^{L}$ record back by between 1 and 10 years indicates a peak correlation with sand percent at an offset of 5 years (Fig. 7.9), with $R^2 = 0.18$ ($p < 0.001$, n = 405). Although only a weak relationship, due to the high level of scatter in the data, this does suggests that there is some correlation between Sand% and $TEX_{86}^{L}$ and indicates the presence of a ca. 5-year lag. However, it must be acknowledged that the artificial increase in resolution (i.e. n = 405 as opposed to n = 126) introduced by the resampling may create some bias in the calculation of $R^2$ and *p*-value.

Re-plotting the two re-sampled datasets, with the 5-year $TEX_{86}^{L}$ lag, highlights the similarity between them, especially in the youngest ca. 100 years (Fig. 7.10). Thus, understanding the processes which drive changes in grain size may help interpreting the $TEX_{86}^{L}$. Grain size

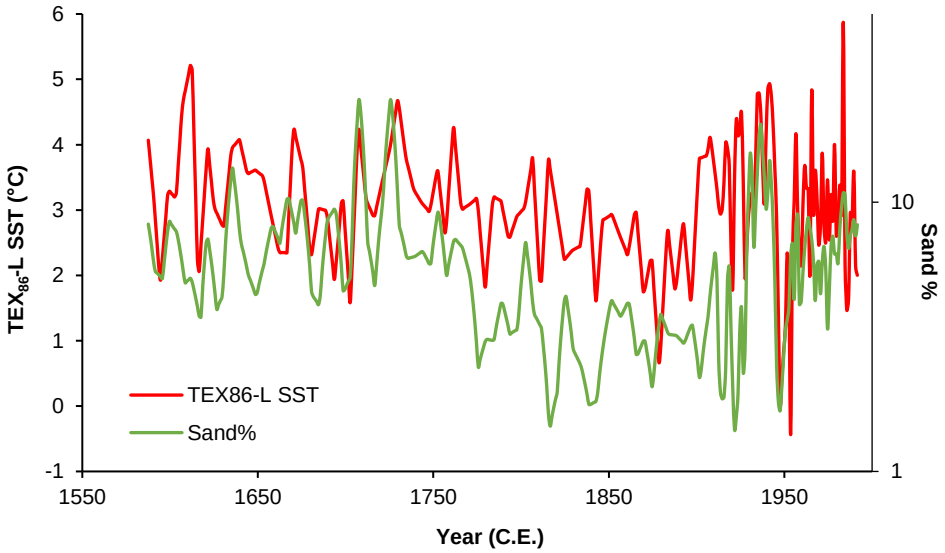



**Figure 7.10** Sand percent (red line, plotted on a log scale) and $TEX_{86}^{L}$ derived sea surface temperatures (green line) from core DTGC2011 after resampling by linear interpolation and shifting the age scale of the $TEX_{86}^{L}$ back by 5 years.

distributions are predominantly associated with flow speed and generally the stronger the flow, the larger the grains which can be transported and deposited (McCave and Hall, 2006). In DTGC2011, grain sizes range from 0.54 µm (clay) up to 493 µm (medium sand), with no course sand which could represent ice-rafted debris (IRD). The lack of IRD indicates that grain size distributions are predominantly current driven rather than being affected by other processes such as ice transport. Sand percent in the core is broadly correlated with mean sortable silt, which has been established as a grain-size flow speed proxy (McCave et al., 2017). However, Sand% is used here to provide a record of the upper current speed limit (R. McKay, 2019, Pers. Comms).

Offshore Adélie Land, katabatic winds blow off the Antarctic ice sheet towards the open ocean and are deflected westward. This drives the westward Antarctic Coastal Current which is instrumental in transporting material around the coast (Chapter 2.1 and Chapter 4 S1) and to our core site, resulting in the east – west orientation of the drift deposit from which the core was retrieved (Escutia et al., 2011).

Therefore, changes in sand percent are interpreted as a proxy for the strength of the Antarctic Coastal Current along the Adélie Coast. It is possible therefore that changes in the strength of currents may affect the transportation of material, including GDGTs, to the core site. For example, a stronger current (leading to a higher percentage of sand deposited) may result in advection of material from further east where conditions may be different (leading to different GDGT distributions).

For changes in advection to be driving sea surface temperatures over the core site, there would need to be a substantially warmer source of water upstream from Adélie Land to drive the large temperature changes suggested by the $TEX_{86}^{L}$ record. The spatial variation in

temperature of modern surface water (1995 – 2004 average) from Adélie Land to the Ross Sea, according to WOA18, is shown in Fig. 7.2. These data indicate that surface waters around the coast vary between ca. -0.3 and -1.8°C. This variation is significantly smaller than the range in temperatures implied by the $TEX_{86}^{L}$ (-0.92 to 5.98°C), suggesting that advection of warmer water is unlikely to be driving the $TEX_{86}^{L}$ record in DTGC2011.

Although already considered to be an unlikely control on $TEX_{86}^{L}$, it is possible that changes in current strength and the advection of water masses could affect ammonia oxidation rate, through advection of material, including GDGTs, from an area with different productivity levels. The core site is located just downstream of the highly productive Mertz Glacier Polynya (MGP), which has higher rates of primary productivity than the Dumont D'Urville polynya in which the core site is located (Arrigo and van Dijken, 2003). Therefore, stronger advection could lead to greater inputs of GDGTs from the MGP, which would be hypothesised to record lower $TEX_{86}^{L}$ values (due to greater primary productivity and associated nitrification) if ammonia oxidation rate was a key driver. However, Fig. 7.10 instead shows that greater sand percent (representing greater advection) occurs with higher $TEX_{86}^{L}$ values, which is the opposite of what would be predicted in this situation.

Archaeal community composition has been shown to vary significantly between different water masses in the Antarctic coastal zone (Alonso-Sáez et al., 2011). Therefore, advection of different water masses to the core site could result in contributions of archaea with different GDGT distributions. In particular, Alonso-Sáez et al. (2011) showed that CDW (and its modified form, MCDW) have a significantly higher archaea species richness than the AASW.

MCDW is a warm and salty water mass which upwells onto the continental shelf around Antarctica providing a source of heat to the coastal regions (Thompson et al., 2018). The core

site itself is located in a deep trough protected by the Adélie bank to the north meaning it is relatively sheltered from direct upwelling of MCDW. However, MCDW has been shown to upwell into the Adélie Depression near the Mertz Glacier, further upstream from the core site (Bindoff et al., 2000; Williams and Bindoff, 2003). Therefore, greater advection of material from the east could result in greater transport from the Adélie Depression including different archaea communities and any GDGTs they produce.

A study by Park et al. (2019) made a similar conclusion for GDGTs from different water depths in the Antarctic Polar Front. They found that $TEX_{86}^{L}$ values were significantly higher deeper in the water column compared to shallow water and argued that this increase in $TEX_{86}^{L}$-derived temperature at depth may be due to contributions of GDGTs from other types of archaea, present within the CDW which is found at depth at the Antarctic Polar Front.

The difficulty in testing this hypothesis is that there is little knowledge of the type of GDGTs (if any) these different types of archaea actually produce, and thus it is difficult to know how the presence of different species would affect $TEX_{86}^{L}$ values. However, close assessment of GDGT distributions in core DTGC2011 indicate that generally, higher $TEX_{86}^{L}$ values (which give temperature estimates much higher than expected in the region) deviate more from global core top distributions (which the temperature calibrations are based on) than lower $TEX_{86}^{L}$ values. In particular, $TEX_{86}^{L}$ values correlate positively with ΔRI, an indicator for non-thermal effects (Zhang et al., 2016) suggesting that higher $TEX_{86}^{L}$ values are less influenced by temperature. These higher $TEX_{86}^{L}$ values are broadly associated with higher sand percent, and thus may indicate that greater advection is leading to inputs of more abnormal GDGT distributions. Although many uncertainties remain, this appears to be the most parsimonious explanation for the relationship between $TEX_{86}^{L}$ and sand percent.

Although the exact timing of the lag between the sand percent and $TEX_{86}^{L}$ record is difficult to determine, it appears to be on the order of several years. Grain size distributions are likely to respond almost instantaneously to a change in flow speed, since the sand is sourced from near the sea floor and thus will be deposited quickly compared to pelagic settling. In contrast, if $TEX_{86}^{L}$ in the sediments is responding to upwelling and advection of archaea in the water column it is likely to take longer to be deposited in the sediment than the sand. In particular, the seafloor where the DTGC2011 was recovered is 1,000 m deep and thus small sinking particles could take a long time to reach the sea floor, in addition to recycling of material in the water column.

The majority of particulate organic matter in the water column will aggregate together to form larger particles which aid vertical transport to the sea floor, known as marine snow. Marine snow aggregates have been measured to sink at a wide range of speeds ranging from less than 1 m $day^{-1}$ up to 370 m $day^{-1}$ (Asper, 1987; Alldredge and Gotschalk, 1988; Turner, 2002). Sinking speed generally increases with diameter of the aggregate (Alldredge and Gotschalk, 1988) although this may also depend on its porosity (Asper, 1987).

Little is known about how archaea cells reach the sea floor. Sinking rates of archaea in the ocean are difficult to determine due to the fact that archaea can inhabit different depths throughout the water column. Archaea cell sizes are typically on the order of a few µm in diameter or less (Stieglmeier et al., 2014; Portillo et al., 2013; Kirchman et al., 2007) meaning it is unlikely they will be able to sink by themselves. Archaea cells have been observed to form aggregates with bacteria ranging between 5 and 30 µm in diameter (Boetius et al., 2015; Orphan et al., 2001). These are typically much smaller than the marine snow aggregates for which sinking speed has been measured (e.g. 1 to 5 mm in Asper, 1987). This suggests they could have sinking speeds on the lower end of the spectrum, perhaps on the order of 1 m day-

[1], which, for the 1,000 m water column at the core site, could result in a travel time of several years.

### 7.7 Conclusions

A new record of $TEX_{86}^{L}$ covering the past four centuries from off the coast of Adélie Land has been presented on an annual to sub-decadal timescale. This provides a unique opportunity to test the use of $TEX_{86}^{L}$ as a SST proxy in this region. The temporal overlap between this record and instrumental air temperature measurements from nearby indicate the lack of correlation. This, in addition to the consistent over-prediction of temperatures compared to known SSTs in the region, and the deviation of GDGT distributions from the global core top dataset, suggest that $TEX_{86}^{L}$ is not recording SST. A correlation between $TEX_{86}$-L and Sand% (after correcting for a several-year lag) suggests that $TEX_{86}^{L}$ is being driven by changes in the strength of the westward coastal currents. The most plausible hypothesis appears to be that stronger currents are leading to greater advection of GDGTs from further east, where MCDW upwells. MCDW is known to have a greater diversity of archaeal communities and thus, greater advection may lead to greater inputs of GDGTs produced by different archaea, for which the relationship between GDGT cyclisation and temperature may differ. This suggests that $TEX_{86}^{L}$ is not applicable as a SST proxy in this location. However, further research is required to test the relationship between GDGT distributions and MCDW upwelling and to determine the GDGTs which other types of archaea may produce.

## Chapter 8

# PRODUCTIVITY, ICE AND WATER MASS CHANGE IN THE DUMONT D'URVILLE TROUGH OVER THE PAST FOUR CENTURIES


## Abstract

High-resolution palaeoenvironmental records from the Antarctic coastal zone over the recent period can provide important information about past environmental conditions, with potential to extend instrumental records in space and time. This chapter presents new proxy data from rapidly accumulated sediment core from off the coast of Adélie Land, East Antarctica to reconstruct a record of productivity, water masses and sea and glacial ice over the past four centuries. These data highlight the key role of sea-ice concentration in driving changes in ice-edge primary productivity, inputs of glacial meltwater and strength of the westward coastal current. Ice-edge primary productivity broadly increases when both fast and pack ice are low. Productivity in open water, however, appears to be less sensitive to changes in sea ice. Inputs of glacial meltwater also appear to be affected by sea-ice concentrations, perhaps due to isotopically-depleted meltwater being locked up in sea ice and released when extensive melting of sea ice occurs. The strength of the westward current appears to be affected by the concentration of fast ice attached to the coast. Comparison with instrumental data is difficult due to the short-term nature of the overlapping datasets. However, there is some indication that wind direction may play a key role in determining sea-ice concentrations in this location which, in turn, affects many other environmental conditions offshore Adélie Land.


## 8.1 Introduction

High-resolution palaeoenvironmental records can provide important insights into changes in environmental conditions over time. Those records which cover the recent period can be

compared with instrumental records to allow better insights into the role of weather and climate in driving environmental conditions, as well as providing the possibility of extending instrumental records back through time using proxy data. This is particularly important for the Southern Ocean where both instrumental and palaeo data are sparse (Steig et al., 2009; Mayewski et al., 2004). In the Antarctic, the main palaeoclimatic information comes from ice cores, helping us understand changes in atmospheric variability (Jouzel et al., 2007; Masson-Delmotte et al., 2011; Masson et al., 2000; Steig et al., 2000; Petit et al., 1999). However, only few oceanic records exist, which are required for understanding changes in conditions such as water masses, primary productivity and sea ice (Pike et al., 2013; Shevenell et al., 2004; Crosta et al., 2007). Complex relationships between the ocean, ice, productivity and climate have been indicated by short term records from satellites, weather station data and direct water mass measurements (Paolo et al., 2015; Steig et al., 2009; Miles et al., 2013; Jacobs et al., 2002; Schmidtko et al., 2014), but their short term nature makes it difficult to fully unravel the complexities of their interactions. Palaeo-records can provide a longer-term picture of environmental change and provide a baseline from which more recent changes can be viewed.

The rapidly accumulating sediments of the Adélie drift in the Dumont d'Urville Trough (DDUT) provide a highly resolved archive of local environmental conditions. Core DTGC2011 was drilled in 2011 with the core top layer dated to ca. 2000 C.E. and extends 460 cm covering ca. 415 years. This allows the potential for reconstructing environmental conditions in high resolution using a range of proxies.

Here we use compound-specific fatty acid (FA) carbon and hydrogen isotopes, distributions of glycerol dialkyl glycerol tetraethers (GDGTs; $TEX_{86}^{L}$), sand percentage (Sand%), highly branched isoprenoid alkene (HBI) biomarker concentrations and diatom abundances to

provide an insight into productivity, water masses and sea and glacial ice over the DDUT offshore Adélie Land over the period 1587 to 1999 C.E.

### 8.2 Methods

Methods for compound-specific carbon and hydrogen isotopes analysis and GDGT quantification are described in Chapter 2. Grain size analyses were conducted at Victoria University Wellington following the methods described in Chapter 4.5.3.

### 8.3 Interpretation of proxy records

Carbon isotopes of the $C_{18}$ and $C_{24}$ FAs ($\delta^{13}C_{18FA}$ and $\delta^{13}C_{24FA}$) are hypothesised to reflect dissolved $CO_2$ in the surface waters offshore Adélie Land, with primary productivity argued to be the predominant driver of surface water $CO_2$, as discussed in Chapter 5. We argue that $\delta^{13}C_{18FA}$ is predominantly reflecting productivity changes in the marginal ice zone, where it is sensitive to changes in ice cover. In contrast, $\delta^{13}C_{24FA}$ may be reflecting summer productivity in more open waters, perhaps further offshore where it is less sensitive to fast ice changes.

Hydrogen isotopes of the $C_{18}$ FA ($\delta^{2}H_{FA}$) are used as a proxy for inputs of isotopically-depleted glacial meltwater, as discussed in Chapter 1.6.2 and Chapter 4 (S3.1). More negative $\delta^{2}H_{FA}$ values are interpreted as greater meltwater input and vice versa.

Sand% is used as a measure of the strength of the westward coastal currents (i.e. Antarctic Coastal Current and Antarctic Surface Water), with stronger currents depositing greater amounts of sand. $TEX_{86}^{L}$ at this site is also suggested to be responding to changing current strength, through advection of different archaeal communities, with higher $TEX_{86}^{L}$ values reflecting greater advection. Both are discussed in Chapter 7.

These data are compared with highly branched isoprenoid alkene (HBI) concentrations and diatom abundances in DTGC2011 from Campagne (2015). HBIs are used as a proxy for sea-ice concentrations. The HBI diene has been shown to be produced within land fast ice attached to the coast, therefore, higher HBI diene concentrations are interpreted to reflect greater concentrations of fast ice (Belt et al., 2016). *Fragilariopsis curta* is a sea ice diatom which blooms in open water within the marginal ice zone with their distribution generally corresponding to winter sea ice (Leventer and Dunbar, 1996). *Fragilariopsis kerguelensis*, on the other hand, is known as an open water diatom species, commonly found further from the coast (Pike et al., 2013; Crosta et al., 2007; Riaux-Gobin et al., 2011). *Chaetoceros* resting spores (CRS) are associated with high nutrient levels and stratification, and are often used to track high productivity events at the receding sea-ice edge (Crosta et al., 2008).

### 8.4 Reconstruction of palaeoenvironmental conditions offshore Adélie Land

Based on variations within the different proxy records, the record can be broadly divided into three different climatic periods within the core, also identified in Campagne (2015). These periods are defined as 1587 to 1725, 1725 to 1980 and 1890 to 1999 C.E.

#### 8.4.1 The 1587 to 1725 C.E. period

This period is characterised by high sea-ice concentrations as indicated by high abundances of *F. curta*. However, HBI diene concentrations are relatively low. This suggests that pack ice, further from the shore, is high while fast ice, attached to the coast, remains low (Campagne, 2015). Sand% is also high during this period suggesting strong westward currents. This is perhaps surprising given that extensive sea ice would reduce wind stress. This may indicate that advection remained strong along the coast in the absence of land fast ice.  Indeed, Sand%

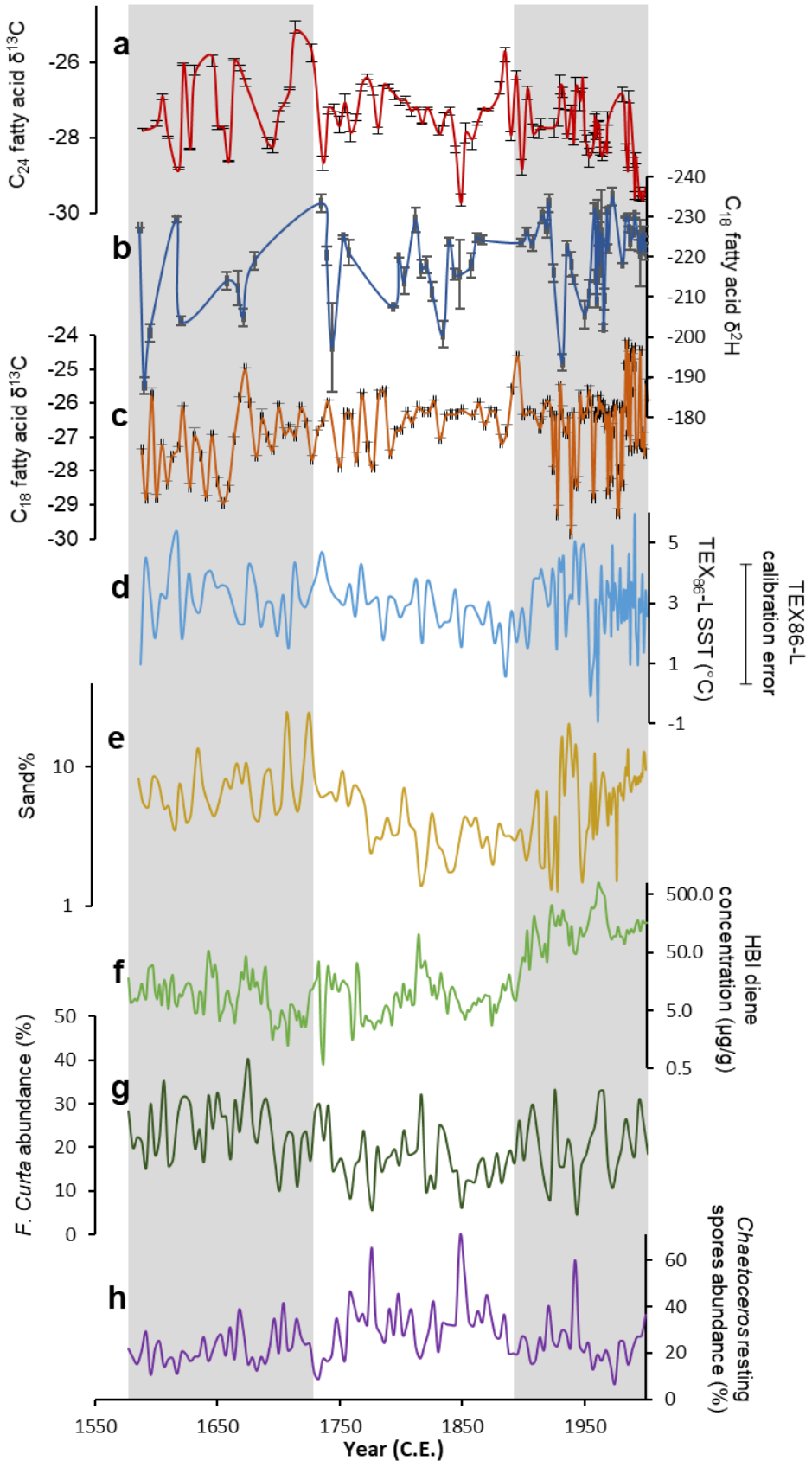



**Figure 8.1** Proxy data from core DTGC2011 a) $C_{24}$ fatty acid $\delta^{13}C$ b) $C_{18}$ fatty acid $\delta^{2}H$ c) $C_{18}$ fatty acid $\delta^{13}C$ d) $TEX_{86}L$-derived sea-surface temperatures e) Sand percentage f) HBI diene concentrations (µg/g) g) *Fragilariopsis curta* relative abundance (%) (Campgane, 2015) h) *Chaetoceros* resting spore relative abundances (%) (Campgane, 2015). Grey shading indicates the three periods discussed in the text: 1587 to 1725, 1725 to 1980 and 1980 to 1999 C.E.

increases though this period while HBI diene decreases, potentially indicating that fast ice and current strength are anticorrelated. Abundances of *Chaetoceros* resting spores (CRS), which are associated with stratification along the sea ice edge (Crosta et al., 2008), are low during this period. This may suggest a reduced polynya during this time, as would be expected with high sea-ice concentrations, with limited areas of stratified water. Indeed, $\delta^{13}C_{18FA}$ values are also low, indicating low ice edge productivity. This may be due to a shorter open-water period at this time leading to a shorter growing season for phytoplankton.

In contrast, $\delta^{13}C_{24FA}$ has, on average, the highest values during this period, indicating high open water productivity. It is also the most variable over this period which could perhaps be in response to large inter-annual changes in sea-ice concentrations, as indicated by high variability in *F. curta* abundances (ranging from 10 to 40% of the assemblage). $\delta^{13}C_{24FA}$ peaks towards the end of this period (1712 C.E.) at which point HBI diene and *F. curta* reach their lowest levels of the period, and Sand% peaks. This suggests the greater presence of open water, allowing greater advection of water, and creating a more favourable environment for open water phytoplankton species.

Meltwater input, as recorded by $\delta^{2}H_{FA}$, appears to start low but increase over time, however, this period is covered by only a handful of measurements making it difficult to fully assess the trend at this time. The increase in meltwater over this period towards one of the most negative $\delta^{2}H_{FA}$ values in the core may be reflecting an increase in advection of isotopically-depleted meltwater from the east, or the increased melting of sea ice which was formed from glacial meltwater. In Chapter 3, the Ross Sea was argued to be a key source of glacial meltwater to the site, transported westward in the AASW, but there may be a mixture of sources including the Mertz Glacier Tongue, also to the east of the core site. The end of this period includes both the highest Sand% values of the record, and lower sea-ice concentrations (HBI diene and

*F. curta*). Thus, as sea ice cover reduces (potentially resulting in an initial increase in sea ice melt) and advection increases at the end of this period, this may increase the supply of glacial meltwater to the site.

### 8.4.2 The 1725 to 1890 C.E. period

A shift in sea ice conditions marks the start of a new period, characterised by lower *F. curta* abundances, while HBI diene concentrations start low but increase. This suggests the increased growth of fast ice at the coast but reduced pack ice concentration, resulting in a large area of open water offshore. Ice edge productivity, as recorded by $\delta^{13}C_{18FA}$ is relatively high during this period and also very stable, potentially benefiting from the increased presence of fast ice, along with a sufficient area of open water. CRS abundances are also elevated during this period (Campagne, 2015). This may also indicate a longer open water season, with earlier sea ice melt, resulting in a longer growing season for phytoplankton. Sand% decreased and reaches its lowest values during this period, along with a decline in $TEX_{86}^{L}$, suggesting a reduction in the westward currents and advection of water masses. Sand% and HBI diene remain anti-correlated, again suggesting that land fast ice affects current strength along the coast.

Open water productivity, recorded by $\delta^{13}C_{24FA}$ reaches its lowest value during this period, broadly following *F. kerguelensis* abundances (Fig, 5.6), both of which reach their lowest values at 1847-8 C.E. This is perhaps surprising given the decline in sea-ice concentrations suggests the presence of open water which would be expected to benefit open water species. The stark difference between $\delta^{13}C_{18FA}$ (high and stable ice-edge productivity) and $\delta^{13}C_{24FA}$ (low and highly variable open water productivity) during this period suggests that while conditions close to the coast may be beneficial to the ice edge phytoplankton, further offshore,

conditions are less optimum for those open water phytoplankton. Alternatively, these two proxies may be reflecting different seasons, since open water species such as *F. kerguelensis* are known to bloom quite late into the open water season after sea ice melt (Crosta et al., 2007), and therefore may indicate that conditions became less favourable to phytoplankton as the season progressed.

### 8.4.3 The 1890 to 1999 C.E. period

Sea-ice concentrations are relatively high again during this period, as recorded by both HBI diene and *F. curta*, with HBI diene reaching the highest concentrations of the record. Both sea ice proxies follow a similar pattern in this period, with a notable short-lived reduction in sea-ice evident ca. 1942 C.E. The HBI record, however, must be viewed with some caution due to the changing preservation in the more recent sediments (discussed in Chapter 5). However, the broad similarity in the two sea ice proxies suggests they are responding to real changes in sea ice.

Large fluctuations are evident in most proxies during this period. The increase in sea-ice concentrations ca. 1920 C.E. coincides with a drop in both ice-edge productivity ($\delta^{13}C_{18FA}$) and a reduction in meltwater input ($\delta^{2}H_{FA}$), and remain low while sea-ice concentration is high. Both of these proxies then rapidly increase towards the end of the period (1970-80 C.E.) after sea-ice concentrations have declined, according to both HBI diene and *F. curta*. This suggests a close association between sea-ice concentration and both ice-edge productivity and meltwater input. The decline in ice-edge productivity and glacial meltwater input after ca. 1920 C.E. may be due to a lack of sea ice melt and stratification, which is also indicated by low CRS abundances during this period (Campagne, 2015), or a shorter ice-free season. Low sea ice melt may lead to less stratified water and low nutrients levels, since sea ice melt is an

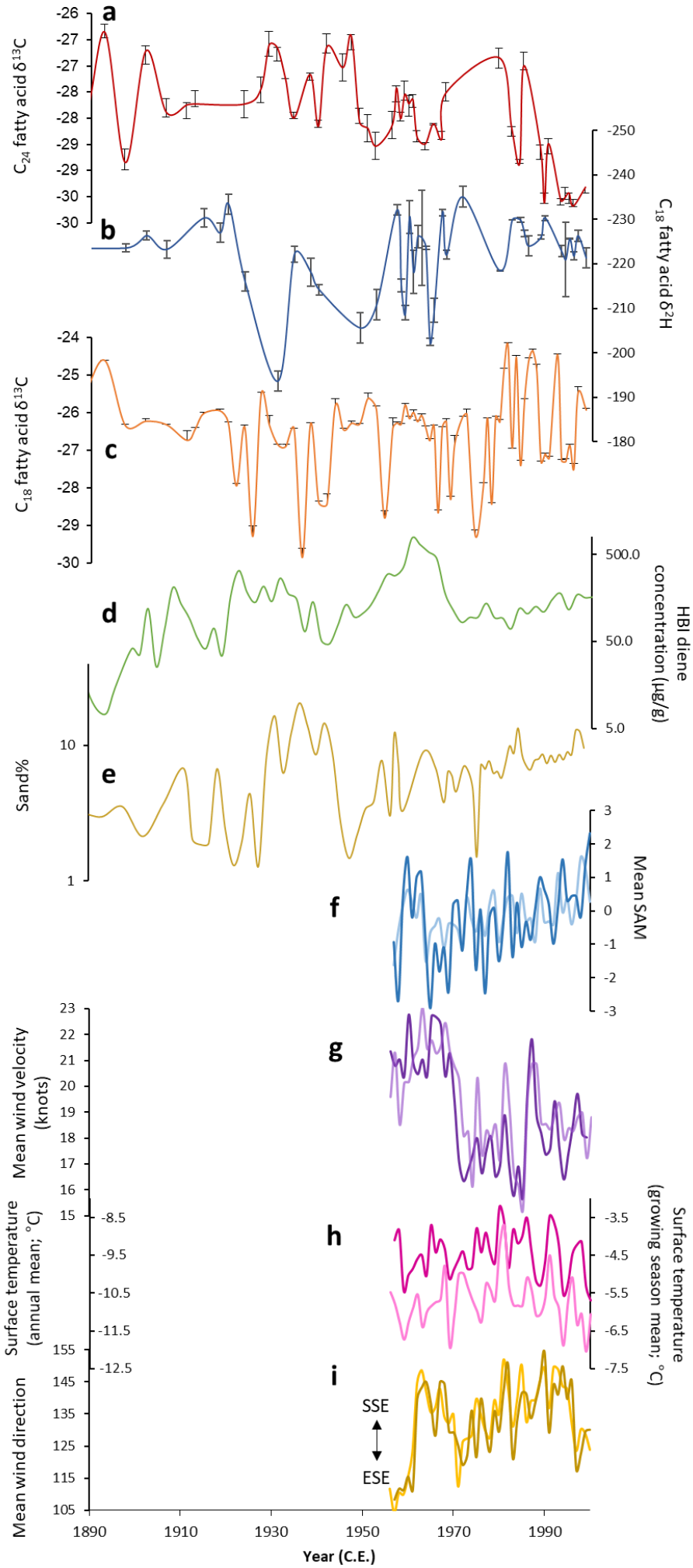

a
b
c
d
e
f
g
h
i
C24 fatty acid δ13C
C18 fatty acid δ2H
C18 fatty acid δ13C
HBI diene concentration (µg/g)
Sand%
Mean SAM
Mean wind velocity (knots)
Surface temperature (annual mean; °C)
Surface temperature (growing season mean; °C)
Mean wind direction
SSE
ESE
Year (C.E.)

**Figure 8.2** Proxy data from core DTGC2011 for the most recent period (1890 to 1999 C.E.) a) $C_{24}$ fatty acid $\delta^{13}C$ (‰) b) $C_{18}$ fatty acid $\delta^{2}H$ (‰) c) $C_{18}$ fatty acid $\delta^{13}C$ (‰) d) HBI diene concentrations (µg/g) e) Sand percentage f) Southern Annular Mode Index (dark blue = mean during the growing season (November to March), light blue = annual mean) (Marshall, 2003) g) Wind velocity measured at Dumont d'Urville station (dark purple = mean during the growing season, light purple = annual mean) h) Surface temperature measured at Dumont d'Urville station (dark pink = mean during the growing season, light pink = annual mean) i) Wind direction measured at Dumont d'Urville station (dark yellow = mean during the growing season, light yellow = annual mean).

important source of dissolved Fe in the surface waters (Sedwick and DiTullio, 1997; Death et al., 2014). This would result in low ice edge productivity, and reduced input of isotopically-depleted meltwater locked up in sea ice. The decline in glacial meltwater input may also have reduced input of nutrients such as Fe for phytoplankton (Arrigo et al., 2015). This may explain the synchronicity in the decline of meltwater and ice-edge productivity.

Large shifts occur in Sand% and $TEX_{86}^{L}$, with both the lowest and highest $TEX_{86}^{L}$ values of the whole record occurring during this period, and the lowest and third highest Sand%. This suggests high variability in the strength of the westward coastal current. Wind speed is a key driver of the Antarctic Coastal Current (also known as the East Wind Drift) but it will also be affected by changes in sea ice cover, which will reduce wind stress. Considering long-term changes observed throughout the record, Sand% and HBI diene are mostly anti-correlated, suggesting that the presence of extensive fast ice attached to the coast reduces the strength of the coastal current, and vice versa. Sea ice proxies also indicate high variability during the 1890 to 1999 C.E. period, which may be related to flow speed variability, however, their timing differs with that of Sand%. This may be due to currents responding to different drivers during this period or on this shorter timescale. For example, changes in the speed of easterly winds (not recorded by proxy data in the core) may have a bigger control on current strength than sea ice cover. Alternatively, there may be a lag between the records which is less clear on longer time scales, for example, current strength responding slowly to changes in sea-ice concentrations, or due to the way the proxies are incorporated into the core (i.e. sand versus diatoms).

For the latter part of this period, proxy data can be compared to instrumental records, including meteorological data (surface temperature, wind velocity and direction, mean sea level pressure) from the Dumont d'Urville station, as well as wider climatological features such as the Southern Annual Mode (SAM). These records begin in 1956 C.E. providing 44 years of overlap with proxy data from core DTGC2011 (Fig 8.2). A notable feature in these instrumental data, is a drop in mean wind velocity (both for the annual mean and the mean over the phytoplankton growing season; November to March), around 1970 C.E. (Fig. 8.2g) This coincides with a rapid decrease in fast ice, recorded by HBI diene concentrations which might initially suggest a connection between the two. However, Periard and Pettré (1993) note that prior to 1970, the weather station was equipped with a 'Papillon anemometer' for measuring wind, which is known to overestimate wind speed. Thus, they suggest that the difference between the pre-1970 period (high wind speeds) and the post-1972 period (lower wind speeds) is a result of these measurement differences. Thus, it remains unclear what role changes in wind speed have on environmental dynamics offshore Adélie land at this time.

Wind direction data, however, are thought to be robust throughout this period (Massom et al., 2009; Periard and Pettré, 1993). A notable shift in wind direction also occurs ca. 1962 C.E (Fig. 8.2i). Between 1956 and 1961, wind direction ranges from 104 to 112° (east-southeast) at which point HBI diene is at its maximum concentration (Fig. 8.2d), indicating substantial fast ice at the coast. This is followed by a rapid shift to 149° (south-southeast) in 1963, after which HBI diene declines, along with an increase in meltwater and, a few years later, an increase in ice edge productivity. Massom et al. (2009) noted the importance of wind direction in fast ice behaviour offshore Adélie Land between 1992 and 1999. Extensive fast ice during 1994 was observed to coincide with winds predominantly from the east-southeast, whereas lower-than-average fast ice extent in 1993 was associated with winds from the south-

southeast. This is consistent with what is seen in DTGC2011 and suggests that wind direction plays a key role in fast ice dynamics – with more southerly winds reducing fast ice concentration – and, ultimately, ice-edge productivity and meltwater input which also respond after fast ice declines. Although wind direction continues to show high variability through the rest of the period, there is an overall trend towards more southerly winds, reaching a peak mean annual wind direction of 152° in 1981, and a peak during the phytoplankton growing season (November to March) of 154° in 1990. HBI diene concentrations remain low for the rest of the period, consistent with the hypothesis that more southerly winds reduce fast ice extent. This is likely due to southerly winds from the continent breaking up sea ice and pushing it away from the coast (Massom et al., 2009; Bindoff et al., 2000).

Surface temperature and mean sea level pressure (MSLP) measured at the Dumont d'Urville station show year-to-year fluctuations throughout the 44-year period of overlap, along with inter-annual variability of the SAM index which also shows a broad trend towards a more positive SAM. The SAM is the dominant mode of atmospheric variability in the Southern Hemisphere. It is defined as the difference in MSLP between 40° and 60°S, and was calculated by Marshall (2003) using MSLP data from various weather stations including Dumont d'Urville. MSLP at Dumont d'Urville is thus associated with changes in the SAM. A positive SAM has been shown to lead to an intensification of the westerlies encircling Antarctica (Marshall, 2003), which leads to greater upwelling near the coast (Hall and Visbeck, 2002). However, comparison with proxy records in DTGC2011 show no clear correlations with changes in the SAM over this period. There is also an apparent lack of correlation between surface temperature and proxy data, which suggests that fluctuations in sea-ice concentration and productivity may be occurring independently of air temperature changes, driven instead by other factors such as glacial ice melt, upwelling and wind strength.

However, the short-term nature of this overlap makes it difficult to draw any conclusions on the role of air temperature or SAM, as well as other meteorological conditions, on environmental conditions in this location. In particular, the largest shifts in the proxy data occur prior to the start of the instrumental record, such as for Sand% which is highly variable between 1920 and 1957, but relatively stable thereafter. Fast ice, recorded by HBI concentrations, is already near its peak concentration at the start of the instrumental record, making it difficult to determine the role of meteorological conditions in driving it.

### 8.5 Conclusions

Environmental conditions offshore Adélie Land have been reconstructed over the past four centuries using a variety of proxies at decadal to annual resolution. Three distinct periods can be recognised based on fluctuations in proxy data. The most recent period, 1980 to 1999 C.E., shows the highest variability of the record in almost all proxy records.

Changes in sea-ice concentration appear to play a key role in driving changes in ice-edge primary productivity, inputs of glacial meltwater and strength of the westward coastal current. Ice-edge primary productivity broadly increases when both fast and pack ice are low, allowing a greater area of nutrient-rich, stratified water and perhaps also a longer growing season for phytoplankton. Productivity further offshore, however, appears to be less sensitive to changes in sea-ice concentration, the drivers of which are less clear. Inputs of glacial meltwater are suggested to be affected by sea-ice concentrations, perhaps due to isotopically-depleted meltwater being locked up in sea ice and released when extensive melting of sea ice occurs. The strength of the westward current is affected by the concentration of fast ice attached to the coast, with high concentrations of fast ice reducing current strength, likely due to a reduction in wind stress. However, this relationship becomes less clear in the latter period

when fluctuations in both sea-ice concentration and current strength are both high. Comparison with instrumental data is difficult due to the short-term nature of the overlapping datasets. However, there is some indication that wind direction may play a key role in determining sea-ice concentrations in this location which, in turn, affects other environmental conditions offshore Adélie Land.

# Chapter 9

# CONCLUSIONS AND FUTURE WORK

## 9.1 Main findings from this thesis

This thesis has presented new data from two unique sediment cores recovered from offshore Adélie Land, East Antarctica. This location is a very dynamic environment, with complex interactions between the atmosphere, ocean, ice and the carbon cycle. Chapter 2 summarised the current understanding of these relationships, including observations of recent trends and our knowledge of Holocene climate and environmental changes. It is clear from this review that many uncertainties exist, which has implications for our understanding of future changes. Palaeoenvironmental proxies from coastal marine sediment cores have the potential to provide an insight into air-ocean-ice interactions where instrumental records are unavailable. A good understanding of how different proxies work and the type of environmental information they record is vital if they are to provide a useful insight into past environmental changes.

As a result, the aims of this thesis were twofold:

1) *Assess the utility of biomarker proxies for reconstructing palaeoenvironmental conditions offshore Adélie Land, East Antarctica.*

To meet this aim, this thesis attempted to assess the use of two biomarker proxies in particular, namely the compound-specific carbon isotope composition of fatty acids and the $TEX_{86}^{L}$ sea surface temperature proxy in Chapters 5 and 7.

Chapter 5 presented the results of two fatty acids, the $C_{18}$ and $C_{24}$, from core DTGC2011. Down-core concentrations and carbon isotope composition were analysed and compared with

other proxy data which are better constrained in their use as a palaeoenvironmental proxy. Along with an assessment of the different potential drivers of surface water $CO_2$, this allowed an insight into the most likely producers of the fatty acids and thus habitat of formation, and ultimately the most likely signal which fatty acid $\delta^{13}C$ is recording. It was concluded that fatty acid $\delta^{13}C$ has the potential to be used as a primary production proxy in this setting. The $C_{18}$ fatty acid is hypothesised to be predominantly produced by *Phaeocystis antarctica* and is responding to changes in primary productivity in the marginal ice zone. In contrast, the $C_{24}$ is more likely to be produced in open waters further offshore, although the exact producer remains unknown. However, many uncertainties remain in the interpretation of fatty acid $\delta^{13}C$, thus more work would be required to determine the extent to which they are recording productivity over other factors such as upwelling.

Chapter 7 assessed the use of $TEX_{86}^{L}$ as a SST proxy. A lack of correlation between air temperatures measured nearby (over the period of overlap), the consistent over-prediction of SSTs compared to those known in the region, and the deviation of GDGT distributions from the global core top dataset, suggest that $TEX_{86}^{L}$ is not recording SST in core DTGC2011. A correlation between $TEX_{86}^{L}$ and Sand% (after correcting for a several-year lag) suggests that $TEX_{86}^{L}$ is being driven by changes in the strength of the westward coastal currents. The most plausible hypothesis is that stronger currents are leading to greater advection of GDGTs from further east, where MCDW upwells. MCDW is known to have a greater diversity of archaeal communities and thus, greater advection may lead to greater inputs of GDGTs produced by different archaea, for which the relationship between GDGT cyclisation and temperature may differ.

2) *Reconstruct changes in palaeoenvironmental conditions offshore Adélie Land, East Antarctica.*

The second aim was to apply these biomarker proxies, along with various others, and ultimately use the new insight from Chapters 5 and 7 about their interpretation, to reconstruct changes in past environmental conditions. Chapter 4, however, precedes the chapters assessing the biomarkers and uses a different suite of palaeoenvironmental proxies to reconstruct changes in glacial meltwater, sea ice and water masses over the Holocene. Fatty acid $\delta^2H$ records a peak in meltwater input during the mid-Holocene which coincides with a widespread increase in sea-ice around the coast, which persists towards the modern day. This is hypothesised to reflect the development of a large ice-shelf cavity in the Ross Sea which fundamentally alters ice-ocean interactions and surface water properties. These freshened surface waters are transported westward around the coast, enhancing sea ice formation around the coast. This provides a new insight into ice shelf-ocean-sea ice interactions with implications for the incorporation of ice shelves into climate models, as well as introducing a new biomarker proxy for glacial meltwater input.

Chapter 6 builds on the results of both Chapters 4 and 5, using fatty acid $\delta^{13}C$ to reconstruct changes in primary productivity offshore Adélie Land over the Holocene. Both sea ice and glacial meltwater appear to play a role in driving ice-edge productivity, which is generally higher under stratified, nutrient-rich conditions with relatively low sea-ice cover during the phytoplankton-growing season. Open water productivity, as recorded by the $C_{24}$ fatty acid, appears to be much less sensitive to changes in sea ice. Both records, however, show a short-lived peak in productivity coincident with the peak in meltwater, suggesting that this temporarily provided conditions beneficial to a wide range of phytoplankton, perhaps through increased delivery of nutrients such as Fe.

Chapter 8 summarises all the data from core DTGC2011, drawing on the conclusions of Chapters 4, 5 and 7 for interpretations of biomarker proxies, in addition to comparisons with

instrumental records where temporal overlap occurs. Close assessment of changes in the reconstructed environmental conditions, and their relationship to each other, highlights the key role of sea ice in driving changes in ice-edge primary productivity, inputs of glacial meltwater to the core site and the strength of the westward coastal current. There is also some indication that wind-direction plays an important role in driving such sea ice changes, however, the short-term nature of the instrumental records limits the conclusions which can be drawn about the role of atmospheric variability on these environmental conditions. The data from this core also highlight that conditions offshore Adélie Land in the most recent period, ca. 1890 to 1999 C.E. have been highly variable.

## 9.2 Directions for future work

This thesis has provided new insights into the dynamics of various environmental conditions offshore Adélie Land, East Antarctica, and the suitability of certain biomarker proxies for reconstructing such changes in the past. However, many questions remain, and more work is clearly required to further improve our understanding of these things. In particular, while progress has been made in interpreting certain biomarker proxies, further research is required to fully ground-truth them. Some outstanding questions and suggestions for areas of further research are outlined as follows:

1) *Fatty acid $\delta^{13}C$ as a primary productivity proxy.*

How important are other factors, such as upwelling, in driving fatty acid $\delta^{13}C$? Can the source of the $C_{18}$ and especially the $C_{24}$ FA, be better constrained? How localised is the productivity signal which is recorded? While FA $\delta^{13}C$ may record relative changes in $CO_2$ drawdown in the surface waters, can we determine how much of this carbon is sequestered to the deep ocean?

Collection and analysis of sediment trap data from the region may help with answering some of these questions, in addition to analyses of DIC in the surface waters. For example, analysis of fatty acids and phytoplankton assemblages in seawater prior to the effects of degradation may help establish the precursor organism(s) for the fatty acids.

2) *What is driving $TEX_{86}^{L}$?*

This thesis concluded that the most plausible hypothesis for the driver of $TEX_{86}^{L}$ is inputs of GDGTs from different types of archaea upwelled in MCDW. However, this hypothesis is difficult to test since very little is known about the producers of GDGTs in this region. How many archaea species produce GDGTs? Is MCDW likely to contain different GDGT-producing archaea? Are these types of GDGTs likely to lead to a warm bias?

Coupled DNA and GDGT analyses in surface waters may be able to spread light on the likely producers of GDGTs. Analyses of GDGTs in the surface waters across the region may help to establish whether GDGT distributions differ in regions where MCDW upwells.

3) *FA $\delta^2H$ as a glacial meltwater proxy.*

The low resolution of FA $\delta^2H$ in DTGC2011 meant it was difficult to assess its use as a proxy in the way that FA $\delta^{13}C$ and $TEX_{86}^{L}$ were. Measurements of fatty acid $\delta^2H$ in surface waters, along with measurements of surface water $\delta^2H$ and salinity for example, from a range of sites around the Antarctic, may help to determine the extent to which it is recording changes in glacial meltwater input.

## REFERENCES


Adcroft, A., Campin, J.-M., Hill, C., et al. (2004) Implementation of an Atmosphere–Ocean General Circulation Model on the Expanded Spherical Cube. *Monthly Weather Review*, 132 (12): 2845–2863. doi:10.1175/MWR2823.1.

Alderkamp, A.C., Kulk, G., Buma, A.G.J., et al. (2012) The effect of iron limitation on the photophysiology of Phaeocystis antarctica (Prymnesiophyceae) and Fragilariopsis cylindrus (Bacillariophyceae) under dynamic irradiance. *Journal of Phycology*, 48 (1): 45–59. doi:10.1111/j.1529-8817.2011.01098.x.

Alldredge, A.L. and Gotschalk, C. (1988) In situ settling behavior of marine snow. *Limnology and Oceanography*. doi:10.4319/lo.1988.33.3.0339.

Alonso-Sáez, L., Andersson, A., Heinrich, F., et al. (2011) High archaeal diversity in Antarctic circumpolar deep waters. *Environmental Microbiology Reports*, 3 (6): 689–697. doi:10.1111/j.1758-2229.2011.00282.x.

Anderson, H.J., Moy, C.M., Vandergoes, M.J., et al. (2018) Southern Hemisphere westerly wind influence on southern New Zealand hydrology during the Lateglacial and Holocene. *Journal of Quaternary Science*, 33 (6): 689–701. doi:10.1002/jqs.3045.

Anderson, J.B., Conway, H., Bart, P.J., et al. (2014) Ross Sea paleo-ice sheet drainage and deglacial history during and since the LGM. *Quaternary Science Reviews*, 100: 31–54. doi:10.1016/j.quascirev.2013.08.020.

Anderson, R.F., Ali, S., Bradtmiller, L.I., et al. (2009) Wind-driven upwelling in the Southern Ocean and the deglacial rise in atmospheric CO2. *Science (New York, N.Y.)*, 323 (5920): 1443–1448. doi:10.1126/science.1167441.

Andrews, J.T., Domack, E.W., Cunningham, W.L., et al. (1999) Problems and possible solutions concerning radiocarbon dating of surface marine sediments, Ross Sea, Antarctica. *Quaternary Research*, 52 (2): 206–216. doi:10.1006/qres.1999.2047.

Aoki, S., Kitade, Y., Shimada, K., et al. (2013) Widespread freshening in the Seasonal Ice

Zone near 140°E off the Adélie Land Coast, Antarctica, from 1994 to 2012. *Journal of Geophysical Research: Oceans*, 118 (11): 6046–6063. doi:10.1002/2013JC009009.

Archambeau, A.S., Pierre, C., Poisson, A., et al. (1998) Distributions of oxygen and carbon stable isotopes and CFC-12 in the water masses of the Southern Ocean at 30°E from South Africa to Antarctica: Results of the CIVA1 cruise. *Journal of Marine Systems*, 17 (1–4): 25–38. doi:10.1016/S0924-7963(98)00027-X.

Arrigo, K.R. (2007) Chapter 7 Physical Control of Primary Productivity in Arctic and Antarctic Polynyas. *Elsevier Oceanography Series*, 74 (06): 223–238. doi:10.1016/S0422-9894(06)74007-7.

Arrigo, K.R. and van Dijken, G.L. (2003) Phytoplankton dynamics within 37 Antarctic coastal polynya systems. *Journal of Geophysical Research*, 108 (C8): 3271. doi:10.1029/2002JC001739.

Arrigo, K.R., Robinson, D.H., Worthen, D.L., et al. (1999) Community Phytoplankton Structure and the Drawdown of and CO2 in the Nutrients Southern Ocean. *Science*, 283 (5400): 365–367.

Arrigo, K.R., van Dijken, G. and Long, M. (2008) Coastal Southern Ocean: A strong anthropogenic CO2 sink. *Geophysical Research Letters*, 35 (21): 1–6. doi:10.1029/2008GL035624.

Arrigo, K.R., van Dijken, G.L. and Strong, A.L. (2015) Environmental controls of marine productivity hot spots around Antarctica Kevin. *Journal of Geophysical Research: Oceans*, pp. 2121–2128. doi:10.1002/jgrc.20224.

Arrigo, K.R., Worthen, D.L. and Robinson, D.H. (2003) A coupled ocean-ecosystem model of the Ross Sea: 2. Iron regulation of phytoplankton taxonomic variability and primary production. *Journal of Geophysical Research C: Oceans*, 108 (7): 24–1. doi:10.1029/2001JC000856.

Arrigo, K.R., Worthen, D.L., Schnell, A., et al. (1998) Primary production in Southern Ocean waters. *Journal of Geophysical Research*, 103 (C8): 15587–15600.

Asper, V.L. (1987) Measuring the flux and sinking speed of marine snow aggregates. *Deep Sea Research Part A, Oceanographic Research Papers*, 34 (1): 1–17. doi:10.1016/0198-0149(87)90117-8.

Asper, V.L. and Smith, W.O. (1999) Particle fluxes during austral spring and summer in the southern Ross Sea, Antarctica. *Journal of Geophysical Research: Oceans*, 104 (C3): 5345–5359. doi:10.1029/1998JC900067.

Atkins, C.B. and Dunbar, G.B. (2009) Aeolian sediment flux from sea ice into Southern McMurdo Sound, Antarctica. *Global and Planetary Change*, 69 (3): 133–141. doi:10.1016/j.gloplacha.2009.04.006.

Baggenstos, D., Severinghaus, J.P., Mulvaney, R., et al. (2018) A Horizontal Ice Core From Taylor Glacier, Its Implications for Antarctic Climate History, and an Improved Taylor Dome Ice Core Time Scale. *Paleoceanography and Paleoclimatology*, 33 (7): 778–794. doi:10.1029/2017PA003297.

Bahr, A., Jiménez-Espejo, F.J., Kolasinac, N., et al. (2014) Deciphering bottom current velocity and paleoclimate signals from contourite deposits in the Gulf of Cádiz during the last 140 kyr: An inorganic geochemical approach. *Geochemistry, Geophysics, Geosystems*, 15 (8): 3145–3160. doi:10.1002/2014GC005356.

Barbara, L., Crosta, X., Massé, G., et al. (2010) Deglacial environments in eastern Prydz Bay, East Antarctica. *Quaternary Science Reviews*, 29 (19–20): 2731–2740. doi:10.1016/j.quascirev.2010.06.027.

BAS (2019) *Dumont_Durville (data supplied by Meteo-France) temperature*. Available at: https://legacy.bas.ac.uk/met/READER/surface/Dumont_Durville.All.temperature.html.

Beaman, R.J., O'Brien, P.E., Post, A.L., et al. (2011) A new high-resolution bathymetry model for the Terre Adélie and George V continental margin, East Antarctica. *Antarctic Science*, 23 (1): 95–103. doi:10.1017/S095410201000074X.

Beans, C., Hecq, J.H., Koubbi, P., et al. (2008) A study of the diatom-dominated microplankton summer assemblages in coastal waters from Terre Adelie to the Mertz Glacier, East Antarctica (139E-145E). *Polar Biology*, 31 (9): 1101–1117.

doi:10.1007/s00300-008-0452-x.

Belt, S.T. (2018) Source-specific biomarkers as proxies for Arctic and Antarctic sea ice. *Organic Geochemistry*, 125: 277–298. doi:10.1016/j.orggeochem.2018.10.002.

Belt, S.T. and Müller, J. (2013) The Arctic sea ice biomarker IP 25 : a review of current understanding , recommendations for future research and applications in palaeo sea ice reconstructions. *Quaternary Science Reviews*, 79: 9–25. doi:10.1016/j.quascirev.2012.12.001.

Belt, S.T., Allard, W.G., Rintatalo, J., et al. (2000) Clay and acid catalysed isomerisation and cyclisation reactions of highly branched isoprenoid (HBI) alkenes: Implications for sedimentary reactions and distributions. *Geochimica et Cosmochimica Acta*, 64 (19): 3337–3345. doi:10.1016/S0016-7037(00)00444-0.

Belt, S.T., Brown, T.A., Smik, L., et al. (2017) Identification of C25 highly branched isoprenoid (HBI) alkenes in diatoms of the genus Rhizosolenia in polar and sub-polar marine phytoplankton. *Organic Geochemistry*, 110: 65–72. doi:10.1016/j.orggeochem.2017.05.007.

Belt, S.T., Massé, G., Rowland, S.J., et al. (2007) A novel chemical fossil of palaeo sea ice: IP25. *Organic Geochemistry*, 38 (1): 16–27. doi:10.1016/j.orggeochem.2006.09.013.

Belt, S.T., Smik, L., Brown, T.A., et al. (2016) Source identification and distribution reveals the potential of the geochemical Antarctic sea ice proxy IPSO25. *Nature Communications*, 7: 12655. doi:10.1038/ncomms12655.

Berger, A. and Loutre, M.F. (1991) Insolation values for the climate of the last 10 million years. *Quaternary Science Reviews*, 10 (4): 297–317. doi:10.1016/0277-3791(91)90033-Q.

Bindoff, N., Rintoul, S. and Massom, R. (2000) Bottom water formation and polynyas in Adelie Land, Antarctica. *Papers and Proceedings of the Royal Society of Tasmania*, 133 (3): 51–56. doi:10.26749/rstpp.133.3.51.

Bintanja, R., Van Oldenborgh, G.J. and Katsman, C.A. (2015) The effect of increased

fresh water from Antarctic ice shelves on future trends in Antarctic sea ice. *Annals of Glaciology*, 56 (69): 120–126. doi:10.3189/2015AoG69A001.

Bintanja, R., van Oldenborgh, G.J., Drijfhout, S.S., et al. (2013) Important role for ocean warming and increased ice-shelf melt in Antarctic sea-ice expansion. *Nature Geoscience*, 6 (5): 376–379. doi:10.1038/ngeo1767.

Blaauw, M. and Christeny, J.A. (2011) Flexible paleoclimate age-depth models using an autoregressive gamma process. *Bayesian Analysis*, 6 (3): 457–474. doi:10.1214/11-BA618.

Blain, S., Quéguiner, B., Armand, L., et al. (2007) Effect of natural iron fertilization on carbon sequestration in the Southern Ocean. *Nature*, 446 (7139): 1070–1074. doi:10.1038/nature05700.

Boetius, A., Anesio, A.M., Deming, J.W., et al. (2015) Microbial ecology of the cryosphere: sea ice and glacial habitats. *Nature Reviews Microbiology*, 13 (11): 677–690. doi:10.1038/nrmicro3522.

BOSCORF (2019) *Accumulation Rates*. Available at: https://boscorf.org/repository/curatorial-reference/accumulation-rates.

Boyd, E.S., Pearson, A. and Pi, Y. (2011) Temperature and pH controls on glycerol dibiphytanyl glycerol tetraether lipid composition in the hyperthermophilic crenarchaeon Acidilobus sulfurireducens. *Extremophiles*, 15: 59–65. doi:10.1007/s00792-010-0339-y.

Boyd, P.W., Watson, A.J., Law, C.S., et al. (2000) A mesoscale phytoplankton bloom in the polar Southern Ocean stimulated by iron fertilization. *Nature*, 407 (6805): 695–702. doi:10.1038/35037500.

Bradley, R.S. (2015) "Chapter 6 - Marine Sediments." In *Paleoclimatology (Third Edition)*. doi:http://dx.doi.org/10.1016/B978-0-12-386913-5.00006-5.

Bradley, S.L., Milne, G.A., Horton, B.P., et al. (2016) Modelling sea level data from China and Malay-Thailand to estimate Holocene ice-volume equivalent sea level change. *Quaternary Science Reviews*, 137: 54–68. doi:10.1016/j.quascirev.2016.02.002.

Brassell, S.C., Eglinton, G., Marlowe, I.T., et al. (1986) Molecular stratigraphy: A new tool for climatic assessment. *Nature*. doi:10.1038/320129a0.

Brook, E.J., White, J.W.C., Schilla, A.S.M., et al. (2005) Timing of millennial-scale climate change at Siple Dome, West Antarctica, during the last glacial period. Quaternary Science Reviews, 24 (12–13): 1333–1343. doi:10.1016/j.quascirev.2005.02.002.

Brown, J., Colling, A., Park, D., et al. (1989) *Ocean Circulation*. 1st ed. Bearman, G. (ed.). Butterworth-Heinemann, Oxford.

Budge, S.M., Wooller, M.J., Springer, A.M., et al. (2008) Tracing carbon flow in an arctic marine food web using fatty acid-stable isotope analysis. *Oecologia*, 157 (1): 117–129. doi:10.1007/s00442-008-1053-7.

Burke, A. and Robinson, L.F. (2012) The Southern Ocean's Role in Carbon Exchange During the Last Deglaciation. *Science*, 335: 557–561.

Cabedo Sanz, P., Smik, L. and Belt, S.T. (2016) On the stability of various highly branched isoprenoid (HBI) lipids in stored sediments and sediment extracts. *Organic Geochemistry*, 97: 74–77. doi:10.1016/j.orggeochem.2016.04.010.

Campagne, P. (2015) *Étude de la variabilité des conditions océanographiques et climatiques en Antarctique de l'Est (Terre Adélie-Georges V) au cours de l'Holocène tardif et de la période instrumentale*. L'Université de Bordeaux. Available at: https://tel.archives-ouvertes.fr/tel-01306576/file/CAMPAGNE_PHILIPPINE_2015.pdf.

Campagne, P., Crosta, X., Houssais, M.N., et al. (2015) Glacial ice and atmospheric forcing on the Mertz Glacier Polynya over the past 250 years. *Nature communications*, 6: 6642. doi:10.1038/ncomms7642.

Castañeda, I.S., Schefuß, E., Pätzold, J., et al. (2010) Millennial-scale sea surface temperature changes in the eastern Mediterranean (Nile River Delta region) over the last 27,000 years. *Paleoceanography*. doi:10.1029/2009PA001740.

Chewings, J.M., Atkins, C.B., Dunbar, G.B., et al. (2014) Aeolian sediment transport and deposition in a modern high-latitude glacial marine environment. *Sedimentology*, 61 (6):

1535–1557. doi:10.1111/sed.12108.

Chiba, S., Hirawake, T., Ushio, S., et al. (2000) An overview of the biological/oceanographic survey by the RTV Umitaka-Maru III off Adelie Land, Antarctica in January-February 1996. *Deep-Sea Research Part II: Topical Studies in Oceanography*, 47 (12–13): 2589–2613. doi:10.1016/S0967-0645(00)00037-0.

Collins, L.G., Pike, J., Allen, C.S., et al. (2012) High-resolution reconstruction of southwest Atlantic sea-ice and its role in the carbon cycle during marine isotope stages 3 and 2. *Paleoceanography*, 27 (3). doi:10.1029/2011PA002264.

Collins, W.D., Bitz, C.M., Blackmon, M.L., et al. (2006) The Community Climate System Model version 3 (CCSM3). *Journal of Climate*. doi:10.1175/JCLI3761.1.

Colombo, J.C., Silverberg, N. and Gearing, J.N. (1997) Lipid biogeochemistry in the Laurentian Trough--ll. Changes in composition of fatty acids, sterols and aliphatic hydrocarbons during early diagenesis. *Org. Geochem.*, 26 (3): 257–274.

Condron, A. and Winsor, P. (2012) Meltwater routing and the Younger Dryas. *Proceedings of the National Academy of Sciences*, 109 (49): 19928–19933. doi:10.1073/pnas.1207381109.

Conte, M.H., Sicre, M.A., Rühlemann, C., et al. (2006) Global temperature calibration of the alkenone unsaturation index (U 37k) in surface waters and comparison with surface sediments. *Geochemistry, Geophysics, Geosystems*, 7 (2). doi:10.1029/2005GC001054.

Conway, H., Hall, B.L., Denton, G.H., et al. (1999) Past and Future Grounding-Line Retreat of the West Antarctic Ice Sheet. *Science*, 286 (5438): 280–283. doi:10.1126/science.286.5438.280.

Cook, A.J., Fox, A.J., Vaughan, D.G., et al. (2005) Retreating Glacier Fronts on the Antarctic Peninsula over the Past Half-Century. *Science*, 308 (April): 541–545.

Cook, A.J., Holland, P.R., Meredith, M.P., et al. (2016) Ocean forcing of glacier retreat in the western Antarctic Peninsula. *Science*, 353 (6296): 283–286. doi:10.1126/science.aae0017.

Cook, C.P., Flierdt, T. Van De, Williams, T., et al. (2013) Dynamic behaviour of the East Antarctic ice sheet during Pliocene warmth. *Nature Geoscience*, 6 (July): 765–769. doi:10.1038/ngeo1889.

Crosta, X., Crespin, J., Billy, I., et al. (2005) Major factors controlling Holocene d13Corg changes in a seasonal sea-ice environment, Adelie Land, East Antarctica. *Global Biogeochemical Cycles*, 19 (4). doi:10.1029/2004GB002426.

Crosta, X., Debret, M., Denis, D., et al. (2007) Holocene long- and short-term climate changes off Adélie Land, East Antarctica. *Geochemistry, Geophysics, Geosystems*, 8 (11). doi:10.1029/2007GC001718.

Crosta, X., Denis, D. and Ther, O. (2008) Sea ice seasonality during the Holocene, Adelie Land, East Antarctica. *Marine Micropaleontology*, 66 (3–4): 222–232. doi:10.1016/j.marmicro.2007.10.001.

Dalsgaard, J., St. John, M., Kattner, G., et al. (2003) Fatty acid trophic markers in the pelagic marine environment. *Advances in Marine Biology*. 46 pp. 225–340. doi:10.1016/S0065-2881(03)46005-7.

Dansgaard, W. (1964) Stable isotopes in precipitation. *Tellus*, pp. 436–468. doi:10.3402/tellusa.v16i4.8993.

Dawson, K.S., Freeman, K.H. and Macalady, J.L. (2012) Molecular characterization of core lipids from halophilic archaea grown under different salinity conditions. *Organic Geochemistry*, 48: 1–8. doi:10.1016/j.orggeochem.2012.04.003.

Death, R., Wadham, J.L., Monteiro, F., et al. (2014) Antarctic ice sheet fertilises the Southern Ocean. *Biogeosciences*, 11 (10): 2635–2643. doi:10.5194/bg-11-2635-2014.

DeConto, R., Pollard, D. and Harwood, D. (2007) Sea ice feedback and Cenozoic evolution of Antarctic climate and ice sheets. *Paleoceanography*, 22 (3). doi:10.1029/2006PA001350.

DeMaster, D.J. (1981) The supply and accumulation of silica in the marine environment. *Geochimica et Cosmochimica Acta*, 45 (10): 1715–1732. doi:10.1016/0016-

7037(81)90006-5.

Denis, D., Crosta, X., Barbara, L., et al. (2010) Sea ice and wind variability during the Holocene in East Antarctica: Insight on middle-high latitude coupling. *Quaternary Science Reviews*, 29 (27–28): 3709–3719. doi:10.1016/j.quascirev.2010.08.007.

Denis, D., Crosta, X., Schmidt, S., et al. (2009a) Holocene glacier and deep water dynamics, Adélie Land region, East Antarctica. *Quaternary Science Reviews*. doi:10.1016/j.quascirev.2008.12.024.

Denis, D., Crosta, X., Schmidt, S., et al. (2009b) Holocene productivity changes off Adélie land (East Antarctica). *Paleoceanography*, 24 (3): 1–12. doi:10.1029/2008PA001689.

DiTullio, G.R., Grebmeier, J.M., Arrigo, K.R., et al. (2000) Rapid and early export of Phaeocystis antarctica blooms in the Ross Sea, Antarctica. *Nature*, 404 (6778): 595–598. doi:10.1038/35007061.

Domack, E., Amblàs, D., Gilbert, R., et al. (2006) Subglacial morphology and glacial evolution of the Palmer deep outlet system, Antarctic Peninsula. *Geomorphology*, 75 (1–2 SPEC. ISS.): 125–142. doi:10.1016/j.geomorph.2004.06.013.

Dunbar, R.B., Anderson, J.B., Domack, E.W., et al. (1985) "Oceanographic influences on sedimentation along the Antarctic continental shelf." In *Oceanology of the Antarctic Continental Shelf (eds S. Jacobs)*. pp. 291–312. doi:10.1029/AR043p0291.

Duprat, L.P.A.M., Bigg, G.R. and Wilton, D.J. (2016) Enhanced Southern Ocean marine productivity due to fertilization by giant icebergs. *Nature Geoscience*, 9 (January): 219–221. doi:10.1038/ngeo2633.

Elling, F.J., Könneke, M., Mußmann, M., et al. (2015) Influence of temperature, pH, and salinity on membrane lipid composition and TEX86 of marine planktonic thaumarchaeal isolates. *Geochimica et Cosmochimica Acta*, 171: 238–255. doi:10.1016/j.gca.2015.09.004.

Escutia, C., Brinkhuis, H., Klaus, A., et al. (2011) *Expedition 318 summary*.

doi:10.2204/iodp.proc.318.101.2011.

Etourneau, J., Collins, L.G., Willmott, V., et al. (2013) Holocene climate variations in the western Antarctic Peninsula: Evidence for sea ice extent predominantly controlled by changes in insolation and ENSO variability. Climate of the Past, 9 (4): 1431–1446. doi:10.5194/cp-9-1431-2013.

Etourneau, J., Collins, L.G., Willmott, V., et al. (2013) Holocene climate variations in the western Antarctic Peninsula: Evidence for sea ice extent predominantly controlled by changes in insolation and ENSO variability. *Climate of the Past*, 9 (4): 1431–1446. doi:10.5194/cp-9-1431-2013.

Expedition 318 Scientists (2011) Site U1357. *Proc. IODP, 318*, 318. doi:10.2204/iodp.proc.318.105.2011.

Farquhar, G.D., O'Leary, M.H. and Berry, J.A. (1982) On the Relationship between Carbon Isotope Discrimination and the Intercellular Carbon dioxide Concentration in Leaves. *Australian Journal of Plant Physiology*, 9: 121–137.

Feakins, S.J., Warny, S. and Lee, J.-E. (2012) Hydrologic cycling over Antarctica during the middle Miocene warming. *Nature Geoscience*, 5. doi:10.1038/NGEO1498.

Fischer, G., Schneider, R., Müller, P.J., et al. (1997) Anthropogenic CO2 in Southern Ocean surface waters: Evidence from stable organic carbon isotopes. *Terra Nova*, 9 (4): 153–157. doi:10.1046/j.1365-3121.1997.d01-29.x.

Fogwill, C.J., Turney, C.S.M., Meissner, K.J., et al. (2014) Testing the sensitivity of the East Antarctic Ice Sheet to Southern Ocean dynamics: Past changes and future implications. *Journal of Quaternary Science*. doi:10.1002/jqs.2683.

Folk, R.L. and Ward, W.C. (1957) Brazos River bar [Texas]; a study in the significance of grain size parameters. *Journal of Sedimentary Research*, 27 (1): 3–26. doi:10.1306/74D70646-2B21-11D7-8648000102C1865D.

Francey, R.J., Allison, C.E., Etheridge, D.M., et al. (1999) A 1000-year high precision record of δ13C in atmospheric CO2. *Tellus, Series B: Chemical and Physical*

*Meteorology*, 51 (2): 170–193.

Freeman, K.H. and Hayes, J.M. (1992) Fractionation of Carbon Isotopes by Phytoplankton and Estimates of Ancient CO2 Levels. *Global Biogeochemical Cyclesiogeochemical cycles*, 6 (2): 185–198.

Frohlich, K., Grabczak, J. and Rozansk, K. (1988) Deuterium and Oxygen-18 in the Baltic Sea. *Chemical Geology*, 72: 77–83.

Gagné, M.-È., Gillett, N.P., Fyfe, J.C., et al. (2015) Observed and simulated changes in Antarctic sea ice extent over the past 50 years. Geophysical Research Letters, 42 (1): 90–95. doi:10.1002/2014GL062231.

Gaines, S.M., Eglinton, G. and Rullkötter, J. (2009) *Echos of Life: What Fossil Molecules Reveal about Earth History*,. Oxford University Press.

Gardner, A.S., Moholdt, G., Scambos, T., et al. (2018) Increased West Antarctic and unchanged East Antarctic ice discharge over the last 7 years. *Cryosphere*, 12 (2): 521–547. doi:10.5194/tc-12-521-2018.

Gat, R., Shemesh, A., Tziperman, E., et al. (1996) The stable isotope composition of waters of the eastern Mediterranean Sea. *Journal of Geophysical Research*, 101 (95): 6441–6451.

Gibson, J.A.E., Trull, T., Nichols, P.D., et al. (1999) Sedimentation of 13 C-rich organic matter from Antarctic sea-ice algae: A potential indicator of past sea-ice extent. *Geology*, 27 (4): 331–334. doi:10.1130/0091-7613(1999)027<0331:SOCROM>2.3.CO;2.

Gilchrist, H. (2018) *A high-resolution record of sea ice, glacial and biological dynamics from an Antarctic coast environment*. University of Birmingham.

Gliozzi, A., Paoli, G., De Rosa, M., et al. (1983) Effect of isoprenoid cyclization on the transition temperature of lipids in thermophilic archaebacteria. *BBA - Biomembranes*. doi:10.1016/0005-2736(83)90298-5.

Golledge, N.R., Menviel, L., Carter, L., et al. (2014) Antarctic contribution to meltwater

pulse 1A from reduced Southern Ocean overturning. *Nature communications*, 5: 5107. doi:10.1038/ncomms6107.

Griffith, E.M. and Paytan, A. (2012) Barite in the ocean - occurrence, geochemistry and palaeoceanographic applications. *Sedimentology*, 59 (6): 1817–1835. doi:10.1111/j.1365-3091.2012.01327.x.

Haddad, R.I., Martens, C.S. and Farrington, J.W. (1992) Quantifying early diagenesis of fatty acids in a rapidly accumulating coastal marine sediment. *Organic Geochemistry*, 19 (1–3): 205–216. doi:10.1016/0146-6380(92)90037-X.

Hall, A. and Visbeck, M. (2002) Synchronous Variability in the Southern Hemisphere Atmosphere, Sea Ice, and Ocean Resulting from the Annular Mode. *Journal of Climate*, 15: 3043–3057.

Hall, B.L., Baroni, C. and Denton, G.H. (2004) Holocene relative sea-level history of the Southern Victoria Land Coast, Antarctica. *Global and Planetary Change*, 42 (1–4): 241–263. doi:10.1016/j.gloplacha.2003.09.004.

Hall, B.L., Henderson, G.M., Baroni, C., et al. (2010) Constant Holocene Southern-Ocean14C reservoir ages and ice-shelf flow rates. *Earth and Planetary Science Letters*, 296 (1–2): 115–123. doi:10.1016/j.epsl.2010.04.054.

Hammer, Ø., Harper, D.A.T. and Ryan, P.D. (2001) Past: Paleontological statistics software package for education and data analysis. *Palaeontologia Electronica*.

Hein, A.S., Marrero, S.M., Woodward, J., et al. (2016) Mid-Holocene pulse of thinning in the Weddell Sea sector of the West Antarctic ice sheet. *Nature Communications*, 7: 12511. doi:10.1038/ncomms12511.

Hellmer, H.H. (2004) Impact of Antarctic ice shelf basal melting on sea ice and deep ocean properties. *Geophysical Research Letters*, 31 (10): 1–4. doi:10.1029/2004GL019506.

Henley, S.F., Annett, A.L., Ganeshram, R.S., et al. (2012) Factors influencing the stable carbon isotopic composition of suspended and sinking organic matter in the coastal

Antarctic sea ice environment. *Biogeosciences*, 9 (3): 1137–1157. doi:10.5194/bg-9-1137-2012.

Herfort, L., Schouten, S., Abbas, B., et al. (2007) Variations in spatial and temporal distribution of Archaea in the North Sea in relation to environmental variables. *FEMS Microbiology Ecology*. doi:10.1111/j.1574-6941.2007.00397.x.

Hillenbrand, C.D., Smith, J.A., Hodell, D.A., et al. (2017) West Antarctic Ice Sheet retreat driven by Holocene warm water incursions. *Nature*, 547 (7661): 43–48. doi:10.1038/nature22995.

Holland, A.R., Petsch, S.T., Castañeda, I.S., et al. (2013) A biomarker record of Lake El'gygytgyn, Far East Russian arctic: Investigating sources of organic matter and carbon cycling during marine isotope stages 1-3. *Climate of the Past*, 9 (1): 243–260. doi:10.5194/cp-9-243-2013.

Holland, D.M., Jacobs, S.S. and Jenkins, A. (2003) Modelling the ocean circulation beneath the Ross Ice Shelf. *Antarctic Science*, 15 (1): 13–23. doi:10.1017/S0954102003001019.

Holland, P.R. and Kwok, R. (2012) Wind-driven trends in Antarctic sea-ice drift. *Nature Geoscience*, 5 (12): 872–875. doi:10.1038/ngeo1627.

Hollander, D.J. and McKenzie, J.A. (1991) CO2 control on carbon-isotope fractionation during aqueous photosynthesis: a paleo-pCO2 barometer. *Geology*, 19 (9): 929–932. doi:10.1130/0091-7613(1991)019<0929:CCOCIF>2.3.CO;2.

Hopmans, E. C., Schouten, S. and Sinninghe Damsté, J. S. (2016) The effect of improved chromatography on GDGT-based palaeoproxies, *Organic Geochemistry*. doi: 10.1016/j.orggeochem.2015.12.006.

Hopmans, E.C., Weijers, J.W.H., Schefuß, E., et al. (2004) A novel proxy for terrestrial organic matter in sediments based on branched and isoprenoid tetraether lipids. *Earth and Planetary Science Letters*, 224: 107–116. doi:10.1016/j.epsl.2004.05.012.

Huang, Y., Clemens, S.C., Liu, W., et al. (2007) Large scale hydrological change drove

the late Miocene C4 plant expansion in the Himalayan foreland Arabian Peninsula. *Geology*, 35 (6): 531–534. doi:10.1130/G23666A.1.

Huang, Y., Street-Perrott, F.A., Perrott, R.A., et al. (1999) Glacial-interglacial environmental changes inferred from molecular and compound-specific δ13C analyses of sediments from Sacred Lake, Mt. Kenya. *Geochimica et Cosmochimica Acta*, 63 (9): 1383–1404. doi:10.1016/S0016-7037(99)00074-5.

Hughes, K., Langhorne, P.J., Leonard, G.H., et al. (2014) Extension of an Ice ShelfWater plumemodel beneath sea ice with application inMcMurdo Sound, Antarctica. *Journal of Geophysical Research: Oceans*, 119: 8662–8687. doi:10.1002/2014JC010248.Received.

Huguet, C., Kim, J.H., Damsté, J.S.S., et al. (2006) Reconstruction of sea surface temperature variations in the Arabian Sea over the last 23 kyr using organic proxies (TEX86 and U 37K′). *Paleoceanography*, 21 (3): 1–13. doi:10.1029/2005PA001215.

Hurley, S.J., Elling, F.J., Könneke, M., et al. (2016) Influence of ammonia oxidation rate on thaumarchaeal lipid composition and the TEX86 temperature proxy. *Proceedings of the National Academy of Sciences of the United States of America*, 113 (28): 7762–7767. doi:10.1073/pnas.1518534113.

IODP (n.d.) *Coring Tools and Technology*. Available at: http://iodp.tamu.edu/tools/index.html (Accessed: 1 October 2019).

IPCC (2013) Climate Change 2013: The Physical Science Basis. Contribution of Working Group I to the Fifth Assessment Report of the Intergovernmental Panel on Climate Change.

Jacobs, S.S. and Giulivi, C.F. (2010) Large multidecadal salinity trends near the Pacific-Antarctic continental margin. Journal of Climate, 23 (17): 4508–4524. doi:10.1175/2010JCLI3284.1.

Jacobs, S.S., Giulivi, C.F. and Mele, P.A. (2002) Freshening of the Ross Sea During the Late 20th Century. *Science*, 297 (5580): 386–389. doi:10.1126/science.1069574.

Jacobs, S.S., Mele, P.A., Smethie, W.M., et al. (2004) *Summer Oceanographic*

*Measurements near the Mertz Polynya ( 140-150E ) on NB Palmer Cruise 00-08*. doi:10.15784/601161.

Jenkyns, H.C., Schouten-Huibers, L., Schouten, S., et al. (2012) Warm Middle Jurassic-Early Cretaceous high-latitude sea-surface temperatures from the Southern Ocean. *Climate of the Past*, 8 (1): 215–225. doi:10.5194/cp-8-215-2012.

Jensen, S., Renberg, L. and Reutergårdh, L. (1977) Residue Analysis of Sediment and Sewage Sludge for Organochlorines in the Presence of Elemental Sulfur. *Analytical Chemistry*, 49 (2): 316–318. doi:10.1021/ac50010a033.

Johns, L., Wraige, E.J., Belt, S.T., et al. (1999) Identification of a C25highly branched isoprenoid (HBI) diene in Antarctic sediments, Antarctic sea-ice diatoms and cultured diatoms. *Organic Geochemistry*, 30 (11): 1471–1475. doi:10.1016/S0146-6380(99)00112-6.

Jones, J.M., Gille, S.T., Goosse, H., et al. (2016) Assessing recent trends in high-latitude Southern Hemisphere surface climate. *Nature Climate Change*, 6 (10): 917–926. doi:10.1038/nclimate3103.

Jones, R.S., Mackintosh, A.N., Norton, K.P., et al. (2015) Rapid Holocene thinning of an East Antarctic outlet glacier driven by marine ice sheet instability. *Nature Communications*, 6: 8910. doi:10.1038/ncomms9910.

Jourdain, N.C., Mathiot, P., Merino, N., et al. (2017) Ocean circulation and sea-ice thinning induced bymelting ice shelves in the Amundsen Sea. *Journal of Geophysical Research: Oceans*, 122 (3): 2550–2573. doi:10.1002/2016JC012509.Received.

Jouzel, J., Masson-Delmotte, V., Cattani, O., et al. (2007) Orbital and millennial Antarctic climate variability over the past 800,000 years. *Science (New York, N.Y.)*, 317 (5839): 793–796. doi:10.1126/science.1141038.

Keeling, C.D., Piper, S.C., Bacastow, R.B., et al. (2005) "Atmospheric CO2 and 13CO2 Exchange with the Terrestrial Biosphere and Oceans from 1978 to 2000: Observations and Carbon Cycle Implications." In A History of Atmospheric CO2 and Its Effects on Plants, Animals, and Ecosystems. doi:10.1007/0-387-27048-5_5.

Khazendar, A., Rignot, E., Schroeder, D.M., et al. (2016) Rapid submarine ice melting in the grounding zones of ice shelves in West Antarctica. *Nature Communications*, 7: 13243. doi:10.1038/ncomms13243.

Killops, S. and Killops, V. (2004) *Introduction to Organic Geochemistry*. doi:10.1002/9781118697214.

Kim, J.H., Crosta, X., Willmott, V., et al. (2012) Holocene subsurface temperature variability in the eastern Antarctic continental margin. Geophysical Research Letters, 39 (6): 1–7. doi:10.1029/2012GL051157.

Kim, J.H., Schneider, R.R., Müller, P.J., et al. (2002) Interhemispheric comparison of deglacial sea-surface temperature patterns in Atlantic eastern boundary currents. *Earth and Planetary Science Letters*, 194 (3–4): 383–393. doi:10.1016/S0012-821X(01)00545-3.

Kim, J.H., Schouten, S., Hopmans, E.C., et al. (2008) Global sediment core-top calibration of the TEX86 paleothermometer in the ocean. *Geochimica et Cosmochimica Acta*. doi:10.1016/j.gca.2007.12.010.

Kim, J.H., van der Meer, J., Schouten, S., et al. (2010) New indices and calibrations derived from the distribution of crenarchaeal isoprenoid tetraether lipids: Implications for past sea surface temperature reconstructions. *Geochimica et Cosmochimica Acta*, 74 (16): 4639–4654. doi:10.1016/j.gca.2010.05.027.

Kingslake, J., Scherer, R.P., Albrecht, T., et al. (2018) Extensive retreat and re-advance of the West Antarctic Ice Sheet during the Holocene. *Nature*, 558 (7710): 430–434. doi:10.1038/s41586-018-0208-x.

Kirchman, D.L., Elifantz, H., Dittel, A.I., et al. (2007) Standing stocks and activity of Archaea and Bacteria in the western Arctic Ocean. *Limnology and Oceanography*. doi:10.4319/lo.2007.52.2.0495.

Kleinschmidt, G. and Talarico, F. (2000) The Mertz shear zone. *Terra Antarctica Reports*, pp. 109–115.

Köhler, P. and Fischer, H. (2006) Simulating low frequency changes in atmospheric CO2 during the last 740 000 years. *Climate of the Past*, 2 (2): 57–78. doi:10.5194/cp-2-57-2006.

König-Langlo, G., King, J.C. and Pettré, P. (1998) Climatology of the three coastal Antarctic stations Dumont d'Urville, Neumayer, and Halley. *Journal of Geophysical Research D: Atmospheres*, 103: 10935–10946. doi:10.1029/97jd00527.

Könneke, M., Bernhard, A.E., De La Torre, J.R., et al. (2005) Isolation of an autotrophic ammonia-oxidizing marine archaeon. *Nature*, 437 (7058): 543–546. doi:10.1038/nature03911.

Koopmans, M., van Rijswijk, P., Boschker, H.T.S., et al. (2014) Seasonal Variation of Fatty Acids and Stable Carbon Isotopes in Sponges as Indicators for Nutrition: Biomarkers in Sponges Identified. *Marine Biotechnology*, 17 (1): 43–54. doi:10.1007/s10126-014-9594-8.

Kopczynska, E.E., Goeyens, L., Semeneh, M., et al. (1995) Phytoplankton Composition and Cell Carbon Distribution in Prydz Bay, Antarctica - Relation To Organic Particulate Matter and Its Delta-C-13 Values. *Journal of Plankton Research*, 17 (4): 685–707. doi:10.1093/plankt/17.4.685.

Kusahara, K., Hasumi, H. and Tamura, T. (2010) Modeling sea ice production and dense shelf water formation in coastal polynyas around East Antarctica. *Journal of Geophysical Research: Oceans*, 115 (10): C10006. doi:10.1029/2010JC006133.

Lacarra, M., Houssais, M.N., Sultan, E., et al. (2011) Summer hydrography on the shelf off Terre Adélie/George V Land based on the ALBION and CEAMARC observations during the IPY. *Polar Science*, 5 (2): 88–103. doi:10.1016/j.polar.2011.04.008.

Laine, V. (2008) Antarctic ice sheet and sea ice regional albedo and temperature change , 1981 – 2000 , from AVHRR Polar Pathfinder data. *Remote Sensing of Environment*, 112: 646–667. doi:10.1016/j.rse.2007.06.005.

Lambeck, K. and Purcell, A. (2005) Sea-level change in the Mediterranean Sea since the LGM: Model predictions for tectonically stable areas. *Quaternary Science Reviews*, 24

(18–19): 1969–1988. doi:10.1016/j.quascirev.2004.06.025.

Lawson, M.P., Bergquist, P.R. and Cambie, R.C. (1986) The cellular localization of long chain fatty acids in sponges. *Tissue and Cell*, 18 (1): 19–26. doi:10.1016/0040-8166(86)90004-2.

Le Quéré, C., Rödenbeck, C., Buitenhuis, E.T., et al. (2007) Saturation of the southern ocean CO2 sink due to recent climate change. *Science*, 316 (5832): 1735–1738. doi:10.1126/science.1136188.

Leblond, J.D. and Chapman, P.J. (2000) Lipid class distribution of highly unsaturated long chain fatty acids in marine dinoflagellates. *Journal of Phycology*, 36: 1103–1108.

Lee, K.E., Kim, J.H., Wilke, I., et al. (2008) A study of the alkenone, TEX86, and planktonic foraminifera in the benguela upwelling system: Implications for past sea surface temperature estimates. *Geochemistry, Geophysics, Geosystems*. doi:10.1029/2008GC002056.

Lenton, A., Tilbrook, B., Law, R., et al. (2013) Sea-air $CO_2$ fluxes in the Southern Ocean for the period 1990–2009. *Biogeosciences Discussions*, 10 (1): 285–333. doi:10.5194/bgd-10-285-2013.

Leventer, A. and Dunbar, R.B. (1996) Factors influencing the distribution of diatoms and other algae in the Ross Sea. *Journal of Geophysical Research C: Oceans*. doi:10.1029/96JC00204.

Leventer, A., Domack, E.W., Dunbar, R., et al. (2006) Marine sediment record from the East Antarctic margin reveals dynamics of ice sheet recession. *GSA Today*, 16 (12): 4–10. doi:10.1130/GSAT01612A.1.

Li, X., Rignot, E., Mouginot, J., et al. (2016) Ice flow dynamics and mass loss of Totten Glacier, East Antarctica, from 1989 to 2015. *Geophysical Research Letters*, 43: 6366–6373. doi:10.1002/2016GL069173.1.

Lincoln, S.A., Wai, B., Eppley, J.M., et al. (2014a) Planktonic euryarchaeota are a significant source of archaeal tetraether lipids in the ocean. *Proceedings of the National*

*Academy of Sciences of the United States of America*, 111 (27): 9858–9863. doi:10.1073/pnas.1409439111.

Lincoln, S.A., Wai, B., Eppley, J.M., et al. (2014b) Reply to Schouten et al.: Marine Group II planktonic Euryarchaeota are significant contributors to tetraether lipids in the ocean. *Proceedings of the National Academy of Sciences of the United States of America*, 111 (41): E4286. doi:10.1073/pnas.1416736111.

Liu, Z., Zhu, J., Rosenthal, Y., et al. (2014) The Holocene temperature conundrum. *Proceedings of the National Academy of Sciences*, 111 (34): E3501--E3505. doi:10.1073/pnas.1407229111.

Locarnini, R.A., Mishonov, A.V., Baranova, O.K., et al. (2018) World Ocean Atlas 2018, Volume 1: Temperature. A. Mishonov, Technical Editor. *NOAA Atlas NESDIS*, 51 (1).

Macalady, J.L., Vestling, M.M., Baumler, D., et al. (2004) Tetraether-linked membrane monolayers in Ferroplasma spp: A key to survival in acid. *Extremophiles*, 8 (5): 411–419. doi:10.1007/s00792-004-0404-5.

MacFarling Meure, C., Etheridge, D., Trudinger, C., et al. (2006) Law Dome CO2, CH4 and N2O ice core records extended to 2000 years BP. *Geophysical Research Letters*, 33 (14): 1–4. doi:10.1029/2006GL026152.

Mackensen, A. (2001) Oxygen and carbon stable isotope tracers of Weddell sea water masses: New data and some paleoceanographic implications. *Deep-Sea Research Part I: Oceanographic Research Papers*, 48 (6): 1401–1422. doi:10.1016/S0967-0637(00)00093-5.

Mackintosh, A., Golledge, N.R., Domack, E.W., et al. (2011) Retreat of the East Antarctic ice sheet during the last glacial termination. *Nature Geoscience*, 4 (3): 195–202. doi:10.1038/ngeo1061.

Mackintosh, A.N., Verleyen, E., O'Brien, P.E., et al. (2014) Retreat history of the East Antarctic Ice Sheet since the Last Glacial Maximum. *Quaternary Science Reviews*, 100: 10–30. doi:10.1016/j.quascirev.2013.07.024.

Mahowald, N., Kohfeld, K., Hansson, M., et al. (1999) Dust sources and deposition during the last glacial maximum and current climate: A comparison of model results with paleodata from ice cores and marine sediments. *Journal of Geophysical Research*, 104 (D13): 15895–15916. doi:10.1029/1999JD900084.

Manabe, S., Spelman, M.J. and Stouffer, R.J. (1992) Transient Responses of a Coupled Ocean-Atmosphere Model to Gradual Changes of Atmospheric CO2. Part II: Seasonal Response. *Journal of Climate*, 5: 105–126.

Manabe, S., Strouffer, R.J., Spelman, M.J., et al. (1991) Transient Responses of a Coupled Ocean–Atmosphere Model to Gradual Changes of Atmospheric CO2. Part I: Mean Annual Response. *Journal of Climate*, 4: 785–818.

Marcott, S. a., Shakun, J.D., Clark, P.U., et al. (2013) A Reconstruction of Regional and Global Temperature for the Past 11,300 Years. *Science (New York, N.Y.)*, 339 (6124): 1198–1201. doi:10.1126/science.1228026.

Marshall, G.J. (2003) Trends in the Southern Annular Mode from observations and reanalyses. *Journal of Climate*, 16 (24): 4134–4143. doi:10.1175/1520-0442(2003)016<4134:TITSAM>2.0.CO;2.

Marshall, J., Adcroft, A., Hill, C., et al. (1997) A finite-volume, incompressible Navier Stokes model for studies of the ocean on parallel computers. *Journal of Geophysical Research: Oceans*, 102 (C3): 5753–5766. doi:10.1029/96JC02775.

Marsland, S.J., Bindoff, N.L., Williams, G.D., et al. (2004) Modeling water mass formation in the Mertz Glacier Polynya and Adélie Depression, East Antarctica. *Journal of Geophysical Research: Oceans*, 109 (11): C11003. doi:10.1029/2004JC002441.

Martin, A., Houssais, M., Le, H., et al. (2017) Circulation and water mass transports on the East Antarctic shelf in the Mertz Glacier region. *Deep-Sea Research Part I*, 126: 1–20. doi:10.1016/j.dsr.2017.05.007.

Martin, J.H., Fitzwater, S.E. and Gordon, R.M. (1990) Iron Deficiency Limits Phytoplankton Growth In Antarctic Waters. *Global Biogeochemical Cycles*, 4 (1): 5–12.

Martínez-Garcia, A., Rosell-Melé, A., Jaccard, S.L., et al. (2011) Southern Ocean dust-climate coupling over the past four million years. Nature. doi:10.1038/nature10310.

Massé, G., Belt, S.T., Crosta, X., et al. (2011) Highly branched isoprenoids as proxies for variable sea ice conditions in the Southern Ocean. *Antarctic Science*, 23 (5): 487–498. doi:10.1017/S0954102011000381.

Massom, R.A., Giles, A.B., Fricker, H.A., et al. (2010) Examining the interaction between multi-year landfast sea ice and the Mertz Glacier Tongue, East Antarctica: Another factor in ice sheet stability? *Journal of Geophysical Research: Oceans*, 115 (12): 1–15. doi:10.1029/2009JC006083.

Massom, R.A., Hill, K., Barbraud, C., et al. (2009) Fast ice distribution in Adélie Land, East Antarctica: Interannual variability and implications for emperor penguins Aptenodytes forsteri. *Marine Ecology Progress Series*, 374: 243–257. doi:10.3354/meps07734.

Massom, R.A., Hill, K.L., Lytle, V.I., et al. (2001) Effects of regional fast-ice and iceberg distributions on the behaviour of the Mertz Glacier polynya, East Antarctica. *Annals of Glaciology*, 33: 391–398. doi:10.3189/172756401781818518.

Massom, R.A., Scambos, T.A., Bennetts, L.G., et al. (2018) Antarctic ice shelf disintegration triggered by sea ice loss and ocean swell. *Nature*, 558 (7710): 383–389. doi:10.1038/s41586-018-0212-1.

Masson, V., Vimeux, F., Jouzel, J., et al. (2000) Holocene climate variability in Antartica based on 11 ice-core isotopic records. *Quaternary Research*. doi:10.1006/qres.2000.2172.

Masson-Delmotte, V., Buiron, D., Ekaykin, A., et al. (2011) A comparison of the present and last interglacial periods in six Antarctic ice cores. *Climate of the Past*, 7 (2): 397–423. doi:10.5194/cp-7-397-2011.

Masuda, S., Awaji, T., Sugiura, N., et al. (2010) Simulated Rapid Warming of Abyssal North Pacific Waters. *Science*, 329 (5989): 319–322. doi:10.1126/science.1188703.

Matsuda, H. (1978) Early diagenesis of fatty acids in lacustrine sediments-III. Changes in

fatty acid composition in the sediments from a brackish water lake. *Geochimica et Cosmochimica Acta*, 42: 1027–1034.

Matsuda, H. and Koyama, T. (1977) Early diagenesis of fatty acids in lacustrine sediments-I. Identification and distribution of fatty acids in recent sediment from a freshwater lake. *Geochimica et Cosmochimica Acta*, 41 (6): 777–783. doi:10.1016/0016-7037(77)90048-5.

Mayer, L.M. (1993) "Organic Matter at the Sediment-Water Interface." In *Organic Geochemistry: principles and applications*. pp. 171–184. doi:10.1007/978-1-4615-2890-6_7.

Mayewski, P.A., Rohling, E.E., Stager, J.C., et al. (2004) Holocene climate variability. *Quaternary Research*, 62 (3): 243–255. doi:10.1016/j.yqres.2004.07.001.

McCartney, M.S. and Donohue, K.A. (2007) A deep cyclonic gyre in the Australian-Antarctic Basin. *Progress in Oceanography*, 75 (4): 675–750. doi:10.1016/j.pocean.2007.02.008.

McCave, I.N. and Hall, I.R. (2006) Size sorting in marine muds: Processes, pitfalls, and prospects for paleoflow-speed proxies. *Geochemistry, Geophysics, Geosystems*, 7 (10). doi:10.1029/2006GC001284.

McCave, I.N., Manighetti, B. and Robinson, S.G. (1995) Sortable silt and fine sediment size/composition slicing: Parameters for palaeocurrent speed and palaeoceanography. *Paleoceanography*, 10 (3): 593–610. doi:10.1029/94PA03039.

McCave, I.N., Thornalley, D.J.R. and Hall, I.R. (2017) Relation of sortable silt grain-size to deep-sea current speeds: Calibration of the 'Mud Current Meter'. *Deep-Sea Research Part I: Oceanographic Research Papers*, 127 (February): 1–12. doi:10.1016/j.dsr.2017.07.003.

McKay, R., Browne, G., Carter, L., et al. (2009) The stratigraphic signature of the late Cenozoic Antarctic Ice Sheets in the Ross Embayment. *Bulletin of the Geological Society of America*, 121 (11–12): 1537–1561. doi:10.1130/B26540.1.

McKay, R., Golledge, N.R., Maas, S., et al. (2016) Antarctic marine ice-sheet retreat in the Ross Sea during the early Holocene. *Geology*, 44 (1): 7–10. doi:10.1130/G37315.1.

McKay, R.M., Dunbar, G.B., Naish, T.R., et al. (2008) Retreat history of the Ross Ice Sheet (Shelf) since the Last Glacial Maximum from deep-basin sediment cores around Ross Island. *Palaeogeography, Palaeoclimatology, Palaeoecology*, 260 (1–2): 245–261. doi:10.1016/j.palaeo.2007.08.015.

Mengel, M. and Levermann, A. (2014) Ice plug prevents irreversible discharge from East Antarctica. *Nature Climate Change*, 4 (May): 451–455. doi:10.1038/nclimate2226.

Meyers, P.A. and Ishiwatari, R. (1993) Lacustrine organic geochemistry-an overview of indicators of organic matter sources and diagenesis in lake sediments. *Organic Geochemistry*, 20 (7): 867–900. doi:10.1016/0146-6380(93)90100-P.

Mezgec, K., Stenni, B., Crosta, X., et al. (2017) Holocene sea ice variability driven by wind and polynya efficiency in the Ross Sea. *Nature Communications*, 8 (1). doi:10.1038/s41467-017-01455-x.

Miles, B.W.J., Stokes, C.R. and Jamieson, S.S.R. (2016) Pan-ice-sheet glacier terminus change in East Antarctica reveals sensitivity of Wilkes Land to sea-ice changes. *Science Advances*, 2 (5): 1–8. doi:10.1126/sciadv.1501350.

Miles, B.W.J., Stokes, C.R. and Jamieson, S.S.R. (2017) Simultaneous disintegration of outlet glaciers in Porpoise Bay (Wilkes Land), East Antarctica, driven by sea ice break-up. *Cryosphere*, 11 (1): 427–442. doi:10.5194/tc-11-427-2017.

Miles, B.W.J., Stokes, C.R., Vieli, A., et al. (2013) Rapid, climate-driven changes in outlet glaciers on the Pacific coast of East Antarctica. *Nature*, 500 (7464): 563–566. doi:10.1038/nature12382.

Mills, M.M., Kropuenske, L.R., Van Dijken, G.L., et al. (2010) Photophysiology in two southern ocean phytoplankton taxa: Photosynthesis of Phaeocystis Antarctica (prymnesiophyceae) and Fragilariopsis Cylindrus (bacillariophyceae) under simulated mixed-layer irradiance. *Journal of Phycology*, 46 (6): 1114–1127. doi:10.1111/j.1529-8817.2010.00923.x.

Moisan, T.A. and Mitchell, B.G. (1999) Photophysiological acclimation of Phaeocystis antarctica Karsten under light limitation. *Limnology and Oceanography*, 44 (2): 247–258. doi:10.4319/lo.1999.44.2.0247.

Mu, L., Stammerjohn, S.E., Lowry, K.E., et al. (2014) Spatial variability of surface pCO2 and air-sea CO2 flux in the Amundsen Sea Polynya, Antarctica. *Elementa: Science of the Anthropocene*, 2: 000036. doi:10.12952/journal.elementa.000036.

Naraoka, H. and Ishiwatari, R. (2000) Molecular and isotopic abundances of long-chain n-fatty acids in open marine sediments of the western North Pacific. *Chemical Geology*, 165 (1–2): 23–36. doi:10.1016/S0009-2541(99)00159-X.

Newton, K.E. (2015) Holocene climate variability off East Antarctica: biogenic, oceanic and glacial interactions. University of Birmingham.

Nicol, S., Pauly, T., Bindoff, N.L., et al. (2000) Ocean circulation off east Antarctica affects ecosystem structure and sea-ice extent. *Nature*, 406 (6795): 504–507. doi:10.1038/35020053.

Nicolas, J.P., Vogelmann, A.M., Scott, R.C., et al. (2017) Antarctica favoured by strong El Nino. *Nature Communications*, 8 (January 2016): 1–10. doi:10.1038/ncomms15799.

Nielsen, S.H.H., Hodell, D.A., Kamenov, G., et al. (2007) Origin and significance of ice-rafted detritus in the Atlantic sector of the Southern Ocean. *Geochemistry, Geophysics, Geosystems*, 8 (12): n/a-n/a. doi:10.1029/2007GC001618.

Orphan, V.J., Hinrichs, K.U., Ussler, W., et al. (2001) Comparative Analysis of Methane-Oxidizing Archaea and Sulfate-Reducing Bacteria in Anoxic Marine Sediments. *Applied and Environmental Microbiology*. doi:10.1128/AEM.67.4.1922-1934.2001.

Orsi, A.H., Johnson, G.C. and Bullister, J.L. (1999) Circulation, mixing, and production of Antarctic Bottom Water. *Progress in Oceanography*, 43 (1): 55–109. doi:10.1016/S0079-6611(99)00004-X.

Pagani, M. (2014) *Biomarker-Based Inferences of Past Climate: The Alkenone pCO2 Proxy*. 2nd ed. Elsevier Ltd. doi:10.1016/B978-0-08-095975-7.01027-5.

Pagani, M., Pedentchouk, N., Huber, M., et al. (2006) Arctic hydrology during global warming at the Palaeocene/Eocene thermal maximum. *Nature*, 442 (7103): 671–675. doi:10.1038/nature05043.

Pancost, R.D. and Boot, C.S. (2004) The palaeoclimatic utility of terrestrial biomarkers in marine sediments. *Marine Chemistry*, 92 (1–4 SPEC. ISS.): 239–261. doi:10.1016/j.marchem.2004.06.029.

Paolo, F.S., Fricker, H.A. and Padman, L. (2015) Volume loss from Antarctic ice shelves is accelerating. *Science*, 348 (6232): 327–331. doi:10.1126/science.aaa0940.

Park, E., Hefter, J., Fischer, G., et al. (2019) Seasonality of archaeal lipid flux and GDGT-based thermometry in sinking particles of high-latitude oceans: Fram Strait (79°N) and Antarctic Polar Front (50°S). *Biogeosciences*, 16 (11): 2247–2268. doi:10.5194/bg-16-2247-2019.

Parkinson, C.L. and Cavalieri, D.J. (2012) Antarctic sea ice variability and trends, 1979-2010. *Cryosphere*, 6 (4): 871–880. doi:10.5194/tc-6-871-2012.

Pauling, A.G., Bitz, C.M., Smith, I.J., et al. (2016) The response of the Southern Ocean and Antarctic sea ice to freshwater from ice shelves in an earth system model. *Journal of Climate*, 29 (5): 1655–1672. doi:10.1175/JCLI-D-15-0501.1.

Paytan, A., Mearon, S., Cobb, K., et al. (2002) Origin of marine barite deposits: Sr and S isotope characterization. *Geology*, 30 (8): 747–750. doi:10.1130/0091-7613(2002)030<0747:OOMBDS>2.0.CO;2.

Periard, C. and Pettré, P. (1993) Some aspects of the climatology of Dumont d'Urville, Adélie Land, Antarctica. *International Journal of Climatology*, 13: 313–317.

Petit, R.J., Raynaud, D., Basile, I., et al. (1999) Climate and atmospheric history of the past 420,000 years from the Vostok ice core, Antarctica. *Nature*, 399: 429–413. doi:10.1038/20859.

Pike, J., Swann, G.E.A., Leng, M.J., et al. (2013) Glacial discharge along the west Antarctic Peninsula during the Holocene. *Nature Geoscience*, 6 (3): 199–202.

doi:10.1038/ngeo1703.

Plewa, K., Meggers, H. and Kasten, S. (2006) Barium in sediments off northwest Africa: A tracer for paleoproductivity or meltwater events? *Paleoceanography*, 21 (2): 1–15. doi:10.1029/2005PA001136.

Pollard, D. and Deconto, R.M. (2016) Contribution of Antarctica to past and future sea-level rise. *Nature*, 531 (7596): 591–597. doi:10.1038/nature17145.

Portillo, M.C., Leff, J.W., Lauber, C.L., et al. (2013) Cell size distributions of soil bacterial and archaeal taxa. *Applied and Environmental Microbiology*. doi:10.1128/AEM.02710-13.

Potter, J.R. and Paren, J.G. (1985) "Interaction between ice shelf and ocean in George VI Sound, Antarctica." In *Oceanology of the Antarctic Continental Shelf (ed S. S. Jacobs)*. pp. 35–58. doi:10.1029/AR043p0035.

Poulton, A.J., Mark Moore, C., Seeyave, S., et al. (2007) Phytoplankton community composition around the Crozet Plateau, with emphasis on diatoms and Phaeocystis. *Deep-Sea Research Part II: Topical Studies in Oceanography*, 54 (18–20): 2085–2105. doi:10.1016/j.dsr2.2007.06.005.

Powell, R. and Domack, E. (1995) "Glaciomarine processes and sediments." In *Modern Glacial Environments (Eds J. Menzies)*. Butterworth-Heinemann, Oxford.

Presti, M., Barbara, L., Denis, D., et al. (2011) Sediment delivery and depositional patterns off Adélie Land (East Antarctica) in relation to late Quaternary climatic cycles. *Marine Geology*, 284 (1–4): 96–113. doi:10.1016/j.margeo.2011.03.012.

Pritchard, H.D., Ligtenberg, S.R.M., Fricker, H.A., et al. (2012) Antarctic ice-sheet loss driven by basal melting of ice shelves. *Nature*, 484 (7395): 502–505. doi:10.1038/nature10968.

Qin, W., Carlson, L.T., Armbrust, E.V., et al. (2015) Confounding effects of oxygen and temperature on the TEX 86 signature of marine Thaumarchaeota. *Proceedings of the National Academy of Sciences of the United States of America*, 112 (35): 10979–10984.

doi:10.1073/pnas.1501568112.

Rau, G.H., Takahashi, T. and Des Marais, D.J. (1989) Latitudinal variations in plankton $\delta^{13}C$: Implications for CO<inf>2</inf>and productivity in past oceans. *Nature*, 341 (6242): 516–518.

Renssen, H., Goosse, H., Crosta, X., et al. (2010) Early holocene laurentide ice sheet deglaciation causes cooling in the high-latitude southern hemisphere through oceanic teleconnection. *Paleoceanography*, 25 (3): 1–15. doi:10.1029/2009PA001854.

Rhodes, R.H., Bertler, N.A.N., Baker, J.A., et al. (2012) Little Ice Age climate and oceanic conditions of the Ross Sea, Antarctica from a coastal ice core record. *Climate of the Past*, pp. 1223–1238. doi:10.5194/cp-8-1223-2012.

Riaux-Gobin, C., Dieckmann, G.S., Poulin, M., et al. (2013) Environmental conditions, particle flux and sympagic microalgal succession in spring before the sea-ice break-up in Adélie Land, East Antarctica. *Polar Research*, 32 (SUPPL.): 0–25. doi:10.3402/polar.v32i0.19675.

Riaux-Gobin, C., Poulin, M., Dieckmann, G., et al. (2011) Spring phytoplankton onset after the ice break-up and sea-ice signature (Adélie Land, East Antarctica). *Polar Research*, 30 (SUPPL.1). doi:10.3402/polar.v30i0.5910.

Rignot, E., Jacobs, S., Mouginot, J., et al. (2013) Ice Shelf Melting Around Antarctica. *Science*, 1 (June): 1–15. doi:10.1126/science.1235798.

Rignot, E., Mouginot, J., Morlighem, M., et al. (2014) Widespread, rapid grounding line retreat of Pine Island, Thwaites, Smith, and Kohler glaciers, West Antarctica, from 1992 to 2011. Geophysical Research Letters, 41 (10): 3502–3509. doi:10.1002/2014GL060140.

Riis, V. and Babel, W. (1999) Removal of sulfur interfering in the analysis of organochlorines by GC-ECD. *Analyst*, 124 (12): 1771–1773. doi:10.1039/a907504f.

Rintoul, S.R. (2007) Rapid freshening of Antarctic Bottom Water formed in the Indian and Pacific oceans. *Geophysical Research Letters*, 34 (6): L06606. doi:10.1029/2006GL028550.

Rintoul, S.R. and Bullister, J.L. (1999) A late winter hydrographic section from Tasmania to Antarctica. *Deep-Sea Research Part I: Oceanographic Research Papers*, 46 (8): 1417–1454. doi:10.1016/S0967-0637(99)00013-8.

Robel, A.A., Seroussi, H. and Roe, G.H. (2019) Marine ice sheet instability amplifies and skews uncertainty in projections of future sea-level rise. *Proceedings of the National Academy of Sciences*, 116 (30): 14887–14892. doi:10.1073/pnas.1904822116.

Robinson, N.J., Williams, M.J.M., Stevens, C.L., et al. (2014) Evolution of a supercooled Ice Shelf Water plume with an actively growing subice platelet matrix. *Journal of Geophysical Research : Oceans*, pp. 3425–3446. doi:10.1002/2013JC009399.Received.

Robson, J.N. and Rowland, S.J. (1988) Biodegradation of highly branched isoprenoid hydrocarbons: A possible explanation of sedimentary abundance. *Organic Geochemistry*, 13 (4–6): 691–695. doi:10.1016/0146-6380(88)90090-3.

Roden, N.P., Shadwick, E.H., Tilbrook, B., et al. (2013) Annual cycle of carbonate chemistry and decadal change in coastal Prydz Bay, East Antarctica. *Marine Chemistry*, 155: 135–147. doi:10.1016/j.marchem.2013.06.006.

Rogerson, J.H. and Johns, R.B. (1996) "A geolipid characterization of Organic Lake - A hypersaline meromictic Antarctic lake." In *Organic Geochemistry*. 1996. pp. 1–8. doi:10.1016/S0146-6380(96)00109-X.

Sachse, D., Billault, I., Bowen, G.J., et al. (2012) Molecular Paleohydrology: Interpreting the Hydrogen-Isotopic Composition of Lipid Biomarkers from Photosynthesizing Organisms. *Annual Review of Earth and Planetary Sciences*, 40 (1): 221–249. doi:10.1146/annurev-earth-042711-105535.

Salminen, T.A., Eklund, D.M., Joly, V., et al. (2018) Deciphering the evolution and development of the cuticle by studying lipid transfer proteins in mosses and liverworts. *Plants*, 7 (1). doi:10.3390/plants7010006.

Sambrotto, R.N., Matsuda, A., Vaillancourt, R., et al. (2003) Summer plankton production and nutrient consumption patterns in the Mertz Glacier Region of East Antarctica. *Deep-Sea Research Part II: Topical Studies in Oceanography*, 50 (8–9): 1393–1414.

doi:10.1016/S0967-0645(03)00076-6.

Schmidt, G.A., Bigg, G.R. and Rohling, E.J. (1999) *Global Seawater Oxygen-18 Database - v1.22*. Available at: https://data.giss.nasa.gov/o18data/.

Schmidtko, S., Heywood, K.J., Thompson, A.F., et al. (2014) Multidecadal warming of Antarctic waters. *Science*, 346 (6214): 1227–1231. doi:10.1126/science.1256117.

Schoemann, V., Becquevort, S., Stefels, J., et al. (2005) Phaeocystis blooms in the global ocean and their controlling mechanisms: A review. *Journal of Sea Research*. 53 (1-2 SPEC. ISS.) pp. 43–66. doi:10.1016/j.seares.2004.01.008.

Schoemann, V., Becquevort, S., Stefels, J., et al. (2005) Phaeocystis blooms in the global ocean and their controlling mechanisms: A review. *Journal of Sea Research*. 53 (1–2 SPEC. ISS.) pp. 43–66. doi:10.1016/j.seares.2004.01.008.

Schouten, S., Hopmans, E.C. and Sinninghe Damsté, J.S. (2013) The organic geochemistry of glycerol dialkyl glycerol tetraether lipids: A review. *Organic Geochemistry*, 54: 19–61. doi:10.1016/j.orggeochem.2012.09.006.

Schouten, S., Hopmans, E.C., Schefuß, E., et al. (2002) Distributional variations in marine crenarchaeotal membrane lipids: A new tool for reconstructing ancient sea water temperatures? *Earth and Planetary Science Letters*. doi:10.1016/S0012-821X(02)00979-2.

Schouten, S., Klein Breteler, W.C.., Blokker, P., et al. (1998) Biosynthetic effects on the stable carbon isotopic compositions of algal lipids: implications for deciphering the carbon isotopic biomarker record. *Geochimica et Cosmochimica Acta*, 62 (8): 1397–1406. doi:10.1016/S0016-7037(98)00076-3.

Schouten, S., Ossebaar, J., Schreiber, K., et al. (2006) The effect of temperature, salinity and growth rate on the stable hydrogen isotopic composition of long chain alkenones produced by *Emiliania huxleyi* and *Gephyrocapsa oceanica*. *Biogeosciences*, 3 (1): 113–119. doi:10.5194/bg-3-113-2006.

Schouten, S., Villanueva, L., Hopmans, E.C., et al. (2014) Are Marine Group II

Euryarchaeota significant contributors to tetraether lipids in the ocean? *Proceedings of the National Academy of Sciences of the United States of America*, 111 (41): E4285. doi:10.1073/pnas.1416176111.

Screen, J.A. and Simmonds, I. (2010) The central role of diminishing sea ice in recent Arctic temperature amplification. *Nature*, 464 (7293): 1334–1337. doi:10.1038/nature09051.

Sedwick, P.N. and DiTullio, G.R. (1997) Regulation of algal blooms in Antarctic shelf waters by the release of iron from melting sea ice. *Geophysical Research Letters*, 24 (20): 2515–2518.

Sedwick, P.N., Di Tullio, G.R. and Mackey, D.J. (2000) Iron and manganese in the Ross Sea, Seasonal iron limitation in Antarctic. *Journal of Geophysical Research: Oceans*. doi:10.1029/2000JC000256.

Seki, O., Bendle, J.A., Harada, N., et al. (2014) Assessment and calibration of TEX86 paleothermometry in the Sea of Okhotsk and sub-polar North Pacific region: Implications for paleoceanography. *Progress in Oceanography*, 126: 254–266. doi:10.1016/j.pocean.2014.04.013.

Sen Gupta, A., Santoso, A., Taschetto, A.S., et al. (2009) Projected Changes to the Southern Hemisphere Ocean and Sea Ice in the IPCC AR4 Climate Models. J. Clim., 22 (11): 3047–3078. doi:10.1175/2008JCLI2827.1.

Serreze, M.C. and Stroeve, J.C. (2015) Arctic sea ice trends, variability and implications for seasonal ice forecasting. *Philosophical Transactions of the Royal Society A: Mathematical, Physical and Engineering Sciences*, 373 (2045): 20140159. doi:10.1098/rsta.2014.0159.

Sessions, A.L., Burgoyne, T.W., Schimmelmann, A., et al. (1999) Fractionation of hydrogen isotopes in lipid biosynthesis, Org. *Organic Geochemistry*, 30: 1193–1200. doi:10.1016/S0146-6380(99)00094-7.

Sessions, A.L., Sylva, S.P., Summons, R.E., et al. (2004) Isotopic exchange of carbon-bound hydrogen over geologic timescales. *Geochimica et Cosmochimica Acta*, 68 (7):

1545–1559. doi:10.1016/j.gca.2003.06.004.

Shackleton, N.J. and Kennett, J.P. (1975) Paleotemperature history of the Cenozoic and the initiation of Antarctic glaciation; Oxygen and carbon isotope analyses in DSDP sites 277, 279 and 281. *Initial Reports of the Deep Sea Drilling Project*, 29: 743–755. doi:10.2973/dsdp.proc.37.1977.

Shadwick, E.H., Tilbrook, B. and Williams, G.D. (2014) Carbonate chemistry in the Mertz Polynya (East Antarctica): Biological and physical modification of dense water outflows and the export of anthropogenic CO2. *Journal of Geophysical Research: Oceans*, 119 (1): 1–14. doi:10.1002/2013JC009286.

Shepherd, A., Wingham, D. and Rignot, E. (2004) Warm ocean is eroding West Antarctic Ice Sheet. *Geophysical Research Letters*, 31 (23): 1–4. doi:10.1029/2004GL021106.

Shevenell, A.E. and Kennett, J.P. (2002) *Antarctic Holocene climate change : A benthic foraminiferal stable isotope record from Palmer Deep*., 17 (2).

Shevenell, A.E., Ingalls, A.E., Domack, E.W., et al. (2011) Holocene Southern Ocean surface temperature variability west of the Antarctic Peninsula. Nature, 470 (7333): 250–4. doi:10.1038/nature09751.

Shevenell, A.E., Kennett, J.P. and Lea, D.W. (2004) Middle Miocene Southern Ocean Cooling and Antarctic Cryosphere Expansion. *Science*, 305 (5691): 1766–1770. doi:10.1126/science.1100061.

Shimada, H., Nemoto, N., Shida, Y., et al. (2008) Effects of pH and temperature on the composition of polar lipids in Thermoplasma acidophilum HO-62. *Journal of Bacteriology*, 190 (15): 5404–5411. doi:10.1128/JB.00415-08.

Shin, S.-I., Liu, Z., Otto-Bliesner, B.L., et al. (2003) Southern Ocean sea-ice control of the glacial North Atlantic thermohaline circulation. *Geophysical Research Letters*, 30 (2). doi:10.1029/2002GL015513.

Sigman, D. and Boyle, E. (2000) Glacial/interglacial variations in atmospheric carbon dioxide. *Nature*, 407 (6806): 859–869.

Sigman, D.M., Hain, M.P. and Haug, G.H. (2010) The polar ocean and glacial cycles in atmospheric CO2 concentration. *Nature*, 466 (7302): 47–55. doi:10.1038/nature09149.

Sikes, E.L., Volkman, J.K., Robertson, L.G., et al. (1997) Alkenones and alkenes in surface waters and sediments of the Southern Ocean: Implications for paleotemperature estimation in polar regions. *Geochimica et Cosmochimica Acta*, 61 (7): 1495–1505. doi:10.1016/S0016-7037(97)00017-3.

Silvano, A., Rintoul, S.R., Pena-Molino, B., et al. (2017) Distribution of water masses and meltwater on the continental shelf near the Totten and Moscow University ice shelves. *Journal of Geophysical Research: Oceans*, 122: 2050–2068. doi:10.1002/2016JC012115.Received.

Singer, J.K. and Anderson, J.B. (1984) Use of total grain-size distributions to define bed erosion and transport for poorly sorted sediment undergoing simulated bioturbation. *Marine Geology*, 57 (1–4): 335–359. doi:10.1016/0025-3227(84)90204-4.

Sinninghe Damsté, J.S., Rijpstra, W.I.C., Coolen, M.J.L., et al. (2007) Rapid sulfurisation of highly branched isoprenoid (HBI) alkenes in sulfidic Holocene sediments from Ellis Fjord, Antarctica. *Organic Geochemistry*, 38 (1): 128–139. doi:10.1016/j.orggeochem.2006.08.003.

Skerratt, J.H., Davidson, A.D., Nichols, P.D., et al. (1998) Effect of UV-B on lipid content of three antarctic marine phytoplankton. *Phytochemistry*, 49 (4): 999–1007. doi:10.1016/S0031-9422(97)01068-6.

Smethie, W.M. and Jacobs, S.S. (2005) Circulation and melting under the Ross Ice Shelf: Estimates from evolving CFC, salinity and temperature fields in the Ross Sea. *Deep-Sea Research Part I: Oceanographic Research Papers*, 52 (6): 959–978. doi:10.1016/j.dsr.2004.11.016.

Smik, L., Belt, S.T., Lieser, J.L., et al. (2016) Distributions of highly branched isoprenoid alkenes and other algal lipids in surface waters from East Antarctica: Further insights for biomarker-based paleo sea-ice reconstruction. *Organic Geochemistry*, 95: 71–80. doi:10.1016/j.orggeochem.2016.02.011.

Smith Jr., W.O., Sedwick, P.N., Arrigo, K.R., et al. (2012) the Ross Sea in a Sea of Change. *Oceanography*, 25 (3, SI): 90–103.

Solomina, O.N., Bradley, R.S., Hodgson, D.A., et al. (2015) Holocene glacier fluctuations. *Quaternary Science Reviews*. 111 pp. 9–34. doi:10.1016/j.quascirev.2014.11.018.

Spector, P., Stone, J., Cowdery, S.G., et al. (2017) Rapid early-Holocene deglaciation in the Ross Sea, Antarctica. *Geophysical Research Letters*, 44 (15): 7817–7825. doi:10.1002/2017GL074216.

Steig, E.J., Hart, C., White, J., et al. (1998) Changes in climate, ocean and ice sheet conditions in the Ross Embayment at 6 ka. *Annals of Glaciology*, 27: 305–310. doi:10.3198/1998AoG27-1-305-310.

Steig, E.J., Morse, D.L., Waddington, E.D., et al. (2000) Wisconsinan and Holocene Climate History from an Ice Core at Taylor Dome, Western Ross Embayment, Antarctica. *Geografiska Annaler Series A Physical Geography*, 82A (2&3): 213–235. doi:10.1111/1468-0459.00122.

Steig, E.J., Schneider, D.P., Rutherford, S.D., et al. (2009) Warming of the Antarctic ice-sheet surface since the 1957 International Geophysical Year. *Nature*, 457 (7228): 459–462. doi:10.1038/nature08286.

Stieglmeier, M., Alves, R.J.E. and Schleper, C. (2014) "The phylum thaumarchaeota." In *The Prokaryotes: Other Major Lineages of Bacteria and The Archaea*. doi:10.1007/978-3-642-38954-2_338.

Strickland, J.D. and Parsons, T.R. (1970) "J. D. H. Strickland and T. R. Parsons: A Practical Handbook of Seawater Analysis. Ottawa: Fisheries Research Board of Canada, Bulletin 167, 1968. 293 pp. $ 7.50." In *Internationale Revue der gesamten Hydrobiologie und Hydrographie*. pp. 167–167. doi:10.1002/iroh.19700550118.

Sun, M.Y., Zou, L., Dai, J., et al. (2004) Molecular carbon isotopic fractionation of algal lipids during decomposition in natural oxic and anoxic seawaters. *Organic Geochemistry*, 35 (8): 895–908. doi:10.1016/j.orggeochem.2004.04.001.

Swart, N.C. and Fyfe, J.C. (2013) The influence of recent Antarctic ice sheet retreat on simulated sea ice area trends. *Geophysical Research Letters*, 40 (16): 4328–4332. doi:10.1002/grl.50820.

Sweeney, C. (2003) "The annual cycle of surface water CO2 And O2 in the Ross Sea: A model for gas exchange on the continental shelves of Antarctica." In *Antarctic Research Series Vol 78*. doi:10.1029/078ars19.

Takahashi, T., Sutherland, S.C., Wanninkhof, R., et al. (2009) Climatological mean and decadal change in surface ocean pCO2, and net sea-air CO2 flux over the global oceans. *Deep-Sea Research Part II: Topical Studies in Oceanography*, 56 (8–10): 554–577. doi:10.1016/j.dsr2.2008.12.009.

Tang, K.W., Smith, W.O., Elliott, D.T., et al. (2008) Colony size of Phaeocystis antarctica (Prymnesiophyceae) as influenced by zooplankton grazers. *Journal of Phycology*, 44 (6): 1372–1378. doi:10.1111/j.1529-8817.2008.00595.x.

Thomas, D.N. (2011) "Biogeochemistry of Sea Ice." In *Encyclopedia of Snow, Ice and Glaciers (eds Singh V.P., Singh P., Haritashya U.K.)*. pp. 98–102. doi:10.1007/978-90-481-2642-2_639.

Thomas, R.H. and Bentley, C.R. (1978) A model for Holocene retreat of the West Antarctic Ice Sheet. *Quaternary Research*, 10 (2): 150–170. doi:10.1016/0033-5894(78)90098-4.

Thompson, A.F., Stewart, A.L., Spence, P., et al. (2018) The Antarctic Slope Current in a Changing Climate. *Reviews of Geophysics*, 56 (4): 741–770. doi:10.1029/2018RG000624.

Tierney, J.E. and Tingley, M.P. (2015) A TEX 86 surface sediment database and extended Bayesian calibration. *Scientific Data*, 2: 1–10. doi:10.1038/sdata.2015.29.

Todd, C., Stone, J., Conway, H., et al. (2010) Late Quaternary evolution of Reedy Glacier, Antarctica. *Quaternary Science Reviews*, 29 (11–12): 1328–1341. doi:10.1016/j.quascirev.2010.02.001.

Tortell, P.D., DiTullio, G.R., Sigman, D.M., et al. (2002) CO2 effects on taxonomic

composition and nutrient utilization in an Equatorial Pacific phytoplankton assemblage. *Marine Ecology Progress Series*, 236: 37–43. doi:10.3354/meps236037.

Tortell, P.D., Guéguen, C., Long, M.C., et al. (2011) Spatial variability and temporal dynamics of surface water pCO2, δO2/Ar and dimethylsulfide in the Ross Sea, Antarctica. *Deep-Sea Research Part I: Oceanographic Research Papers*, 58 (3): 241–259. doi:10.1016/j.dsr.2010.12.006.

Tully, B.J., Nelson, W.C. and Heidelberg, J.F. (2012) Metagenomic analysis of a complex marine planktonic thaumarchaeal community from the Gulf of Maine. *Environmental Microbiology*, 14 (1): 254–267. doi:10.1111/j.1462-2920.2011.02628.x.

Turner, J., Scott Hosking, J., Marshall, G.J., et al. (2016) Antarctic sea ice increase consistent with intrinsic variability of the Amundsen sea low. *Climate Dynamics*, 46 (7–8): 2391–2402. doi:10.1007/s00382-015-2708-9.

Turner, J.T. (2002) Zooplankton fecal pellets, marine snow and sinking phytoplankton blooms. *Aquatic Microbial Ecology*. doi:10.3354/ame027057.

Vaillancourt, R.D., Sambrotto, R.N., Green, S., et al. (2003) Phytoplankton biomass and photosynthetic competency in the summertime Mertz Glacier region of East Antarctica. *Deep-Sea Research Part II: Topical Studies in Oceanography*, 50 (8–9): 1415–1440. doi:10.1016/S0967-0645(03)00077-8.

Vaughan, D.G., Marshall, G.J., Connolley, W.., et al. (2003) Recent Rapid Regional Climate Warming On The Antarctic Peninsula. *Climatic Change*, 60: 243–274.

Villinski, J.C., Hayes, J.M., Brassell, S.C., et al. (2008) Sedimentary sterols as biogeochemical indicators in the Southern Ocean. *Organic Geochemistry*, 39 (5): 567–588. doi:10.1016/j.orggeochem.2008.01.009.

Viso, A.-C., Pesando, D., Bernard, P., et al. (1993) Lipid components of the mediterranean seagrass Posidonia Oceanica. *Phytochemistry*, 34 (2): 381–387. doi:10.1016/0031-9422(93)80012-H.

Volkman, J.K., Eglinton, G. and Corner, E.D.S. (1980) Sterols and fatty acids of the

marine diatom biddulphia sinensis. *Phytochemistry*, 19 (8): 1809–1813. doi:10.1016/S0031-9422(00)83818-2.

Wakeham, S.G., Lee, C., Farrington, J.W., et al. (1984) Biogeochemistry of particulate organic matter in the oceans: results from sediment trap experiments. *Deep Sea Research Part A, Oceanographic Research Papers*, 31 (5): 509–528. doi:10.1016/0198-0149(84)90099-2.

Walker, C.B., De La Torre, J.R., Klotz, M.G., et al. (2010) Nitrosopumilus maritimus genome reveals unique mechanisms for nitrification and autotrophy in globally distributed marine crenarchaea. *Proceedings of the National Academy of Sciences of the United States of America*, 107 (19): 8818–8823. doi:10.1073/pnas.0913533107.

Weijers, J.W.H., Schouten, S., Spaargaren, O.C., et al. (2006) Occurrence and distribution of tetraether membrane lipids in soils: Implications for the use of the TEX86 proxy and the BIT index. *Organic Geochemistry*, 37 (12): 1680–1693. doi:10.1016/j.orggeochem.2006.07.018.

Whitworth, T., Orsi, A.H., Kim, S.-J., et al. (1998) "Water masses and mixing near the Antarctic slope front." In *Ocean, Ice, and Atmosphere: Interactions at the Antarctic Continental Margin (eds S. S. Jacobs and R. F. Weiss)*. pp. 1–27. doi:10.1029/AR075p0001.

Williams, G.D. and Bindoff, N.L. (2003) Wintertime oceanography of the Adélie Depression. *Deep-Sea Research Part II: Topical Studies in Oceanography*, 50 (8–9): 1373–1392. doi:10.1016/S0967-0645(03)00074-2.

Williams, G.D., Bindoff, N.L., Marsland, S.J., et al. (2008) Formation and export of dense shelf water from the Adélie depression, East Antarctica. *Journal of Geophysical Research: Oceans*, 113 (4): 1–12. doi:10.1029/2007JC004346.

Wilson, D.L., Smith, W.O. and Nelson, David, M. (1986) Phytoplankton bloom dynamics of the western Ross Sea ice edge - I. Primary productivity and species-specific production. *Deep-Sea Research*, 33 (10): 1375–1387.

Wong, W.W. and Sackett, W.M. (1978) Fractionation of stable carbon isotopes by marine

phytoplankton. *Geochimica et Cosmochimica Acta*, 42 (12): 1809–1815. doi:10.1016/0016-7037(78)90236-3.

Wright, S.W., van den Enden, R.L., Pearce, I., et al. (2010) Phytoplankton community structure and stocks in the Southern Ocean (30-80°E) determined by CHEMTAX analysis of HPLC pigment signatures. *Deep-Sea Research Part II: Topical Studies in Oceanography*, 57 (9–10): 758–778. doi:10.1016/j.dsr2.2009.06.015.

Yang, Y., Gao, C., Dang, X., et al. (2018) Assessing hydroxylated isoprenoid GDGTs as a paleothermometer for the tropical South China Sea. *Organic Geochemistry*, 115: 156–165. doi:10.1016/j.orggeochem.2017.10.014.

Yunker, M.B., Belicka, L.L., Harvey, H.R., et al. (2005) Tracing the inputs and fate of marine and terrigenous organic matter in Arctic Ocean sediments: A multivariate analysis of lipid biomarkers. *Deep-Sea Research Part II: Topical Studies in Oceanography*, 52 (24–26): 3478–3508. doi:10.1016/j.dsr2.2005.09.008.

Zeng, Z., Liu, X.-L., Farley, K.R., et al. (2019) GDGT cyclization proteins identify the dominant archaeal sources of tetraether lipids in the ocean. *Proceedings of the National Academy of Sciences*, p. 201909306. doi:10.1073/pnas.1909306116.

Zhang, J. (2007) Increasing Antarctic Sea Ice under Warming Atmospheric and Oceanic Conditions. *American Meteorological Society*, 20: 2515–2529. doi:10.1175/JCLI4136.1.

Zhang, J. and Hibler, W.D. (1997) On an efficient numerical method for modeling sea ice dynamics. *Journal of Geophysical Research*, 102 (C4): 8691. doi:10.1029/96JC03744.

Zhang, R., Zheng, M., Chen, M., et al. (2014) An isotopic perspective on the correlation of surface ocean carbon dynamics and sea ice melting in Prydz Bay (Antarctica) during austral summer. *Deep-Sea Research Part I: Oceanographic Research Papers*, 83: 24–33. doi:10.1016/j.dsr.2013.08.006.

Zhang, Y.G., Pagani, M. and Wang, Z. (2016) Ring Index: A new strategy to evaluate the integrity of TEX 86 paleothermometry. *Paleoceanography*, 31 (2): 220–232. doi:10.1002/2015PA002848.

Zhang, Y.G., Zhang, C.L., Liu, X.L., et al. (2011) Methane Index: A tetraether archaeal lipid biomarker indicator for detecting the instability of marine gas hydrates. *Earth and Planetary Science Letters*, 307 (3–4): 525–534. doi:10.1016/j.epsl.2011.05.031.

Zhang, Z., Sachs, J.P. and Marchetti, A. (2009) Hydrogen isotope fractionation in freshwater and marine algae: II. Temperature and nitrogen limited growth rate effects. *Organic Geochemistry*, 40 (3): 428–439. doi:10.1016/j.orggeochem.2008.11.002.

Zwally, H.J., Comiso, J.C. and Gordon, A.L. (1985) Antarctic offshore leads and polynyas and oceanographic effects. *Oceanology of the Antarctic Continental Shelf*, 43: 203–226. doi:10.1029/AR043p0203.

A1: CHAPTER 4 DATA

| Top depth (m) | Age (year) | Mud % | C18 d2H mean | d2H error + | d2H error - | %BSi | BSi stdev |
|---|---|---|---|---|---|---|---|
| 1.11 | | | | | | 31.1 | 0.5 |
| 1.9 | 64.7 | | -189.47 | -24.53 | -16.47 | 33.7 | 0.1 |
| 1.92 | 65.9 | | -164.47 | | | 34.8 | |
| 2.99 | 133.3 | 89.00 | | | | 34.3 | 0.2 |
| 3 | 134.5 | 92.06 | | | | 37.7 | 0.5 |
| 4 | 191.4 | 85.49 | -182.60 | | | 35.7 | 1.0 |
| 4.02 | 192.5 | 90.41 | -133.19 | | | 38.9 | 0.1 |
| 5.07 | 244.8 | 91.72 | | | | 37.5 | |
| 5.09 | 245.7 | 96.10 | | | | 40.6 | |
| 6.11 | 297.4 | 92.11 | -179.39 | | | 38.7 | |
| 6.13 | 298.4 | 93.38 | -184.67 | | | 36.8 | 1.2 |
| 6.98 | 339.9 | 95.97 | | | | 32.5 | |
| 7 | 340.9 | 98.87 | | | | 39.3 | 0.6 |
| 7.95 | 391.1 | 95.07 | -174.21 | | | 41.4 | 1.6 |
| 7.97 | 392.2 | 96.24 | -201.17 | | | 38.4 | 0.3 |
| 9 | 446.5 | 92.06 | | | | 38.0 | 0.7 |
| 9.84 | 491.1 | 94.82 | | | | 40.0 | |
| 9.86 | 492 | 96.81 | -166.45 | -37.55 | -37.45 | 49.2 | |
| 10.85 | 542.6 | 89.73 | | | | 49.3 | |
| 10.87 | 544.2 | 92.66 | | | | 39.8 | |
| 11.77 | 601.7 | 89.28 | | | | 31.4 | |
| 11.79 | 603.1 | 83.73 | | | | 48.9 | |
| 12.12 | 625.5 | 94.63 | | | | 39.9 | |
| 12.14 | 627 | 97.11 | | | | 41.1 | |
| 12.9 | 678.9 | 88.54 | | | | 37.8 | |
| 12.91 | 679.6 | 89.47 | -186.82 | | | 39.8 | |
| 13.84 | 739.5 | 95.65 | | | | 40.8 | 0.2 |
| 13.86 | 740.7 | 85.83 | | | | 33.1 | 0.4 |
| 14.84 | 795 | 95.66 | -184.91 | -5.09 | -6.91 | 37.3 | 0.0 |
| 14.86 | 796.1 | 95.17 | -187.18 | -10.82 | -15.18 | 39.2 | 0.1 |
| 15.75 | 844.4 | 89.23 | | | | 37.2 | 0.9 |
| 15.77 | 845.4 | 94.06 | | | | 39.8 | 0.6 |
| 16.81 | 892.9 | 88.02 | | | | 37.8 | |
| 16.83 | 893.7 | 96.87 | -205.45 | | | 44.2 | 0.1 |
| 17.8 | 937.2 | 95.47 | | | | 46.6 | 1.3 |
| 17.82 | 938.1 | 96.31 | | | | 43.7 | 1.5 |
| 18.44 | 967.9 | 96.46 | -195.70 | | | 37.4 | 0.4 |
| 18.45 | 968.4 | 95.31 | -181.61 | | | 52.4 | |
| 19.6 | 1020.3 | 94.43 | | | | 33.6 | 0.1 |
| 19.61 | 1020.7 | 94.89 | | | | 52.0 | 0.2 |
| 20.39 | 1054.8 | 81.19 | -187.23 | -9.77 | -10.23 | 38.4 | 0.9 |
| 20.41 | 1055.6 | 83.63 | -205.85 | | | 42.0 | 0.0 |
| 22.12 | 1123.6 | 88.02 | | | | 41.5 | 0.2 |
| 22.14 | 1124.4 | 90.26 | | | | 47.1 | |
| 22.95 | 1158.2 | 89.75 | | | | 41.7 | |
| 22.97 | 1159 | 95.14 | | | | 54.6 | |
| 23.78 | 1193.6 | 92.24 | -190.51 | | | 42.9 | 0.0 |
| 23.8 | 1194.5 | 97.46 | | | | 46.3 | 0.4 |
| 24.86 | 1244.8 | 88.94 | -196.99 | -2.01 | -1.99 | 38.8 | |
| 24.88 | 1245.8 | 88.71 | | | | 44.1 | 0.4 |

| | | | | | | | |
|---|---|---|---|---|---|---|---|
| 25.83 | 1300.7 | 89.33 | | | | 36.2 | |
| 25.85 | 1301.8 | 95.57 | | | | 37.9 | 0.2 |
| 26.79 | 1357.5 | 94.39 | -163.82 | | | 46.1 | |
| 26.81 | 1358.6 | 95.97 | | | | 48.0 | 0.1 |
| 27.69 | 1406.3 | 99.27 | | | | 42.8 | |
| 27.7 | 1406.8 | 86.11 | | | | 50.2 | 0.2 |
| 28.65 | 1456.6 | 93.24 | -182.94 | | | 37.1 | |
| 28.67 | 1457.7 | 95.29 | -194.06 | -4.94 | -5.06 | 48.7 | 1.0 |
| 29.39 | 1497.1 | 83.42 | | | | 45.5 | 1.0 |
| 29.41 | 1498.3 | 89.37 | | | | 42.6 | 0.4 |
| 30.22 | 1548.9 | 92.40 | | | | 40.0 | 0.3 |
| 30.24 | 1550.4 | 92.03 | -168.58 | | | 36.4 | 0.7 |
| 31.05 | 1613.5 | 89.80 | | | | 41.7 | 1.5 |
| 31.06 | 1614.4 | 94.98 | | | | 44.4 | 0.2 |
| 32.12 | 1703.4 | 88.63 | | | | 44.6 | 0.4 |
| 32.14 | 1704.6 | 95.30 | | | | 45.3 | 0.3 |
| 32.82 | 1742.5 | 91.11 | | | | 42.2 | 0.7 |
| 32.84 | 1743.7 | 95.53 | | | | 48.0 | 0.7 |
| 33.82 | 1804.9 | 91.04 | | | | 40.2 | 0.4 |
| 33.83 | 1805.6 | | -200.92 | | | 41.3 | 0.3 |
| 34.86 | 1871.7 | 90.08 | | | | 42.1 | 0.5 |
| 34.87 | 1872.3 | 99.32 | | | | 50.9 | |
| 35.63 | 1921.5 | 88.89 | | | | 38.1 | 0.4 |
| 35.65 | 1922.7 | 95.27 | -180.80 | | | 46.1 | 0.4 |
| 36.64 | 1996.3 | 95.23 | | | | 41.5 | 0.1 |
| 36.66 | 1998.6 | | | | | 37.9 | 1.3 |
| 37.58 | 2059.4 | 83.03 | | | | 36.5 | |
| 37.6 | 2061.1 | 93.40 | | | | 38.9 | 0.3 |
| 38.45 | 2136.1 | 94.47 | | | | 48.0 | 0.2 |
| 38.47 | 2138.2 | 96.23 | | | | 47.7 | 0.3 |
| 39.34 | 2236.1 | 93.21 | -180.13 | | | 39.2 | 0.2 |
| 39.35 | 2237.3 | | -177.59 | | | 48.2 | 0.1 |
| 41.05 | 2438 | 88.85 | | | | 37.5 | 0.3 |
| 41.07 | 2441.2 | 96.10 | | | | 45.3 | 0.5 |
| 42.08 | 2526.6 | 83.47 | -174.68 | | | 43.5 | 0.3 |
| 42.1 | 2528.8 | 92.68 | | | | 49.7 | 0.5 |
| 43.11 | 2617.4 | 84.04 | | | | 34.9 | 0.8 |
| 43.13 | 2619.2 | | | | | 48.1 | 0.1 |
| 43.78 | 2673.6 | 92.10 | -199.38 | | | 37.9 | 0.4 |
| 43.79 | 2674.4 | 96.96 | | | | 53.1 | 0.5 |
| 44.95 | 2774 | 98.87 | | | | 38.8 | |
| 44.97 | 2776.9 | 93.76 | | | | 46.2 | |
| 45.63 | 2870.9 | 91.73 | -139.18 | | | 38.0 | 0.3 |
| 45.65 | 2872.7 | | -184.17 | | | 46.0 | |
| 46.69 | 2923.2 | 93.41 | | | | 43.9 | 0.9 |
| 46.71 | 2924.9 | 93.54 | | | | 45.8 | 0.3 |
| 47.7 | 2994.3 | 89.73 | | | | 46.8 | |
| 47.72 | 2996 | 95.47 | -211.56 | -9.44 | -8.56 | 50.5 | |
| 48.73 | 3094 | 90.72 | | | | 41.8 | |
| 48.75 | 3096 | 85.06 | | | | 42.0 | 0.1 |
| 49.65 | 3203.7 | 79.61 | | | | 39.6 | |
| 49.67 | 3206.3 | 95.74 | | | | 52.9 | |

| | | | | | | | |
|---|---|---|---|---|---|---|---|
| 50.04 | 3405.5 | 95.12 | | | | 44.1 | |
| 50.06 | 3408.1 | 97.65 | | | | 48.2 | 0.2 |
| 51.07 | 3531.1 | 95.22 | | | | 45.6 | 0.7 |
| 51.09 | 3533.8 | 93.80 | -231.78 | | | 39.2 | 0.2 |
| 51.87 | 3612.3 | 79.24 | | | | 36.7 | 0.7 |
| 51.89 | 3614.8 | 95.54 | | | | 44.4 | |
| 53.05 | 3727.2 | 91.17 | -189.88 | | | 42.5 | 0.3 |
| 53.07 | 3729 | 92.81 | -195.02 | | | 41.8 | |
| 54.01 | 3798.1 | 95.46 | | | | 46.7 | |
| 54.03 | 3799.9 | 94.15 | | | | 49.4 | 0.3 |
| 55.04 | 3864.7 | 95.07 | | | | 47.4 | 0.2 |
| 55.06 | 3866.3 | 94.45 | -209.41 | | | 44.2 | 0.9 |
| 56.07 | 3947.3 | 88.61 | | | | 37.4 | 0.9 |
| 56.08 | 3948.2 | 93.11 | | | | 44.9 | |
| 56.95 | 4022 | | | | | 48.0 | 0.2 |
| 56.96 | 4022.7 | 94.19 | -205.48 | | | 52.5 | 0.6 |
| 58.18 | 4105.2 | 96.10 | | | | 46.8 | 0.4 |
| 58.2 | 4106.6 | 96.39 | | | | 51.6 | 0.1 |
| 60.16 | 4307.7 | 90.61 | -218.77 | -1.23 | -0.77 | 47.6 | 0.8 |
| 60.18 | 4308.8 | 95.83 | -238.22 | -2.78 | -2.22 | 50.2 | |
| 61.09 | 4359.5 | 86.86 | | | | 48.9 | |
| 61.1 | 4360.2 | 88.08 | | | | 49.6 | |
| 62.09 | 4416.3 | 87.23 | | | | 50.4 | |
| 62.11 | 4417.5 | 90.60 | | | | 51.8 | |
| 63.04 | 4465.7 | 88.90 | | | | 49.4 | 0.5 |
| 63.06 | 4466.8 | 91.27 | | | | 55.1 | |
| 64.11 | 4520 | 78.95 | | | | 52.8 | |
| 64.12 | 4520.5 | 90.95 | -234.21 | | | 54.6 | |
| 65.06 | 4562.4 | 75.01 | | | | 50.7 | |
| 65.08 | 4563.4 | 91.18 | | | | 57.6 | |
| 66.27 | 4612.4 | 87.86 | | | | 54.8 | |
| 66.29 | 4613.5 | 91.51 | -207.94 | | | 51.2 | |
| 69.12 | 4783.9 | 86.78 | | | | 50.7 | 0.2 |
| 69.14 | 4784.9 | 92.15 | | | | 51.8 | |
| 70.12 | 4827.3 | 84.02 | | | | 51.0 | |
| 70.14 | 4828.3 | 93.84 | | | | 49.5 | |
| 71.14 | 4873.7 | 84.79 | | | | 55.3 | 0.2 |
| 71.16 | 4874.8 | 81.50 | | | | 58.0 | 0.2 |
| 71.92 | 4911.2 | 90.23 | -207.84 | | | 56.0 | |
| 71.94 | 4912.3 | 92.79 | -185.08 | -4.92 | -4.08 | 56.7 | 1.7 |
| 73.1 | 4962.9 | 84.28 | | | | 47.6 | |
| 73.12 | 4964 | 85.35 | | | | 49.7 | |
| 74.08 | 5007.4 | 85.94 | | | | 52.2 | 0.2 |
| 74.1 | 5008.5 | 90.01 | -190.88 | | | 52.8 | 0.4 |
| 75.12 | 5059.2 | 83.28 | | | | 53.0 | |
| 75.14 | 5060.4 | 84.10 | | | | 56.4 | |
| 76.16 | 5115.9 | 83.31 | -206.62 | -2.38 | -2.62 | 49.6 | |
| 76.17 | 5116.5 | 88.11 | | | | 56.5 | |
| 77.22 | 5167.4 | 83.78 | | | | 44.8 | |
| 77.24 | 5168.6 | 88.99 | | | | 51.9 | 0.1 |
| 78.54 | 5317.5 | 88.35 | -201.95 | | | 48.4 | |
| 78.55 | 5318.1 | 94.99 | | | | 59.2 | |

| | | | | | | | |
|---|---|---|---|---|---|---|---|
| 79.08 | 5350.5 | 85.79 | | | | 50.9 | 0.5 |
| 79.1 | 5351.6 | 90.40 | | | | 47.6 | |
| 80.28 | 5401.5 | 93.09 | -198.47 | -4.53 | -4.47 | 56.7 | 0.7 |
| 80.3 | 5402.7 | 94.64 | | | | 62.6 | |
| 81.27 | 5445.8 | 95.14 | | | | 53.9 | |
| 81.29 | 5446.9 | 88.27 | | | | 57.0 | 0.2 |
| 82.26 | 5483.8 | 84.50 | -220.54 | | | 49.5 | |
| 82.28 | 5484.8 | 95.70 | | | | 45.6 | 0.3 |
| 83.05 | 5519.9 | 87.23 | | | | 47.6 | |
| 83.07 | 5520.9 | 87.43 | | | | 60.9 | |
| 83.9 | 5551.4 | 79.14 | | | | 51.9 | |
| 83.91 | 5551.9 | 85.42 | -199.30 | | | 59.9 | |
| 84.63 | 5587.7 | 85.50 | | | | 53.0 | 0.4 |
| 84.65 | 5588.7 | 91.80 | | | | 58.0 | 0.5 |
| 85.16 | 5611.2 | 87.01 | | | | 49.4 | 0.0 |
| 85.17 | 5611.7 | 91.43 | | | | 55.8 | |
| 86.11 | 5659 | 83.56 | | | | 57.1 | |
| 86.13 | 5660.1 | 86.04 | | | | 60.3 | 0.6 |
| 87.09 | 5711.5 | 90.30 | -185.70 | -11.30 | -10.70 | 56.8 | |
| 87.11 | 5712.6 | 90.69 | -191.24 | -8.76 | -10.24 | 56.1 | |
| 88.14 | 5856.1 | 91.88 | | | | 57.6 | |
| 88.16 | 5857.4 | 85.46 | | | | 58.0 | 0.4 |
| 89.13 | 5909.4 | 86.43 | | | | 52.3 | 0.2 |
| 89.15 | 5910.7 | 94.16 | -175.58 | | | 55.8 | 0.8 |
| 89.94 | 5946.5 | 89.29 | | | | 51.0 | |
| 89.96 | 5947.7 | 90.14 | | | | 52.8 | 0.1 |
| 91.12 | 5999.9 | 88.90 | -184.15 | | | 54.5 | 0.3 |
| 91.14 | 6001.2 | 93.60 | -184.74 | | | 57.0 | |
| 92.24 | 6052.6 | 89.54 | | | | 45.6 | |
| 92.26 | 6053.9 | 95.10 | | | | 60.6 | 0.4 |
| 93.04 | 6097 | 89.04 | | | | 50.6 | |
| 93.06 | 6098.4 | 92.35 | -190.56 | | | 50.7 | |
| 94.07 | 6147.7 | 81.33 | | | | 45.7 | |
| 94.09 | 6148.8 | 97.09 | | | | 53.6 | 0.5 |
| 95.14 | 6199.4 | 88.62 | -169.90 | -20.10 | -19.90 | 55.6 | |
| 95.16 | 6200.5 | 90.77 | -212.59 | -18.41 | -17.59 | 56.5 | 0.5 |
| 96.11 | 6242.6 | 90.10 | | | | 55.0 | |
| 96.13 | 6243.7 | 93.43 | | | | 54.6 | |
| 97.18 | 6288.7 | 85.04 | -189.88 | | | 54.2 | 0.2 |
| 97.2 | 6289.7 | 90.55 | -213.03 | | | 49.6 | 0.5 |
| 97.55 | 6387.8 | 84.98 | | | | 52.2 | 0.4 |
| 97.57 | 6388.8 | 88.41 | | | | 56.6 | 0.3 |
| 98.07 | 6409 | 86.66 | | | | 53.7 | 0.4 |
| 98.14 | 6412.4 | 82.25 | | | | 56.6 | 0.6 |
| 98.99 | 6452.1 | 85.74 | | | | 40.7 | |
| 99.01 | 6453 | 94.54 | | | | 46.6 | 0.2 |
| 99.99 | 6487.6 | 85.48 | | | | 50.9 | |
| 100.01 | 6488.7 | 89.04 | -199.59 | -3.41 | -3.59 | 46.7 | |
| 101.07 | 6522.8 | 83.45 | | | | 50.5 | |
| 101.09 | 6523.8 | 95.22 | | | | 58.8 | |
| 102.03 | 6571.4 | 92.21 | -184.63 | | | 49.5 | |
| 102.05 | 6572.5 | 90.73 | -188.03 | -4.97 | -5.03 | 47.8 | |

| | | | | | | | |
|---|---|---|---|---|---|---|---|
| 103.11 | 6609.2 | 88.00 | | | | 55.6 | |
| 103.13 | 6610.3 | 93.31 | | | | 61.1 | |
| 103.97 | 6648.5 | 78.01 | | | | 59.8 | |
| 103.99 | 6649.5 | 78.62 | -170.62 | | | 55.3 | 1.0 |
| 105.17 | 6701.3 | 72.88 | | | | 48.5 | |
| 105.18 | 6701.8 | 92.20 | | | | 58.6 | |
| 106.18 | 6739.5 | 91.17 | -204.56 | | | 57.0 | 0.2 |
| 106.2 | 6740.5 | 89.11 | -152.66 | | | 58.1 | |
| 107.19 | 6890.2 | 85.68 | | | | 52.3 | |
| 107.2 | 6890.8 | 93.97 | | | | 46.6 | |
| 108.02 | 6941.2 | 84.31 | | | | 51.7 | |
| 108.03 | 6941.7 | 80.60 | -211.09 | | | 48.3 | |
| 109.02 | 6982.7 | 86.07 | | | | 52.5 | |
| 109.04 | 6983.7 | 95.18 | | | | 50.7 | |
| 109.86 | 7028.5 | 83.35 | -211.63 | -9.37 | -9.63 | 38.4 | 0.1 |
| 109.88 | 7029.7 | 93.56 | | | | 48.1 | |
| 110.75 | 7073.3 | 93.70 | | | | 51.3 | |
| 110.77 | 7075.2 | 94.87 | | | | 56.3 | |
| 111.8 | 7139.4 | 82.53 | -221.02 | | | 50.8 | |
| 111.82 | 7140.6 | 89.88 | | | | 51.4 | 0.5 |
| 112.69 | 7186.6 | 89.08 | | | | 50.9 | |
| 112.71 | 7188 | 93.95 | | | | 51.8 | |
| 113.75 | 7248.6 | 87.35 | -221.79 | -4.21 | -4.79 | 47.8 | |
| 113.77 | 7250.1 | 95.29 | | | | 50.7 | |
| 114.74 | 7326.4 | 83.77 | | | | 46.4 | 0.8 |
| 114.76 | 7327.9 | 92.90 | | | | 60.9 | |
| 115.5 | 7382 | 77.41 | | | | 56.5 | |
| 115.51 | 7383.5 | 90.90 | -182.04 | | | 57.8 | |
| 116.71 | 7525.3 | 92.23 | | | | 48.4 | |
| 116.73 | 7526.9 | 94.97 | | | | 52.4 | |
| 118.08 | 7618.4 | 90.78 | | | | 54.6 | |
| 118.09 | 7619.3 | 90.88 | -187.37 | -1.63 | -1.37 | 54.4 | |
| 119.15 | 7689.6 | 87.51 | | | | 49.0 | |
| 119.17 | 7690.9 | 94.70 | | | | 54.8 | 1.1 |
| 120.12 | 7736.8 | 80.59 | | | | 44.8 | |
| 120.13 | 7737.5 | 91.65 | -208.93 | | | 46.9 | |
| 121.04 | 7786.7 | 89.47 | | | | 46.3 | |
| 121.05 | 7787.2 | 81.65 | | | | 56.1 | |
| 122.06 | 7837.3 | 87.01 | -191.54 | | | 52.5 | |
| 122.07 | 7837.7 | 85.17 | -193.90 | -23.10 | -22.90 | 46.3 | 0.9 |
| 122.92 | 7857.9 | 88.03 | | | | 47.3 | |
| 122.94 | 7858.9 | 90.64 | | | | 57.6 | |
| 123.97 | 7906.6 | 71.60 | | | | 45.7 | |
| 123.99 | 7907.6 | 85.50 | | | | 56.8 | |
| 124.91 | 7943.7 | 82.09 | | | | 52.2 | |
| 124.92 | 7944.2 | 90.53 | | | | 54.3 | |
| 126.11 | 8050.3 | 87.25 | -198.78 | | | 52.1 | 0.2 |
| 126.12 | 8050.6 | 90.29 | -202.43 | | | 47.2 | 0.4 |
| 127.1 | 8081.8 | 90.23 | | | | 54.5 | |
| 127.11 | 8082.1 | 93.35 | | | | 57.9 | |
| 128.25 | 8116.8 | 84.95 | -180.79 | | | 44.5 | |
| 128.28 | 8118 | 92.53 | | | | 59.7 | 0.7 |

| | | | | | | | |
|---|---|---|---|---|---|---|---|
| 129.2 | 8151.4 | 80.21 | | | | 45.4 | 0.2 |
| 129.21 | 8151.8 | 81.33 | | | | 49.2 | |
| 130.3 | 8184.2 | 80.93 | -228.94 | | | 45.6 | |
| 130.31 | 8184.6 | 92.86 | | | | 55.3 | |
| 131.29 | 8212.3 | 89.64 | | | | 51.5 | |
| 131.31 | 8213.1 | 87.46 | | | | 49.4 | 1.5 |
| 132.13 | 8246.5 | 87.62 | -182.01 | | | 52.1 | |
| 132.14 | 8246.9 | 87.94 | -185.40 | | | 48.1 | |
| 133.11 | 8287.3 | 83.26 | | | | 46.1 | 0.7 |
| 133.13 | 8288.2 | 80.68 | | | | 59.6 | 0.4 |
| 134.07 | 8324.3 | 71.79 | | | | 46.6 | |
| 134.08 | 8324.7 | 92.61 | | | | 54.1 | 0.9 |
| 135.08 | 8371.6 | 85.77 | | | | 56.4 | |
| 135.1 | 8372.6 | 90.03 | | | | 56.6 | |
| 136.12 | 8496.3 | 95.64 | | | | 59.1 | |
| 136.14 | 8497.5 | 87.31 | | | | 48.2 | |
| 137.08 | 8545.7 | 87.05 | | | | 50.6 | |
| 137.1 | 8546.9 | 88.34 | | | | 53.0 | |
| 138.21 | 8596.5 | 97.61 | -219.64 | | | 60.7 | |
| 138.23 | 8597.8 | 90.44 | | | | 47.1 | |
| 139.01 | 8642.2 | 88.68 | | | | 54.4 | 1.3 |
| 139.03 | 8643.4 | 91.43 | | | | 57.0 | 0.0 |
| 140.08 | 8695.2 | 78.57 | | | | 39.4 | |
| 140.09 | 8695.7 | 91.41 | | | | 47.8 | |
| 141.04 | 8747.4 | 81.22 | | | | 41.2 | |
| 141.05 | 8748.7 | 87.59 | | | | 51.4 | 0.4 |
| 142.16 | 8820.4 | 86.52 | | | | 48.6 | 0.4 |
| 142.18 | 8821.7 | 88.46 | | | | 60.3 | |
| 142.89 | 8869.3 | 90.61 | | | | 48.5 | |
| 142.91 | 8870.6 | 84.22 | | | | 55.6 | |
| 143.93 | 8936.1 | 87.33 | | | | 42.5 | 0.3 |
| 143.95 | 8937.3 | 94.52 | -242.11 | | | 58.1 | 0.0 |
| 145.17 | 9064.7 | 86.22 | | | | 48.3 | |
| 145.19 | 9066 | 93.99 | | | | 45.5 | |
| 146.09 | 9126 | 87.87 | | | | 54.5 | |
| 146.11 | 9127.5 | 88.59 | -223.88 | | | 55.2 | 1.2 |
| 147.17 | 9185.9 | 83.37 | | | | 53.1 | 0.6 |
| 147.19 | 9187.3 | 89.68 | | | | 45.9 | 0.6 |
| 147.92 | 9227.8 | 91.96 | | | | 44.7 | |
| 147.94 | 9229.4 | 93.38 | -229.32 | | | 55.3 | 0.3 |

| | | | | | | | |
|---|---|---|---|---|---|---|---|
| 148.76 | 9295.2 | 80.51 | | | | 42.4 | 0.3 |
| 148.78 | 9296.9 | 90.12 | | | | 50.3 | |
| 149.77 | 9378.9 | 75.23 | -187.18 | -3.82 | -4.18 | 41.4 | |
| 149.78 | 9379.7 | 94.53 | | | | 47.4 | 0.4 |
| 150.71 | 9450.2 | 85.56 | | | | 49.1 | |
| 150.73 | 9452.9 | 93.40 | | | | 48.7 | |
| 151.49 | 9512 | 93.45 | -195.32 | | | 55.7 | 1.6 |
| 151.51 | 9513.8 | 94.49 | -202.34 | -7.66 | -7.34 | 56.5 | 0.6 |
| 152.5 | 9600.5 | 81.82 | | | | 43.2 | 0.0 |
| 152.52 | 9603 | 89.48 | | | | 48.2 | |
| 153.52 | 9695.6 | 83.44 | | | | 50.4 | 0.1 |
| 153.54 | 9697.3 | 92.44 | -256.71 | | | 53.2 | |
| 154.34 | 9771.8 | 84.59 | | | | 44.2 | 0.4 |
| 154.35 | 9772.7 | 93.37 | | | | 52.8 | |
| 155.05 | 9896.3 | 67.17 | | | | 38.8 | 0.5 |
| 155.06 | 9897.2 | 81.22 | | | | 48.8 | 0.2 |
| 155.98 | 9970.8 | 77.32 | | | | 45.9 | |
| 156 | 9972.6 | 91.92 | | | | 55.6 | |
| 156.93 | 10088.2 | 87.19 | | | | 47.8 | |
| 156.94 | 10089.4 | 93.02 | | | | 52.3 | |
| 157.69 | 10178.5 | 87.83 | | | | 46.9 | 0.4 |
| 157.71 | 10181 | 85.95 | | | | 47.5 | 0.8 |
| 158.66 | 10290.3 | 83.30 | -229.19 | | | 42.7 | |
| 158.68 | 10292.9 | 94.32 | -201.52 | -13.48 | -13.52 | 56.3 | |
| 159.62 | 10398.4 | 66.77 | | | | 42.7 | 0.1 |
| 159.64 | 10402.3 | 79.33 | | | | 53.7 | |
| 160.58 | 10517.1 | 81.05 | | | | 44.0 | 0.3 |
| 160.6 | 10519.4 | 82.66 | | | | 56.7 | |
| 161.53 | 10634.3 | 90.19 | | | | 45.5 | |
| 161.55 | 10636.6 | 90.06 | | | | 56.8 | |
| 162.52 | 10740.2 | 86.38 | | | | 43.8 | |
| 162.53 | 10741.1 | 93.22 | | | | 48.6 | |
| 163.45 | 10820.1 | 82.43 | | | | 39.8 | 1.2 |
| 163.47 | 10821.7 | 89.86 | | | | 53.0 | 0.3 |
| 164.05 | 10877.6 | 90.06 | -218.61 | | | 38.5 | |
| 164.06 | 10878.5 | 88.98 | -214.37 | | | 47.0 | 0.2 |
| 164.08 | 10880.1 | 94.95 | | | | 54.4 | 0.2 |
| 165.04 | 10962.4 | 88.10 | | | | 36.7 | |
| 165.05 | 10963.2 | 88.40 | | | | 44.3 | |
| 165.07 | 10964.9 | 91.47 | | | | 49.8 | |
| 165.86 | 11030.7 | 86.09 | -238.49 | -0.51 | -0.49 | 36.5 | |
| 165.87 | 11031.5 | 93.33 | | | | 53.6 | |
| 167.12 | 11123.1 | 77.32 | | | | 39.9 | |
| 167.13 | 11124 | 76.53 | | | | 57.5 | 0.3 |
| 168.05 | 11201.7 | 75.57 | -206.98 | | | 33.5 | |
| 168.06 | 11202.6 | 86.58 | | | | 47.2 | |
| 168.97 | 11286 | 74.17 | | | | 42.4 | 1.3 |
| 168.98 | 11287 | 88.11 | | | | 61.2 | |
| 169.62 | 11343.5 | 79.97 | -206.35 | -28.65 | -27.35 | 34.6 | |
| 169.64 | 11345.3 | 86.51 | | | | 48.7 | |
| 170.35 | 11383.7 | 73.69 | -216.21 | | | 37.0 | |

| age (years) | NGR | age (years) | NGR | age (years) | NGR |
|---|---|---|---|---|---|
| 101.8 | 3.31 | 359.2 | 3.52 | 674.1 | 2.75 |
| 108.1 | 2.06 | 364.3 | 2.87 | 680.8 | 3.40 |
| 114.4 | 1.88 | 369.4 | 3.09 | 687.4 | 3.36 |
| 120.8 | 1.91 | 374.6 | 2.83 | 692.2 | 3.45 |
| 127.0 | 2.13 | 379.8 | 2.88 | 698.4 | 3.04 |
| 133.3 | 2.12 | 385.0 | 2.73 | 704.5 | 3.06 |
| 139.2 | 2.20 | 390.2 | 2.57 | 709.4 | 4.00 |
| 145.1 | 2.09 | 395.2 | 2.94 | 715.6 | 3.09 |
| 151.0 | 2.34 | 400.3 | 2.96 | 721.6 | 3.20 |
| 157.0 | 2.34 | 405.5 | 2.63 | 727.7 | 3.74 |
| 162.9 | 2.10 | 410.6 | 4.07 | 733.7 | 3.42 |
| 168.9 | 1.87 | 415.8 | 4.31 | 739.8 | 3.22 |
| 174.8 | 2.10 | 420.9 | 3.84 | 745.9 | 2.96 |
| 180.5 | 2.19 | 426.0 | 3.78 | 751.7 | 2.84 |
| 186.3 | 2.34 | 431.1 | 4.04 | 757.4 | 2.95 |
| 188.6 | 3.00 | 436.2 | 3.42 | 763.2 | 3.03 |
| 194.0 | 2.75 | 441.3 | 2.90 | 767.9 | 3.47 |
| 198.7 | 2.57 | 446.5 | 3.11 | 773.6 | 3.60 |
| 203.5 | 2.18 | 451.7 | 2.93 | 779.3 | 4.12 |
| 208.3 | 2.13 | 456.8 | 3.19 | 782.1 | 3.51 |
| 213.2 | 2.74 | 462.1 | 3.59 | 787.8 | 2.83 |
| 218.0 | 2.78 | 467.2 | 3.54 | 790.6 | 3.46 |
| 223.0 | 2.83 | 472.4 | 3.28 | 796.3 | 3.75 |
| 227.8 | 2.59 | 477.7 | 3.05 | 802.0 | 3.31 |
| 232.7 | 2.56 | 482.9 | 3.18 | 807.6 | 3.82 |
| 237.5 | 2.58 | 488.0 | 3.97 | 812.8 | 3.83 |
| 242.4 | 2.52 | 493.1 | 3.79 | 818.1 | 3.74 |
| 247.1 | 2.61 | 498.2 | 3.37 | 823.3 | 3.53 |
| 252.0 | 2.67 | 501.9 | 3.34 | 828.4 | 3.58 |
| 257.0 | 3.21 | 507.0 | 3.32 | 833.6 | 2.77 |
| 261.9 | 4.21 | 512.2 | 2.99 | 836.2 | 2.75 |
| 266.8 | 3.03 | 516.4 | 3.30 | 841.4 | 3.26 |
| 271.6 | 2.67 | 521.6 | 3.63 | 846.5 | 4.03 |
| 276.6 | 2.53 | 526.9 | 3.60 | 851.7 | 3.88 |
| 281.5 | 3.14 | 532.0 | 3.67 | 856.9 | 4.05 |
| 286.4 | 3.02 | 537.3 | 3.45 | 862.0 | 4.15 |
| 291.3 | 2.70 | 542.6 | 3.02 | 863.3 | 3.77 |
| 296.3 | 2.84 | 548.6 | 3.04 | 867.5 | 3.60 |
| 301.4 | 2.99 | 552.7 | 3.35 | 871.6 | 3.10 |
| 306.5 | 2.46 | 559.7 | 3.01 | 875.9 | 3.24 |
| 314.0 | 2.58 | 567.0 | 3.33 | 880.0 | 3.97 |
| 319.0 | 2.73 | 623.3 | 2.94 | 884.2 | 3.99 |
| 324.1 | 2.82 | 629.9 | 3.08 | 888.5 | 3.76 |
| 329.1 | 3.09 | 636.6 | 3.17 | 892.7 | 3.84 |
| 334.0 | 4.30 | 643.2 | 2.61 | 896.9 | 4.67 |
| 338.9 | 3.02 | 649.8 | 2.88 | 901.2 | 3.87 |
| 343.9 | 3.05 | 656.5 | 2.71 | 905.3 | 3.93 |
| 349.0 | 3.24 | 663.3 | 2.64 | 909.5 | 4.29 |
| 354.1 | 3.75 | 670.0 | 2.34 | 913.8 | 4.08 |

| age (years) | NGR | age (years) | NGR | age (years) | NGR |
|---|---|---|---|---|---|
| 918.0 | 3.99 | 1132.7 | 3.80 | 1363.8 | 3.70 |
| 922.2 | 3.83 | 1136.6 | 3.20 | 1369.1 | 3.63 |
| 925.3 | 4.49 | 1140.5 | 3.20 | 1374.1 | 4.40 |
| 929.6 | 4.11 | 1144.4 | 2.76 | 1379.1 | 3.58 |
| 933.8 | 3.92 | 1148.2 | 2.77 | 1384.0 | 3.94 |
| 938.1 | 3.62 | 1152.2 | 2.77 | 1389.0 | 3.61 |
| 942.4 | 3.23 | 1156.0 | 3.12 | 1394.0 | 2.97 |
| 946.8 | 3.41 | 1159.8 | 2.99 | 1399.0 | 2.71 |
| 951.1 | 3.56 | 1163.8 | 3.13 | 1403.9 | 3.35 |
| 955.6 | 3.65 | 1167.9 | 2.82 | 1408.8 | 3.13 |
| 960.2 | 3.53 | 1171.9 | 3.12 | 1413.8 | 3.61 |
| 964.7 | 3.55 | 1175.9 | 2.78 | 1418.5 | 3.91 |
| 969.2 | 3.15 | 1179.8 | 2.90 | 1423.5 | 4.40 |
| 973.6 | 3.60 | 1183.9 | 3.49 | 1428.3 | 4.15 |
| 978.1 | 3.40 | 1187.8 | 3.68 | 1433.1 | 3.73 |
| 982.5 | 3.99 | 1191.8 | 3.68 | 1438.0 | 3.75 |
| 987.0 | 4.43 | 1195.7 | 3.73 | 1443.0 | 3.66 |
| 990.5 | 4.64 | 1199.6 | 3.60 | 1447.9 | 4.47 |
| 995.0 | 3.77 | 1203.6 | 3.54 | 1452.8 | 3.92 |
| 999.1 | 4.11 | 1208.1 | 3.38 | 1457.8 | 3.76 |
| 1003.1 | 4.29 | 1212.5 | 3.04 | 1462.7 | 3.51 |
| 1007.2 | 3.78 | 1217.0 | 3.77 | 1467.7 | 4.22 |
| 1011.3 | 3.92 | 1221.7 | 3.16 | 1472.5 | 3.88 |
| 1015.3 | 3.50 | 1226.1 | 3.40 | 1477.6 | 3.66 |
| 1019.4 | 3.18 | 1230.8 | 3.62 | 1482.8 | 3.93 |
| 1023.4 | 3.04 | 1235.2 | 3.41 | 1488.0 | 3.51 |
| 1027.4 | 3.06 | 1239.9 | 3.78 | 1493.4 | 3.63 |
| 1031.6 | 3.35 | 1244.4 | 4.61 | 1498.7 | 3.44 |
| 1035.6 | 3.13 | 1249.0 | 4.76 | 1504.0 | 3.69 |
| 1039.7 | 2.88 | 1254.1 | 4.59 | 1509.3 | 2.95 |
| 1043.6 | 3.32 | 1259.5 | 4.63 | 1514.7 | 2.62 |
| 1047.5 | 4.34 | 1265.0 | 4.34 | 1520.1 | 3.00 |
| 1051.5 | 5.46 | 1270.4 | 3.74 | 1525.3 | 4.88 |
| 1055.5 | 4.36 | 1276.0 | 3.15 | 1530.6 | 4.52 |
| 1059.4 | 4.30 | 1281.4 | 3.15 | 1537.2 | 4.18 |
| 1063.4 | 3.98 | 1287.0 | 3.12 | 1544.4 | 3.97 |
| 1067.3 | 3.60 | 1292.5 | 4.40 | 1551.6 | 3.71 |
| 1071.2 | 3.86 | 1298.0 | 3.58 | 1558.9 | 4.35 |
| 1075.2 | 3.82 | 1303.4 | 3.84 | 1566.2 | 4.79 |
| 1078.0 | 4.29 | 1308.9 | 3.97 | 1573.3 | 4.56 |
| 1098.6 | 3.16 | 1314.5 | 3.58 | 1580.6 | 4.70 |
| 1102.4 | 2.70 | 1320.0 | 3.66 | 1609.2 | 3.90 |
| 1106.2 | 2.85 | 1325.5 | 4.11 | 1617.6 | 3.04 |
| 1109.9 | 3.22 | 1331.1 | 4.64 | 1626.0 | 3.36 |
| 1113.6 | 3.70 | 1336.5 | 4.35 | 1634.4 | 3.63 |
| 1117.4 | 3.92 | 1342.2 | 4.11 | 1642.7 | 3.83 |
| 1121.2 | 4.17 | 1347.6 | 4.36 | 1651.1 | 4.12 |
| 1124.9 | 4.14 | 1353.2 | 4.57 | 1659.4 | 3.87 |
| 1128.7 | 4.33 | 1358.6 | 4.08 | 1667.8 | 3.45 |

| age (years) | NGR | age (years) | NGR | age (years) | NGR |
|---|---|---|---|---|---|
| 1676.2 | 3.52 | 1966.4 | 4.40 | 2468.6 | 3.85 |
| 1680.4 | 3.95 | 1973.7 | 4.65 | 2479.5 | 3.90 |
| 1688.7 | 4.63 | 1980.9 | 4.77 | 2490.5 | 3.64 |
| 1696.6 | 4.17 | 1988.0 | 5.16 | 2501.4 | 3.18 |
| 1702.6 | 3.81 | 1995.2 | 3.95 | 2510.1 | 3.99 |
| 1708.4 | 3.59 | 2002.4 | 3.73 | 2521.1 | 3.59 |
| 1712.0 | 3.14 | 2011.6 | 3.60 | 2532.1 | 2.95 |
| 1717.9 | 3.90 | 2019.1 | 3.65 | 2541.3 | 3.89 |
| 1723.9 | 3.17 | 2024.5 | 4.18 | 2550.5 | 4.27 |
| 1729.8 | 3.65 | 2032.4 | 4.11 | 2559.7 | 4.45 |
| 1732.2 | 3.93 | 2040.3 | 4.66 | 2568.8 | 4.38 |
| 1738.2 | 3.78 | 2048.3 | 5.07 | 2577.9 | 4.23 |
| 1744.0 | 4.15 | 2056.2 | 4.56 | 2587.1 | 4.62 |
| 1749.8 | 4.71 | 2064.3 | 4.56 | 2596.2 | 5.21 |
| 1755.7 | 4.29 | 2072.3 | 4.69 | 2605.4 | 4.88 |
| 1761.7 | 3.44 | 2080.3 | 4.34 | 2614.5 | 4.08 |
| 1767.7 | 3.27 | 2082.0 | 5.23 | 2623.7 | 3.60 |
| 1773.7 | 3.48 | 2090.0 | 4.37 | 2632.8 | 3.56 |
| 1779.6 | 3.49 | 2098.2 | 4.73 | 2635.4 | 3.50 |
| 1785.8 | 3.69 | 2108.1 | 5.68 | 2644.2 | 3.78 |
| 1789.4 | 3.21 | 2117.8 | 5.43 | 2653.1 | 3.47 |
| 1795.4 | 3.08 | 2127.6 | 4.63 | 2661.9 | 3.46 |
| 1801.2 | 5.28 | 2137.5 | 4.23 | 2670.9 | 3.47 |
| 1807.0 | 4.34 | 2147.4 | 5.08 | 2679.8 | 3.46 |
| 1813.0 | 4.12 | 2157.3 | 5.38 | 2692.3 | 4.21 |
| 1818.7 | 4.91 | 2167.3 | 5.07 | 2701.2 | 4.41 |
| 1824.7 | 4.83 | 2176.9 | 5.58 | 2713.7 | 4.27 |
| 1830.7 | 4.71 | 2186.5 | 5.05 | 2724.1 | 4.19 |
| 1836.6 | 4.02 | 2196.2 | 4.79 | 2738.3 | 4.22 |
| 1842.7 | 4.39 | 2207.3 | 4.72 | 2752.6 | 4.13 |
| 1848.6 | 3.89 | 2218.6 | 4.65 | 2759.6 | 3.71 |
| 1854.6 | 4.10 | 2229.9 | 4.91 | 2766.9 | 3.47 |
| 1860.6 | 4.00 | 2241.2 | 4.09 | 2781.2 | 3.45 |
| 1866.5 | 4.45 | 2252.6 | 4.20 | 2795.4 | 3.48 |
| 1872.4 | 4.30 | 2263.9 | 3.85 | 2809.9 | 3.01 |
| 1878.3 | 4.04 | 2275.1 | 3.62 | 2824.1 | 2.95 |
| 1884.2 | 4.30 | 2286.2 | 3.57 | 2838.5 | 3.66 |
| 1890.2 | 4.39 | 2297.2 | 3.32 | 2852.8 | 3.85 |
| 1896.3 | 3.97 | 2308.4 | 3.08 | 2865.5 | 3.94 |
| 1902.3 | 4.51 | 2319.6 | 3.18 | 2874.6 | 3.25 |
| 1908.2 | 4.36 | 2330.9 | 3.94 | 2878.1 | 3.47 |
| 1914.2 | 4.56 | 2371.7 | 5.13 | 2887.0 | 4.11 |
| 1920.2 | 4.60 | 2383.7 | 4.59 | 2895.8 | 4.37 |
| 1926.2 | 4.67 | 2395.3 | 3.73 | 2904.6 | 3.88 |
| 1932.2 | 4.63 | 2407.1 | 3.36 | 2905.5 | 3.25 |
| 1938.2 | 4.22 | 2418.8 | 3.39 | 2914.3 | 3.33 |
| 1944.9 | 3.94 | 2430.5 | 3.66 | 2923.2 | 3.60 |
| 1952.0 | 3.68 | 2441.2 | 3.96 | 2931.9 | 4.57 |
| 1959.3 | 3.86 | 2452.1 | 3.71 | 2940.8 | 4.57 |

| age (years) | NGR | age (years) | NGR | age (years) | NGR |
|---|---|---|---|---|---|
| 2949.6 | 3.76 | 3681.4 | 5.46 | 4093.9 | 5.51 |
| 2958.1 | 3.75 | 3691.1 | 4.99 | 4100.9 | 4.63 |
| 2966.7 | 3.87 | 3700.8 | 4.50 | 4108.0 | 4.97 |
| 2975.4 | 4.44 | 3710.6 | 4.99 | 4115.0 | 4.52 |
| 2980.5 | 4.34 | 3720.3 | 5.45 | 4122.0 | 3.90 |
| 2989.1 | 3.44 | 3730.0 | 4.45 | 4129.1 | 3.41 |
| 2997.8 | 3.81 | 3738.0 | 4.51 | 4137.5 | 4.58 |
| 3006.3 | 4.17 | 3747.7 | 4.99 | 4264.9 | 4.27 |
| 3015.0 | 4.75 | 3761.9 | 5.25 | 4271.7 | 3.87 |
| 3023.5 | 5.35 | 3771.0 | 4.99 | 4278.4 | 4.21 |
| 3032.2 | 5.13 | 3779.9 | 4.50 | 4285.0 | 4.72 |
| 3041.2 | 4.96 | 3789.1 | 4.84 | 4291.7 | 4.79 |
| 3051.2 | 4.29 | 3792.7 | 4.68 | 4298.5 | 4.67 |
| 3061.2 | 3.93 | 3801.8 | 4.19 | 4304.2 | 4.60 |
| 3071.2 | 4.35 | 3810.8 | 4.66 | 4310.0 | 4.05 |
| 3081.2 | 4.68 | 3817.1 | 4.51 | 4315.9 | 4.18 |
| 3091.1 | 5.04 | 3826.3 | 3.56 | 4321.7 | 4.71 |
| 3101.1 | 4.66 | 3835.3 | 2.65 | 4327.6 | 4.94 |
| 3111.0 | 5.09 | 3845.5 | 4.22 | 4333.4 | 4.77 |
| 3121.0 | 4.80 | 3854.3 | 3.92 | 4336.8 | 4.22 |
| 3130.8 | 4.75 | 3862.9 | 3.90 | 4342.6 | 4.09 |
| 3141.9 | 4.76 | 3871.6 | 4.28 | 4348.4 | 3.89 |
| 3154.3 | 4.58 | 3880.4 | 4.79 | 4354.3 | 4.17 |
| 3167.0 | 4.08 | 3894.5 | 5.14 | 4360.2 | 3.74 |
| 3179.7 | 3.66 | 3903.3 | 5.20 | 4366.1 | 3.83 |
| 3192.2 | 3.66 | 3912.2 | 4.99 | 4372.0 | 3.61 |
| 3205.0 | 3.27 | 3918.4 | 4.40 | 4378.0 | 3.12 |
| 3400.1 | 4.26 | 3927.2 | 4.07 | 4383.9 | 3.42 |
| 3413.4 | 4.40 | 3934.3 | 4.66 | 4388.8 | 3.35 |
| 3426.7 | 4.25 | 3943.1 | 5.38 | 4394.8 | 3.12 |
| 3440.2 | 4.08 | 3951.6 | 5.30 | 4400.8 | 2.66 |
| 3453.7 | 3.48 | 3960.2 | 4.82 | 4406.8 | 2.52 |
| 3467.3 | 2.91 | 3968.9 | 4.37 | 4411.0 | 2.49 |
| 3480.8 | 2.90 | 3977.5 | 4.28 | 4416.9 | 2.22 |
| 3494.5 | 3.54 | 3984.5 | 5.52 | 4420.3 | 2.53 |
| 3508.1 | 3.64 | 3993.2 | 5.67 | 4426.1 | 2.26 |
| 3521.6 | 3.89 | 4001.9 | 5.80 | 4432.0 | 2.41 |
| 3535.1 | 3.97 | 4010.6 | 5.50 | 4436.6 | 2.89 |
| 3547.7 | 4.48 | 4019.5 | 5.20 | 4442.5 | 2.77 |
| 3560.1 | 5.04 | 4026.7 | 5.51 | 4448.2 | 2.72 |
| 3572.6 | 5.31 | 4033.3 | 5.52 | 4451.7 | 2.98 |
| 3585.0 | 5.20 | 4040.0 | 5.48 | 4457.5 | 3.10 |
| 3597.5 | 4.62 | 4046.8 | 5.39 | 4463.4 | 2.96 |
| 3613.6 | 4.28 | 4053.5 | 5.06 | 4469.2 | 3.30 |
| 3625.8 | 5.82 | 4060.2 | 5.22 | 4474.8 | 3.26 |
| 3646.7 | 5.95 | 4067.0 | 5.32 | 4480.0 | 3.37 |
| 3659.1 | 5.90 | 4073.6 | 5.28 | 4485.2 | 3.00 |
| 3663.9 | 5.99 | 4080.4 | 5.23 | 4490.3 | 3.32 |
| 3673.5 | 6.05 | 4087.0 | 5.27 | 4495.5 | 2.91 |

| age (years) | NGR | age (years) | NGR | age (years) | NGR |
|---|---|---|---|---|---|
| 4500.7 | 2.70 | 4894.9 | 3.85 | 5315.0 | 4.35 |
| 4505.9 | 2.58 | 4900.5 | 3.61 | 5321.2 | 3.65 |
| 4510.9 | 2.84 | 4904.0 | 3.72 | 5327.3 | 3.74 |
| 4514.5 | 3.24 | 4909.5 | 3.53 | 5333.4 | 3.61 |
| 4519.4 | 2.83 | 4915.2 | 3.59 | 5339.6 | 3.12 |
| 4524.7 | 2.92 | 4920.8 | 3.75 | 5345.7 | 3.30 |
| 4529.6 | 2.92 | 4926.5 | 3.57 | 5351.6 | 2.93 |
| 4532.1 | 2.63 | 4932.2 | 2.95 | 5357.4 | 2.31 |
| 4537.1 | 2.85 | 4935.5 | 3.37 | 5363.4 | 2.91 |
| 4541.2 | 3.42 | 4940.9 | 3.46 | 5369.5 | 3.44 |
| 4546.2 | 3.23 | 4946.1 | 3.01 | 5375.4 | 3.93 |
| 4551.3 | 2.68 | 4951.5 | 2.64 | 5381.5 | 3.35 |
| 4554.4 | 2.92 | 4956.9 | 3.17 | 5384.5 | 3.60 |
| 4559.4 | 2.49 | 4962.3 | 3.23 | 5390.6 | 3.40 |
| 4564.4 | 2.40 | 4967.7 | 3.52 | 5396.7 | 3.14 |
| 4570.8 | 3.04 | 4969.3 | 3.79 | 5402.7 | 2.97 |
| 4575.7 | 3.02 | 4974.9 | 2.46 | 5408.2 | 2.76 |
| 4579.8 | 3.01 | 4980.4 | 3.41 | 5412.1 | 3.40 |
| 4584.9 | 2.54 | 4985.8 | 3.30 | 5417.1 | 3.69 |
| 4590.0 | 2.77 | 4991.3 | 3.82 | 5422.1 | 3.31 |
| 4595.1 | 2.44 | 4996.8 | 3.58 | 5427.1 | 3.22 |
| 4600.2 | 2.35 | 5002.3 | 3.33 | 5432.2 | 3.04 |
| 4605.2 | 1.56 | 5007.9 | 3.81 | 5437.2 | 3.63 |
| 4608.8 | 2.72 | 5013.6 | 3.73 | 5442.3 | 3.48 |
| 4614.0 | 2.80 | 5019.1 | 3.57 | 5447.4 | 3.28 |
| 4619.1 | 2.90 | 5028.2 | 3.47 | 5449.9 | 3.03 |
| 4777.9 | 3.92 | 5033.8 | 3.62 | 5455.0 | 2.73 |
| 4782.9 | 3.47 | 5039.4 | 3.23 | 5460.2 | 2.91 |
| 4787.8 | 3.19 | 5041.7 | 3.75 | 5465.4 | 3.47 |
| 4792.8 | 3.24 | 5047.4 | 3.63 | 5470.7 | 3.43 |
| 4797.7 | 3.13 | 5053.3 | 3.46 | 5475.9 | 3.25 |
| 4802.7 | 2.77 | 5057.4 | 3.69 | 5481.1 | 3.39 |
| 4807.6 | 2.97 | 5063.3 | 3.48 | 5484.8 | 3.63 |
| 4811.2 | 2.70 | 5067.5 | 3.35 | 5490.0 | 3.45 |
| 4816.1 | 3.05 | 5073.3 | 3.64 | 5495.2 | 3.22 |
| 4821.2 | 3.41 | 5079.3 | 3.84 | 5500.4 | 4.03 |
| 4826.3 | 3.25 | 5088.2 | 3.68 | 5505.4 | 3.96 |
| 4831.3 | 2.84 | 5094.2 | 4.07 | 5510.7 | 4.66 |
| 4836.4 | 3.37 | 5100.1 | 3.91 | 5513.5 | 4.75 |
| 4841.4 | 3.36 | 5106.0 | 3.60 | 5518.8 | 4.13 |
| 4843.0 | 3.53 | 5111.8 | 3.51 | 5524.2 | 3.70 |
| 4848.3 | 2.95 | 5117.7 | 4.14 | 5529.4 | 3.44 |
| 4853.4 | 2.89 | 5118.8 | 3.76 | 5534.8 | 2.82 |
| 4858.6 | 2.80 | 5124.6 | 3.59 | 5540.1 | 2.84 |
| 4866.4 | 3.40 | 5130.5 | 3.81 | 5545.5 | 2.78 |
| 4871.7 | 3.25 | 5136.4 | 3.83 | 5547.7 | 3.31 |
| 4876.9 | 3.23 | 5142.2 | 3.06 | 5553.0 | 3.56 |
| 4882.2 | 3.57 | 5148.1 | 2.97 | 5558.4 | 3.51 |
| 4889.3 | 3.72 | 5154.0 | 2.80 | 5561.0 | 3.64 |

| age (years) | NGR | age (years) | NGR | age (years) | NGR |
|---|---|---|---|---|---|
| 5566.4 | 3.54 | 5940.0 | 3.43 | 6221.1 | 3.14 |
| 5571.7 | 3.65 | 5945.8 | 3.63 | 6226.2 | 2.88 |
| 5577.0 | 4.12 | 5951.7 | 3.82 | 6231.0 | 3.12 |
| 5582.4 | 2.88 | 5953.0 | 5.43 | 6232.9 | 3.20 |
| 5587.7 | 2.97 | 5958.8 | 4.11 | 6390.2 | 4.15 |
| 5593.6 | 3.76 | 5964.7 | 4.35 | 6394.9 | 3.83 |
| 5599.0 | 3.90 | 5971.0 | 4.15 | 6399.8 | 3.82 |
| 5604.3 | 3.79 | 5977.9 | 3.94 | 6404.6 | 3.17 |
| 5609.6 | 3.92 | 5984.7 | 3.14 | 6408.5 | 4.00 |
| 5614.9 | 3.80 | 5991.5 | 1.98 | 6413.4 | 3.50 |
| 5623.1 | 3.92 | 5992.9 | 3.87 | 6418.3 | 3.26 |
| 5628.7 | 4.01 | 5999.9 | 3.72 | 6426.1 | 2.67 |
| 5634.1 | 3.80 | 6006.6 | 3.86 | 6431.0 | 2.74 |
| 5639.7 | 3.26 | 6013.3 | 3.49 | 6435.9 | 2.66 |
| 5645.2 | 3.42 | 6014.7 | 4.54 | 6440.8 | 2.97 |
| 5649.1 | 3.30 | 6021.4 | 4.09 | 6445.7 | 3.05 |
| 5654.5 | 2.87 | 6028.0 | 3.85 | 6450.5 | 3.21 |
| 5660.1 | 2.93 | 6032.0 | 3.86 | 6455.4 | 3.57 |
| 5665.6 | 3.45 | 6038.7 | 3.47 | 6460.3 | 3.66 |
| 5671.1 | 3.47 | 6045.2 | 2.07 | 6465.1 | 3.57 |
| 5676.4 | 3.43 | 6051.2 | 3.07 | 6470.5 | 3.36 |
| 5681.7 | 3.91 | 6057.9 | 3.06 | 6475.4 | 3.39 |
| 5687.0 | 4.15 | 6064.6 | 3.68 | 6480.5 | 3.18 |
| 5692.4 | 3.94 | 6074.7 | 3.32 | 6485.6 | 3.10 |
| 5697.6 | 3.50 | 6081.5 | 3.74 | 6490.7 | 2.91 |
| 5703.0 | 4.05 | 6082.2 | 3.28 | 6495.7 | 1.93 |
| 5703.5 | 3.97 | 6088.9 | 3.71 | 6500.8 | 1.41 |
| 5708.9 | 3.42 | 6095.7 | 3.12 | 6505.7 | 2.79 |
| 5714.2 | 3.33 | 6104.5 | 3.27 | 6510.7 | 3.19 |
| 5719.4 | 3.37 | 6110.2 | 3.53 | 6517.9 | 3.36 |
| 5725.0 | 3.15 | 6115.9 | 3.54 | 6522.8 | 2.79 |
| 5731.3 | 2.98 | 6124.6 | 3.40 | 6527.7 | 3.20 |
| 5737.5 | 3.59 | 6130.4 | 3.42 | 6532.7 | 2.93 |
| 5847.8 | 3.91 | 6136.2 | 3.62 | 6537.7 | 3.12 |
| 5853.7 | 3.76 | 6139.1 | 4.10 | 6542.7 | 3.04 |
| 5859.7 | 3.23 | 6144.8 | 4.20 | 6547.7 | 2.81 |
| 5865.7 | 3.25 | 6150.5 | 3.65 | 6552.6 | 3.52 |
| 5871.8 | 3.29 | 6156.2 | 3.26 | 6557.6 | 3.34 |
| 5877.9 | 3.05 | 6161.7 | 3.20 | 6562.9 | 3.59 |
| 5879.7 | 4.01 | 6165.0 | 4.18 | 6568.3 | 3.47 |
| 5885.6 | 2.85 | 6170.5 | 2.88 | 6573.6 | 3.16 |
| 5891.6 | 3.29 | 6179.1 | 3.75 | 6577.3 | 3.95 |
| 5897.7 | 3.46 | 6184.4 | 3.63 | 6582.6 | 3.86 |
| 5903.6 | 3.02 | 6189.8 | 3.49 | 6587.8 | 4.44 |
| 5909.4 | 3.14 | 6193.0 | 3.62 | 6593.2 | 4.42 |
| 5915.4 | 3.29 | 6198.4 | 3.40 | 6598.5 | 4.00 |
| 5921.3 | 3.31 | 6203.7 | 3.38 | 6601.7 | 3.86 |
| 5928.3 | 3.25 | 6209.2 | 3.48 | 6607.1 | 3.59 |
| 5934.2 | 3.66 | 6214.3 | 3.82 | 6612.3 | 3.50 |

| age (years) | NGR | age (years) | NGR | age (years) | NGR |
|---|---|---|---|---|---|
| 6615.5 | 3.26 | 6984.2 | 4.08 | 7294.3 | 4.01 |
| 6620.4 | 3.64 | 6989.3 | 4.27 | 7298.3 | 4.19 |
| 6624.1 | 3.53 | 6995.3 | 4.17 | 7306.1 | 4.13 |
| 6629.3 | 3.35 | 7001.2 | 4.06 | 7314.0 | 4.62 |
| 6634.5 | 3.60 | 7007.2 | 4.30 | 7321.9 | 4.47 |
| 6639.6 | 3.31 | 7011.3 | 5.04 | 7329.4 | 4.86 |
| 6643.2 | 5.22 | 7017.2 | 4.11 | 7336.8 | 4.81 |
| 6648.5 | 3.53 | 7023.1 | 3.61 | 7344.1 | 5.00 |
| 6656.7 | 3.93 | 7029.0 | 3.98 | 7348.5 | 3.98 |
| 6661.8 | 4.14 | 7035.6 | 3.87 | 7355.8 | 3.70 |
| 6666.8 | 3.77 | 7041.4 | 4.12 | 7363.0 | 3.46 |
| 6669.8 | 3.61 | 7047.3 | 3.93 | 7370.3 | 3.88 |
| 6674.7 | 3.98 | 7053.5 | 4.19 | 7377.6 | 3.85 |
| 6678.6 | 4.01 | 7059.6 | 4.42 | 7384.9 | 3.86 |
| 6683.6 | 4.06 | 7065.9 | 4.20 | 7392.2 | 3.74 |
| 6688.5 | 4.40 | 7072.1 | 3.97 | 7398.0 | 4.47 |
| 6693.5 | 4.60 | 7078.3 | 3.75 | 7405.0 | 4.55 |
| 6696.4 | 4.29 | 7084.6 | 3.81 | 7412.0 | 4.80 |
| 6701.3 | 4.02 | 7087.1 | 4.43 | 7418.9 | 4.89 |
| 6706.1 | 4.17 | 7093.3 | 3.62 | 7508.0 | 5.35 |
| 6709.4 | 3.03 | 7099.6 | 3.59 | 7516.3 | 4.17 |
| 6714.2 | 2.97 | 7105.8 | 4.61 | 7524.5 | 4.25 |
| 6719.0 | 2.93 | 7112.0 | 4.61 | 7532.6 | 3.50 |
| 6727.4 | 3.99 | 7118.4 | 4.39 | 7540.8 | 3.27 |
| 6732.3 | 3.68 | 7124.7 | 4.02 | 7549.0 | 3.76 |
| 6737.2 | 3.07 | 7131.1 | 3.72 | 7549.8 | 4.73 |
| 6739.0 | 2.95 | 7137.4 | 3.87 | 7558.3 | 3.86 |
| 6744.0 | 3.46 | 7143.9 | 4.04 | 7566.8 | 3.31 |
| 6748.8 | 3.70 | 7150.3 | 4.08 | 7575.4 | 3.58 |
| 6753.6 | 4.07 | 7156.7 | 4.19 | 7583.9 | 3.61 |
| 6878.5 | 5.93 | 7163.1 | 3.85 | 7594.2 | 3.93 |
| 6884.4 | 4.73 | 7166.3 | 4.86 | 7602.9 | 4.09 |
| 6890.2 | 4.46 | 7172.7 | 3.35 | 7611.5 | 4.17 |
| 6896.1 | 5.10 | 7179.6 | 3.76 | 7620.2 | 4.78 |
| 6902.0 | 4.57 | 7186.6 | 4.33 | 7628.7 | 5.13 |
| 6907.8 | 3.56 | 7193.8 | 4.18 | 7636.7 | 5.39 |
| 6913.8 | 3.81 | 7200.9 | 4.64 | 7643.3 | 4.86 |
| 6919.6 | 3.82 | 7208.1 | 4.48 | 7649.9 | 4.80 |
| 6925.3 | 3.69 | 7211.7 | 3.94 | 7653.1 | 5.28 |
| 6931.2 | 3.56 | 7218.8 | 3.98 | 7659.8 | 4.24 |
| 6937.0 | 3.95 | 7223.8 | 3.88 | 7666.5 | 4.42 |
| 6942.3 | 3.76 | 7231.0 | 4.36 | 7673.1 | 4.20 |
| 6947.4 | 3.00 | 7238.2 | 4.76 | 7679.7 | 4.45 |
| 6952.7 | 3.47 | 7247.0 | 4.87 | 7686.3 | 4.27 |
| 6957.9 | 3.79 | 7254.9 | 4.79 | 7692.9 | 3.94 |
| 6963.1 | 3.72 | 7262.9 | 4.61 | 7699.5 | 4.42 |
| 6968.5 | 4.01 | 7270.7 | 4.21 | 7706.0 | 4.68 |
| 6974.1 | 4.33 | 7278.7 | 4.62 | 7706.7 | 4.85 |
| 6979.2 | 4.37 | 7286.5 | 4.19 | 7713.4 | 4.66 |

| age (years) | NGR | age (years) | NGR | age (years) | NGR |
|---|---|---|---|---|---|
| 7720.1 | 4.39 | 7960.1 | 4.93 | 8217.4 | 4.83 |
| 7726.7 | 4.20 | 7964.6 | 4.67 | 8221.6 | 4.61 |
| 7733.4 | 4.26 | 7969.2 | 4.97 | 8225.9 | 4.81 |
| 7741.5 | 4.25 | 8046.3 | 5.32 | 8228.8 | 5.34 |
| 7748.2 | 3.85 | 8049.9 | 3.98 | 8233.0 | 4.58 |
| 7754.9 | 4.47 | 8053.5 | 4.02 | 8237.3 | 4.42 |
| 7761.5 | 4.25 | 8057.0 | 3.89 | 8241.6 | 5.01 |
| 7768.0 | 4.32 | 8060.7 | 4.50 | 8245.7 | 5.04 |
| 7773.4 | 4.47 | 8064.3 | 4.55 | 8249.8 | 5.02 |
| 7778.7 | 4.31 | 8067.5 | 4.47 | 8253.9 | 4.95 |
| 7784.0 | 4.30 | 8071.1 | 4.24 | 8258.1 | 5.43 |
| 7789.4 | 4.44 | 8074.7 | 4.70 | 8262.2 | 5.58 |
| 7794.7 | 5.14 | 8078.2 | 4.65 | 8266.3 | 5.21 |
| 7800.0 | 4.83 | 8081.8 | 4.44 | 8270.5 | 5.19 |
| 7805.3 | 4.68 | 8085.4 | 3.82 | 8274.7 | 5.07 |
| 7810.6 | 4.93 | 8089.2 | 3.86 | 8278.8 | 4.85 |
| 7812.2 | 5.20 | 8092.6 | 5.06 | 8283.0 | 4.35 |
| 7817.6 | 4.21 | 8096.3 | 3.89 | 8287.3 | 3.91 |
| 7822.7 | 3.14 | 8100.0 | 3.95 | 8290.7 | 6.76 |
| 7827.9 | 2.30 | 8103.8 | 4.46 | 8295.0 | 6.00 |
| 7833.0 | 2.50 | 8107.5 | 4.45 | 8299.3 | 5.48 |
| 7838.2 | 3.36 | 8111.2 | 4.28 | 8303.7 | 5.60 |
| 7840.3 | 3.49 | 8115.0 | 4.22 | 8310.5 | 5.94 |
| 7845.4 | 3.52 | 8118.7 | 4.13 | 8314.8 | 5.63 |
| 7850.6 | 3.78 | 8122.5 | 5.21 | 8319.1 | 5.43 |
| 7855.8 | 4.32 | 8126.3 | 5.21 | 8326.6 | 5.63 |
| 7860.9 | 4.61 | 8130.3 | 6.07 | 8331.2 | 5.64 |
| 7864.0 | 5.20 | 8133.0 | 5.21 | 8335.9 | 5.76 |
| 7869.2 | 4.68 | 8136.8 | 4.50 | 8340.7 | 5.76 |
| 7874.1 | 4.96 | 8140.6 | 4.74 | 8345.5 | 5.70 |
| 7879.0 | 4.15 | 8144.4 | 4.56 | 8350.3 | 5.37 |
| 7883.9 | 4.20 | 8148.3 | 4.43 | 8354.1 | 5.39 |
| 7885.4 | 4.41 | 8152.2 | 4.30 | 8358.8 | 4.33 |
| 7890.3 | 5.02 | 8155.8 | 4.44 | 8363.6 | 3.76 |
| 7895.2 | 5.15 | 8159.7 | 4.49 | 8368.3 | 3.15 |
| 7900.2 | 4.90 | 8163.8 | 4.41 | 8373.2 | 2.93 |
| 7905.1 | 4.63 | 8167.9 | 4.58 | 8378.7 | 3.40 |
| 7908.1 | 4.71 | 8172.0 | 4.26 | 8458.0 | 5.38 |
| 7913.0 | 4.98 | 8176.1 | 4.47 | 8463.9 | 4.64 |
| 7917.9 | 4.82 | 8180.2 | 4.67 | 8470.0 | 5.27 |
| 7922.8 | 4.35 | 8181.0 | 4.99 | 8476.0 | 4.93 |
| 7927.4 | 4.35 | 8185.0 | 4.03 | 8482.2 | 4.39 |
| 7930.7 | 4.69 | 8188.9 | 2.77 | 8488.2 | 5.04 |
| 7935.3 | 3.60 | 8192.9 | 3.13 | 8494.4 | 5.77 |
| 7940.0 | 3.45 | 8196.8 | 3.85 | 8500.5 | 5.40 |
| 7945.1 | 2.58 | 8200.8 | 3.95 | 8506.7 | 5.35 |
| 7950.3 | 2.95 | 8205.1 | 4.02 | 8512.9 | 4.91 |
| 7950.8 | 4.24 | 8208.9 | 4.90 | 8519.1 | 5.43 |
| 7955.5 | 4.55 | 8213.1 | 4.47 | 8525.3 | 5.51 |

| age (years) | NGR | age (years) | NGR | age (years) | NGR |
|---|---|---|---|---|---|
| 8531.5 | 5.07 | 8817.0 | 5.75 | 9198.9 | 3.34 |
| 8535.2 | 5.97 | 8823.7 | 5.12 | 9207.0 | 4.03 |
| 8541.4 | 4.39 | 8830.4 | 5.08 | 9215.0 | 4.44 |
| 8547.5 | 3.37 | 8837.0 | 6.22 | 9217.4 | 5.34 |
| 8553.7 | 2.54 | 8843.6 | 5.06 | 9225.4 | 4.76 |
| 8560.1 | 2.00 | 8850.3 | 5.26 | 9233.4 | 5.30 |
| 8566.4 | 2.79 | 8856.8 | 5.29 | 9241.2 | 5.70 |
| 8572.7 | 3.57 | 8863.3 | 5.38 | 9249.2 | 5.84 |
| 8579.1 | 4.43 | 8870.0 | 5.17 | 9257.0 | 5.70 |
| 8585.6 | 4.57 | 8876.5 | 5.40 | 9265.0 | 5.76 |
| 8590.7 | 6.89 | 8883.1 | 5.59 | 9267.3 | 5.39 |
| 8597.1 | 5.01 | 8889.7 | 5.90 | 9275.4 | 5.67 |
| 8603.6 | 4.79 | 8896.4 | 6.13 | 9284.0 | 6.39 |
| 8610.0 | 4.51 | 8902.7 | 6.13 | 9292.6 | 6.62 |
| 8616.3 | 4.76 | 8909.2 | 5.35 | 9301.1 | 6.06 |
| 8622.5 | 4.82 | 8915.6 | 5.25 | 9309.9 | 5.56 |
| 8628.5 | 4.69 | 8921.8 | 5.61 | 9318.5 | 5.44 |
| 8635.4 | 5.48 | 8928.1 | 6.32 | 9327.2 | 5.33 |
| 8641.6 | 5.34 | 8934.3 | 6.39 | 9337.7 | 5.45 |
| 8647.7 | 5.33 | 8939.1 | 4.87 | 9346.4 | 5.64 |
| 8654.0 | 5.73 | 8945.3 | 4.90 | 9350.8 | 5.95 |
| 8660.0 | 5.80 | 8951.3 | 4.81 | 9359.7 | 6.92 |
| 8666.2 | 6.02 | 8957.4 | 4.69 | 9368.4 | 5.69 |
| 8668.1 | 5.42 | 8963.5 | 4.77 | 9377.2 | 4.98 |
| 8674.3 | 4.47 | 8969.7 | 5.25 | 9386.1 | 5.46 |
| 8680.0 | 4.59 | 8975.9 | 6.16 | 9392.2 | 5.33 |
| 8685.5 | 4.23 | 8982.1 | 5.34 | 9401.2 | 5.00 |
| 8691.2 | 3.76 | 9052.5 | 6.11 | 9410.3 | 5.33 |
| 8693.5 | 4.68 | 9059.2 | 5.69 | 9419.2 | 5.52 |
| 8699.2 | 4.88 | 9066.0 | 5.64 | 9428.2 | 5.71 |
| 8705.0 | 4.32 | 9072.7 | 5.16 | 9437.0 | 5.35 |
| 8710.7 | 4.29 | 9079.5 | 4.75 | 9439.6 | 5.81 |
| 8713.0 | 4.93 | 9082.9 | 4.52 | 9448.5 | 5.65 |
| 8718.7 | 6.26 | 9089.6 | 5.26 | 9457.4 | 5.95 |
| 8724.4 | 5.88 | 9096.4 | 4.95 | 9470.8 | 5.43 |
| 8730.2 | 4.91 | 9107.3 | 5.34 | 9479.8 | 5.51 |
| 8736.2 | 4.58 | 9114.0 | 5.07 | 9488.8 | 5.19 |
| 8741.2 | 5.72 | 9120.7 | 5.10 | 9497.7 | 4.96 |
| 8747.4 | 5.15 | 9128.2 | 5.06 | 9506.7 | 5.28 |
| 8753.7 | 5.00 | 9135.6 | 4.62 | 9515.6 | 5.04 |
| 8760.1 | 5.06 | 9143.0 | 4.54 | 9524.5 | 5.42 |
| 8766.4 | 5.42 | 9145.9 | 5.18 | 9533.4 | 5.73 |
| 8772.7 | 6.10 | 9153.3 | 4.44 | 9542.0 | 5.19 |
| 8778.8 | 5.93 | 9160.7 | 3.23 | 9550.6 | 5.65 |
| 8785.0 | 6.11 | 9168.2 | 2.35 | 9556.4 | 7.14 |
| 8791.0 | 6.54 | 9175.5 | 2.66 | 9565.0 | 6.80 |
| 8797.3 | 6.43 | 9183.0 | 2.93 | 9573.5 | 6.45 |
| 8803.9 | 6.65 | 9183.7 | 4.55 | 9582.1 | 6.90 |
| 8810.5 | 6.63 | 9191.1 | 4.35 | 9590.5 | 6.09 |

| age (years) | NGR | age (years) | NGR | age (years) | NGR |
|---|---|---|---|---|---|
| 9597.2 | 5.81 | 10147.7 | 5.45 | 10715.9 | 9.33 |
| 9605.5 | 6.11 | 10160.0 | 6.22 | 10724.9 | 10.63 |
| 9613.7 | 6.32 | 10172.3 | 6.35 | 10733.9 | 10.27 |
| 9622.2 | 6.39 | 10184.6 | 5.84 | 10742.9 | 7.46 |
| 9630.9 | 6.81 | 10196.6 | 5.63 | 10751.9 | 6.45 |
| 9639.6 | 7.58 | 10208.7 | 8.08 | 10760.9 | 6.33 |
| 9648.2 | 7.11 | 10220.7 | 6.90 | 10766.2 | 7.76 |
| 9657.1 | 6.83 | 10233.3 | 6.90 | 10775.1 | 6.25 |
| 9665.9 | 6.55 | 10245.9 | 7.35 | 10784.1 | 6.15 |
| 9674.6 | 6.91 | 10258.5 | 6.29 | 10792.8 | 6.82 |
| 9683.3 | 7.20 | 10271.2 | 6.39 | 10801.0 | 7.53 |
| 9692.0 | 6.35 | 10283.9 | 6.58 | 10805.3 | 8.09 |
| 9700.7 | 6.77 | 10290.3 | 7.62 | 10813.5 | 7.99 |
| 9709.4 | 6.35 | 10302.9 | 6.10 | 10821.7 | 8.09 |
| 9718.4 | 5.67 | 10315.5 | 7.61 | 10830.1 | 8.65 |
| 9727.6 | 6.02 | 10323.1 | 8.74 | 10873.4 | 7.69 |
| 9736.5 | 6.00 | 10335.7 | 7.71 | 10881.8 | 6.49 |
| 9745.6 | 5.86 | 10348.2 | 6.48 | 10890.2 | 6.79 |
| 9754.7 | 5.19 | 10361.0 | 6.97 | 10898.7 | 7.34 |
| 9844.8 | 6.47 | 10381.4 | 7.50 | 10915.6 | 9.42 |
| 9853.5 | 5.82 | 10394.5 | 7.06 | 10924.1 | 9.11 |
| 9862.3 | 5.57 | 10407.6 | 6.86 | 10932.5 | 7.63 |
| 9870.9 | 5.26 | 10420.8 | 7.53 | 10941.2 | 9.26 |
| 9879.7 | 5.51 | 10434.0 | 8.35 | 10949.6 | 9.33 |
| 9888.3 | 4.96 | 10446.9 | 7.85 | 10958.1 | 8.56 |
| 9897.2 | 4.85 | 10454.9 | 8.02 | 10966.6 | 7.79 |
| 9906.0 | 5.14 | 10468.0 | 7.04 | 10975.1 | 8.80 |
| 9914.8 | 5.08 | 10480.1 | 7.42 | 10983.5 | 8.18 |
| 9923.6 | 5.21 | 10485.9 | 9.23 | 10992.1 | 9.27 |
| 9935.9 | 6.18 | 10497.3 | 8.77 | 10999.8 | 10.94 |
| 9944.6 | 6.33 | 10509.0 | 8.22 | 11008.4 | 10.42 |
| 9953.3 | 6.42 | 10520.6 | 7.83 | 11016.9 | 10.46 |
| 9962.0 | 6.77 | 10532.4 | 8.10 | 11023.0 | 11.25 |
| 9970.8 | 6.08 | 10544.1 | 8.08 | 11031.5 | 10.44 |
| 9980.7 | 7.11 | 10555.8 | 8.76 | 11040.1 | 10.25 |
| 9992.9 | 6.76 | 10567.4 | 9.49 | 11048.0 | 9.57 |
| 10005.0 | 5.76 | 10579.0 | 9.94 | 11055.5 | 9.89 |
| 10017.0 | 6.11 | 10590.7 | 9.34 | 11062.9 | 9.65 |
| 10029.2 | 6.50 | 10601.6 | 8.43 | 11070.3 | 9.51 |
| 10036.3 | 6.57 | 10612.5 | 9.36 | 11077.8 | 8.82 |
| 10048.6 | 6.72 | 10623.5 | 8.01 | 11085.3 | 9.47 |
| 10060.7 | 6.63 | 10634.3 | 6.48 | 11092.8 | 8.08 |
| 10072.8 | 6.18 | 10645.3 | 7.21 | 11100.2 | 7.23 |
| 10084.6 | 6.26 | 10653.9 | 7.52 | 11107.5 | 7.78 |
| 10096.5 | 5.91 | 10665.0 | 7.73 | 11110.5 | 8.37 |
| 10108.7 | 5.62 | 10675.9 | 8.25 | 11117.8 | 9.52 |
| 10120.6 | 4.95 | 10686.9 | 7.25 | 11126.7 | 10.28 |
| 10123.2 | 7.15 | 10697.8 | 7.64 | 11135.6 | 10.64 |
| 10135.4 | 5.38 | 10707.0 | 7.66 | 11144.5 | 9.95 |

A1: CHAPTER 4 DATA

| age (years) | NGR |
|---|---|
| 11153.4 | 9.60 |
| 11162.4 | 10.27 |
| 11174.9 | 9.68 |
| 11183.8 | 8.58 |
| 11192.8 | 10.66 |
| 11201.7 | 11.85 |
| 11210.7 | 10.40 |
| 11219.8 | 8.74 |
| 11228.9 | 7.58 |
| 11238.2 | 9.80 |
| 11247.2 | 9.21 |
| 11256.4 | 9.62 |
| 11265.3 | 10.09 |
| 11274.4 | 9.49 |
| 11283.4 | 8.81 |
| 11292.4 | 8.70 |
| 11301.2 | 7.69 |
| 11310.0 | 8.17 |
| 11318.5 | 8.08 |
| 11327.0 | 8.71 |
| 11335.7 | 9.24 |
| 11344.4 | 9.79 |
| 11353.1 | 8.26 |
| 11361.6 | 8.10 |
| 11369.3 | 25.62 |
| 11377.8 | 23.36 |

| age (years) | Diene | Triene | Diene/Triene |
|---|---|---|---|
| 56.70 | 4.37 | 194.48 | 0.02 |
| 99.30 | 21.14 | 218.06 | 0.10 |
| 151.70 | 0.27 | 30.96 | 0.01 |
| 199.20 | 0.92 | 20.88 | 0.04 |
| 250.10 | 0.57 | 17.66 | 0.03 |
| 299.90 | 1.06 | 17.57 | 0.06 |
| 349.50 | 1.37 | 24.65 | 0.06 |
| 400.90 | 0.70 | 26.61 | 0.03 |
| 449.60 | 1.55 | 30.65 | 0.05 |
| 501.03 | 1.48 | 40.30 | 0.04 |
| 549.30 | 0.51 | 10.95 | 0.05 |
| 599.50 | 1.86 | 30.78 | 0.06 |
| 650.50 | 0.25 | 7.29 | 0.03 |
| 698.98 | 0.54 | 34.67 | 0.02 |
| 749.51 | 1.23 | 20.96 | 0.06 |
| 799.74 | 0.17 | 14.12 | 0.01 |
| 849.74 | 0.37 | 38.33 | 0.01 |
| 899.44 | 1.20 | 10.02 | 0.12 |
| 949.28 | 0.20 | 12.36 | 0.02 |
| 999.54 | 0.04 | 12.23 | 0.00 |
| 1049.97 | 0.22 | 2.54 | 0.09 |
| 1100.94 | 0.16 | 10.84 | 0.02 |
| 1150.67 | 0.05 | 58.24 | 0.00 |
| 1200.04 | 0.13 | 17.10 | 0.01 |
| 1251.82 | 0.34 | 4.04 | 0.08 |
| 1298.52 | 0.25 | 29.57 | 0.01 |
| 1351.01 | 0.10 | 24.36 | 0.00 |
| 1399.46 | 0.10 | 178.11 | 0.00 |
| 1450.86 | 0.10 | 13.54 | 0.01 |
| 1499.76 | 0.08 | 2.32 | 0.03 |
| 1548.71 | 0.09 | 10.01 | 0.01 |
| 1599.17 | 0.11 | 12.92 | 0.01 |
| 1651.94 | 0.30 | 6.68 | 0.05 |
| 1700.13 | 0.16 | 3.89 | 0.04 |
| 1750.42 | 0.03 | 1.72 | 0.02 |
| 1801.72 | 0.00 | 5.07 | 0.00 |
| 1849.17 | 0.00 | 12.13 | 0.00 |
| 1899.83 | 0.15 | 11.13 | 0.01 |
| 1949.11 | 0.16 | 7.05 | 0.02 |
| 2000.88 | 0.08 | 4.57 | 0.02 |
| 2049.07 | 0.38 | 11.01 | 0.03 |
| 2099.15 | 0.60 | 6.55 | 0.09 |
| 2148.37 | 0.09 | 6.93 | 0.01 |
| 2197.19 | 0.27 | 12.11 | 0.02 |
| 2248.01 | 0.17 | 11.92 | 0.01 |
| 2298.41 | 0.60 | 46.38 | 0.01 |
| 2349.05 | 0.22 | 8.59 | 0.03 |
| 2396.50 | 0.19 | 25.30 | 0.01 |
| 2480.60 | 0.23 | 12.43 | 0.02 |
| 2502.50 | 0.00 | 6.16 | 0.00 |

| age (years) | Diene | Triene | Diene/Triene |
|---|---|---|---|
| 2542.30 | 0.00 | 7.02 | 0.00 |
| 2597.20 | 0.81 | 6.47 | 0.13 |
| 2653.90 | 0.00 | 15.73 | 0.00 |
| 2693.20 | 2.08 | 9.07 | 0.23 |
| 2754.00 | 0.41 | 10.71 | 0.04 |
| 2811.40 | 0.23 | 18.77 | 0.01 |
| 2866.40 | 0.00 | 5.53 | 0.00 |
| 2896.70 | 0.71 | 10.63 | 0.07 |
| 2959.00 | 0.67 | 6.88 | 0.10 |
| 3015.80 | 0.72 | 8.73 | 0.08 |
| 3052.10 | 0.00 | 10.85 | 0.00 |
| 3092.10 | 0.23 | 6.30 | 0.04 |
| 3168.30 | 0.22 | 11.66 | 0.02 |
| 3193.50 | 0.00 | 8.03 | 0.00 |
| 3236.70 | 0.32 | 15.48 | 0.02 |
| 3401.50 | 0.25 | 58.40 | 0.00 |
| 3455.10 | 0.23 | 13.04 | 0.02 |
| 3495.80 | 0.03 | 7.69 | 0.00 |
| 3548.90 | 0.38 | 3.95 | 0.10 |
| 3607.30 | 0.33 | 16.73 | 0.02 |
| 3659.27 | 0.40 | 5.51 | 0.07 |
| 3701.70 | 0.21 | 54.61 | 0.00 |
| 3762.80 | 0.28 | 1.88 | 0.15 |
| 3811.70 | 0.19 | 1.43 | 0.14 |
| 3846.40 | 0.00 | 23.86 | 0.00 |
| 3895.40 | 0.27 | 4.91 | 0.05 |
| 3943.90 | 0.12 | 1.09 | 0.11 |
| 4002.80 | 0.25 | 2.43 | 0.10 |
| 4047.40 | 0.34 | 5.64 | 0.06 |
| 4094.60 | 0.14 | 0.71 | 0.20 |
| 4145.30 | 0.28 | 1.04 | 0.27 |
| 4265.60 | 0.22 | 3.40 | 0.06 |
| 4304.80 | 1.19 | 3.67 | 0.32 |
| 4349.00 | 0.11 | 2.72 | 0.04 |
| 4401.40 | 0.13 | 24.48 | 0.01 |
| 4458.10 | 0.08 | 5.21 | 0.02 |
| 4501.20 | 0.72 | 11.68 | 0.06 |
| 4551.80 | 0.00 | 22.13 | 0.00 |
| 4600.70 | 0.00 | 1.27 | 0.00 |
| 4633.80 | 0.00 | 6.87 | 0.00 |
| 4808.10 | 0.00 | 5.42 | 0.00 |
| 4853.90 | 0.00 | 3.48 | 0.00 |
| 4901.10 | 0.00 | 7.84 | 0.00 |
| 4952.00 | 0.00 | 2.79 | 0.00 |
| 4997.40 | 0.00 | 2.73 | 0.00 |
| 5052.70 | 0.00 | 11.75 | 0.00 |
| 5106.60 | 0.00 | 1.45 | 0.00 |
| 5154.70 | 0.00 | 7.77 | 0.00 |
| 5197.90 | 0.00 | 4.59 | 0.00 |
| 5315.60 | 0.23 | 4.79 | 0.05 |

| age (years) | Diene | Triene | Diene/Triene |
|---|---|---|---|
| 5352.70 | 0.10 | 9.03 | 0.01 |
| 5397.30 | 0.00 | 7.22 | 0.00 |
| 5450.40 | 0.00 | 2.19 | 0.00 |
| 5500.90 | 0.00 | 6.37 | 0.00 |
| 5553.50 | 0.00 | 12.28 | 0.00 |
| 5594.10 | 0.00 | 7.64 | 0.00 |
| 5649.60 | 0.00 | 1.89 | 0.00 |
| 5702.50 | 0.00 | 20.68 | 0.00 |
| 5752.50 | 0.00 | 7.37 | 0.00 |
| 5848.40 | 0.00 | 3.36 | 0.00 |
| 5904.20 | 0.00 | 3.81 | 0.00 |
| 5952.30 | 0.00 | 0.38 | 0.00 |
| 5999.10 | 0.00 | 4.43 | 0.00 |
| 6051.90 | 0.00 | 7.78 | 0.00 |
| 6100.57 | 0.00 | 9.93 | 0.00 |
| 6151.10 | 0.00 | 4.52 | 0.00 |
| 6204.20 | 0.00 | 1.14 | 0.00 |
| 6251.30 | 0.00 | 2.72 | 0.00 |
| 6292.80 | 0.00 | 5.78 | 0.00 |
| 6382.03 | 0.00 | 4.63 | 0.00 |
| 6405.10 | 0.00 | 15.36 | 0.00 |
| 6455.80 | 0.00 | 3.29 | 0.00 |
| 6506.30 | 0.00 | 0.98 | 0.00 |
| 6553.10 | 0.00 | 17.39 | 0.00 |
| 6602.20 | 0.00 | 0.95 | 0.00 |
| 6652.00 | 0.00 | 8.76 | 0.00 |
| 6696.90 | 0.00 | 0.75 | 0.00 |
| 6749.30 | 0.18 | 6.67 | 0.03 |
| 6879.10 | 0.00 | 6.40 | 0.00 |
| 6902.60 | 0.00 | 5.31 | 0.00 |
| 6953.30 | 0.15 | 10.37 | 0.01 |
| 7001.80 | 0.00 | 5.82 | 0.00 |
| 7047.90 | 0.00 | 3.22 | 0.00 |
| 7100.20 | 0.00 | 3.62 | 0.00 |
| 7150.90 | 0.00 | 24.26 | 0.00 |
| 7201.60 | 0.00 | 0.00 | 0.00 |
| 7255.70 | 0.27 | 1.39 | 0.19 |
| 7299.00 | 0.00 | 7.89 | 0.00 |
| 7349.10 | 0.00 | 4.17 | 0.00 |
| 7398.70 | 0.00 | 6.43 | 0.00 |
| 7438.60 | 0.07 | 3.32 | 0.02 |
| 7508.79 | 0.00 | 5.64 | 0.00 |
| 7550.70 | 0.00 | 5.78 | 0.00 |
| 7603.80 | 0.00 | 12.65 | 0.00 |
| 7649.90 | 0.00 | 9.42 | 0.00 |
| 7706.04 | 0.00 | 3.88 | 0.00 |
| 7748.90 | 0.00 | 2.46 | 0.00 |
| 7800.50 | 0.00 | 2.13 | 0.00 |
| 7851.10 | 0.38 | 5.56 | 0.07 |
| 7900.70 | 0.00 | 2.31 | 0.00 |
| 7949.90 | 0.00 | 7.56 | 0.00 |

| age (years) | Diene | Triene | Diene/Triene |
|---|---|---|---|
| 7980.10 | 0.00 | 12.94 | 0.00 |
| 8046.70 | 0.00 | 9.63 | 0.00 |
| 8053.90 | 0.00 | 15.09 | 0.00 |
| 8100.40 | 0.00 | 3.16 | 0.00 |
| 8148.60 | 0.00 | 3.12 | 0.00 |
| 8197.10 | 0.00 | 5.51 | 0.00 |
| 8254.30 | 0.00 | 2.16 | 0.00 |
| 8299.80 | 0.00 | 1.68 | 0.00 |
| 8350.80 | 0.00 | 1.25 | 0.00 |
| 8393.20 | 0.00 | 9.82 | 0.00 |
| 8458.60 | 0.00 | 8.15 | 0.00 |
| 8495.10 | 0.00 | 5.36 | 0.00 |
| 8549.40 | 0.00 | 13.77 | 0.00 |
| 8604.20 | 0.00 | 2.45 | 0.00 |
| 8648.40 | 0.00 | 8.82 | 0.00 |
| 8694.00 | 0.00 | 13.93 | 0.00 |
| 8754.40 | 0.18 | 3.28 | 0.05 |
| 8804.50 | 0.00 | 4.25 | 0.00 |
| 8850.90 | 0.00 | 7.59 | 0.00 |
| 8903.40 | 0.00 | 4.38 | 0.00 |
| 8945.90 | 0.00 | 2.69 | 0.00 |
| 8999.30 | 0.00 | 3.32 | 0.00 |
| 9053.20 | 0.00 | 1.75 | 0.00 |
| 9101.24 | 0.00 | 16.00 | 0.00 |
| 9146.60 | 0.00 | 8.62 | 0.00 |
| 9199.70 | 0.00 | 1.99 | 0.00 |
| 9249.90 | 0.00 | 9.51 | 0.00 |
| 9293.50 | 0.00 | 2.57 | 0.00 |
| 9347.30 | 0.00 | 7.73 | 0.00 |
| 9393.20 | 0.00 | 3.54 | 0.00 |
| 9458.30 | 0.00 | 1.37 | 0.00 |
| 9498.60 | 0.00 | 2.58 | 0.00 |
| 9550.80 | 0.00 | 16.47 | 0.00 |
| 9606.40 | 0.14 | 3.16 | 0.04 |
| 9658.00 | 0.00 | 11.90 | 0.00 |
| 9701.60 | 0.00 | 7.80 | 0.00 |
| 9755.60 | 0.00 | 3.51 | 0.00 |
| 9845.70 | 0.00 | 4.45 | 0.00 |
| 9895.40 | 0.00 | 8.13 | 0.00 |
| 9954.20 | 0.00 | 5.55 | 0.00 |
| 10006.20 | 0.00 | 18.74 | 0.00 |
| 10049.80 | 0.00 | 4.18 | 0.00 |
| 10097.80 | 0.00 | 1.94 | 0.00 |
| 10148.90 | 0.00 | 2.67 | 0.00 |
| 10197.80 | 0.00 | 4.19 | 0.00 |
| 10259.70 | 0.00 | 2.87 | 0.00 |
| 10296.60 | 0.00 | 7.91 | 0.00 |
| 10362.30 | 0.00 | 3.85 | 0.00 |
| 10395.80 | 0.00 | 3.28 | 0.00 |
| 10448.40 | 0.00 | 1.08 | 0.00 |
| 10498.50 | 0.00 | 7.77 | 0.00 |

| age (years) | Diene | Triene | Diene/Triene |
|---|---|---|---|
| 10545.30 | 0.00 | 10.06 | 0.00 |
| 10591.80 | 0.00 | 4.41 | 0.00 |
| 10646.40 | 0.00 | 1.77 | 0.00 |
| 10700.90 | 0.09 | 2.55 | 0.04 |
| 10744.70 | 0.00 | 8.76 | 0.00 |
| 10801.80 | 0.00 | 9.59 | 0.00 |
| 10899.60 | 0.00 | 2.44 | 0.00 |
| 10855.50 | 0.00 | 4.04 | 0.00 |
| 10897.90 | 0.00 | 4.48 | 0.00 |
| 10992.90 | 0.00 | 1.70 | 0.00 |
| 10942.00 | 0.00 | 1.25 | 0.00 |
| 11000.60 | 0.00 | 1.51 | 0.00 |
| 11048.70 | 0.00 | 1.80 | 0.00 |
| 11103.10 | 0.00 | 1.54 | 0.00 |
| 11145.40 | 0.00 | 2.40 | 0.00 |
| 11211.60 | 0.00 | 2.16 | 0.00 |
| 11254.50 | 0.04 | 3.50 | 0.01 |
| 11257.30 | 0.00 | 2.01 | 0.00 |
| 11298.50 | 0.00 | 4.02 | 0.00 |
| 11350.30 | 0.58 | 4.06 | 0.14 |
| 11370.20 | 0.00 | 0.33 | 0.00 |

| Age (years) | Biogenic_MAR ($g/cm^2/yr$) | Terrigenous_MAR ($g/cm^2/yr$) |
|---|---|---|
| 191.147 | 0.0076 | 0.0137 |
| 192.320 | 0.0083 | 0.0130 |
| 244.738 | 0.0087 | 0.0143 |
| 245.662 | 0.0094 | 0.0136 |
| 297.410 | 0.0087 | 0.0138 |
| 298.441 | 0.0083 | 0.0142 |
| 339.738 | 0.0073 | 0.0150 |
| 340.769 | 0.0088 | 0.0134 |
| 390.955 | 0.0091 | 0.0128 |
| 392.019 | 0.0084 | 0.0134 |
| 446.421 | 0.0083 | 0.0134 |
| 491.303 | 0.0086 | 0.0128 |
| 492.281 | 0.0106 | 0.0108 |
| 542.894 | 0.0096 | 0.0096 |
| 543.930 | 0.0077 | 0.0113 |
| 601.909 | 0.0050 | 0.0109 |
| 603.351 | 0.0078 | 0.0082 |
| 625.229 | 0.0065 | 0.0097 |
| 626.713 | 0.0067 | 0.0095 |
| 679.078 | 0.0064 | 0.0105 |
| 679.810 | 0.0067 | 0.0102 |
| 739.315 | 0.0074 | 0.0108 |
| 740.570 | 0.0060 | 0.0122 |
| 794.804 | 0.0073 | 0.0123 |
| 795.982 | 0.0077 | 0.0119 |
| 844.403 | 0.0082 | 0.0137 |
| 845.458 | 0.0088 | 0.0132 |
| 892.937 | 0.0098 | 0.0159 |
| 893.793 | 0.0115 | 0.0143 |
| 937.090 | 0.0118 | 0.0133 |
| 938.027 | 0.0111 | 0.0141 |
| 967.762 | 0.0095 | 0.0157 |
| 968.251 | 0.0133 | 0.0120 |
| 1020.313 | 0.0090 | 0.0176 |
| 1020.732 | 0.0139 | 0.0127 |
| 1054.625 | 0.0106 | 0.0169 |
| 1055.497 | 0.0116 | 0.0159 |
| 1123.600 | 0.0115 | 0.0160 |
| 1124.400 | 0.0130 | 0.0144 |
| 1158.200 | 0.0113 | 0.0155 |
| 1159.000 | 0.0147 | 0.0121 |
| 1193.600 | 0.0110 | 0.0144 |
| 1194.500 | 0.0119 | 0.0135 |
| 1244.800 | 0.0085 | 0.0132 |
| 1245.800 | 0.0096 | 0.0120 |
| 1300.700 | 0.0069 | 0.0122 |
| 1301.800 | 0.0073 | 0.0119 |
| 1357.500 | 0.0093 | 0.0108 |
| 1358.600 | 0.0097 | 0.0104 |
| 1406.300 | 0.0091 | 0.0121 |
| 1406.800 | 0.0107 | 0.0106 |
| 1456.600 | 0.0078 | 0.0131 |
| 1457.700 | 0.0103 | 0.0107 |
| 1497.100 | 0.0090 | 0.0106 |
| 1498.300 | 0.0084 | 0.0111 |
| 1548.900 | 0.0066 | 0.0097 |
| 1550.400 | 0.0060 | 0.0103 |
| 1613.739 | 0.0058 | 0.0080 |
| 1614.687 | 0.0061 | 0.0076 |
| 1703.458 | 0.0073 | 0.0092 |
| 1704.742 | 0.0075 | 0.0092 |
| 1742.567 | 0.0079 | 0.0107 |
| 1743.831 | 0.0089 | 0.0096 |
| 1804.625 | 0.0075 | 0.0110 |
| 1805.316 | 0.0077 | 0.0108 |
| 1871.739 | 0.0078 | 0.0107 |
| 1872.383 | 0.0094 | 0.0090 |
| 1921.593 | 0.0067 | 0.0108 |
| 1922.883 | 0.0081 | 0.0094 |
| 1996.716 | 0.0063 | 0.0088 |
| 1998.338 | 0.0057 | 0.0093 |
| 2059.495 | 0.0050 | 0.0085 |
| 2061.290 | 0.0053 | 0.0082 |
| 2136.063 | 0.0054 | 0.0058 |
| 2138.263 | 0.0053 | 0.0058 |
| 2235.729 | 0.0038 | 0.0059 |
| 2236.993 | 0.0047 | 0.0051 |
| 2438.490 | 0.0038 | 0.0064 |
| 2440.738 | 0.0047 | 0.0056 |
| 2526.767 | 0.0049 | 0.0064 |
| 2529.067 | 0.0056 | 0.0057 |
| 2617.214 | 0.0044 | 0.0082 |
| 2619.113 | 0.0061 | 0.0065 |
| 2673.462 | 0.0048 | 0.0079 |
| 2674.313 | 0.0068 | 0.0060 |
| 2774.199 | 0.0032 | 0.0049 |
| 2777.226 | 0.0038 | 0.0043 |
| 2871.098 | 0.0043 | 0.0072 |
| 2873.010 | 0.0052 | 0.0063 |
| 2923.214 | 0.0057 | 0.0073 |
| 2924.998 | 0.0060 | 0.0071 |
| 2993.971 | 0.0062 | 0.0070 |
| 2995.680 | 0.0067 | 0.0065 |
| 3094.252 | 0.0047 | 0.0066 |

| Age (years) | Biogenic_MAR ($g/cm^2/yr$) | Terrigenous_MAR ($g/cm^2/yr$) |
|---|---|---|
| 3096.376 | 0.0048 | 0.0065 |
| 3204.241 | 0.0035 | 0.0054 |
| 3206.958 | 0.0047 | 0.0042 |
| 3405.500 | 0.0038 | 0.0048 |
| 3408.100 | 0.0041 | 0.0044 |
| 3531.100 | 0.0040 | 0.0048 |
| 3533.800 | 0.0035 | 0.0054 |
| 3612.300 | 0.0035 | 0.0061 |
| 3614.800 | 0.0042 | 0.0054 |
| 3727.200 | 0.0051 | 0.0068 |
| 3729.000 | 0.0050 | 0.0069 |
| 3798.100 | 0.0060 | 0.0068 |
| 3799.900 | 0.0063 | 0.0064 |
| 3864.700 | 0.0061 | 0.0068 |
| 3866.300 | 0.0057 | 0.0072 |
| 3947.300 | 0.0050 | 0.0083 |
| 3948.200 | 0.0059 | 0.0073 |
| 4022.000 | 0.0074 | 0.0082 |
| 4022.700 | 0.0082 | 0.0075 |
| 4105.200 | 0.0078 | 0.0088 |
| 4106.600 | 0.0086 | 0.0080 |
| 4307.700 | 0.0090 | 0.0099 |
| 4308.800 | 0.0095 | 0.0094 |
| 4359.500 | 0.0097 | 0.0100 |
| 4360.200 | 0.0098 | 0.0099 |
| 4416.300 | 0.0099 | 0.0097 |
| 4417.500 | 0.0102 | 0.0095 |
| 4465.700 | 0.0104 | 0.0106 |
| 4466.800 | 0.0117 | 0.0095 |
| 4520.000 | 0.0121 | 0.0107 |
| 4520.500 | 0.0125 | 0.0103 |
| 4562.400 | 0.0117 | 0.0113 |
| 4563.400 | 0.0133 | 0.0097 |
| 4612.400 | 0.0126 | 0.0103 |
| 4613.500 | 0.0118 | 0.0111 |
| 4783.900 | 0.0118 | 0.0114 |
| 4784.900 | 0.0121 | 0.0112 |
| 4827.300 | 0.0117 | 0.0111 |
| 4828.300 | 0.0114 | 0.0115 |
| 4873.700 | 0.0121 | 0.0097 |
| 4874.800 | 0.0126 | 0.0091 |
| 4911.200 | 0.0119 | 0.0093 |
| 4912.300 | 0.0121 | 0.0092 |
| 4962.900 | 0.0101 | 0.0111 |
| 4964.000 | 0.0106 | 0.0106 |
| 5007.400 | 0.0109 | 0.0099 |
| 5008.500 | 0.0110 | 0.0098 |
| 5059.200 | 0.0107 | 0.0094 |
| 5060.400 | 0.0114 | 0.0087 |
| 5115.900 | 0.0099 | 0.0099 |
| 5116.500 | 0.0112 | 0.0086 |
| 5167.400 | 0.0088 | 0.0108 |
| 5168.600 | 0.0102 | 0.0094 |
| 5317.500 | 0.0093 | 0.0099 |
| 5318.100 | 0.0114 | 0.0078 |
| 5350.500 | 0.0100 | 0.0096 |
| 5351.600 | 0.0094 | 0.0102 |
| 5401.500 | 0.0120 | 0.0091 |
| 5402.700 | 0.0133 | 0.0079 |
| 5445.800 | 0.0123 | 0.0105 |
| 5446.900 | 0.0130 | 0.0098 |
| 5483.800 | 0.0111 | 0.0113 |
| 5484.800 | 0.0103 | 0.0121 |
| 5519.900 | 0.0106 | 0.0115 |
| 5520.900 | 0.0135 | 0.0086 |
| 5551.400 | 0.0114 | 0.0105 |
| 5551.900 | 0.0132 | 0.0087 |
| 5587.700 | 0.0116 | 0.0102 |
| 5588.700 | 0.0127 | 0.0092 |
| 5611.200 | 0.0107 | 0.0109 |
| 5611.700 | 0.0121 | 0.0095 |
| 5659.000 | 0.0123 | 0.0092 |
| 5660.100 | 0.0130 | 0.0085 |
| 5711.500 | 0.0120 | 0.0090 |
| 5712.600 | 0.0118 | 0.0091 |
| 5856.100 | 0.0111 | 0.0082 |
| 5857.400 | 0.0112 | 0.0081 |
| 5909.400 | 0.0103 | 0.0093 |
| 5910.700 | 0.0110 | 0.0087 |
| 5946.500 | 0.0101 | 0.0095 |
| 5947.700 | 0.0105 | 0.0091 |
| 5999.900 | 0.0094 | 0.0078 |
| 6001.200 | 0.0099 | 0.0074 |
| 6052.600 | 0.0081 | 0.0097 |
| 6053.900 | 0.0108 | 0.0070 |
| 6097.000 | 0.0096 | 0.0093 |
| 6098.400 | 0.0096 | 0.0093 |
| 6147.700 | 0.0096 | 0.0113 |
| 6148.800 | 0.0112 | 0.0096 |
| 6199.400 | 0.0125 | 0.0099 |
| 6200.500 | 0.0127 | 0.0097 |
| 6242.600 | 0.0129 | 0.0105 |
| 6243.700 | 0.0128 | 0.0106 |
| 6288.700 | 0.0128 | 0.0108 |
| 6289.700 | 0.0117 | 0.0119 |
| 6387.800 | 0.0127 | 0.0115 |
| 6388.800 | 0.0137 | 0.0105 |
| 6409.000 | 0.0131 | 0.0112 |

| Age (years) | Biogenic_MAR ($g/cm^2/yr$) | Terrigenous_MAR ($g/cm^2/yr$) |
|---|---|---|
| 6412.400 | 0.0138 | 0.0105 |
| 6452.100 | 0.0099 | 0.0142 |
| 6453.000 | 0.0113 | 0.0128 |
| 6487.600 | 0.0122 | 0.0116 |
| 6488.700 | 0.0111 | 0.0126 |
| 6522.800 | 0.0119 | 0.0115 |
| 6523.800 | 0.0138 | 0.0096 |
| 6571.400 | 0.0114 | 0.0114 |
| 6572.500 | 0.0110 | 0.0118 |
| 6609.200 | 0.0126 | 0.0100 |
| 6610.300 | 0.0139 | 0.0088 |
| 6648.500 | 0.0139 | 0.0093 |
| 6649.500 | 0.0129 | 0.0103 |
| 6701.300 | 0.0117 | 0.0123 |
| 6701.800 | 0.0142 | 0.0099 |
| 6739.500 | 0.0134 | 0.0100 |
| 6740.500 | 0.0136 | 0.0098 |
| 6890.224 | 0.0105 | 0.0095 |
| 6890.857 | 0.0094 | 0.0107 |
| 6940.992 | 0.0113 | 0.0105 |
| 6941.519 | 0.0106 | 0.0112 |
| 6982.728 | 0.0113 | 0.0101 |
| 6983.783 | 0.0109 | 0.0104 |
| 7028.293 | 0.0078 | 0.0123 |
| 7029.535 | 0.0097 | 0.0103 |
| 7073.616 | 0.0099 | 0.0093 |
| 7074.982 | 0.0108 | 0.0083 |
| 7139.564 | 0.0094 | 0.0091 |
| 7140.868 | 0.0095 | 0.0089 |
| 7186.702 | 0.0087 | 0.0083 |
| 7188.204 | 0.0088 | 0.0081 |
| 7248.558 | 0.0075 | 0.0081 |
| 7250.146 | 0.0079 | 0.0076 |
| 7326.693 | 0.0073 | 0.0084 |
| 7328.233 | 0.0096 | 0.0062 |
| 7382.368 | 0.0093 | 0.0072 |
| 7383.165 | 0.0096 | 0.0070 |
| 7525.388 | 0.0071 | 0.0075 |
| 7526.997 | 0.0076 | 0.0069 |
| 7618.265 | 0.0082 | 0.0070 |
| 7619.153 | 0.0082 | 0.0071 |
| 7689.876 | 0.0088 | 0.0091 |
| 7691.184 | 0.0098 | 0.0081 |
| 7736.793 | 0.0083 | 0.0101 |
| 7737.437 | 0.0087 | 0.0097 |
| 7786.895 | 0.0100 | 0.0116 |
| 7787.437 | 0.0121 | 0.0095 |
| 7837.256 | 0.0121 | 0.0109 |
| 7837.673 | 0.0107 | 0.0123 |
| 7858.089 | 0.0111 | 0.0123 |
| 7859.095 | 0.0135 | 0.0099 |
| 7906.566 | 0.0112 | 0.0133 |
| 7907.571 | 0.0140 | 0.0106 |
| 7943.913 | 0.0136 | 0.0123 |
| 7944.373 | 0.0142 | 0.0118 |
| 8050.304 | 0.0170 | 0.0154 |
| 8050.605 | 0.0154 | 0.0169 |
| 8081.835 | 0.0177 | 0.0146 |
| 8082.147 | 0.0188 | 0.0135 |
| 8116.895 | 0.0142 | 0.0174 |
| 8118.072 | 0.0190 | 0.0126 |
| 8151.535 | 0.0140 | 0.0165 |
| 8151.935 | 0.0152 | 0.0154 |
| 8184.381 | 0.0136 | 0.0159 |
| 8184.781 | 0.0165 | 0.0131 |
| 8212.123 | 0.0150 | 0.0140 |
| 8212.923 | 0.0144 | 0.0146 |
| 8246.358 | 0.0151 | 0.0136 |
| 8246.759 | 0.0139 | 0.0148 |
| 8287.199 | 0.0130 | 0.0151 |
| 8288.075 | 0.0168 | 0.0113 |
| 8324.240 | 0.0124 | 0.0140 |
| 8324.640 | 0.0144 | 0.0120 |
| 8371.582 | 0.0132 | 0.0100 |
| 8372.579 | 0.0132 | 0.0099 |
| 8496.405 | 0.0116 | 0.0079 |
| 8497.628 | 0.0094 | 0.0100 |
| 8545.696 | 0.0097 | 0.0094 |
| 8546.919 | 0.0102 | 0.0090 |
| 8596.581 | 0.0115 | 0.0074 |
| 8597.903 | 0.0089 | 0.0099 |
| 8641.990 | 0.0105 | 0.0088 |
| 8643.213 | 0.0111 | 0.0083 |
| 8695.007 | 0.0082 | 0.0127 |
| 8695.548 | 0.0100 | 0.0110 |
| 8747.748 | 0.0081 | 0.0113 |
| 8748.409 | 0.0100 | 0.0094 |
| 8820.133 | 0.0090 | 0.0094 |
| 8821.460 | 0.0112 | 0.0073 |
| 8869.301 | 0.0089 | 0.0094 |
| 8870.628 | 0.0102 | 0.0081 |
| 8936.084 | 0.0082 | 0.0111 |
| 8937.306 | 0.0112 | 0.0081 |
| 9064.864 | 0.0086 | 0.0092 |
| 9066.266 | 0.0081 | 0.0097 |
| 9125.933 | 0.0093 | 0.0076 |
| 9127.544 | 0.0093 | 0.0075 |
| 9185.709 | 0.0083 | 0.0073 |

| Age (years) | Biogenic_MAR ($g/cm^2/yr$) | Terrigenous_MAR ($g/cm^2/yr$) |
|---|---|---|
| 9187.235 | 0.0072 | 0.0084 |
| 9227.967 | 0.0068 | 0.0084 |
| 9229.683 | 0.0084 | 0.0068 |
| 9295.448 | 0.0060 | 0.0080 |
| 9297.309 | 0.0071 | 0.0069 |
| 9378.581 | 0.0056 | 0.0079 |
| 9379.474 | 0.0064 | 0.0071 |
| 9450.625 | 0.0066 | 0.0068 |
| 9452.556 | 0.0066 | 0.0069 |
| 9512.138 | 0.0076 | 0.0060 |
| 9514.055 | 0.0077 | 0.0059 |
| 9600.926 | 0.0062 | 0.0082 |
| 9602.695 | 0.0069 | 0.0074 |
| 9695.494 | 0.0069 | 0.0068 |
| 9697.325 | 0.0073 | 0.0064 |
| 9771.670 | 0.0059 | 0.0075 |
| 9772.620 | 0.0071 | 0.0063 |
| 9896.713 | 0.0053 | 0.0084 |
| 9897.686 | 0.0067 | 0.0070 |
| 9970.797 | 0.0057 | 0.0065 |
| 9972.710 | 0.0068 | 0.0053 |
| 10087.835 | 0.0048 | 0.0052 |
| 10089.133 | 0.0052 | 0.0048 |
| 10178.327 | 0.0046 | 0.0052 |
| 10181.022 | 0.0047 | 0.0052 |
| 10290.239 | 0.0041 | 0.0055 |
| 10292.744 | 0.0054 | 0.0042 |
| 10399.049 | 0.0040 | 0.0053 |
| 10401.825 | 0.0050 | 0.0043 |
| 10517.436 | 0.0046 | 0.0058 |
| 10519.931 | 0.0059 | 0.0045 |
| 10634.279 | 0.0050 | 0.0060 |
| 10636.756 | 0.0063 | 0.0048 |
| 10740.204 | 0.0058 | 0.0075 |
| 10741.177 | 0.0065 | 0.0069 |
| 10819.687 | 0.0058 | 0.0087 |
| 10821.463 | 0.0077 | 0.0068 |
| 10877.647 | 0.0055 | 0.0088 |
| 10878.550 | 0.0067 | 0.0076 |
| 10880.175 | 0.0078 | 0.0065 |
| 10962.469 | 0.0053 | 0.0090 |
| 10963.278 | 0.0063 | 0.0079 |
| 10964.995 | 0.0071 | 0.0071 |
| 11030.649 | 0.0055 | 0.0096 |
| 11031.463 | 0.0081 | 0.0070 |

| Age (years) | Ba/Ti | Age (years) | Ba/Ti | Age (years) | Ba/Ti |
|---|---|---|---|---|---|
| 56.70 | 1.26 | 1698.67 | 0.24 | 4270.30 | 0.33 |
| 125.50 | 0.54 | 1740.91 | 0.22 | 4277.10 | 0.48 |
| 157.90 | 2.11 | 1773.43 | 0.29 | 4281.55 | 0.32 |
| 188.56 | | 1807.61 | 0.21 | 4285.35 | 0.27 |
| 214.90 | 1.30 | 1847.04 | 1.86 | 4290.40 | 0.32 |
| 243.65 | 2.03 | 1877.71 | 0.38 | 4295.80 | 0.22 |
| 267.55 | 2.17 | 1913.94 | 0.35 | 4299.90 | 0.21 |
| 294.30 | 0.48 | 1954.67 | 0.36 | 4306.80 | 0.38 |
| 327.85 | 0.58 | 2002.75 | 0.32 | 4310.90 | 0.32 |
| 355.45 | 2.24 | 2031.15 | 0.21 | 4315.60 | 0.41 |
| 383.65 | 1.08 | 2075.13 | 0.38 | 4320.20 | 0.33 |
| 408.85 | 0.61 | 2128.57 | 0.26 | 4324.95 | 0.29 |
| 436.95 | 0.43 | 2182.83 | 0.31 | 4328.80 | 0.29 |
| 465.20 | 0.66 | 2246.28 | 0.40 | 4332.60 | 0.27 |
| 493.10 | 0.34 | 2407.70 | 0.20 | 4339.20 | 0.57 |
| 522.95 | 0.44 | 2471.35 | 0.36 | 4344.70 | 0.39 |
| 551.65 | 0.36 | 2528.80 | 0.32 | 4348.15 | 0.35 |
| 626.21 | 0.51 | 2586.20 | 0.34 | 4351.60 | 0.34 |
| 662.16 | 1.32 | 2636.75 | 0.22 | 4356.00 | 0.73 |
| 707.21 | 0.53 | 2691.40 | 0.30 | 4359.50 | 0.49 |
| 735.57 | 0.94 | 2752.60 | 0.62 | 4363.10 | 0.77 |
| 772.40 | 2.51 | 2833.40 | 0.24 | 4366.70 | |
| 799.16 | 0.59 | 2901.20 | 0.34 | 4370.40 | 3.31 |
| 830.70 | 0.35 | 2944.30 | 0.33 | 4373.80 | 0.80 |
| 856.66 | 1.62 | 2990.80 | 0.26 | 4377.50 | 0.55 |
| 877.37 | 1.23 | 2996.00 | 0.23 | 4381.00 | 1.02 |
| 900.31 | 0.92 | 3054.75 | 0.23 | 4385.80 | 0.51 |
| 919.49 | 0.76 | 3451.00 | 0.21 | 4389.40 | 0.69 |
| 941.80 | 0.31 | 3536.40 | 0.31 | 4394.80 | 0.60 |
| 966.92 | 0.39 | 3607.95 | 0.36 | 4398.40 | |
| 988.97 | 0.18 | 3672.00 | 0.25 | 4402.00 | 0.63 |
| 1017.97 | 0.42 | 3735.55 | 0.21 | 4405.60 | 0.68 |
| 1116.31 | 0.27 | 3786.50 | 0.41 | 4409.20 | 4.50 |
| 1139.92 | 0.27 | 3839.98 | 0.31 | 4414.60 | 0.91 |
| 1162.43 | 0.70 | 3892.80 | 0.25 | 4418.10 | |
| 1186.75 | 0.29 | 3943.50 | 0.22 | 4422.40 | 1.45 |
| 1211.38 | 0.46 | 3995.80 | 0.18 | 4425.85 | 2.29 |
| 1210.55 | 0.33 | 4044.10 | 0.22 | 4429.40 | 4.02 |
| 1237.82 | 0.20 | 4085.80 | 0.25 | 4432.85 | 36.15 |
| 1268.50 | 0.39 | 4099.85 | 0.32 | 4437.50 | 0.51 |
| 1298.52 | 0.53 | 4107.00 | 0.29 | 4443.00 | 0.37 |
| 1333.78 | 0.27 | 4111.15 | 0.20 | 4446.80 | 0.36 |
| 1362.52 | 0.43 | 4115.70 | 1.86 | 4450.60 | 0.53 |
| 1394.51 | 0.61 | 4120.35 | 0.57 | 4454.35 | 0.38 |
| 1423.71 | 0.21 | 4124.50 | 0.23 | 4458.70 | 0.49 |
| 1458.34 | 0.45 | 4129.10 | 0.32 | 4463.10 | 0.87 |
| 1494.43 | 0.22 | 4134.00 | 0.33 | 4469.70 | 0.29 |
| 1531.93 | 0.23 | 4138.60 | 0.25 | 4473.40 | 0.52 |
| 1646.03 | 0.31 | 4142.85 | 0.32 | 4477.65 | 0.48 |

| Age (years) | Ba/Ti | Age (years) | Ba/Ti | Age (years) | Ba/Ti |
|---|---|---|---|---|---|
| 4482.85 | 0.32 | 4783.10 | 0.36 | 4940.60 | 0.41 |
| 4486.20 | 0.93 | 4787.30 | 0.40 | 4943.90 | 0.50 |
| 4490.05 | 0.32 | 4790.30 | 0.30 | 4947.70 | 0.33 |
| 4493.40 | 5.23 | 4793.30 | 0.32 | 4951.25 | 0.40 |
| 4496.85 | 1.09 | 4796.95 | 0.57 | 4954.70 | 0.56 |
| 4500.70 | 18.28 | 4799.95 | 0.41 | 4959.50 | 0.32 |
| 4504.05 | 0.53 | 4803.20 | 0.40 | 4962.90 | 0.39 |
| 4507.90 | 0.28 | 4806.20 | 0.62 | 4966.35 | 0.28 |
| 4511.15 | 0.85 | 4809.95 | 0.83 | 4971.30 | 0.51 |
| 4514.13 | 0.57 | 4813.20 | 0.52 | 4976.00 | 0.40 |
| 4517.60 | 0.51 | 4816.35 | 0.45 | 4979.32 | 0.44 |
| 4520.50 |  | 4819.80 | 0.43 | 4982.75 | 0.51 |
| 4523.60 | 0.49 | 4822.95 | 0.43 | 4986.10 | 0.55 |
| 4526.85 | 0.78 | 4826.30 | 0.43 | 4991.30 | 0.36 |
| 4529.85 | 0.78 | 4830.40 | 0.38 | 4995.70 | 0.30 |
| 4532.60 | 0.61 | 4833.60 | 0.31 | 4999.60 | 0.28 |
| 4535.60 | 1.02 | 4836.65 | 0.60 | 5004.35 | 0.41 |
| 4538.85 | 0.70 | 4839.55 | 0.64 | 5007.65 | 0.33 |
| 4541.85 | 0.60 | 4844.25 | 0.91 | 5011.60 | 0.40 |
| 4544.95 | 0.51 | 4847.45 | 0.19 | 5015.80 | 0.39 |
| 4548.05 | 0.47 | 4850.65 | 0.22 | 5019.10 | 0.58 |
| 4551.10 | 0.78 | 4853.65 | 0.44 | 5022.50 | 0.48 |
| 4554.80 | 1.00 | 4856.80 | 0.67 | 5026.50 | 0.56 |
| 4557.80 | 0.70 | 4860.45 | 0.26 | 5029.80 | 0.39 |
| 4560.80 | 1.59 | 4863.03 | 0.26 | 5033.20 | 0.44 |
| 4563.90 | 1.12 | 4864.15 | 0.34 | 5054.50 | 0.45 |
| 4567.05 | 1.41 | 4867.15 | 0.44 | 5094.45 | 0.33 |
| 4571.30 | 0.55 | 4870.25 | 0.33 | 5130.50 | 0.48 |
| 4574.20 | 0.76 | 4873.45 | 0.40 | 5164.50 | 0.34 |
| 4577.30 | 1.08 | 4877.10 | 0.41 | 5316.60 | 0.39 |
| 4579.60 |  | 4880.50 | 0.46 | 5350.50 | 0.44 |
| 4582.80 | 0.70 | 4883.80 | 0.53 | 5383.30 | 0.53 |
| 4586.15 | 0.92 | 4885.20 | 0.44 | 5416.10 | 0.39 |
| 4589.15 | 1.33 | 4886.90 | 0.64 | 5445.30 | 0.32 |
| 4592.30 | 2.06 | 4890.10 | 0.22 | 5473.80 | 0.39 |
| 4595.35 | 1.53 | 4893.50 | 0.27 | 5502.15 | 0.43 |
| 4598.40 | 1.90 | 4896.90 | 0.23 | 5533.70 | 0.49 |
| 4601.45 | 0.87 | 4900.20 | 0.20 | 5565.05 | 0.50 |
| 4604.50 | 3.70 | 4903.48 | 0.19 | 5592.30 | 0.42 |
| 4608.55 | 7.02 | 4909.00 | 0.60 | 5622.60 | 0.38 |
| 4611.90 | 0.78 | 4912.30 | 0.66 | 5654.25 | 0.40 |
| 4615.10 | 1.45 | 4915.80 | 0.30 | 5687.85 | 0.37 |
| 4618.10 | 0.85 | 4920.00 | 0.46 | 5721.85 | 0.44 |
| 4621.20 | 0.81 | 4923.40 | 0.39 | 5870.00 | 0.46 |
| 4625.30 | 2.31 | 4926.80 | 0.49 | 5908.10 | 0.58 |
| 4628.40 | 0.66 | 4930.20 | 0.43 | 5939.40 | 0.34 |
| 4631.30 | 2.86 | 4933.55 | 0.61 | 5971.00 | 0.54 |
| 4635.10 | 0.90 | 4934.38 | 1.45 | 5992.76 |  |
| 4779.90 | 0.98 | 4937.35 | 0.42 | 6025.90 | 0.33 |

| Age (years) | Ba/Ti |
|---|---|
| 6061.30 | 0.33 |
| 6098.70 | 0.64 |
| 6128.60 | 0.30 |
| 6158.75 | 0.34 |
| 6256.80 | 0.49 |
| 6286.95 | 0.38 |
| 6403.70 | 0.38 |
| 6429.85 | 1.08 |
| 6458.30 | 0.68 |
| 6486.10 | 0.39 |
| 6517.65 | 0.32 |
| 6546.95 | 0.80 |
| 6585.10 | 0.28 |
| 6612.80 | 0.36 |
| 6646.05 | 0.55 |
| 6674.20 | 0.85 |
| 6702.55 | 0.51 |
| 6735.95 | 0.30 |
| 6880.00 | 0.31 |
| 6914.40 | 0.34 |
| 6942.23 | 0.44 |
| 6956.90 | 0.48 |
| 6971.47 | 0.34 |
| 6984.95 | 0.31 |
| 7000.30 | 0.28 |
| 7023.70 | 0.58 |
| 7056.60 | 0.47 |
| 7086.93 | 0.36 |
| 7124.40 | 0.35 |
| 7165.91 | 0.64 |
| 7193.80 | |
| 7226.70 | 0.28 |
| 7262.50 | 0.54 |
| 7306.90 | 0.26 |
| 7347.35 | 0.31 |
| 7391.52 | 0.29 |
| 7523.70 | 0.34 |
| 7572.80 | 0.33 |
| 7625.75 | 0.35 |
| 7664.10 | 0.38 |
| 7701.50 | 0.39 |
| 7736.18 | |
| 7770.70 | 0.46 |
| 7801.60 | 0.36 |
| 7830.70 | 0.36 |
| 7862.20 | 0.32 |
| 7891.80 | 0.40 |
| 7922.80 | 0.37 |
| 7956.90 | 0.37 |

| Age (years) | Ba/Ti |
|---|---|
| 8058.70 | 0.39 |
| 8078.90 | 0.41 |
| 8101.20 | 0.37 |
| 8123.50 | 0.28 |
| 8146.30 | 0.34 |
| 8167.65 | 0.37 |
| 8191.15 | 0.32 |
| 8213.80 | 0.47 |
| 8242.60 | 0.81 |
| 8266.50 | 0.56 |
| 8295.50 | 0.31 |
| 8318.70 | 0.38 |
| 8342.20 | 0.28 |
| 8458.85 | 0.68 |
| 8492.20 | 0.30 |
| 8526.50 | 0.35 |
| 8560.45 | 0.29 |
| 8596.80 | 0.31 |
| 8632.72 | 0.34 |
| 8667.92 | 0.57 |
| 8703.30 | 0.47 |
| 8759.15 | 0.32 |
| 8795.40 | 0.33 |
| 8831.00 | 0.44 |
| 8869.65 | 0.35 |
| 8909.50 | 0.70 |
| 9073.30 | 0.25 |
| 9109.00 | 0.45 |
| 9145.30 | 0.32 |
| 9182.67 | |
| 9217.04 | 0.58 |
| 9257.35 | 0.44 |
| 9298.60 | 0.31 |
| 9341.65 | 0.34 |
| 9386.55 | 0.35 |
| 9463.15 | 0.26 |
| 9498.15 | 0.33 |
| 9547.60 | 0.24 |
| 9593.90 | 0.25 |
| 9646.40 | 0.45 |
| 9695.60 | 0.34 |
| 9883.20 | 0.37 |
| 9956.40 | 0.89 |
| 10014.05 | 0.83 |
| 10080.50 | 0.54 |
| 10133.50 | 0.78 |
| 10206.79 | 0.47 |
| 10261.65 | 0.60 |
| 10325.15 | 0.49 |

| Age (years) | Ba/Ti |
|---|---|
| 10391.90 | 0.31 |
| 10456.20 | 0.34 |
| 10515.90 | 0.34 |
| 10568.60 | 0.66 |
| 10633.30 | 0.67 |
| 10692.30 | 0.54 |
| 10737.05 | 0.38 |
| 10783.10 | 0.48 |
| 10914.35 | 0.34 |
| 10962.40 | 0.44 |
| 11008.40 | 0.34 |
| 11053.90 | 0.34 |
| 11095.40 | 0.31 |
| 11140.90 | 0.58 |
| 11189.65 | 0.74 |
| 11238.20 | 0.37 |
| 11287.45 | 0.33 |
| 11337.40 | 0.40 |
| 11379.40 | 0.29 |

| | | Fatty acid concentration - Total ng/g of dried sediment | | | | | | |
|---|---|---|---|---|---|---|---|---|
| **Depth** | **Age (C.E.)** | **C16** | **C17** | **C18** | **C20** | **C22** | **C24** | **C26** |
| 3 | 1998.59 | 617.28 | 26.78 | 1047.10 | 18.94 | 16.98 | 28.74 | 13.72 |
| 5 | 1996.78 | 394.91 | 21.76 | 844.68 | 7.87 | 3.70 | 7.18 | 13.66 |
| 6 | 1995.88 | 484.78 | 19.23 | 626.60 | 27.24 | 63.30 | 437.50 | 77.72 |
| 7 | 1994.98 | 975.73 | 34.46 | 1386.92 | 36.73 | 60.20 | 368.41 | 68.91 |
| 8 | 1994.07 | 935.92 | 39.84 | 1603.51 | 51.23 | 57.73 | 543.99 | 62.61 |
| 9 | 1993.17 | 1042.51 | 42.94 | 1982.40 | 48.09 | 51.09 | 663.37 | 56.68 |
| 10 | 1992.27 | 37.41 | 3.72 | 180.57 | 0.00 | 4.88 | 7.67 | 0.00 |
| 12 | 1990.46 | 955.66 | 31.57 | 730.38 | 63.14 | 340.08 | 1018.80 | 439.09 |
| 13 | 1989.56 | 3004.20 | 103.73 | 5493.70 | 162.82 | 384.72 | 1042.54 | 449.05 |
| 14 | 1988.66 | 13201.00 | 455.15 | 21009.97 | 521.59 | 903.65 | 2897.01 | 918.60 |
| 15 | 1987.75 | 40.78 | 5.53 | 184.19 | 7.60 | 13.13 | 17.97 | 6.91 |
| 16 | 1986.85 | 116.25 | 6.66 | 234.83 | 15.66 | 4.33 | 8.66 | 0.00 |
| 17 | 1985.95 | 280.17 | 13.43 | 553.13 | 4.59 | 6.23 | 14.42 | 4.92 |
| 18 | 1985.04 | 731.40 | 38.25 | 1633.60 | 21.55 | 21.82 | 88.36 | 24.51 |
| 19 | 1984.14 | 2137.05 | 74.20 | 3112.72 | 93.64 | 201.56 | 654.29 | 221.40 |
| 20 | 1983.24 | 188.50 | 8.17 | 315.30 | 5.92 | 7.33 | 10.99 | 3.66 |
| 21 | 1982.33 | 26467.91 | 943.49 | 46760.06 | 1017.72 | 826.15 | 1810.34 | 658.52 |
| 22 | 1981.43 | 138.26 | 5.30 | 196.21 | 12.88 | 4.92 | 0.00 | 0.00 |
| 23 | 1980.53 | 103.37 | 8.34 | 216.94 | 7.88 | 8.81 | 13.44 | 0.00 |
| 24 | 1979.62 | 993.97 | 42.69 | 2071.59 | 37.79 | 24.52 | 58.27 | 21.06 |
| 25 | 1978.72 | 157.08 | 9.62 | 401.00 | 11.07 | 14.28 | 31.47 | 8.45 |
| 26 | 1977.82 | 487.66 | 0.00 | 348.52 | 15.46 | 19.33 | 42.52 | 9.02 |
| 27 | 1976.91 | 259.22 | 9.13 | 366.92 | 7.76 | 6.85 | 18.25 | 9.58 |
| 28 | 1976.01 | 159.03 | 0.00 | 125.20 | 0.00 | 0.00 | 15.79 | 0.00 |
| 29 | 1975.11 | 412.97 | 0.00 | 264.33 | 16.17 | 0.00 | 96.40 | 0.00 |
| 30 | 1974.20 | 373.95 | 0.00 | 229.61 | 0.00 | 0.00 | 25.17 | 0.00 |
| 31 | 1973.30 | 18.56 | 0.00 | 99.31 | 6.87 | 0.00 | 0.00 | 0.00 |
| 32 | 1972.40 | 177.85 | 8.87 | 262.81 | 7.00 | 9.80 | 21.47 | 7.47 |
| 33 | 1971.49 | 4977.01 | 133.05 | 6485.90 | 97.49 | 45.98 | 125.38 | 37.40 |
| 34 | 1970.59 | 285.33 | 0.00 | 422.91 | 13.13 | 13.46 | 63.37 | 4.27 |
| 35 | 1969.69 | 328.51 | 0.00 | 287.90 | 14.14 | 19.62 | 79.85 | 0.00 |
| 36 | 1968.78 | 291.94 | 0.00 | 270.70 | 12.08 | 12.49 | 26.24 | 5.83 |
| 37 | 1967.88 | 1887.64 | 70.53 | 4195.76 | 74.27 | 44.88 | 89.76 | 28.85 |
| 38 | 1966.98 | 4166.62 | 174.49 | 11051.62 | 219.02 | 103.38 | 195.38 | 59.55 |
| 39 | 1966.08 | 186.16 | 0.00 | 152.29 | 7.07 | 9.75 | 14.86 | 0.00 |
| 40 | 1965.17 | 1591.04 | 65.61 | 2689.37 | 81.17 | 153.06 | 407.56 | 179.96 |
| 41 | 1964.27 | 4956.65 | 170.70 | 8283.80 | 181.67 | 118.54 | 267.18 | 93.03 |
| 42 | 1963.37 | 1783.00 | 60.04 | 2797.35 | 52.32 | 46.29 | 101.99 | 31.59 |
| 43 | 1962.46 | 4197.35 | 119.66 | 5173.38 | 87.03 | 39.16 | 89.37 | 37.82 |
| 44 | 1961.56 | 1908.01 | 60.33 | 2881.07 | 58.37 | 50.09 | 126.10 | 49.65 |
| 45 | 1960.66 | 2840.57 | 97.40 | 4605.32 | 76.06 | 49.80 | 130.24 | 48.70 |
| 46 | 1959.75 | 1148.21 | 40.03 | 1861.00 | 43.30 | 56.37 | 150.32 | 54.33 |
| 47 | 1958.85 | 2984.42 | 80.41 | 2940.10 | 43.86 | 36.55 | 78.59 | 29.70 |
| 48 | 1957.95 | 2262.36 | 73.74 | 3127.56 | 68.12 | 79.86 | 212.02 | 58.94 |
| 49 | 1957.04 | 1320.75 | 46.62 | 1949.69 | 51.00 | 86.99 | 249.69 | 84.17 |
| 50 | 1956.14 | 294.19 | 10.41 | 302.00 | 9.98 | 23.00 | 29.94 | 6.07 |
| 52 | 1954.33 | 117.87 | 0.00 | 60.98 | 3.42 | 4.61 | 4.78 | 0.00 |
| 54 | 1952.53 | 1320.94 | 39.14 | 1671.18 | 24.84 | 15.05 | 27.35 | 13.55 |

| | | | | | | | | |
|---|---|---|---|---|---|---|---|---|
| 56 | 1950.72 | 149.73 | 5.46 | 216.92 | 6.50 | 9.75 | 23.77 | 8.27 |
| 58 | 1948.91 | 1103.51 | 34.82 | 1723.65 | 28.54 | 15.37 | 31.99 | 14.12 |
| 60 | 1947.11 | 392.18 | 11.21 | 205.87 | 20.28 | 78.48 | 156.97 | 27.91 |
| 62 | 1945.30 | 123.62 | 3.24 | 95.79 | 4.21 | 10.84 | 18.12 | 3.72 |
| 64 | 1943.50 | 95.80 | 3.40 | 112.30 | 3.40 | 7.76 | 8.97 | 3.64 |
| 66 | 1941.69 | 40.87 | 4.15 | 21.32 | 3.85 | 18.36 | 32.28 | 5.33 |
| 68 | 1939.88 | 1287.94 | 37.75 | 546.13 | 23.76 | 30.96 | 62.73 | 13.04 |
| 70 | 1938.08 | 1615.31 | 51.64 | 1777.10 | 52.60 | 66.48 | 129.46 | 48.62 |
| 72 | 1936.27 | 75.48 | 0.00 | 43.82 | 2.11 | 2.35 | 2.35 | 0.00 |
| 74 | 1934.46 | 968.86 | 29.67 | 1154.72 | 32.12 | 55.08 | 97.58 | 36.82 |
| 76 | 1932.66 | 434.44 | 12.22 | 241.50 | 14.28 | 36.81 | 36.18 | 7.30 |
| 78 | 1930.85 | 534.17 | 18.89 | 338.88 | 20.09 | 35.76 | 77.69 | 17.55 |
| 80 | 1929.04 | 394.56 | 11.51 | 400.32 | 12.79 | 17.27 | 36.45 | 11.51 |
| 82 | 1927.24 | 406.46 | 7.96 | 95.48 | 11.27 | 18.90 | 31.16 | 11.60 |
| 84 | 1925.43 | 217.64 | 0.00 | 125.37 | 8.39 | 12.02 | 13.15 | 3.40 |
| 86 | 1923.62 | 410.70 | 12.66 | 368.43 | 11.22 | 14.09 | 18.62 | 5.73 |
| 88 | 1921.82 | 107.92 | 3.07 | 54.62 | 3.95 | 7.02 | 11.85 | 5.26 |
| 90 | 1920.01 | 185.86 | 6.82 | 319.95 | 6.06 | 4.55 | 6.82 | 4.55 |
| 92 | 1918.21 | 244.52 | 7.92 | 326.77 | 5.16 | 3.44 | 3.96 | 2.58 |
| 94 | 1916.40 | 297.41 | 0.00 | 178.44 | 8.75 | 10.79 | 15.16 | 0.00 |
| 96 | 1914.59 | 453.68 | 13.14 | 471.26 | 7.28 | 4.24 | 9.90 | 6.26 |
| 98 | 1912.79 | 136.14 | 4.81 | 133.26 | 7.22 | 9.86 | 26.22 | 5.29 |
| 100 | 1910.98 | 163.75 | 5.34 | 167.16 | 4.54 | 7.38 | 17.72 | 8.18 |
| 105 | 1906.46 | 381.57 | 12.57 | 432.08 | 8.30 | 8.77 | 17.79 | 10.20 |
| 110 | 1901.95 | 232.42 | 7.82 | 324.70 | 8.72 | 9.09 | 16.49 | 5.96 |
| 115 | 1897.43 | 700.39 | 19.91 | 783.66 | 16.29 | 15.96 | 22.87 | 11.19 |
| 120 | 1892.92 | 118.08 | 6.70 | 61.16 | 4.25 | 11.23 | 34.64 | 9.34 |
| 125 | 1888.40 | 361.78 | 8.04 | 110.82 | 10.86 | 27.63 | 37.93 | 8.74 |
| 130 | 1883.88 | 98.17 | 5.45 | 44.26 | 7.13 | 16.57 | 42.37 | 7.76 |
| 135 | 1879.37 | 246.26 | 7.05 | 84.87 | 8.36 | 16.71 | 20.37 | 7.31 |
| 140 | 1874.85 | 581.96 | 18.14 | 430.89 | 12.79 | 15.76 | 27.06 | 7.14 |
| 145 | 1870.34 | 393.66 | 1.92 | 81.25 | 8.61 | 20.29 | 26.70 | 6.80 |
| 150 | 1865.82 | 1020.33 | 153.38 | 836.99 | 30.14 | 100.50 | 200.55 | 37.27 |
| 155 | 1861.30 | 1439.52 | 44.28 | 1857.40 | 40.70 | 42.41 | 107.59 | 33.68 |
| 160 | 1856.79 | 542.05 | 15.81 | 590.64 | 18.16 | 36.62 | 73.83 | 25.33 |
| 166 | 1851.37 | 483.89 | 11.66 | 115.93 | 14.78 | 49.74 | 43.29 | 8.95 |
| 170 | 1847.76 | 2482.48 | 70.08 | 2913.44 | 62.70 | 96.09 | 46.59 | 5.63 |
| 175 | 1843.24 | 904.18 | 25.59 | 977.59 | 26.18 | 28.04 | 49.91 | 18.38 |
| 180 | 1838.72 | 470.93 | 57.89 | 583.72 | 31.93 | 33.70 | 35.20 | 10.92 |
| 185 | 1834.21 | 501.73 | 14.14 | 440.97 | 19.10 | 44.94 | 91.39 | 25.75 |
| 190 | 1829.69 | 166.39 | 4.52 | 83.20 | 9.59 | 58.80 | 33.58 | 4.25 |
| 195 | 1825.18 | 1146.66 | 23.16 | 745.00 | 41.69 | 71.97 | 120.66 | 31.83 |
| 200 | 1820.66 | 500.80 | 12.21 | 401.02 | 21.00 | 66.01 | 172.92 | 41.17 |
| 205 | 1816.14 | 310.91 | 9.67 | 351.67 | 12.50 | 24.10 | 61.14 | 15.32 |
| 210 | 1811.63 | 784.68 | 24.57 | 1043.80 | 30.37 | 40.52 | 100.43 | 37.62 |
| 215 | 1807.11 | 456.18 | 7.08 | 121.14 | 16.20 | 46.04 | 74.68 | 17.05 |
| 220 | 1802.60 | 1006.29 | 24.73 | 853.02 | 39.65 | 114.17 | 327.04 | 80.42 |
| 225 | 1798.08 | 545.82 | 10.49 | 324.05 | 23.82 | 96.85 | 203.15 | 48.19 |
| 230 | 1793.56 | 541.52 | 10.82 | 282.26 | 22.75 | 69.62 | 173.17 | 50.72 |
| 235 | 1789.05 | 155.47 | 4.30 | 62.31 | 9.79 | 32.93 | 51.77 | 8.75 |

| | | | | | | | | |
|---|---|---|---|---|---|---|---|---|
| 240 | 1784.53 | 221.47 | 7.43 | 67.90 | 18.63 | 78.61 | 221.19 | 74.89 |
| 245 | 1780.02 | 930.89 | 7.62 | 96.43 | 15.12 | 59.47 | 114.85 | 29.00 |
| 250 | 1775.50 | 249.93 | 7.64 | 77.85 | 14.70 | 59.81 | 121.51 | 44.67 |
| 255 | 1770.98 | 226.16 | 5.94 | 78.83 | 17.10 | 59.17 | 86.13 | 13.09 |
| 260 | 1766.47 | 210.13 | 5.28 | 39.91 | 8.00 | 41.27 | 67.53 | 9.96 |
| 265 | 1761.95 | 243.87 | 8.24 | 84.72 | 11.70 | 37.63 | 63.94 | 13.11 |
| 270 | 1757.44 | 1237.53 | 32.36 | 1313.67 | 52.03 | 83.99 | 181.08 | 51.14 |
| 275 | 1752.92 | 1395.35 | 43.09 | 1881.14 | 38.08 | 27.76 | 47.94 | 15.48 |
| 280 | 1748.40 | 201.65 | 5.12 | 85.83 | 8.71 | 23.06 | 39.46 | 10.51 |
| 285 | 1743.89 | 284.75 | 8.25 | 260.18 | 13.24 | 35.73 | 95.11 | 28.73 |
| 290 | 1739.37 | 956.77 | 43.96 | 1871.28 | 40.59 | 44.80 | 109.54 | 39.18 |
| 295 | 1734.86 | 828.64 | 147.73 | 1039.09 | 32.27 | 66.01 | 183.29 | 40.43 |
| 300 | 1730.34 | 214.77 | 7.23 | 136.04 | 9.02 | 13.81 | 12.97 | 9.96 |
| 305 | 1725.82 | 71.82 | 2.84 | 25.12 | 4.93 | 12.56 | 14.50 | 1.94 |
| 310 | 1721.31 | 156.05 | 7.09 | 180.78 | 10.71 | 17.64 | 13.07 | 6.93 |
| 315 | 1716.79 | 293.19 | 7.51 | 171.91 | 14.66 | 29.83 | 26.08 | 2.09 |
| 320 | 1712.28 | 293.31 | 10.38 | 134.91 | 15.84 | 40.42 | 37.14 | 12.67 |
| 325 | 1707.76 | 145.55 | 5.18 | 109.01 | 7.36 | 17.66 | 26.52 | 7.29 |
| 330 | 1703.24 | 409.51 | 26.61 | 151.54 | 18.51 | 46.27 | 77.51 | 25.45 |
| 335 | 1698.73 | 127.06 | 5.71 | 77.02 | 11.49 | 25.96 | 33.78 | 7.58 |
| 340 | 1694.21 | 48.25 | 2.64 | 34.34 | 6.52 | 29.65 | 67.80 | 18.23 |
| 345 | 1689.70 | 231.40 | 7.85 | 152.69 | 16.95 | 52.64 | 134.38 | 44.69 |
| 350 | 1685.18 | 24.07 | 1.85 | 18.88 | 2.22 | 3.95 | 4.20 | 2.10 |
| 355 | 1680.66 | 581.96 | 0.00 | 363.82 | 18.41 | 41.97 | 787.05 | 17.37 |
| 361 | 1675.24 | 157.38 | 5.19 | 141.33 | 5.65 | 9.32 | 9.47 | 2.60 |
| 365 | 1671.63 | 257.81 | 8.74 | 215.78 | 11.48 | 20.52 | 20.83 | 4.33 |
| 370 | 1667.12 | 496.89 | 20.03 | 854.47 | 19.78 | 42.34 | 27.76 | 61.39 |
| 375 | 1662.60 | 432.64 | 10.08 | 159.97 | 22.42 | 59.74 | 62.58 | 6.66 |
| 380 | 1658.08 | 403.57 | 0.00 | 198.65 | 12.22 | 33.90 | 70.07 | 23.79 |
| 385 | 1653.57 | 321.24 | 0.00 | 129.93 | 20.53 | 72.77 | 549.04 | 40.88 |
| 390 | 1649.05 | 322.79 | 0.00 | 172.08 | 14.78 | 45.15 | 86.45 | 23.71 |
| 395 | 1644.54 | 273.41 | 4.52 | 57.29 | 9.30 | 33.65 | 47.54 | 6.91 |
| 400 | 1640.02 | 209.78 | 0.00 | 81.24 | 6.69 | 17.30 | 36.16 | 11.69 |
| 405 | 1635.50 | 249.46 | 0.00 | 195.92 | 7.98 | 17.75 | 38.20 | 13.47 |
| 411 | 1630.08 | 221.92 | 6.25 | 82.35 | 11.75 | 34.74 | 45.86 | 8.25 |
| 415 | 1626.47 | 396.08 | 0.00 | 114.31 | 10.49 | 26.32 | 42.60 | 16.98 |
| 421 | 1621.05 | 308.59 | 10.48 | 288.38 | 8.23 | 16.71 | 26.94 | 10.23 |
| 425 | 1617.44 | 316.56 | 0.00 | 369.32 | 15.20 | 24.13 | 58.55 | 21.03 |
| 431 | 1612.02 | 113.30 | 4.98 | 94.06 | 8.15 | 14.04 | 13.02 | 3.17 |
| 435 | 1608.41 | 140.52 | 0.00 | 66.76 | 10.04 | 18.74 | 28.13 | 4.83 |
| 440 | 1603.89 | 174.18 | 7.32 | 127.60 | 13.09 | 57.49 | 183.53 | 43.16 |
| 445 | 1599.38 | 283.11 | 0.00 | 156.37 | 10.80 | 35.09 | 75.58 | 21.49 |
| 449 | 1595.76 | 252.49 | 0.00 | 271.49 | 13.57 | 24.43 | 27.15 | 0.00 |
| 454 | 1591.25 | 702.88 | 0.00 | 527.99 | 0.00 | 48.78 | 100.06 | 41.16 |
| 458 | 1587.63 | 781.89 | 0.00 | 856.14 | 33.93 | 99.72 | 313.15 | 146.49 |

| | | C18 fatty acid d13C | | | | |
|---|---|---|---|---|---|---|
| Depth (cm) top | Age (C.E.) | d13C (‰) FAME 1 | d13C (‰) FAME 2 | average FAME d13C (‰) | Corrected FA d13C (‰) | error (‰) |
| 3 | 1998.59 | -26.20 | -26.28 | -26.24 | -25.43 | 0.04 |
| 5 | 1996.78 | -25.64 | -25.98 | -25.81 | -24.97 | 0.17 |
| 6 | 1995.88 | -27.83 | -27.59 | -27.71 | -26.98 | 0.12 |
| 7 | 1994.98 | -27.10 | -27.14 | -27.12 | -26.36 | 0.02 |
| 8 | 1994.07 | -27.61 | -27.46 | -27.54 | -26.80 | 0.07 |
| 9 | 1993.17 | -27.53 | -27.48 | -27.51 | -26.77 | 0.02 |
| 10 | 1992.27 | -24.86 | -24.82 | -24.84 | -23.95 | 0.02 |
| 12 | 1990.46 | -27.40 | -27.50 | -27.45 | -26.71 | 0.05 |
| 13 | 1989.56 | -27.32 | -27.35 | -27.34 | -26.59 | 0.02 |
| 14 | 1988.66 | -27.57 | -27.53 | -27.55 | -26.81 | 0.02 |
| 15 | 1987.75 | -25.08 | -25.48 | -25.28 | -24.42 | 0.20 |
| 16 | 1986.85 | -24.80 | -24.70 | -24.75 | -23.86 | 0.05 |
| 17 | 1985.95 | -24.92 | -25.09 | -25.01 | -24.13 | 0.08 |
| 18 | 1985.04 | -26.05 | -25.94 | -26.00 | -25.17 | 0.05 |
| 19 | 1984.14 | -27.73 | -27.51 | -27.62 | -26.89 | 0.11 |
| 20 | 1983.24 | -24.87 | -24.95 | -24.91 | -24.03 | 0.04 |
| 21 | 1982.33 | -27.20 | -27.20 | -27.20 | -26.44 | 0.00 |
| 22 | 1981.43 | -24.54 | -24.74 | -24.64 | -23.74 | 0.10 |
| 23 | 1980.53 | -25.30 | -25.19 | -25.24 | -24.38 | 0.05 |
| 24 | 1979.62 | -26.47 | -26.61 | -26.54 | -25.75 | 0.07 |
| 25 | 1978.72 | -26.39 | -26.40 | -26.40 | -25.60 | 0.01 |
| 26 | 1977.82 | -28.57 | -28.64 | -28.61 | -27.93 | 0.04 |
| 27 | 1976.91 | -26.45 | -26.43 | -26.44 | -25.64 | 0.01 |
| 28 | 1976.01 | -28.24 | -28.06 | -28.15 | -27.45 | 0.09 |
| 30 | 1974.20 | -29.53 | -29.24 | -29.38 | -28.75 | 0.14 |
| 32 | 1972.40 | -26.20 | -26.48 | -26.34 | -25.54 | 0.14 |
| 33 | 1971.49 | -26.40 | -26.40 | -26.40 | -25.60 | 0.00 |
| 35 | 1969.69 | -27.12 | N/A | -27.12 | -26.36 | 0.26 |
| 36 | 1968.78 | -28.42 | -28.55 | -28.48 | -27.80 | 0.07 |
| 37 | 1967.88 | -26.46 | -26.61 | -26.53 | -25.74 | 0.07 |
| 38 | 1966.98 | -26.65 | -26.71 | -26.68 | -25.90 | 0.03 |
| 39 | 1966.08 | -28.75 | -28.90 | -28.82 | -28.16 | 0.08 |
| 40 | 1965.17 | -26.61 | -26.68 | -26.64 | -25.86 | 0.04 |
| 41 | 1964.27 | -27.06 | -26.96 | -27.01 | -26.24 | 0.05 |
| 42 | 1963.37 | -26.63 | -26.74 | -26.68 | -25.90 | 0.06 |
| 43 | 1962.46 | -26.34 | -26.41 | -26.37 | -25.57 | 0.04 |
| 44 | 1961.56 | -26.56 | -26.50 | -26.53 | -25.74 | 0.03 |
| 45 | 1960.66 | -26.23 | -26.37 | -26.30 | -25.49 | 0.07 |
| 46 | 1959.75 | -26.39 | -26.51 | -26.45 | -25.66 | 0.06 |
| 47 | 1958.85 | -26.08 | -26.14 | -26.11 | -25.30 | 0.03 |
| 48 | 1957.95 | -26.62 | -26.58 | -26.60 | -25.81 | 0.02 |
| 49 | 1957.04 | -26.54 | -26.58 | -26.56 | -25.77 | 0.02 |
| 50 | 1956.14 | -26.69 | N/A | -26.69 | -25.90 | 0.26 |
| 52 | 1954.33 | -28.76 | -29.15 | -28.95 | -28.30 | 0.19 |
| 54 | 1952.53 | -26.33 | -26.12 | -26.23 | -25.42 | 0.10 |
| 56 | 1950.72 | -26.08 | -25.80 | -25.94 | -25.12 | 0.14 |
| 58 | 1948.91 | -26.58 | -26.59 | -26.58 | -25.79 | 0.01 |

| | | | | | | |
|---|---|---|---|---|---|---|
| 60 | 1947.11 | -26.63 | -26.51 | -26.57 | -25.78 | 0.06 |
| 62 | 1945.30 | -26.77 | -26.70 | -26.74 | -25.95 | 0.04 |
| 64 | 1943.50 | -26.32 | -25.95 | -26.13 | -25.32 | 0.19 |
| 66 | 1941.69 | -28.60 | N/A | -28.60 | -27.92 | 0.26 |
| 68 | 1939.88 | -28.52 | -28.61 | -28.57 | -27.89 | 0.05 |
| 70 | 1938.08 | -26.56 | -26.60 | -26.58 | -25.79 | 0.02 |
| 72 | 1936.27 | -29.71 | -30.18 | -29.95 | -29.34 | 0.23 |
| 74 | 1934.46 | -26.70 | -26.72 | -26.71 | -25.93 | 0.01 |
| 76 | 1932.66 | -27.10 | -27.21 | -27.15 | -26.40 | 0.05 |
| 78 | 1930.85 | -27.10 | -27.10 | -27.10 | -26.34 | 0.00 |
| 80 | 1929.04 | -26.36 | -26.88 | -26.62 | -25.83 | 0.26 |
| 82 | 1927.24 | -25.91 | -25.78 | -25.84 | -25.01 | 0.06 |
| 84 | 1925.43 | -29.15 | -29.67 | -29.41 | -28.78 | 0.26 |
| 86 | 1923.62 | -26.72 | -26.62 | -26.67 | -25.88 | 0.05 |
| 88 | 1921.82 | -28.21 | -28.08 | -28.15 | -27.44 | 0.06 |
| 90 | 1920.01 | -26.55 | -26.56 | -26.55 | -25.76 | 0.01 |
| 92 | 1918.21 | -26.20 | -26.31 | -26.26 | -25.45 | 0.05 |
| 96 | 1914.59 | -26.30 | -26.36 | -26.33 | -25.52 | 0.03 |
| 98 | 1912.79 | -26.75 | -26.67 | -26.71 | -25.93 | 0.04 |
| 100 | 1910.98 | -27.00 | N/A | -27.00 | -26.23 | 0.26 |
| 105 | 1906.46 | -26.60 | -26.62 | -26.61 | -25.82 | 0.01 |
| 110 | 1901.95 | -26.46 | -26.58 | -26.52 | -25.73 | 0.06 |
| 115 | 1897.43 | -26.65 | -26.61 | -26.63 | -25.84 | 0.02 |
| 120 | 1892.92 | -25.00 | -24.99 | -24.99 | -24.11 | 0.01 |
| 125 | 1888.40 | -25.99 | -25.83 | -25.91 | -25.08 | 0.08 |
| 130 | 1883.88 | -26.90 | -27.31 | -27.10 | -26.34 | 0.21 |
| 135 | 1879.37 | -27.42 | N/A | -27.42 | -26.67 | 0.26 |
| 140 | 1874.85 | -26.49 | -26.63 | -26.56 | -25.77 | 0.07 |
| 145 | 1870.34 | -26.63 | -26.44 | -26.53 | -25.74 | 0.09 |
| 150 | 1865.82 | -26.82 | -27.00 | -26.91 | -26.14 | 0.09 |
| 155 | 1861.30 | -26.27 | -26.33 | -26.30 | -25.49 | 0.03 |
| 160 | 1856.79 | -26.61 | -26.67 | -26.64 | -25.85 | 0.03 |
| 170 | 1847.76 | -26.53 | -26.45 | -26.49 | -25.70 | 0.04 |
| 175 | 1843.24 | -26.50 | -26.71 | -26.61 | -25.82 | 0.10 |
| 180 | 1838.72 | -26.50 | -26.70 | -26.60 | -25.81 | 0.10 |
| 185 | 1834.21 | -26.73 | -26.61 | -26.67 | -25.88 | 0.06 |
| 190 | 1829.69 | -27.33 | -27.26 | -27.29 | -26.54 | 0.04 |
| 195 | 1825.18 | -26.23 | -26.28 | -26.25 | -25.44 | 0.03 |
| 200 | 1820.66 | -26.43 | -26.67 | -26.55 | -25.76 | 0.12 |
| 205 | 1816.14 | -26.50 | -26.58 | -26.54 | -25.75 | 0.04 |
| 210 | 1811.63 | -26.40 | -26.41 | -26.41 | -25.61 | 0.01 |
| 215 | 1807.11 | -26.97 | -26.72 | -26.84 | -26.07 | 0.12 |
| 220 | 1802.60 | -26.59 | -26.53 | -26.56 | -25.77 | 0.03 |
| 225 | 1798.08 | -26.99 | -27.08 | -27.04 | -26.27 | 0.05 |
| 230 | 1793.56 | -27.03 | -27.14 | -27.09 | -26.33 | 0.06 |
| 235 | 1789.05 | -27.59 | -27.85 | -27.72 | -26.99 | 0.13 |
| 240 | 1784.53 | -26.08 | -25.87 | -25.98 | -25.15 | 0.10 |
| 245 | 1780.02 | -26.14 | -25.95 | -26.04 | -25.22 | 0.10 |
| 250 | 1775.50 | -28.13 | -28.03 | -28.08 | -27.37 | 0.05 |
| 255 | 1770.98 | -27.40 | -27.64 | -27.52 | -26.78 | 0.12 |

| | | | | | | |
|---|---|---|---|---|---|---|
| 260 | 1766.47 | -26.01 | -26.08 | -26.04 | -25.22 | 0.04 |
| 265 | 1761.95 | -27.93 | N/A | -27.93 | -27.21 | 0.26 |
| 270 | 1757.44 | -26.63 | -26.58 | -26.60 | -25.81 | 0.03 |
| 275 | 1752.92 | -26.59 | -26.60 | -26.59 | -25.80 | 0.01 |
| 280 | 1748.40 | -28.07 | N/A | -28.07 | -27.37 | 0.26 |
| 290 | 1739.37 | -26.20 | -26.38 | -26.29 | -25.49 | 0.09 |
| 295 | 1734.86 | -26.79 | -26.84 | -26.82 | -26.04 | 0.03 |
| 300 | 1730.34 | -27.06 | -27.07 | -27.07 | -26.30 | 0.01 |
| 305 | 1725.82 | -27.99 | -27.76 | -27.88 | -27.16 | 0.11 |
| 310 | 1721.31 | -26.91 | -26.80 | -26.86 | -26.08 | 0.05 |
| 315 | 1716.79 | -26.44 | -26.42 | -26.43 | -25.63 | 0.01 |
| 320 | 1712.28 | -27.21 | N/A | -27.21 | -26.45 | 0.26 |
| 325 | 1707.76 | -26.91 | -27.06 | -26.98 | -26.22 | 0.08 |
| 330 | 1703.24 | -27.35 | -26.98 | -27.16 | -26.41 | 0.19 |
| 335 | 1698.73 | -26.51 | -26.30 | -26.41 | -25.61 | 0.11 |
| 340 | 1694.21 | -27.66 | -27.53 | -27.59 | -26.86 | 0.07 |
| 345 | 1689.70 | -27.32 | -27.16 | -27.24 | -26.49 | 0.08 |
| 350 | 1685.18 | -26.72 | N/A | -26.72 | -25.94 | 0.26 |
| 355 | 1680.66 | -27.76 | -27.82 | -27.79 | -27.07 | 0.03 |
| 361 | 1675.24 | -26.34 | -26.28 | -26.31 | -25.50 | 0.03 |
| 365 | 1671.63 | -25.39 | -25.33 | -25.36 | -24.50 | 0.03 |
| 370 | 1667.12 | -26.14 | -26.16 | -26.15 | -25.34 | 0.01 |
| 375 | 1662.60 | -27.23 | -27.38 | -27.30 | -26.55 | 0.08 |
| 380 | 1658.08 | -28.66 | -28.60 | -28.63 | -27.96 | 0.03 |
| 385 | 1653.57 | -29.03 | -29.16 | -29.10 | -28.45 | 0.06 |
| 390 | 1649.05 | -28.58 | -28.38 | -28.48 | -27.80 | 0.10 |
| 395 | 1644.54 | -27.26 | -27.18 | -27.22 | -26.46 | 0.04 |
| 400 | 1640.02 | -28.92 | -28.89 | -28.91 | -28.24 | 0.02 |
| 405 | 1635.50 | -27.86 | -27.67 | -27.76 | -27.04 | 0.09 |
| 411 | 1630.08 | -27.23 | N/A | -27.23 | -26.47 | 0.26 |
| 415 | 1626.47 | -28.72 | -28.55 | -28.64 | -27.96 | 0.09 |
| 421 | 1621.05 | -26.38 | -26.48 | -26.43 | -25.63 | 0.05 |
| 425 | 1617.44 | -27.52 | -27.56 | -27.54 | -26.80 | 0.02 |
| 431 | 1612.02 | -27.79 | -27.80 | -27.80 | -27.08 | 0.01 |
| 435 | 1608.41 | -28.60 | -28.49 | -28.54 | -27.86 | 0.06 |
| 440 | 1603.89 | -27.44 | -27.45 | -27.45 | -26.71 | 0.01 |
| 445 | 1599.38 | -28.86 | -28.98 | -28.92 | -28.26 | 0.06 |
| 449 | 1595.76 | -25.87 | -26.32 | -26.10 | -25.28 | 0.22 |
| 454 | 1591.25 | -29.08 | -28.83 | -28.95 | -28.29 | 0.12 |
| 458 | 1587.63 | -27.58 | -27.61 | -27.59 | -26.86 | 0.02 |

| | | C24 fatty acid d13C | | | | |
|---|---|---|---|---|---|---|
| Depth (cm) top | Age (years) | d13C (‰) FAME 1 | d13C (‰) FAME 2 | average FAME d13C (‰) | Corrected FA d13C (‰) | error (‰) |
| 3 | 1998.59 | -29.78 | N/A | -29.78 | -29.32 | |
| 6 | 1995.88 | -30.24 | -30.00 | -30.12 | -29.68 | 0.12 |
| 7 | 1994.98 | -29.88 | -29.89 | -29.89 | -29.43 | 0.01 |
| 8 | 1994.07 | -30.17 | -29.77 | -29.97 | -29.52 | 0.20 |
| 9 | 1993.17 | -30.07 | -29.98 | -30.03 | -29.58 | 0.04 |
| 12 | 1990.46 | -28.89 | -29.06 | -28.98 | -28.48 | 0.09 |
| 13 | 1989.56 | -30.26 | -29.87 | -30.07 | -29.62 | 0.20 |
| 14 | 1988.66 | -29.02 | -29.00 | -29.01 | -28.52 | 0.01 |
| 18 | 1985.04 | -27.55 | N/A | -27.55 | -26.99 | |
| 19 | 1984.14 | -29.26 | -29.41 | -29.33 | -28.86 | 0.07 |
| 21 | 1982.33 | -28.66 | -28.68 | -28.67 | -28.17 | 0.01 |
| 24 | 1979.62 | -27.23 | -27.57 | -27.40 | -26.84 | 0.17 |
| 37 | 1967.88 | -28.25 | -27.85 | -28.05 | -27.52 | 0.20 |
| 38 | 1966.98 | -28.74 | -29.04 | -28.89 | -28.40 | 0.15 |
| 40 | 1965.17 | -28.61 | -28.61 | -28.61 | -28.10 | 0.00 |
| 42 | 1963.37 | -28.96 | -29.00 | -28.98 | -28.49 | 0.02 |
| 44 | 1961.56 | -28.97 | -28.73 | -28.85 | -28.36 | 0.12 |
| 45 | 1960.66 | -28.07 | -28.26 | -28.17 | -27.64 | 0.09 |
| 46 | 1959.75 | -28.09 | -28.39 | -28.24 | -27.72 | 0.15 |
| 47 | 1958.85 | -27.83 | -28.32 | -28.07 | -27.54 | 0.25 |
| 48 | 1957.95 | -28.63 | -28.40 | -28.52 | -28.01 | 0.11 |
| 49 | 1957.04 | -28.00 | -27.91 | -27.95 | -27.42 | 0.05 |
| 50 | 1956.14 | -28.63 | N/A | -28.63 | -28.12 | |
| 54 | 1952.53 | -29.02 | N/A | -29.02 | -28.53 | |
| 56 | 1950.72 | -28.69 | N/A | -28.69 | -28.19 | |
| 58 | 1948.91 | -28.58 | N/A | -28.58 | -28.07 | |
| 60 | 1947.11 | -26.97 | -27.03 | -27.00 | -26.42 | 0.03 |
| 62 | 1945.30 | -27.58 | N/A | -27.58 | -27.03 | |
| 66 | 1941.69 | -27.21 | N/A | -27.21 | -26.64 | |
| 68 | 1939.88 | -28.77 | -28.55 | -28.66 | -28.15 | 0.11 |
| 70 | 1938.08 | -27.73 | -27.68 | -27.71 | -27.16 | 0.03 |
| 74 | 1934.46 | -28.62 | -28.39 | -28.51 | -28.00 | 0.11 |
| 76 | 1932.66 | -27.79 | -27.78 | -27.79 | -27.25 | 0.01 |
| 78 | 1930.85 | -27.22 | -27.22 | -27.22 | -26.65 | 0.00 |
| 80 | 1929.04 | -27.16 | N/A | -27.16 | -26.60 | |
| 82 | 1927.24 | -28.20 | -27.75 | -27.98 | -27.44 | 0.22 |
| 86 | 1923.62 | -28.25 | N/A | -28.25 | -27.73 | |
| 98 | 1912.79 | -28.25 | N/A | -28.25 | -27.73 | |
| 100 | 1910.98 | -28.22 | -28.31 | -28.26 | -27.74 | 0.05 |
| 105 | 1906.46 | -28.40 | N/A | -28.40 | -27.89 | |
| 110 | 1901.95 | -27.19 | -27.36 | -27.27 | -26.71 | 0.09 |
| 115 | 1897.43 | -29.32 | N/A | -29.32 | -28.84 | |
| 120 | 1892.92 | -26.78 | -27.07 | -26.93 | -26.35 | 0.14 |
| 125 | 1888.40 | -28.34 | -28.56 | -28.45 | -27.94 | 0.11 |
| 130 | 1883.88 | -26.46 | -26.18 | -26.32 | -25.72 | 0.14 |
| 135 | 1879.37 | -27.33 | N/A | -27.33 | -26.77 | |
| 145 | 1870.34 | -27.76 | -27.89 | -27.83 | -27.29 | 0.06 |

| | | | | | | |
|---|---|---|---|---|---|---|
| 150 | 1865.82 | -27.75 | -27.75 | -27.75 | -27.21 | 0.00 |
| 155 | 1861.30 | -28.15 | -28.10 | -28.13 | -27.60 | 0.02 |
| 160 | 1856.79 | -28.51 | -28.61 | -28.56 | -28.05 | 0.05 |
| 166 | 1851.37 | -28.13 | -28.65 | -28.39 | -27.87 | 0.26 |
| 170 | 1847.76 | -30.18 | N/A | -30.18 | -29.74 | |
| 175 | 1843.24 | -28.71 | -28.86 | -28.79 | -28.29 | 0.07 |
| 180 | 1838.72 | -27.72 | -27.94 | -27.83 | -27.29 | 0.11 |
| 185 | 1834.21 | -27.88 | -28.10 | -27.99 | -27.46 | 0.11 |
| 190 | 1829.69 | -28.66 | -28.19 | -28.42 | -27.91 | 0.24 |
| 200 | 1820.66 | -27.77 | -27.72 | -27.75 | -27.20 | 0.03 |
| 205 | 1816.14 | -28.17 | -28.11 | -28.14 | -27.61 | 0.03 |
| 210 | 1811.63 | -27.72 | -27.76 | -27.74 | -27.20 | 0.02 |
| 215 | 1807.11 | -27.78 | -27.88 | -27.83 | -27.29 | 0.05 |
| 220 | 1802.60 | -27.68 | -27.44 | -27.56 | -27.01 | 0.12 |
| 225 | 1798.08 | -27.51 | -27.62 | -27.56 | -27.01 | 0.06 |
| 230 | 1793.56 | -27.31 | -27.52 | -27.41 | -26.85 | 0.10 |
| 235 | 1789.05 | -27.37 | -27.14 | -27.26 | -26.69 | 0.12 |
| 240 | 1784.53 | -27.16 | -27.15 | -27.16 | -26.59 | 0.01 |
| 245 | 1780.02 | -28.29 | -28.24 | -28.26 | -27.74 | 0.03 |
| 250 | 1775.50 | -27.45 | -27.18 | -27.31 | -26.75 | 0.14 |
| 255 | 1770.98 | -27.08 | -26.87 | -26.97 | -26.40 | 0.11 |
| 260 | 1766.47 | -27.13 | -27.21 | -27.17 | -26.60 | 0.04 |
| 265 | 1761.95 | -27.90 | -28.19 | -28.04 | -27.51 | 0.14 |
| 270 | 1757.44 | -28.40 | -28.34 | -28.37 | -27.86 | 0.03 |
| 275 | 1752.92 | -27.38 | -27.85 | -27.61 | -27.06 | 0.23 |
| 280 | 1748.40 | -28.22 | N/A | -28.22 | -27.69 | |
| 285 | 1743.89 | -28.01 | -27.65 | -27.83 | -27.29 | 0.18 |
| 290 | 1739.37 | -27.74 | -27.74 | -27.74 | -27.20 | 0.00 |
| 295 | 1734.86 | -28.98 | -29.29 | -29.14 | -28.65 | 0.15 |
| 305 | 1725.82 | -26.55 | -26.10 | -26.32 | -25.72 | 0.22 |
| 320 | 1712.28 | -25.78 | N/A | -25.78 | -25.16 | |
| 325 | 1707.76 | -27.21 | -27.29 | -27.25 | -26.68 | 0.04 |
| 330 | 1703.24 | -27.61 | -27.65 | -27.63 | -27.08 | 0.02 |
| 335 | 1698.73 | -27.95 | -27.83 | -27.89 | -27.35 | 0.06 |
| 340 | 1694.21 | -28.95 | -28.54 | -28.74 | -28.24 | 0.21 |
| 345 | 1689.70 | -28.82 | -28.49 | -28.65 | -28.15 | 0.17 |
| 365 | 1671.63 | -27.26 | -26.99 | -27.12 | -26.55 | 0.13 |
| 370 | 1667.12 | -26.64 | -26.80 | -26.72 | -26.13 | 0.08 |
| 375 | 1662.60 | -26.47 | -26.61 | -26.54 | -25.95 | 0.07 |
| 380 | 1658.08 | -29.12 | -29.09 | -29.10 | -28.61 | 0.02 |
| 385 | 1653.57 | -28.22 | -28.27 | -28.24 | -27.72 | 0.03 |
| 390 | 1649.05 | -28.20 | -28.26 | -28.23 | -27.70 | 0.03 |
| 395 | 1644.54 | -26.50 | -26.39 | -26.45 | -25.85 | 0.06 |
| 411 | 1630.08 | -26.90 | N/A | -26.90 | -26.32 | |
| 415 | 1626.47 | -28.78 | -28.81 | -28.79 | -28.29 | 0.02 |
| 421 | 1621.05 | -26.61 | -26.62 | -26.61 | -26.02 | 0.01 |
| 425 | 1617.44 | -29.35 | -29.25 | -29.30 | -28.82 | 0.05 |
| 435 | 1608.41 | -28.46 | -28.47 | -28.46 | -27.95 | 0.01 |
| 440 | 1603.89 | -27.38 | -27.53 | -27.45 | -26.90 | 0.07 |
| 445 | 1599.38 | -28.24 | -28.07 | -28.16 | -27.63 | 0.08 |
| 458 | 1587.63 | -28.27 | -28.40 | -28.34 | -27.82 | 0.07 |

| Age (years) | C24 FA d13C | error |
|---|---|---|
| 191.4 | -29.53 | 0.01 |
| 192.5 | -29.38 | 0.01 |
| 297.4 | -30.17 | 0.00 |
| 1548.9 | -29.26 | 0.13 |
| 391.1 | -29.11 | 0.15 |
| 392.2 | -29.30 | 0.32 |
| 492 | -29.05 | 0.31 |
| 601.7 | -30.42 | 0.13 |
| 603.1 | -29.08 | 0.01 |
| 679.6 | -28.09 | 0.00 |
| 298.4 | -28.39 | 0.45 |
| 796.1 | -29.64 | 0.24 |
| 678.9 | -28.65 | 0.06 |
| 893.7 | -29.98 | 0.15 |
| 967.9 | -29.70 | 0.05 |
| 968.4 | -29.50 | 0.00 |
| 1054.8 | -30.95 | 0.13 |
| 1193.6 | -29.95 | 0.10 |
| 1244.8 | -30.48 | 0.00 |
| 892.9 | -29.32 | 0.20 |
| 1357.5 | -29.61 | 0.03 |
| 1245.8 | -29.43 | 0.08 |
| 1456.6 | -29.03 | 0.01 |
| 1457.7 | -29.53 | 0.03 |
| 11345.3 | -32.05 | 0.05 |
| 1550.4 | -30.23 | 0.00 |
| 1358.6 | -29.83 | 0.00 |
| 1703.4 | -27.87 | 0.02 |
| 1704.6 | -28.07 | 0.00 |
| 1805.6 | -28.98 | 0.02 |
| 1804.9 | -30.49 | 0.00 |
| 1922.7 | -28.40 | 0.22 |
| 1921.5 | -28.97 | 0.03 |
| 2059.4 | -29.82 | 0.05 |
| 2237.3 | -29.10 | 0.03 |
| 2526.6 | -29.89 | 0.26 |
| 2061.1 | -28.54 | 0.08 |
| 2528.8 | -27.46 | 0.03 |
| 2870.9 | -30.02 | 0.00 |
| 2674.4 | -30.29 | 0.00 |
| 2872.7 | -29.13 | 0.05 |
| 2994.3 | -29.32 | 0.05 |
| 3203.7 | -29.34 | 0.15 |
| 3206.3 | -28.96 | 0.15 |
| 2996 | -29.30 | 0.06 |
| 3533.8 | -28.96 | 0.00 |
| 795 | -31.73 | 0.44 |
| 3531.1 | -29.54 | 0.02 |

| Age (years) | C24 FA d13C | error |
|---|---|---|
| 3727.2 | -29.44 | 0.18 |
| 3866.3 | -29.49 | 0.00 |
| 4022.7 | -30.02 | 0.08 |
| 4307.7 | -28.74 | 0.00 |
| 3864.7 | -30.84 | 0.02 |
| 4416.3 | -29.22 | 0.04 |
| 4417.5 | -28.80 | 0.02 |
| 4308.8 | -28.40 | 0.08 |
| 4520 | -27.72 | 0.02 |
| 4520.5 | -28.21 | 0.03 |
| 4612.4 | -29.20 | 0.01 |
| 4827.3 | -29.66 | 0.10 |
| 4613.5 | -30.28 | 0.14 |
| 4911.2 | -28.89 | 0.02 |
| 4828.3 | -29.24 | 0.02 |
| 5008.5 | -28.42 | 0.02 |
| 5115.9 | -28.80 | 0.01 |
| 5007.4 | -28.54 | 0.01 |
| 5317.5 | -28.34 | 0.00 |
| 5318.1 | -31.39 | 0.00 |
| 5401.5 | -28.53 | 0.05 |
| 3729 | -30.29 | 0.50 |
| 5402.7 | -27.90 | 0.03 |
| 5483.8 | -29.43 | 0.12 |
| 5551.4 | -29.50 | 0.06 |
| 5611.2 | -28.63 | 0.08 |
| 5551.9 | -29.02 | 0.07 |
| 5711.5 | -29.65 | 0.00 |
| 5611.7 | -28.66 | 0.00 |
| 5712.6 | -29.55 | 0.05 |
| 5910.7 | -29.43 | 0.00 |
| 5999.9 | -30.38 | 0.13 |
| 6001.2 | -29.80 | 0.00 |
| 6199.4 | -29.61 | 0.15 |
| 6200.5 | -28.99 | 0.03 |
| 6288.7 | -30.65 | 0.00 |
| 5909.4 | -29.25 | 0.04 |
| 6409 | -29.22 | 0.04 |
| 6412.4 | -28.44 | 0.17 |
| 6289.7 | -29.37 | 0.02 |
| 6488.7 | -30.41 | 0.01 |
| 6571.4 | -29.32 | 0.04 |
| 6572.5 | -29.40 | 0.26 |
| 6649.5 | -28.98 | 0.03 |
| 6739.5 | -29.01 | 0.00 |
| 6648.5 | -30.07 | 0.00 |
| 6740.5 | -28.97 | 0.01 |
| 6941.7 | -28.73 | 0.09 |

| Age (years) | C24 FA d13C | error |
|---|---|---|
| 6941.2 | -29.72 | 0.11 |
| 7140.6 | -29.13 | 0.02 |
| 7250.1 | -28.59 | 0.00 |
| 7248.6 | -29.48 | 0.01 |
| 7382 | -29.96 | 0.10 |
| 7383.5 | -30.05 | 0.00 |
| 7737.5 | -28.91 | 0.06 |
| 7906.6 | -31.84 | 0.00 |
| 7837.7 | -29.96 | 0.04 |
| 8050.3 | -29.94 | 0.00 |
| 8050.6 | -29.66 | 0.00 |
| 7907.6 | -29.66 | 0.04 |
| 8116.8 | -29.86 | 0.11 |
| 8184.2 | -31.07 | 0.02 |
| 8246.5 | -30.70 | 0.05 |
| 8184.6 | -31.07 | 0.00 |
| 8496.3 | -30.19 | 0.07 |
| 8497.5 | -32.36 | 0.08 |
| 8597.8 | -30.67 | 0.05 |
| 8695.7 | -31.45 | 0.03 |
| 8820.4 | -30.90 | 0.11 |
| 8821.7 | -30.00 | 0.05 |
| 8246.9 | -30.60 | 0.00 |
| 8937.3 | -30.05 | 0.03 |
| 9127.5 | -30.37 | 0.06 |
| 9126 | -30.82 | 0.04 |
| 9229.4 | -30.09 | 0.03 |
| 9512 | -30.00 | 0.00 |
| 9378.9 | -29.90 | 0.19 |
| 9513.8 | -29.31 | 0.02 |
| 9896.3 | -30.52 | 0.02 |
| 10088.2 | -30.73 | 0.03 |
| 9697.3 | -30.07 | 0.03 |
| 5484.8 | -28.80 | 0.00 |
| 10089.4 | -30.76 | 0.11 |
| 10519.4 | -29.38 | 0.30 |
| 10740.2 | -30.99 | 0.01 |
| 10290.3 | -30.47 | 0.02 |
| 10877.6 | -28.76 | 0.00 |
| 10741.1 | -31.91 | 0.09 |
| 10878.5 | -32.10 | 0.06 |
| 10880.1 | -32.95 | 0.04 |
| 11202.6 | -31.32 | 0.03 |

| Age (years) | C18 FA d13C | error |
|---|---|---|
| 192.5 | -29.5989 | 0.13 |
| 297.4 | -29.6683 | 0.42 |
| 298.4 | -29.5464 | 0.32 |
| 392.2 | -29.6646 | 0.42 |
| 492 | -28.6559 | 0.16 |
| 601.7 | -30.0866 | 0.00 |
| 678.9 | -28.4247 | 0.15 |
| 795 | -31.7791 | 0.26 |
| 796.1 | -28.8436 | 0.03 |
| 893.7 | -29.5239 | 0.19 |
| 967.9 | -31.6058 | 0.19 |
| 968.4 | -29.9076 | 0.42 |
| 1054.8 | -30.1215 | 0.14 |
| 1244.8 | -30.1133 | 0.42 |
| 1245.8 | -29.6305 | 0.05 |
| 1358.6 | -29.9447 | 0.42 |
| 1457.7 | -31.5837 | 0.42 |
| 1548.9 | -29.5726 | 0.10 |
| 1550.4 | -30.6036 | 0.42 |
| 1703.4 | -29.081 | 0.10 |
| 1704.6 | -32.3926 | 0.42 |
| 1804.9 | -29.6768 | 0.42 |
| 1805.6 | -29.2661 | 0.05 |
| 2528.8 | -31.8324 | 0.40 |
| 2674.4 | -28.8151 | 0.42 |
| 2870.9 | -29.7169 | 0.42 |
| 3206.3 | -28.5485 | 0.27 |
| 3533.8 | -30.1677 | 0.42 |
| 3727.2 | -28.6605 | 0.11 |
| 3729 | -29.4759 | 0.42 |
| 4022.7 | -29.4912 | 0.22 |
| 4307.7 | -32.2423 | 0.29 |
| 4308.8 | -28.7943 | 0.20 |
| 4520.5 | -28.3336 | 0.04 |
| 4613.5 | -28.9533 | 0.23 |
| 4827.3 | -30.4898 | 0.40 |
| 4828.3 | -28.8546 | 0.23 |
| 4911.2 | -29.7397 | 0.19 |
| 5007.4 | -30.1991 | 0.10 |
| 5115.9 | | 0.36 |
| 5402.7 | -29.3011 | 0.15 |
| 5483.8 | -29.5193 | 0.03 |
| 5484.8 | -28.8387 | 0.42 |
| 5551.4 | -29.3472 | 0.42 |
| 5551.9 | -30.2003 | 0.06 |
| 5611.7 | -29.2251 | 0.42 |
| 5711.5 | -29.7518 | 0.42 |
| 5712.6 | -28.1189 | 0.03 |
| 5909.4 | -30.9019 | 0.09 |
| 5910.7 | -29.7726 | 0.42 |
| 5999.9 | -30.079 | 0.42 |
| 6001.2 | -29.2996 | 0.42 |
| 6199.4 | -29.3928 | 0.05 |
| 6200.5 | -30.839 | 0.09 |
| 6288.7 | -29.8235 | 0.42 |
| 6289.7 | -30.7138 | 0.13 |
| 6488.7 | -30.0644 | 0.10 |
| 6572.5 | -30.7569 | 0.03 |
| 6648.5 | -30.4098 | 0.42 |
| 6649.5 | -30.042 | 0.16 |
| 6739.5 | -29.6473 | 0.42 |
| 6740.5 | -30.8721 | 0.03 |
| 7250.1 | -29.0568 | 0.42 |
| 7906.6 | -30.8407 | 0.42 |
| 8050.3 | -30.9545 | 0.31 |
| 8116.8 | -29.0123 | 0.14 |
| 8184.6 | -29.2505 | 0.42 |
| 8246.9 | -30.6194 | 0.19 |
| 8497.5 | -29.839 | 0.42 |
| 9896.3 | -30.0428 | 0.31 |
| 10089.4 | -28.2893 | 0.42 |
| 10290.3 | -28.5388 | 0.42 |
| 10519.4 | -28.734 | 0.22 |
| 10878.5 | -31.2006 | 0.34 |
| 11202.6 | -28.864 | 0.42 |

| Age (years) | Bulk acidified $\delta^{13}C_{(PDB)}$ | Age (years) | Bulk acidified $\delta^{13}C_{(PDB)}$ | Age (years) | Bulk acidified $\delta^{13}C_{(PDB)}$ |
|---|---|---|---|---|---|
| 133.3 | -26.10 | 1301.8 | -26.74 | 3096 | -27.27 |
| 134.5 | -26.65 | 1357.5 | -25.96 | 3203.7 | -27.33 |
| 191.4 | -24.99 | 1358.6 | -27.38 | 3206.3 | -29.43 |
| 192.5 | -26.13 | 1406.3 | -25.82 | 3405.5 | -26.90 |
| 244.8 | -26.85 | 1406.8 | -28.38 | 3408.1 | -27.93 |
| 245.7 | -27.53 | 1456.6 | -26.00 | 3531.1 | -27.11 |
| 297.4 | -26.39 | 1457.7 | -27.96 | 3533.8 | -27.94 |
| 298.4 | -27.17 | 1497.1 | -27.14 | 3612.3 | -26.46 |
| 339.9 | -28.21 | 1498.3 | -27.02 | 3614.8 | -27.23 |
| 340.9 | -28.61 | 1548.9 | -27.22 | 3727.2 | -26.72 |
| 391.1 | -28.28 | 1550.4 | -26.72 | 3729 | -27.45 |
| 392.2 | -29.66 | 1613.5 | -26.31 | 3798.1 | -27.69 |
| 446.5 | -26.42 | 1614.4 | -26.81 | 3799.9 | -28.32 |
| 491.1 | -26.90 | 1703.4 | -27.24 | 3864.7 | -28.18 |
| 492 | -28.47 | 1704.6 | -27.79 | 3866.3 | -28.01 |
| 542.6 | -28.77 | 1742.5 | -26.44 | 3947.3 | -26.46 |
| 544.2 | -26.41 | 1743.7 | -26.79 | 3948.2 | -27.04 |
| 601.7 | -26.68 | 1804.9 | -25.85 | 4022 | -27.63 |
| 603.1 | -29.06 | 1805.6 | -26.66 | 4022.7 | -30.54 |
| 625.5 | -26.73 | 1871.7 | -26.08 | 4105.2 | -29.27 |
| 627 | -28.14 | 1872.3 | -27.66 | 4106.6 | -29.05 |
| 678.9 | -27.31 | 1921.5 | -25.78 | 4307.7 | -26.24 |
| 679.6 | -27.54 | 1922.7 | -27.75 | 4308.8 | -27.61 |
| 739.5 | -26.44 | 1996.3 | -26.20 | 4359.5 | -26.79 |
| 740.7 | -27.66 | 1998.6 | -26.17 | 4360.2 | -28.26 |
| 795 | -26.51 | 2059.4 | -26.96 | 4416.3 | -26.98 |
| 796.1 | -27.47 | 2061.1 | -28.40 | 4417.5 | -27.20 |
| 844.4 | -26.87 | 2136.1 | -29.81 | 4465.7 | -27.04 |
| 845.4 | -26.84 | 2138.2 | -27.30 | 4466.8 | -27.59 |
| 892.9 | -26.46 | 2236.1 | -26.05 | 4520 | -26.82 |
| 893.7 | -28.57 | 2237.3 | -27.10 | 4520.5 | -27.99 |
| 937.2 | -27.49 | 2438 | -26.14 | 4562.4 | -26.92 |
| 938.1 | -27.92 | 2441.2 | -27.60 | 4563.4 | -27.32 |
| 967.9 | -27.43 | 2526.6 | -27.01 | 4612.4 | -27.24 |
| 968.4 | -29.73 | 2528.8 | -27.56 | 4613.5 | -28.64 |
| 1020.3 | -26.86 | 2617.4 | -26.65 | 4783.9 | -27.19 |
| 1020.7 | -28.66 | 2619.2 | -29.61 | 4784.9 | -28.28 |
| 1054.8 | -26.53 | 2673.6 | -26.79 | 4827.3 | -26.71 |
| 1055.6 | -27.01 | 2674.4 | -29.83 | 4828.3 | -27.04 |
| 1123.6 | -25.88 | 2774 | -27.23 | 4873.7 | -27.41 |
| 1124.4 | -26.78 | 2776.9 | -28.29 | 4874.8 | -27.12 |
| 1158.2 | -25.65 | 2870.9 | -26.76 | 4911.2 | -27.59 |
| 1159 | -27.03 | 2872.7 | -27.43 | 4912.3 | -28.95 |
| 1193.6 | -27.14 | 2923.2 | -26.66 | 4962.9 | -26.80 |
| 1194.5 | -28.42 | 2924.9 | -27.77 | 4964 | -27.69 |
| 1244.8 | -26.07 | 2994.3 | -27.40 | 5007.4 | -26.87 |
| 1245.8 | -26.78 | 2996 | -29.62 | 5008.5 | -27.17 |
| 1300.7 | -25.78 | 3094 | -26.84 | 5059.2 | -26.57 |

| Age (years) | Bulk acidified $\delta^{13}C_{(PDB)}$ | Age (years) | Bulk acidified $\delta^{13}C_{(PDB)}$ | Age (years) | Bulk acidified $\delta^{13}C_{(PDB)}$ |
|---|---|---|---|---|---|
| 5060.4 | -28.05 | 6452.1 | -26.67 | 7907.6 | -27.80 |
| 5115.9 | -27.45 | 6453 | -28.08 | 7943.7 | -28.58 |
| 5116.5 | -28.41 | 6487.6 | -27.71 | 7944.2 | -28.21 |
| 5167.4 | -26.72 | 6488.7 | -28.12 | 8050.3 | -27.86 |
| 5168.6 | -27.29 | 6522.8 | -27.40 | 8050.6 | -27.92 |
| 5317.5 | -26.64 | 6523.8 | -28.47 | 8081.8 | -27.81 |
| 5318.1 | -27.41 | 6571.4 | -26.90 | 8082.1 | -29.49 |
| 5350.5 | -26.64 | 6572.5 | -27.29 | 8116.8 | -27.29 |
| 5351.6 | -26.47 | 6609.2 | -27.67 | 8118 | -28.87 |
| 5401.5 | -27.71 | 6610.3 | -28.28 | 8151.4 | -27.45 |
| 5402.7 | -27.79 | 6648.5 | -27.12 | 8151.8 | -28.36 |
| 5445.8 | -27.03 | 6649.5 | -27.67 | 8184.2 | -27.56 |
| 5446.9 | -27.42 | 6701.3 | -27.13 | 8184.6 | -29.70 |
| 5483.8 | -26.96 | 6701.8 | -28.18 | 8212.3 | -27.88 |
| 5484.8 | -28.16 | 6739.5 | -27.35 | 8213.1 | -27.67 |
| 5519.9 | -26.88 | 6740.5 | -27.41 | 8246.5 | -28.02 |
| 5520.9 | -27.72 | 6890.2 | -26.65 | 8246.9 | -28.32 |
| 5551.4 | -27.50 | 6890.8 | -26.95 | 8287.3 | -27.09 |
| 5551.9 | -28.06 | 6941.2 | -26.66 | 8288.2 | -29.30 |
| 5587.7 | -27.18 | 6941.7 | -26.43 | 8324.3 | -27.78 |
| 5588.7 | -27.43 | 6982.7 | -27.31 | 8324.7 | -28.88 |
| 5611.2 | -26.91 | 6983.7 | -28.97 | 8371.6 | -28.40 |
| 5611.7 | -27.00 | 7028.5 | -26.93 | 8372.6 | -29.72 |
| 5659 | -26.76 | 7029.7 | -28.01 | 8496.3 | -28.10 |
| 5660.1 | -27.83 | 7073.3 | -29.17 | 8497.5 | -29.52 |
| 5711.5 | -27.05 | 7075.2 | -29.18 | 8545.7 | -28.14 |
| 5712.6 | -27.65 | 7139.4 | -26.97 | 8546.9 | -29.92 |
| 5856.1 | -27.33 | 7140.6 | -27.90 | 8596.5 | -27.62 |
| 5857.4 | -27.95 | 7186.6 | -28.02 | 8597.8 | -27.21 |
| 5909.4 | -27.94 | 7188 | -28.16 | 8642.2 | -28.75 |
| 5910.7 | -28.61 | 7248.6 | -27.51 | 8643.4 | -29.33 |
| 5946.5 | -27.14 | 7250.1 | -28.46 | 8695.2 | -27.58 |
| 5947.7 | -27.59 | 7326.4 | -27.39 | 8695.7 | -27.60 |
| 5999.9 | -26.78 | 7327.9 | -29.00 | 8747.4 | -27.78 |
| 6001.2 | -27.88 | 7382 | -28.36 | 8748.7 | -28.57 |
| 6052.6 | -27.03 | 7383.5 | -27.56 | 8820.4 | -28.12 |
| 6053.9 | -28.32 | 7525.3 | -28.17 | 8821.7 | -28.75 |
| 6097 | -27.78 | 7526.9 | -30.14 | 8869.3 | -27.69 |
| 6098.4 | -28.74 | 7618.4 | -29.31 | 8870.6 | -31.08 |
| 6147.7 | -27.28 | 7619.3 | -29.24 | 8936.1 | -27.73 |
| 6148.8 | -28.92 | 7689.6 | -28.39 | 8937.3 | -30.22 |
| 6199.4 | -27.04 | 7690.9 | -29.95 | 9064.7 | -27.31 |
| 6200.5 | -27.61 | 7736.8 | -28.73 | 9066 | -30.28 |
| 6242.6 | -27.31 | 7737.5 | -29.10 | 9126 | -28.00 |
| 6243.7 | -27.82 | 7786.7 | -27.50 | 9127.5 | -28.78 |
| 6288.7 | -27.58 | 7787.2 | -27.96 | 9185.9 | -28.36 |
| 6289.7 | -27.72 | 7837.3 | -28.55 | 9187.3 | -28.50 |
| 6387.8 | -26.64 | 7837.7 | -27.88 | 9227.8 | -27.98 |
| 6388.8 | -27.78 | 7857.9 | -28.08 | 9229.4 | -29.70 |
| 6409 | -27.08 | 7858.9 | -28.73 | 9295.2 | -27.71 |
| 6412.4 | -28.31 | 7906.6 | -27.55 | 9296.9 | -28.52 |

| Age (years) | Bulk acidified $\delta^{13}C_{(PDB)}$ |
|---|---|
| 9378.9 | -27.16 |
| 9379.7 | -28.36 |
| 9450.2 | -27.73 |
| 9452.9 | -28.01 |
| 9512 | -27.95 |
| 9513.8 | -28.44 |
| 9600.5 | -27.47 |
| 9603 | -27.73 |
| 9695.6 | -27.76 |
| 9697.3 | -28.85 |
| 9771.8 | -27.19 |
| 9772.7 | -27.88 |
| 9896.3 | -27.53 |
| 9897.2 | -28.52 |
| 9970.8 | -27.56 |
| 9972.6 | -29.39 |
| 10088.2 | -28.30 |
| 10089.4 | -30.16 |
| 10178.5 | -28.31 |
| 10181 | -28.16 |
| 10290.3 | -27.51 |
| 10292.9 | -29.01 |
| 10398.4 | -27.18 |
| 10402.3 | -29.94 |
| 10517.1 | -27.79 |
| 10519.4 | -28.37 |
| 10634.3 | -27.30 |
| 10636.6 | -27.46 |
| 10740.2 | -28.46 |
| 10741.1 | -29.47 |
| 10820.1 | -28.09 |
| 10821.7 | -29.86 |
| 10877.6 | -28.43 |
| 10878.5 | -30.97 |
| 10880.1 | -32.60 |
| 10962.4 | -28.34 |
| 10963.2 | -31.14 |
| 10964.9 | -32.55 |
| 11030.7 | -28.52 |
| 11031.5 | -30.81 |
| 11123.1 | -27.90 |
| 11124 | -29.80 |
| 11201.7 | -28.55 |
| 11202.6 | -31.48 |
| 11286 | -29.06 |
| 11287 | -29.90 |
| 11343.5 | -28.50 |
| 11345.3 | -30.40 |
| 11383.7 | -30.13 |

| Ages (C.E.) | GDGT fractional abundances | | | | | | TEX86 | TEX86-L | TEX86-L SST | RI | RI-TEX | ΔRI | MI |
|---|---|---|---|---|---|---|---|---|---|---|---|---|---|
| | GDGT-0 | GDGT-1 | GDGT-2 | GDGT-3 | Cren | Cren isomer | | | | | | | |
| 1998.59 | 0.56 | 0.02 | 0.01 | 0.00 | 0.41 | 0.00 | 0.41 | -0.66 | 2.59 | 1.70 | 1.84 | 0.14 | 0.06 |
| 1997.69 | 0.55 | 0.02 | 0.01 | 0.00 | 0.42 | 0.00 | 0.43 | -0.64 | 3.44 | 1.74 | 1.87 | 0.14 | 0.05 |
| 1996.78 | 0.59 | 0.02 | 0.01 | 0.00 | 0.37 | 0.00 | 0.45 | -0.66 | 2.11 | 1.55 | 1.90 | 0.35 | 0.07 |
| 1995.88 | 0.54 | 0.01 | 0.00 | 0.00 | 0.44 | 0.00 | 0.40 | -0.67 | 1.45 | 1.79 | 1.82 | 0.03 | 0.05 |
| 1994.98 | 0.55 | 0.02 | 0.01 | 0.00 | 0.42 | 0.00 | 0.47 | -0.64 | 3.93 | 1.75 | 1.95 | 0.21 | 0.06 |
| 1994.07 | 0.57 | 0.02 | 0.01 | 0.00 | 0.40 | 0.00 | 0.43 | -0.65 | 3.03 | 1.66 | 1.86 | 0.21 | 0.06 |
| 1993.17 | 0.57 | 0.02 | 0.01 | 0.00 | 0.40 | 0.00 | 0.44 | -0.65 | 2.69 | 1.66 | 1.90 | 0.23 | 0.06 |
| 1992.27 | 0.61 | 0.02 | 0.01 | 0.00 | 0.35 | 0.00 | 0.41 | -0.65 | 3.13 | 1.46 | 1.83 | 0.37 | 0.09 |
| 1991.36 | 0.63 | 0.02 | 0.01 | 0.00 | 0.33 | 0.00 | 0.42 | -0.68 | 1.01 | 1.41 | 1.85 | 0.44 | 0.09 |
| 1990.46 | 0.59 | 0.02 | 0.01 | 0.00 | 0.38 | 0.00 | 0.44 | -0.67 | 1.57 | 1.58 | 1.89 | 0.31 | 0.07 |
| 1989.56 | 0.58 | 0.02 | 0.01 | 0.00 | 0.39 | 0.00 | 0.43 | -0.66 | 2.22 | 1.62 | 1.88 | 0.26 | 0.07 |
| 1988.66 | 0.57 | 0.01 | 0.01 | 0.00 | 0.40 | 0.00 | 0.45 | -0.61 | 5.97 | 1.65 | 1.91 | 0.26 | 0.06 |
| 1987.75 | 0.58 | 0.02 | 0.01 | 0.00 | 0.40 | 0.00 | 0.46 | -0.65 | 2.90 | 1.64 | 1.93 | 0.30 | 0.06 |
| 1986.85 | 0.58 | 0.02 | 0.01 | 0.00 | 0.38 | 0.00 | 0.44 | -0.65 | 3.29 | 1.59 | 1.89 | 0.29 | 0.07 |
| 1985.95 | 0.59 | 0.02 | 0.01 | 0.00 | 0.38 | 0.00 | 0.44 | -0.64 | 3.67 | 1.56 | 1.90 | 0.34 | 0.07 |
| 1985.04 | 0.56 | 0.02 | 0.00 | 0.00 | 0.41 | 0.00 | 0.41 | -0.68 | 0.98 | 1.70 | 1.83 | 0.12 | 0.05 |
| 1984.14 | 0.59 | 0.02 | 0.01 | 0.00 | 0.37 | 0.00 | 0.47 | -0.63 | 4.57 | 1.55 | 1.96 | 0.41 | 0.08 |
| 1983.24 | 0.59 | 0.02 | 0.01 | 0.00 | 0.38 | 0.00 | 0.44 | -0.64 | 3.57 | 1.58 | 1.90 | 0.32 | 0.07 |
| 1982.33 | 0.59 | 0.02 | 0.01 | 0.00 | 0.37 | 0.00 | 0.43 | -0.66 | 2.49 | 1.56 | 1.87 | 0.31 | 0.07 |
| 1981.43 | 0.58 | 0.02 | 0.01 | 0.00 | 0.38 | 0.00 | 0.44 | -0.64 | 3.45 | 1.60 | 1.90 | 0.30 | 0.07 |
| 1980.53 | 0.60 | 0.02 | 0.01 | 0.00 | 0.37 | 0.00 | 0.43 | -0.66 | 2.43 | 1.52 | 1.86 | 0.35 | 0.07 |
| 1979.62 | 0.60 | 0.02 | 0.01 | 0.00 | 0.37 | 0.00 | 0.44 | -0.64 | 3.47 | 1.55 | 1.90 | 0.35 | 0.07 |
| 1978.72 | 0.58 | 0.02 | 0.01 | 0.00 | 0.39 | 0.00 | 0.45 | -0.66 | 2.52 | 1.63 | 1.91 | 0.28 | 0.06 |
| 1977.82 | 0.60 | 0.02 | 0.01 | 0.00 | 0.37 | 0.00 | 0.42 | -0.66 | 2.37 | 1.54 | 1.85 | 0.31 | 0.07 |
| 1976.91 | 0.59 | 0.02 | 0.01 | 0.00 | 0.38 | 0.00 | 0.45 | -0.63 | 4.16 | 1.57 | 1.91 | 0.34 | 0.07 |
| 1976.01 | 0.61 | 0.02 | 0.01 | 0.00 | 0.35 | 0.00 | 0.43 | -0.65 | 3.23 | 1.46 | 1.87 | 0.41 | 0.09 |
| 1975.11 | 0.58 | 0.02 | 0.01 | 0.00 | 0.39 | 0.00 | 0.42 | -0.66 | 2.13 | 1.60 | 1.85 | 0.25 | 0.07 |
| 1974.20 | 0.56 | 0.02 | 0.01 | 0.00 | 0.41 | 0.00 | 0.44 | -0.65 | 2.77 | 1.71 | 1.90 | 0.19 | 0.06 |
| 1973.30 | 0.57 | 0.02 | 0.01 | 0.00 | 0.40 | 0.00 | 0.44 | -0.64 | 3.44 | 1.64 | 1.90 | 0.26 | 0.06 |
| 1972.40 | 0.56 | 0.02 | 0.01 | 0.00 | 0.41 | 0.00 | 0.42 | -0.64 | 3.66 | 1.69 | 1.86 | 0.17 | 0.06 |
| 1971.49 | 0.57 | 0.02 | 0.01 | 0.00 | 0.39 | 0.00 | 0.42 | -0.65 | 2.82 | 1.64 | 1.85 | 0.22 | 0.07 |
| 1970.59 | 0.60 | 0.02 | 0.01 | 0.00 | 0.38 | 0.00 | 0.46 | -0.62 | 4.93 | 1.56 | 1.93 | 0.38 | 0.06 |
| 1969.69 | 0.59 | 0.02 | 0.01 | 0.00 | 0.38 | 0.00 | 0.43 | -0.67 | 1.93 | 1.57 | 1.88 | 0.31 | 0.06 |
| 1968.78 | 0.56 | 0.02 | 0.01 | 0.00 | 0.41 | 0.00 | 0.43 | -0.65 | 3.34 | 1.70 | 1.87 | 0.17 | 0.05 |
| 1967.88 | 0.61 | 0.02 | 0.01 | 0.00 | 0.36 | 0.00 | 0.44 | -0.65 | 3.21 | 1.49 | 1.89 | 0.40 | 0.08 |
| 1966.98 | 0.60 | 0.02 | 0.01 | 0.00 | 0.36 | 0.00 | 0.43 | -0.64 | 3.64 | 1.51 | 1.88 | 0.37 | 0.07 |
| 1966.08 | 0.54 | 0.01 | 0.01 | 0.00 | 0.43 | 0.00 | 0.45 | -0.64 | 3.74 | 1.77 | 1.91 | 0.14 | 0.05 |
| 1965.17 | 0.56 | 0.02 | 0.01 | 0.00 | 0.41 | 0.00 | 0.43 | -0.66 | 2.41 | 1.69 | 1.87 | 0.18 | 0.05 |
| 1964.27 | 0.61 | 0.02 | 0.01 | 0.00 | 0.36 | 0.00 | 0.43 | -0.67 | 2.01 | 1.49 | 1.87 | 0.37 | 0.08 |

| | | | | | | | | | | | | | |
|---|---|---|---|---|---|---|---|---|---|---|---|---|---|
| 1963.37 | 0.57 | 0.02 | 0.01 | 0.00 | 0.41 | 0.00 | 0.44 | -0.66 | 2.55 | 1.68 | 1.89 | 0.22 | 0.06 |
| 1962.46 | 0.56 | 0.02 | 0.01 | 0.00 | 0.41 | 0.00 | 0.47 | -0.65 | 3.08 | 1.68 | 1.95 | 0.27 | 0.06 |
| 1961.56 | 0.57 | 0.02 | 0.01 | 0.00 | 0.40 | 0.00 | 0.48 | -0.63 | 4.26 | 1.66 | 1.98 | 0.32 | 0.06 |
| 1960.66 | 0.57 | 0.02 | 0.01 | 0.00 | 0.40 | 0.00 | 0.43 | -0.65 | 3.15 | 1.65 | 1.88 | 0.23 | 0.06 |
| 1959.75 | 0.59 | 0.02 | 0.01 | 0.00 | 0.39 | 0.00 | 0.43 | -0.65 | 2.78 | 1.59 | 1.87 | 0.28 | 0.06 |
| 1958.85 | 0.55 | 0.02 | 0.00 | 0.00 | 0.42 | 0.00 | 0.42 | -0.71 | -0.93 | 1.75 | 1.85 | 0.10 | 0.05 |
| 1957.04 | 0.59 | 0.02 | 0.01 | 0.00 | 0.38 | 0.00 | 0.43 | -0.65 | 3.09 | 1.58 | 1.86 | 0.28 | 0.07 |
| 1956.14 | 0.56 | 0.02 | 0.01 | 0.00 | 0.41 | 0.00 | 0.43 | -0.67 | 1.44 | 1.71 | 1.88 | 0.17 | 0.06 |
| 1954.33 | 0.58 | 0.02 | 0.01 | 0.00 | 0.39 | 0.00 | 0.42 | -0.68 | 0.72 | 1.62 | 1.86 | 0.24 | 0.06 |
| 1952.53 | 0.55 | 0.02 | 0.00 | 0.00 | 0.42 | 0.00 | 0.40 | -0.69 | 0.00 | 1.73 | 1.81 | 0.08 | 0.05 |
| 1950.72 | 0.57 | 0.02 | 0.01 | 0.00 | 0.40 | 0.00 | 0.43 | -0.65 | 2.79 | 1.66 | 1.88 | 0.22 | 0.06 |
| 1948.91 | 0.61 | 0.02 | 0.01 | 0.00 | 0.36 | 0.00 | 0.43 | -0.63 | 4.17 | 1.50 | 1.87 | 0.38 | 0.08 |
| 1947.11 | 0.57 | 0.02 | 0.01 | 0.00 | 0.40 | 0.00 | 0.42 | -0.62 | 4.97 | 1.64 | 1.85 | 0.21 | 0.06 |
| 1945.30 | 0.62 | 0.02 | 0.01 | 0.00 | 0.34 | 0.00 | 0.44 | -0.62 | 4.82 | 1.43 | 1.89 | 0.46 | 0.09 |
| 1943.50 | 0.61 | 0.02 | 0.01 | 0.00 | 0.35 | 0.00 | 0.44 | -0.65 | 2.96 | 1.46 | 1.89 | 0.42 | 0.08 |
| 1941.69 | 0.56 | 0.02 | 0.01 | 0.00 | 0.41 | 0.00 | 0.45 | -0.63 | 4.45 | 1.70 | 1.92 | 0.22 | 0.06 |
| 1939.88 | 0.56 | 0.02 | 0.01 | 0.00 | 0.40 | 0.00 | 0.46 | -0.62 | 5.03 | 1.68 | 1.94 | 0.25 | 0.07 |
| 1938.08 | 0.56 | 0.02 | 0.01 | 0.00 | 0.41 | 0.00 | 0.44 | -0.65 | 3.16 | 1.70 | 1.88 | 0.19 | 0.06 |
| 1936.27 | 0.60 | 0.02 | 0.01 | 0.00 | 0.37 | 0.01 | 0.46 | -0.65 | 3.29 | 1.54 | 1.93 | 0.39 | 0.08 |
| 1934.46 | 0.59 | 0.02 | 0.01 | 0.00 | 0.38 | 0.00 | 0.42 | -0.65 | 2.88 | 1.58 | 1.85 | 0.26 | 0.07 |
| 1932.66 | 0.61 | 0.02 | 0.01 | 0.00 | 0.36 | 0.00 | 0.42 | -0.67 | 1.93 | 1.49 | 1.84 | 0.35 | 0.07 |
| 1930.85 | 0.59 | 0.02 | 0.01 | 0.00 | 0.38 | 0.00 | 0.46 | -0.63 | 4.54 | 1.59 | 1.95 | 0.36 | 0.06 |
| 1929.04 | 0.61 | 0.02 | 0.01 | 0.00 | 0.36 | 0.00 | 0.44 | -0.63 | 4.04 | 1.49 | 1.90 | 0.41 | 0.07 |
| 1927.24 | 0.60 | 0.02 | 0.01 | 0.00 | 0.37 | 0.00 | 0.45 | -0.63 | 4.47 | 1.52 | 1.92 | 0.40 | 0.07 |
| 1925.43 | 0.56 | 0.02 | 0.01 | 0.00 | 0.41 | 0.00 | 0.40 | -0.67 | 1.47 | 1.69 | 1.82 | 0.13 | 0.05 |
| 1923.62 | 0.62 | 0.02 | 0.01 | 0.00 | 0.35 | 0.00 | 0.45 | -0.64 | 3.70 | 1.46 | 1.92 | 0.45 | 0.08 |
| 1921.82 | 0.63 | 0.02 | 0.01 | 0.00 | 0.33 | 0.01 | 0.46 | -0.63 | 4.15 | 1.39 | 1.94 | 0.55 | 0.09 |
| 1920.01 | 0.62 | 0.02 | 0.01 | 0.00 | 0.35 | 0.00 | 0.44 | -0.65 | 3.05 | 1.46 | 1.89 | 0.43 | 0.08 |
| 1918.21 | 0.62 | 0.02 | 0.01 | 0.00 | 0.34 | 0.00 | 0.43 | -0.65 | 2.90 | 1.43 | 1.88 | 0.45 | 0.09 |
| 1916.40 | 0.62 | 0.02 | 0.01 | 0.00 | 0.35 | 0.00 | 0.42 | -0.64 | 3.38 | 1.47 | 1.86 | 0.39 | 0.08 |
| 1914.59 | 0.59 | 0.02 | 0.01 | 0.00 | 0.38 | 0.00 | 0.43 | -0.64 | 3.77 | 1.56 | 1.88 | 0.32 | 0.07 |
| 1912.79 | 0.57 | 0.02 | 0.01 | 0.00 | 0.40 | 0.00 | 0.44 | -0.63 | 4.14 | 1.66 | 1.89 | 0.24 | 0.07 |

| | | | | | | | | | | | | | |
|---|---|---|---|---|---|---|---|---|---|---|---|---|---|
| 1910.98 | 0.59 | 0.02 | 0.01 | 0.00 | 0.38 | 0.00 | 0.46 | -0.64 | 3.84 | 1.58 | 1.95 | 0.37 | 0.07 |
| 1906.46 | 0.59 | 0.02 | 0.01 | 0.00 | 0.37 | 0.00 | 0.45 | -0.64 | 3.79 | 1.55 | 1.91 | 0.36 | 0.07 |
| 1901.95 | 0.60 | 0.02 | 0.01 | 0.00 | 0.36 | 0.01 | 0.44 | -0.67 | 1.53 | 1.51 | 1.89 | 0.38 | 0.08 |
| 1897.43 | 0.59 | 0.02 | 0.01 | 0.00 | 0.37 | 0.00 | 0.43 | -0.65 | 2.85 | 1.55 | 1.86 | 0.32 | 0.07 |
| 1892.92 | 0.60 | 0.02 | 0.01 | 0.00 | 0.36 | 0.00 | 0.43 | -0.67 | 1.73 | 1.52 | 1.87 | 0.34 | 0.08 |
| 1888.40 | 0.62 | 0.02 | 0.01 | 0.01 | 0.34 | 0.00 | 0.43 | -0.65 | 2.74 | 1.43 | 1.87 | 0.44 | 0.10 |
| 1883.88 | 0.58 | 0.02 | 0.01 | 0.00 | 0.39 | 0.00 | 0.42 | -0.69 | 0.57 | 1.62 | 1.84 | 0.22 | 0.06 |
| 1879.37 | 0.55 | 0.02 | 0.01 | 0.00 | 0.41 | 0.00 | 0.45 | -0.66 | 2.33 | 1.71 | 1.91 | 0.20 | 0.06 |
| 1874.85 | 0.57 | 0.02 | 0.01 | 0.00 | 0.39 | 0.00 | 0.40 | -0.67 | 1.69 | 1.62 | 1.81 | 0.19 | 0.08 |
| 1870.34 | 0.56 | 0.02 | 0.01 | 0.00 | 0.41 | 0.00 | 0.42 | -0.65 | 3.05 | 1.69 | 1.85 | 0.17 | 0.06 |
| 1865.82 | 0.56 | 0.02 | 0.01 | 0.00 | 0.41 | 0.00 | 0.42 | -0.66 | 2.30 | 1.70 | 1.85 | 0.15 | 0.06 |
| 1861.30 | 0.60 | 0.02 | 0.01 | 0.00 | 0.37 | 0.00 | 0.43 | -0.66 | 2.61 | 1.53 | 1.87 | 0.34 | 0.08 |
| 1856.79 | 0.62 | 0.02 | 0.01 | 0.00 | 0.34 | 0.00 | 0.42 | -0.65 | 2.93 | 1.42 | 1.85 | 0.43 | 0.09 |
| 1851.37 | 0.60 | 0.02 | 0.01 | 0.00 | 0.36 | 0.00 | 0.44 | -0.65 | 2.84 | 1.50 | 1.90 | 0.39 | 0.08 |
| 1847.76 | 0.54 | 0.02 | 0.01 | 0.00 | 0.43 | 0.00 | 0.42 | -0.67 | 1.56 | 1.77 | 1.85 | 0.08 | 0.05 |
| 1843.24 | 0.60 | 0.02 | 0.01 | 0.00 | 0.37 | 0.00 | 0.46 | -0.64 | 3.46 | 1.53 | 1.94 | 0.40 | 0.08 |
| 1838.72 | 0.61 | 0.02 | 0.01 | 0.00 | 0.35 | 0.00 | 0.42 | -0.66 | 2.45 | 1.47 | 1.84 | 0.37 | 0.09 |
| 1834.21 | 0.61 | 0.02 | 0.01 | 0.01 | 0.35 | 0.01 | 0.45 | -0.66 | 2.38 | 1.46 | 1.91 | 0.45 | 0.09 |
| 1829.69 | 0.60 | 0.02 | 0.01 | 0.00 | 0.37 | 0.00 | 0.42 | -0.66 | 2.24 | 1.54 | 1.86 | 0.32 | 0.08 |
| 1820.66 | 0.58 | 0.02 | 0.01 | 0.00 | 0.38 | 0.00 | 0.44 | -0.64 | 3.78 | 1.60 | 1.90 | 0.30 | 0.07 |
| 1816.14 | 0.61 | 0.02 | 0.01 | 0.00 | 0.35 | 0.00 | 0.40 | -0.67 | 1.69 | 1.46 | 1.81 | 0.36 | 0.10 |
| 1811.63 | 0.63 | 0.03 | 0.01 | 0.01 | 0.32 | 0.01 | 0.46 | -0.64 | 3.79 | 1.38 | 1.93 | 0.55 | 0.11 |
| 1807.11 | 0.62 | 0.02 | 0.01 | 0.00 | 0.34 | 0.00 | 0.43 | -0.65 | 3.04 | 1.43 | 1.87 | 0.44 | 0.09 |
| 1802.60 | 0.59 | 0.02 | 0.01 | 0.00 | 0.37 | 0.00 | 0.42 | -0.65 | 2.90 | 1.55 | 1.86 | 0.31 | 0.08 |
| 1798.08 | 0.61 | 0.02 | 0.01 | 0.00 | 0.34 | 0.01 | 0.44 | -0.66 | 2.54 | 1.45 | 1.88 | 0.43 | 0.09 |
| 1793.56 | 0.60 | 0.02 | 0.01 | 0.00 | 0.36 | 0.00 | 0.44 | -0.65 | 3.14 | 1.52 | 1.89 | 0.37 | 0.08 |
| 1789.05 | 0.60 | 0.02 | 0.01 | 0.00 | 0.37 | 0.00 | 0.45 | -0.65 | 3.21 | 1.54 | 1.91 | 0.37 | 0.08 |
| 1784.53 | 0.64 | 0.03 | 0.01 | 0.01 | 0.32 | 0.00 | 0.42 | -0.67 | 1.79 | 1.35 | 1.85 | 0.50 | 0.11 |
| 1780.02 | 0.58 | 0.02 | 0.01 | 0.00 | 0.38 | 0.00 | 0.45 | -0.65 | 3.18 | 1.59 | 1.91 | 0.32 | 0.07 |
| 1775.50 | 0.60 | 0.01 | 0.01 | 0.00 | 0.38 | 0.01 | 0.50 | -0.65 | 3.08 | 1.56 | 2.04 | 0.48 | 0.06 |
| 1770.98 | 0.64 | 0.02 | 0.01 | 0.01 | 0.32 | 0.00 | 0.43 | -0.65 | 3.00 | 1.35 | 1.87 | 0.52 | 0.10 |
| 1766.47 | 0.61 | 0.02 | 0.01 | 0.00 | 0.35 | 0.00 | 0.43 | -0.63 | 4.31 | 1.47 | 1.88 | 0.41 | 0.09 |
| 1761.95 | 0.63 | 0.02 | 0.01 | 0.00 | 0.33 | 0.00 | 0.43 | -0.66 | 2.57 | 1.40 | 1.87 | 0.47 | 0.09 |
| 1757.44 | 0.64 | 0.02 | 0.01 | 0.01 | 0.32 | 0.00 | 0.44 | -0.64 | 3.64 | 1.36 | 1.90 | 0.54 | 0.10 |
| 1752.92 | 0.58 | 0.02 | 0.01 | 0.00 | 0.39 | 0.00 | 0.43 | -0.65 | 2.97 | 1.62 | 1.87 | 0.25 | 0.06 |
| 1748.40 | 0.62 | 0.02 | 0.01 | 0.00 | 0.35 | 0.00 | 0.43 | -0.65 | 3.11 | 1.45 | 1.88 | 0.42 | 0.08 |
| 1743.89 | 0.62 | 0.02 | 0.01 | 0.01 | 0.34 | 0.00 | 0.43 | -0.65 | 3.31 | 1.42 | 1.88 | 0.46 | 0.10 |
| 1739.37 | 0.61 | 0.02 | 0.01 | 0.00 | 0.35 | 0.00 | 0.45 | -0.64 | 3.81 | 1.46 | 1.90 | 0.45 | 0.09 |
| 1734.86 | 0.61 | 0.02 | 0.01 | 0.00 | 0.36 | 0.00 | 0.46 | -0.62 | 4.71 | 1.50 | 1.93 | 0.43 | 0.08 |
| 1730.34 | 0.59 | 0.02 | 0.01 | 0.00 | 0.37 | 0.00 | 0.46 | -0.64 | 3.95 | 1.55 | 1.94 | 0.39 | 0.07 |
| 1725.82 | 0.64 | 0.02 | 0.01 | 0.01 | 0.32 | 0.00 | 0.45 | -0.64 | 3.42 | 1.37 | 1.92 | 0.55 | 0.10 |
| 1721.31 | 0.60 | 0.02 | 0.01 | 0.00 | 0.37 | 0.00 | 0.44 | -0.65 | 2.88 | 1.54 | 1.90 | 0.35 | 0.07 |

| | | | | | | | | | | | | | |
|---|---|---|---|---|---|---|---|---|---|---|---|---|---|
| 1716.79 | 0.59 | 0.02 | 0.01 | 0.00 | 0.37 | 0.00 | 0.42 | -0.65 | 3.15 | 1.54 | 1.86 | 0.32 | 0.09 |
| 1712.28 | 0.58 | 0.02 | 0.01 | 0.00 | 0.39 | 0.01 | 0.47 | -0.63 | 4.33 | 1.60 | 1.96 | 0.36 | 0.06 |
| 1707.76 | 0.58 | 0.02 | 0.01 | 0.00 | 0.39 | 0.00 | 0.43 | -0.67 | 1.53 | 1.60 | 1.87 | 0.27 | 0.06 |
| 1703.24 | 0.64 | 0.02 | 0.01 | 0.00 | 0.32 | 0.00 | 0.44 | -0.65 | 3.29 | 1.37 | 1.89 | 0.52 | 0.09 |
| 1698.73 | 0.62 | 0.02 | 0.01 | 0.00 | 0.35 | 0.00 | 0.42 | -0.67 | 1.91 | 1.47 | 1.85 | 0.39 | 0.07 |
| 1694.21 | 0.64 | 0.02 | 0.01 | 0.01 | 0.32 | 0.01 | 0.45 | -0.65 | 2.99 | 1.34 | 1.92 | 0.58 | 0.10 |
| 1689.70 | 0.62 | 0.02 | 0.01 | 0.01 | 0.33 | 0.00 | 0.42 | -0.65 | 3.03 | 1.41 | 1.86 | 0.45 | 0.10 |
| 1685.18 | 0.60 | 0.02 | 0.01 | 0.00 | 0.37 | 0.00 | 0.45 | -0.66 | 2.24 | 1.54 | 1.92 | 0.37 | 0.07 |
| 1680.66 | 0.59 | 0.02 | 0.01 | 0.00 | 0.38 | 0.00 | 0.46 | -0.64 | 3.65 | 1.59 | 1.93 | 0.35 | 0.07 |
| 1675.24 | 0.62 | 0.02 | 0.01 | 0.00 | 0.34 | 0.00 | 0.44 | -0.63 | 4.28 | 1.42 | 1.90 | 0.48 | 0.09 |
| 1671.63 | 0.62 | 0.02 | 0.01 | 0.00 | 0.34 | 0.00 | 0.44 | -0.66 | 2.35 | 1.44 | 1.88 | 0.44 | 0.09 |
| 1667.12 | 0.62 | 0.02 | 0.01 | 0.00 | 0.34 | 0.00 | 0.42 | -0.66 | 2.35 | 1.43 | 1.85 | 0.42 | 0.09 |
| 1662.60 | 0.63 | 0.03 | 0.01 | 0.01 | 0.32 | 0.01 | 0.43 | -0.65 | 2.92 | 1.37 | 1.87 | 0.50 | 0.11 |
| 1658.08 | 0.63 | 0.02 | 0.01 | 0.00 | 0.34 | 0.00 | 0.43 | -0.64 | 3.52 | 1.40 | 1.88 | 0.48 | 0.08 |
| 1653.57 | 0.61 | 0.02 | 0.01 | 0.00 | 0.35 | 0.01 | 0.47 | -0.64 | 3.61 | 1.47 | 1.95 | 0.49 | 0.08 |
| 1649.05 | 0.57 | 0.02 | 0.01 | 0.00 | 0.40 | 0.00 | 0.43 | -0.64 | 3.55 | 1.64 | 1.88 | 0.24 | 0.06 |
| 1644.54 | 0.60 | 0.02 | 0.01 | 0.00 | 0.38 | 0.00 | 0.44 | -0.63 | 4.08 | 1.56 | 1.90 | 0.35 | 0.06 |
| 1640.02 | 0.57 | 0.02 | 0.01 | 0.00 | 0.39 | 0.00 | 0.46 | -0.64 | 3.94 | 1.63 | 1.94 | 0.31 | 0.07 |
| 1635.50 | 0.56 | 0.02 | 0.01 | 0.00 | 0.42 | 0.00 | 0.44 | -0.65 | 2.72 | 1.72 | 1.89 | 0.18 | 0.06 |
| 1630.08 | 0.60 | 0.02 | 0.01 | 0.01 | 0.36 | 0.01 | 0.45 | -0.65 | 3.05 | 1.53 | 1.92 | 0.40 | 0.08 |
| 1626.47 | 0.60 | 0.02 | 0.01 | 0.00 | 0.36 | 0.00 | 0.45 | -0.64 | 3.98 | 1.52 | 1.92 | 0.40 | 0.07 |
| 1621.05 | 0.59 | 0.02 | 0.01 | 0.00 | 0.37 | 0.00 | 0.43 | -0.67 | 1.83 | 1.55 | 1.88 | 0.33 | 0.07 |
| 1617.44 | 0.60 | 0.02 | 0.01 | 0.00 | 0.37 | 0.00 | 0.45 | -0.62 | 5.32 | 1.54 | 1.91 | 0.37 | 0.07 |
| 1612.02 | 0.59 | 0.02 | 0.01 | 0.00 | 0.38 | 0.00 | 0.46 | -0.63 | 4.60 | 1.58 | 1.94 | 0.36 | 0.07 |
| 1608.41 | 0.57 | 0.01 | 0.01 | 0.00 | 0.40 | 0.01 | 0.48 | -0.65 | 3.18 | 1.66 | 1.99 | 0.33 | 0.05 |
| 1603.89 | 0.63 | 0.02 | 0.01 | 0.00 | 0.33 | 0.00 | 0.44 | -0.65 | 3.31 | 1.38 | 1.89 | 0.50 | 0.09 |
| 1599.38 | 0.60 | 0.02 | 0.01 | 0.00 | 0.36 | 0.00 | 0.43 | -0.67 | 1.85 | 1.51 | 1.87 | 0.36 | 0.08 |
| 1595.76 | 0.60 | 0.02 | 0.01 | 0.00 | 0.36 | 0.01 | 0.49 | -0.65 | 3.18 | 1.53 | 2.00 | 0.47 | 0.08 |
| 1591.25 | 0.62 | 0.02 | 0.01 | 0.00 | 0.35 | 0.00 | 0.43 | -0.63 | 4.46 | 1.44 | 1.88 | 0.44 | 0.08 |
| 1587.63 | 0.56 | 0.01 | 0.00 | 0.00 | 0.42 | 0.00 | 0.39 | -0.68 | 0.98 | 1.72 | 1.80 | 0.08 | 0.05 |

| Year (C.E.) | Sand% |
|---|---|
| 1998.5904 | 9.58 |
| 1997.6872 | 12.68 |
| 1996.784 | 12.93 |
| 1995.8808 | 8.55 |
| 1994.9776 | 8.99 |
| 1994.0744 | 7.86 |
| 1993.1712 | 8.58 |
| 1992.268 | 7.53 |
| 1991.3648 | 8.45 |
| 1990.4616 | 7.38 |
| 1989.5584 | 8.61 |
| 1988.6552 | 7.96 |
| 1987.752 | 7.74 |
| 1986.8488 | 6.62 |
| 1985.9456 | 7.1 |
| 1985.0424 | 8.53 |
| 1984.1392 | 13.43 |
| 1983.236 | 8.78 |
| 1982.3328 | 9.94 |
| 1981.4296 | 7.43 |
| 1980.5264 | 5.76 |
| 1979.6232 | 6.43 |
| 1978.72 | 6.27 |
| 1977.8168 | 7.7 |
| 1976.9136 | 6.69 |
| 1976.0104 | 7.19 |
| 1975.1072 | 1.51 |
| 1974.204 | 4.89 |
| 1972.3976 | 7.09 |
| 1970.5912 | 4.57 |
| 1969.688 | 5.97 |
| 1968.7848 | 6.41 |
| 1967.8816 | 3.8 |
| 1966.0752 | 6.86 |
| 1963.3656 | 8.93 |
| 1958.8496 | 3.28 |
| 1957.9464 | 7.31 |
| 1957.0432 | 12.18 |
| 1956.14 | 3.04 |
| 1954.3336 | 7.76 |
| 1952.5272 | 3.86 |
| 1950.7208 | 3.41 |
| 1948.9144 | 2.2 |
| 1947.108 | 1.48 |
| 1945.3016 | 2.68 |
| 1943.4952 | 8.75 |
| 1941.6888 | 14.61 |
| 1939.8824 | 8.56 |
| 1938.076 | 13.82 |

| Year (C.E.) | Sand% |
|---|---|
| 1936.27 | 20.54 |
| 1934.463 | 12.32 |
| 1932.657 | 6.27 |
| 1930.85 | 16.51 |
| 1929.044 | 8.24 |
| 1927.238 | 1.28 |
| 1925.431 | 4.41 |
| 1923.625 | 1.94 |
| 1921.818 | 1.31 |
| 1920.012 | 2.42 |
| 1918.206 | 6.73 |
| 1916.399 | 1.91 |
| 1914.593 | 1.86 |
| 1912.786 | 2.05 |
| 1910.98 | 6.73 |
| 1906.464 | 3.73 |
| 1901.948 | 2.14 |
| 1897.432 | 3.55 |
| 1892.916 | 2.98 |
| 1888.4 | 3.2 |
| 1883.884 | 3.23 |
| 1879.368 | 3.86 |
| 1874.852 | 1.99 |
| 1870.336 | 3.12 |
| 1865.82 | 2.65 |
| 1861.304 | 4.3 |
| 1856.788 | 3.75 |
| 1851.369 | 4.33 |
| 1843.24 | 1.83 |
| 1838.724 | 1.76 |
| 1834.208 | 2.46 |
| 1829.692 | 2.83 |
| 1825.176 | 4.63 |
| 1820.66 | 1.99 |
| 1816.144 | 1.41 |
| 1811.628 | 3.4 |
| 1807.112 | 3.89 |
| 1802.596 | 7.09 |
| 1798.08 | 3.38 |
| 1793.564 | 3.24 |
| 1789.048 | 4.32 |
| 1784.532 | 3.06 |
| 1780.016 | 3.1 |
| 1775.5 | 2.43 |
| 1770.984 | 5.25 |
| 1766.468 | 6.8 |
| 1761.952 | 7.35 |
| 1757.436 | 5.25 |
| 1752.92 | 9.42 |

| Year (C.E.) | Sand% |
|---|---|
| 1748.404 | 5.76 |
| 1743.888 | 6.58 |
| 1739.372 | 6.28 |
| 1734.856 | 6.17 |
| 1730.34 | 8.35 |
| 1725.824 | 24.69 |
| 1721.308 | 10.1 |
| 1716.792 | 4.79 |
| 1712.276 | 7.3 |
| 1707.76 | 24.87 |
| 1703.244 | 5.37 |
| 1698.728 | 4.58 |
| 1694.212 | 9.54 |
| 1689.696 | 8.63 |
| 1685.18 | 4.11 |
| 1680.664 | 4.55 |
| 1675.245 | 10.61 |
| 1671.632 | 7.67 |
| 1667.116 | 10.64 |
| 1662.6 | 7.04 |
| 1658.084 | 8.26 |
| 1653.568 | 5.92 |
| 1649.052 | 4.44 |
| 1644.536 | 5.39 |
| 1640.02 | 7.26 |
| 1635.504 | 13.54 |
| 1630.085 | 4.52 |
| 1626.472 | 3.99 |
| 1621.053 | 7.63 |
| 1617.44 | 3.52 |
| 1612.021 | 5.24 |
| 1608.408 | 5.01 |
| 1603.892 | 7.71 |
| 1599.376 | 8.51 |
| 1595.763 | 5.19 |
| 1591.247 | 5.57 |
| 1587.634 | 8.29 |

| Age (C.E.) | FAME d2H 1 | FAME d2H 2 | Average FAME d2H | Corrected FA d2H | SD |
|---|---|---|---|---|---|
| 1998.59 | -215.55 | -212.46 | -214.0 | -221 | 2.2 |
| 1996.784 | -228.08 | -229.94 | -229.0 | -226 | 1.3 |
| 1995.881 | -218.92 | -217.73 | -218.3 | -222 | 0.8 |
| 1994.978 | -232.89 | -232.67 | -232.8 | -226 | 0.2 |
| 1994.074 | -226.07 | -214.22 | -220.1 | -221 | 8.4 |
| 1993.171 | -233.45 | -231.63 | -232.5 | -223 | 1.3 |
| 1989.558 | -232.08 | -231.32 | -231.7 | -230 | 0.5 |
| 1988.655 | -231.50 | -230.95 | -231.2 | -226 | 0.4 |
| 1985.946 | | | | -224 | |
| 1985.042 | -226.52 | -227.59 | -227.1 | -227 | 0.8 |
| 1984.139 | -228.25 | -229.10 | -228.7 | -230 | 0.6 |
| 1982.333 | -235.39 | -235.48 | -235.4 | -230 | 0.1 |
| 1979.623 | -219.03 | -219.08 | -219.1 | -218 | 0.0 |
| 1971.494 | -227.90 | -231.18 | -229.5 | -235 | 2.3 |
| 1967.882 | -217.77 | -219.14 | -218.5 | -222 | 1.0 |
| 1966.978 | -234.69 | -233.72 | -234.2 | -232 | 0.7 |
| 1965.172 | -207.27 | -211.02 | -209.1 | -210 | 2.6 |
| 1964.269 | -206.46 | -207.54 | -207.0 | -202 | 0.8 |
| 1963.366 | -222.18 | -222.74 | -222.5 | -224 | 0.4 |
| 1962.462 | -230.51 | -215.32 | -222.9 | -226 | 10.7 |
| 1961.559 | -226.82 | -223.30 | -225.1 | -226 | 2.5 |
| 1960.656 | -216.04 | -209.19 | -212.6 | -218 | 4.8 |
| 1959.753 | -223.89 | -229.05 | -226.5 | -231 | 3.7 |
| 1958.85 | -207.12 | -209.43 | -208.3 | -209 | 1.6 |
| 1957.946 | -223.29 | -221.24 | -222.3 | -215 | 1.5 |
| 1957.043 | -227.11 | -228.81 | -228.0 | -232 | 1.2 |
| 1952.527 | -220.77 | -215.86 | -218.3 | -211 | 3.5 |
| 1948.914 | -204.96 | -209.82 | -207.4 | -206 | 3.4 |
| 1939.882 | -222.65 | -220.99 | -221.8 | -214 | 1.2 |
| 1938.076 | -223.96 | -219.53 | -221.7 | -218 | 3.1 |
| 1934.463 | -223.39 | -220.80 | -222.1 | -222 | 1.8 |
| 1930.85 | | | | -194 | |
| 1923.625 | | | | -216 | |
| 1920.012 | | | | -233 | |
| 1918.206 | | | | -227 | |
| 1914.593 | -224.22 | -221.33 | -222.8 | -230 | 2.0 |
| 1906.464 | -214.60 | -211.86 | -213.2 | -223 | 1.9 |
| 1901.948 | -221.81 | -223.11 | -222.5 | -226 | 0.9 |
| 1897.432 | -224.43 | -225.65 | -225.0 | -224 | 0.9 |
| 1865.82 | -225.68 | -224.13 | -224.9 | -224 | 1.1 |
| 1861.304 | -229.94 | -231.56 | -230.8 | -225 | 1.2 |
| 1856.788 | -227.92 | -223.73 | -225.8 | -218 | 3.0 |
| 1847.756 | -219.17 | -207.08 | -213.1 | -216 | 8.5 |
| 1843.24 | -221.82 | -219.97 | -220.9 | -216 | 1.3 |
| 1838.724 | -220.90 | -222.16 | -221.5 | -224 | 0.9 |
| 1834.208 | -202.66 | -197.99 | -200.3 | -201 | 3.3 |
| 1825.176 | -210.47 | -213.78 | -212.1 | -211 | 2.3 |
| 1820.66 | | | | -218 | |

| | | | | | |
|---|---|---|---|---|---|
| 1816.144 | | | | -217 | |
| 1811.628 | -223.00 | -227.41 | -225.2 | -229 | 3.1 |
| 1802.596 | -211.83 | -216.57 | -214.2 | -214 | 3.4 |
| 1798.08 | -216.52 | -216.51 | -216.5 | -220 | 0.0 |
| 1793.564 | -213.09 | -213.23 | -213.2 | -208 | 0.1 |
| 1757.436 | -223.44 | -219.06 | -221.2 | -221 | 3.1 |
| 1752.92 | -224.81 | -224.16 | -224.5 | -225 | 0.5 |
| 1743.888 | -204.97 | -189.35 | -197.2 | -198 | 11.0 |
| 1739.372 | -224.22 | -220.91 | -222.6 | -220 | 2.3 |
| 1734.856 | -229.33 | -226.32 | -227.8 | -233 | 2.1 |
| 1680.664 | | | | -219 | |
| 1671.632 | | | | -205 | |
| 1667.116 | -219.81 | -213.91 | -216.9 | -212 | 4.2 |
| 1658.084 | | | | -214 | |
| 1621.053 | -213.09 | -211.44 | -212.3 | -204 | 1.2 |
| 1617.44 | -225.46 | -226.33 | -225.9 | -229 | 0.6 |
| 1595.763 | | | | -201 | |
| 1591.247 | -179.89 | -182.87 | -181.4 | -188 | 2.1 |
| 1587.634 | -226.18 | -226.29 | -226.2 | -227 | 0.1 |